# Study on the mechanism of wood/bamboo/adhesive activation and bonding enhancement induced by high voltage electric field

Qian He

Ecole Doctorale Sciences et Ingénierie des
Molécules Procédés Produits et Énergie

# Thèse de doctorat

# Étude sur le mécanisme d'activation du bois/bambou/adhésif et amélioration du collage induit par le champ électrique à haute tension

# Study on the mechanism of wood/bamboo/adhesive activation and bonding enhancement induced by high voltage electric field

Présentée en vue de l'obtention du titre de Docteur de

l'Université de Lorraine/ Nanjing Forestry University Spécialité:

Sciences du Bois et des Fibres

Par

**MS. Qian HE**

**Soutenance le 28 Septembre 2021**

Membres du jury:

**Rapporteurs**:

Mr.Kong YUE, researcher, College of Civil Engineering, Nanjing Tech University, P.R.China;

Mr.Nabil GRIMI, professeur, Département Génie des Procédés Industriels, Université de Technologie de Compiègne, France.

**Members**:

**Président de jury:** Mrs.Fatima Charrier, Maître de Conférences HDR, l'Université de Pau et des Pays de l'Adour, France;

**Directeur de thèse:** Mr.Xiaoning LU, professor, college of materials science and engineering, Nanjing Forestry University, P.R.China;

**Directeur de thèse:** Mr.Nicolas BROSSE, professor, LERMAB, EA 4370, Université de Lorraine, France;

Mrs.Yan XIA, professor, college of materials science and engineering, Southwest Forestry University, P.R.China.

LERMAB

University of Lorraine

Boulevard des Aiguillettes BP 70239,54506

Vandœuvre-lès-Nancy, France.

## Acknowledgements

Looking back on my Ph.D. study experience, this is an unforgettable time for me to study, research and live at Lorraine University and Nanjing Forestry University. It has benefited me a lot. There is not only hard work, but also the joy of suffering. At this time, what I want to express most is my gratitude to the school, teachers, family, classmates and friends.

This article was completed under the careful guidance of the tutor Professor Nicolas Brosse and Xiaoning Lu. In terms of the topic selection of the thesis, the design of the test plan, the analysis of the test results, the structure and modification of the thesis and other details, a lot of effort has been devoted to the tutor. As this paper is about to be published, I would like to express my sincere thanks to my supervisor. The mentor's rigorous academic thinking, international scientific research vision, wise and optimistic life style, in terms of scientific research and humanistic care, have given students great enlightenment and encouragement, which has benefited me for life.

Thanks to Associate Professor Isabelle Ziegler-Devin, Associate Professor Laurent Chrusciel, and Associate Professor Arnaud Besserer of the Wood Materials Research Laboratory (LERMAB) of the University of Lorraine, for the opportunity of joint training, as well as the help and guidance in scientific research and material testing.

Thanks to Mei Changtong, Zhu Nanfeng, Xu Xinwu, Jin Juwan, Cui Juqing, Han Shuguang and Zou Ling from the college of Materials Science and Engineering of Nanjing Forestry University for their suggestions and guidance during the design and topic opening stage of this thesis. At the same time, I would like to thank Mr. Tianyi Zhan for his help and guidance in experiment design, analysis and paper modification,

and Mr. Zhang Haiyang for his help and guidance in material procurement, test testing and design during the experiment. Thanks to Mr. Wang Weidong, Mr. Jia Chong, Teachers Lan Ping and Ke Yu provided help and guidance during the experiment, thanks to the instrument detection and help provided by the Modern Analysis Center of Nanjing Forestry University in the experiment.

I would also like to thank my family for their support, companionship, tolerance and understanding for my study and life, and for giving me the courage and strength to overcome difficulties and obstacles, so that I have always been optimistic and active in living, studying and scientific research.

I would like to thank French National Research Agency through the Laboratory of Excellence ARBRE (ANR-12-LABXARBRE-01). Thanks for the financial support from the China Scholarship Council (CSC), Nanjing Forestry University, the School of Materials Science and Engineering for their international exchanges and participation in conference funding during the project, including the "Superior Disciplines of Universities in Jiangsu Province" and "First-class Disciplines" projects. Thanks for the financial support provided by the national key research and development project (2017YFC0703501). Thanks for the funding of the Doctoral Innovation Fund Project of Nanjing Forestry University.

Finally, I would like to thank the experts and teachers of the Doctoral Defense Committee for their careful guidance and help in their busy schedule!

# Table of contents

# Résumé

En tant que matériau polymère naturel, le bois et le bambou sont largement utilisés pour préparer de nouveaux matériaux composites. L'amélioration de la résistance mécanique du composite bois-bambou est un moyen important de promouvoir l'amélioration des produits et le développement industriel. Dans cette étude, les effets de l'interphase de collage du bois et du bambou induite par un champ électrique à haute tension (HVEF) ont été étudiés de façon systématique. Le mécanisme d'induction du champ électrique à haute tension sur l'interphase des matériaux composites a été appréhendé. Ces résultats ont une valeur théorique importante et une signification pratique pour améliorer la qualité et l'efficacité des matériaux composites bois-bambou.

Dans cette étude, des équipements de pointe tels que l'ESR (résonance de spin électronique), le dispositif d'angle de contact dynamique, le spectromètre photoélectronique à rayons X, le rhéomètre rotatif, le microscope à fluorescence et le dispositif de nano-indentation ont été mobilisés afin d'étudier les effets du HVEF sur les propriétés physicochimiques du bois et du bambou, les effets du HVEF sur la structure chimique et les propriétés rhéologiques des adhésifs sous une série de paramètres HVEF. L'effet d'agrégation de l'adhésif à l'interface de collage induit par le HVEF a également été révélé et le modèle de prédiction micro-mécanique est établi. L'organigramme de cette recherche est présenté dans la figure 0-1.

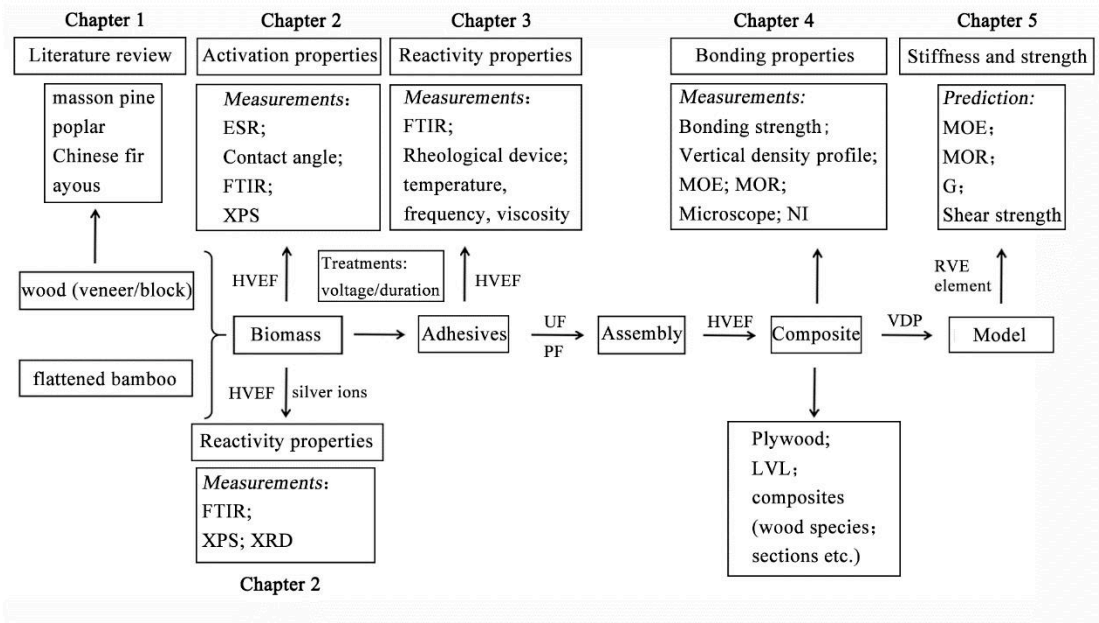


**Fig.0-1** Organigramme des travaux menés

## Chapitre 1

Les propriétés mécaniques des composites à base de bois, de bambou et d'autres biomasses sont étroitement liées à la performance de l'interphase de collage et à la force d'adhérence. Il est très important de promouvoir l'amélioration des produits et le développement industriel pour la préparation de composites de biomasse à haute force d'adhésion. Les matériaux de la biomasse ont une structure complexe et des composants divers. Par exemple, la pénétration des adhésifs sur la surface du bois est inégale en raison de la structure des pores à plusieurs échelles et de l'anisotropie du bois. Il est difficile pour l'adhésif de pénétrer et de s'étendre sur la surface du bambou en raison de la graisse, de la cire et d'autres substances présentes sur sa surface. En conséquence, l'interphase de collage des composites de biomasse est souvent incapable de former une couche adhésive continue et uniforme, ce qui entraîne une diminution de la force de collage. Il est donc important, pour améliorer la force de

liaison des composites de biomasse, d'augmenter l'activité de surface des matériaux de biomasse et d'améliorer la forme de pénétration des adhésifs dans l'interphase de liaison. Il est également important d'améliorer la théorie de l'adhérence des composites de biomasse et de fournir une base théorique pour leur développement industriel. Dans ce chapitre, la théorie de liaison des composites de biomasse et les propriétés structurelles et mécaniques de leur interphase ont été introduites, les méthodes de modification des matériaux composites de bois et de bambou ont été résumées, et les lacunes de ces recherches sur l'interphase de liaison des composites de biomasse à l'heure actuelle ont été analysées. En même temps, l'effet du champ électrique à haute tension sur les performances physico-chimiques des matériaux de biomasse, l'électrohydrodynamique, l'interphase de liaison et d'autres applications ont été présentés. Les avantages et les inconvénients de l'effet du champ électrique à haute tension sur les matériaux lignocellulosiques et leurs matériaux composites ont été résumés dans l'étude. Enfin, le contenu de la recherche de ce document, les objectifs de recherche, l'importance de la recherche et les points innovants ont été exposés.

**Chapitre 2 :**

Le schéma du dispositif de traitement HVEF est présenté à la figure 0-2. Après le traitement HVEF, l'activité de surface du bois et du bambou a augmenté de manière significative. De plus, avec l'augmentation de la tension/du temps, les radicaux libres de surface, le rapport O/C et le nombre de groupes d'oxygène ont augmenté de manière significative tandis que l'angle de contact a diminué. Les rapports de changement des radicaux libres en fonction du temps de traitement et de l'intensité

sont présentés dans les figures 0-3 et 0-4. Les relations entre les angles de contact/rapport de changement d'énergie de surface et le diamètre du lumen, la teneur en lignine et le contact de l'extrait avec quatre espèces ont été montrées dans la Figure 0-5. Sous la condition de 60kV, l'activité de surface a fortement augmenté. L'augmentation des radicaux libres était de 26%, la diminution de l'angle de contact initial était de 22%, la diminution de l'angle de contact d'équilibre était de 23%, l'augmentation de la composante d'énergie libre était de 43% ~ 75%, l'augmentation du rapport O/C était de 34%, l'augmentation des groupes contenant de l'oxygène était de 39% (C-OH), 149% (C-O ou C=O) et 97% (O-C=O), respectivement. Des caractéristiques de surface variées de différentes espèces et de différentes sections ont été obtenues sous traitement HVEF. Le rapport de changement était basé sur les paramètres des caractéristiques de surface : section transversale < section tangentielle < section radiale ; ayous < peuplier < pin masson < sapin chinois. Sous HVEF, les particules d'argent actives ont réagi avec les groupes fonctionnels du bois avec différentes formes d'oxydation de Ag (0), Ag (I) et Ag (III). La concentration la plus élevée de particules d'argent dans les échantillons de bois était de 10,71%. Les nanoparticules d'argent ont été obtenues avec une certaine morphologie cristalline et la taille moyenne des particules était inférieure à 50 nm. Pour le bambou, l'activité de surface de la peau de bambou traitée était significativement plus élevée que celle de la moelle de bambou. Sous la condition de 60kV, le radical libre, le rapport O/C et les groupes contenant de l'oxygène de la peau de bambou ont augmenté de 35%, 32%, 33% (C-OH), 136% (C-O ou C=O) et 71% (O-C=O) respectivement. Par conséquent, sous traitement HVEF, les propriétés physiques et chimiques du bois et du bambou

peuvent être significativement améliorées, ce qui est propice à l'amélioration des propriétés de l'interphase des matériaux composites.

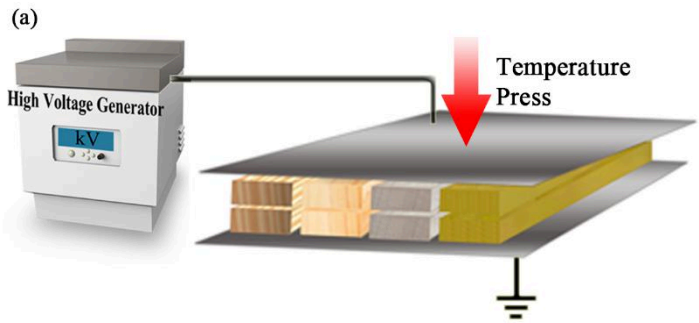


**Fig.0-2** Schéma du dispositive de traitement par champ électrique haute tension

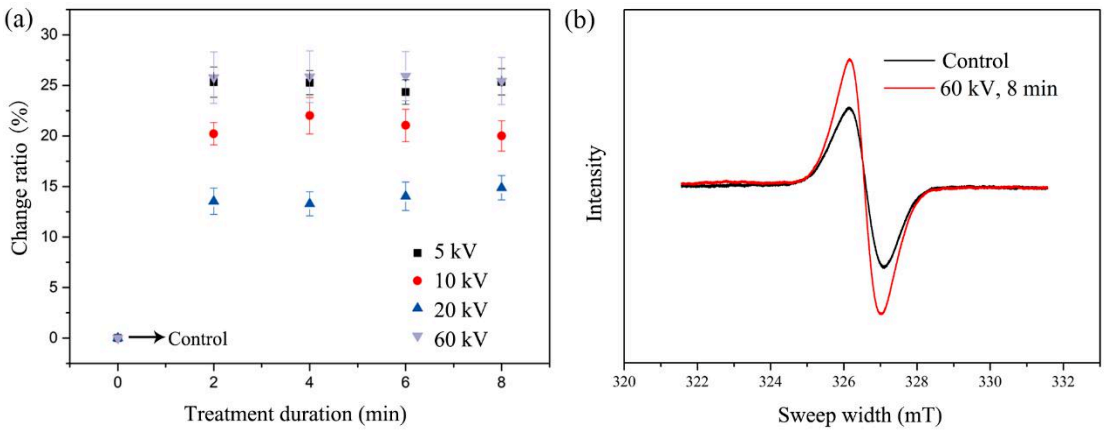


**Fig.0-3** (a) Rapport de changement des radicaux libres en fonction du temps de traitement et de l'intensité, respectivement. (b) Courbe obtenue par la mesure de la résonance de spin électronique (ESR). Le rapport de changement a été calculé comme suit $((value_{treated}-value_{control})/value_{control})\times 100\%$。

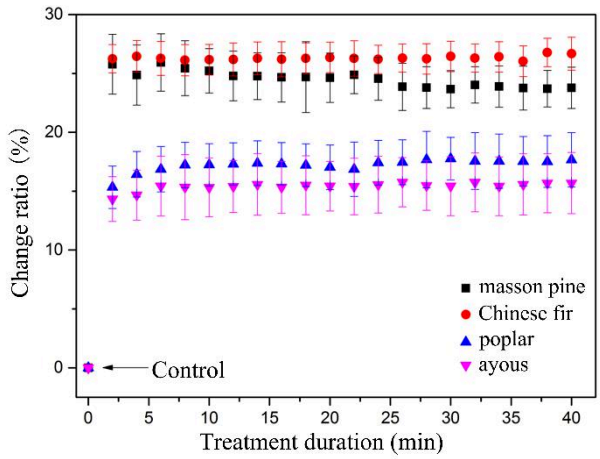


**Fig.0-4** Rapport de changement des radicaux libres pour différentes espèces de bois sous traitement HVEF. Le rapport de changement a été calculé comme suit $[(Value_{treated} - Value_{control})/Value_{control}] \times 100\%$.

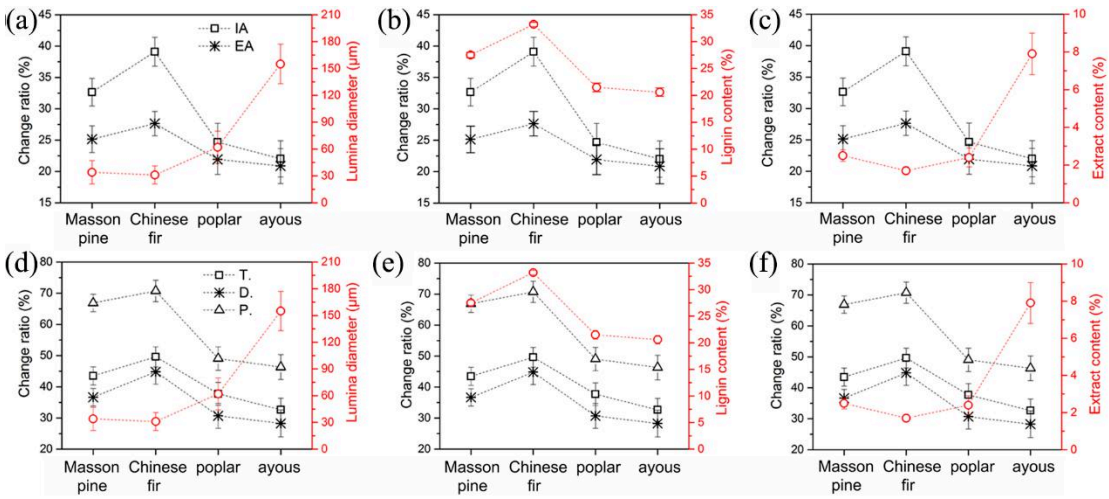


**Fig.0-5** Relation entre le rapport de changement des angles de contact et (a) le diamètre du lumen, (b) la teneur en lignine et (c) le contact avec l'extrait, respectivement, avec quatre espèces. La relation entre le rapport de changement de l'énergie de surface et (d) le diamètre du lumen, (e) la teneur en lignine et (f) le contact avec l'extrait, respectivement, avec quatre espèces.

**Chapitre 3** :

Avec l'augmentation de la tension/du temps, des réactions intermoléculaires significativement améliorées ont été obtenues avec les résines urée-formaldéhyde et

phénol-formaldéhyde. Les spectres FTIR des échantillons d'UF/PF traités par HVEF comparés aux contrôles sont présentés dans les figures 0-6 et 0-7. Après un traitement de 60kV/8 min, une augmentation significative des pics caractéristiques des groupes C-O a été obtenue. Sous traitement HVEF, la dépendance température/fréquence des comportements rhéologiques des deux résines a changé de manière significative. Dans le test du spectre de température, la viscosité, le module de stockage et le module de perte de la résine urée-formaldéhyde et de la résine phénol-formaldéhyde ont augmenté de manière significative après traitement. Il n'y avait pas de différence significative dans l'augmentation des paramètres des propriétés rhéologiques entre les deux résines dans diverses conditions de traitement, mais les caractéristiques de réaction des deux adhésifs étaient différentes avec le facteur eau. Dans le test du spectre de fréquence, avec l'augmentation de la constante de température, l'augmentation de la viscosité, du module de stockage et du module de perte de la résine urée-formaldéhyde et de la résine phénol-formaldéhyde a diminué. Par conséquent, le degré de polymérisation intermoléculaire du phénol-formaldéhyde et de la résine d'urée-formaldéhyde peut être amélioré de manière significative et la viscoélasticité de la résine peut être améliorée sous traitement HVEF.

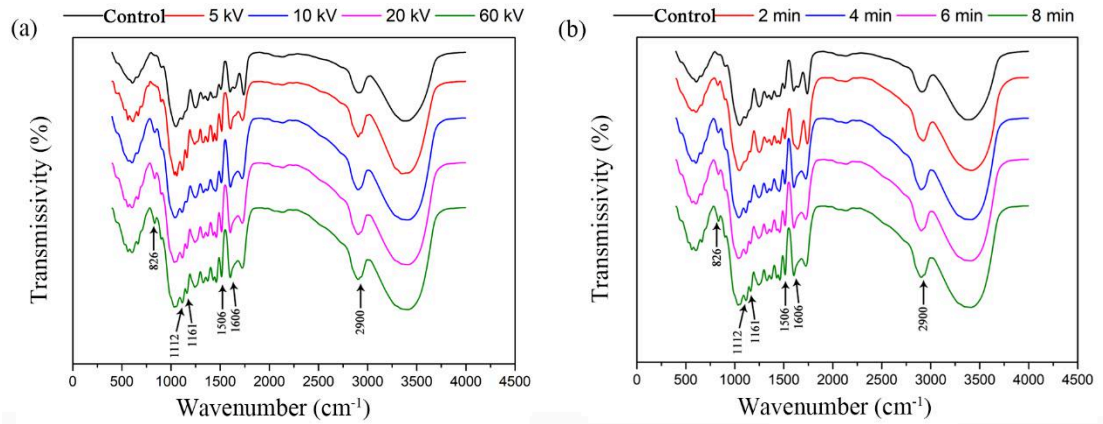


**Fig.0-6** Spectroscopie infrarouge à transformée de Fourier pour les échantillons d'UF traités par HVEF comparés aux témoins, (a) sous différentes tensions et (b) sous différentes durées de traitement.

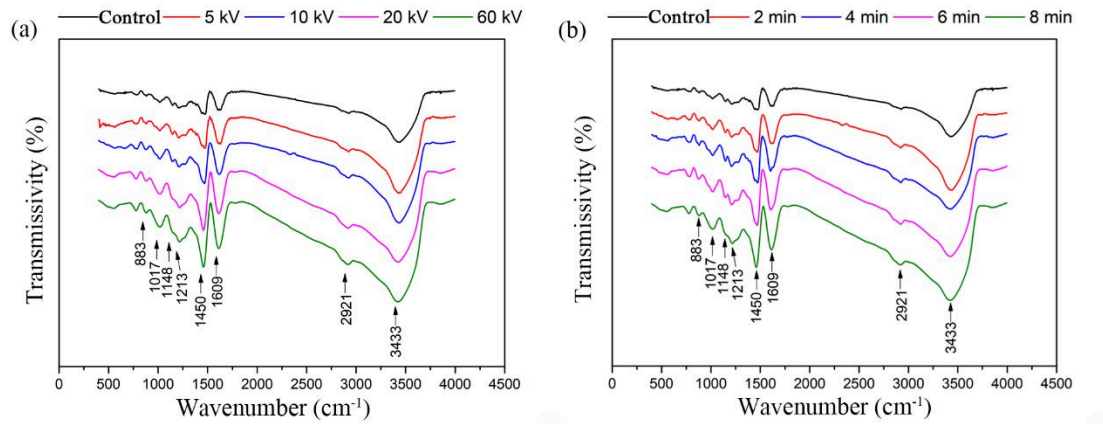


**Fig.0-7** Spectroscopie infrarouge à transformée de Fourier pour les échantillons de PF traités par HVEF comparés aux témoins, (a) sous différentes tensions et (b) sous différentes durées de traitement.

**Chapitre 4 :**

Le schéma de la préparation du contreplaqué de pin Masson-UF sous traitement HVEF est présenté dans la Figure 0-8. La figure 0-9 présente les micrographies des échantillons traités par HVEF obtenues par microscope à fluorescence à l'aide d'une lampe UV à différentes durées et intensités de traitement. La figure 0-10 montre la force d'adhérence et le taux de défaillance du bois des échantillons traités au FEHV. Après le traitement HVEF, la distribution de l'adhésif dans l'interphase de collage était continue et uniforme. La profondeur de pénétration a été considérablement

réduite. La densité et la force d'adhérence au niveau de l'interphase de collage ont augmenté de manière significative, et le taux de délamination a été réduit. Après le traitement, la densité maximale à l'interphase est de 1081 kg/m3, soit 32% de plus que le témoin. La force d'adhérence est passée de 0,66MPa à 1,25MPa, le taux de rupture du bois a augmenté de 85% et le taux de délamination a diminué de 5,97%. Les effets du traitement HVEF sur différentes sections (C, section transversale, T, section tangentielle et R, section radiale) et différentes espèces ont été obtenus. Selon le rapport de changement des caractéristiques de l'interface, la séquence était : C-C < T-T < T-T⊥ < R-T < R-R ; ayous < peuplier < pin masson < sapin chinois. Les résultats ont montré que l'amélioration des propriétés de l'interphase du bois tendre induite par le HVEF était supérieure à celle du bois dur. Selon l'analyse de corrélation, l'augmentation de la teneur en lignine a significativement augmenté avec l'augmentation des radicaux libres, la diminution de la profondeur de pénétration et l'augmentation de la force de liaison. Cependant, il existe une corrélation négative entre la teneur en extrait, le diamètre de la cavité cellulaire, la diminution de la profondeur de pénétration et l'augmentation de la force d'adhérence. Pour le bambou, la force d'adhérence a été significativement améliorée après le traitement HVEF. La force d'adhérence de la peau de bambou et de la peau de bambou était de 9,51MPa, et le taux d'échec du bambou était de 60%. Dans la combinaison de la moelle de bambou et de la moelle de bambou, le taux de rupture maximal du bambou était de 85%, ce qui a augmenté de 70%. Par conséquent, sous traitement HVEF, la distribution continue et uniforme des adhésifs interphases de liaison peut être obtenue, ce qui peut améliorer de manière significative la performance de liaison du composite bois-bambou, et est propice à l'utilisation efficace du composite bois-bambou.

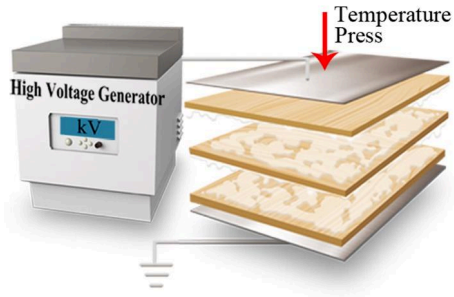


**Fig.0-8** Schéma de la préparation du contreplaqué de pin de Masson-UF sous traitement HVEF

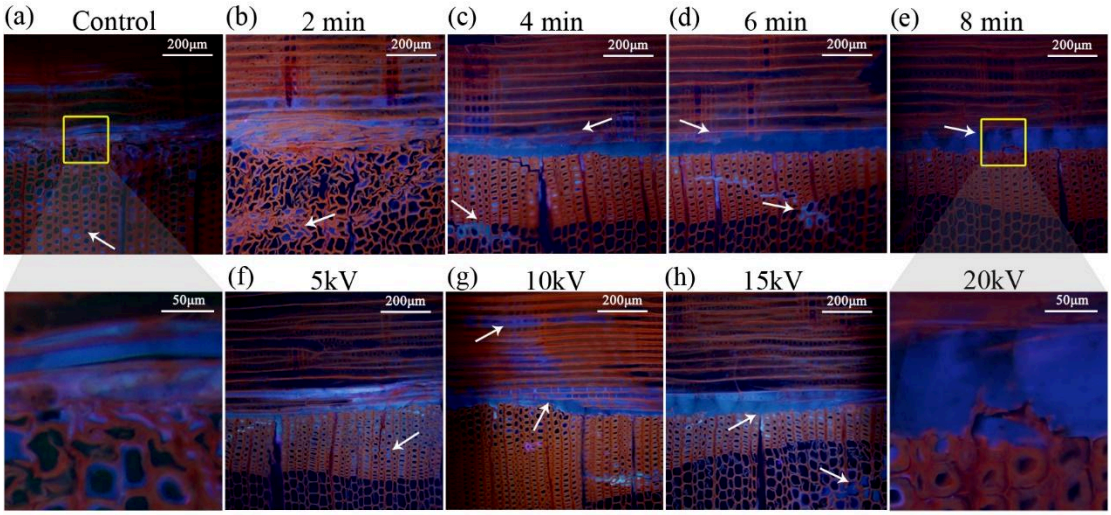


**Fig.0-9** Micrographies des échantillons traités par HVEF obtenues par microscope à fluorescence en utilisant la lumière UV sous différents temps et intensités de traitement respectivement, comparées au contrôle. (a) Micrographies des échantillons témoins. Micrographies des échantillons traités sous 60 kV pendant (b) 2 min, (c) 4 min, (d) 6 min, (e) 8 min. Micrographies des échantillons traités pendant 8 minutes sous (f) 5 kV, (g) 10 kV, (h) 20 kV, (e) 60 kV.

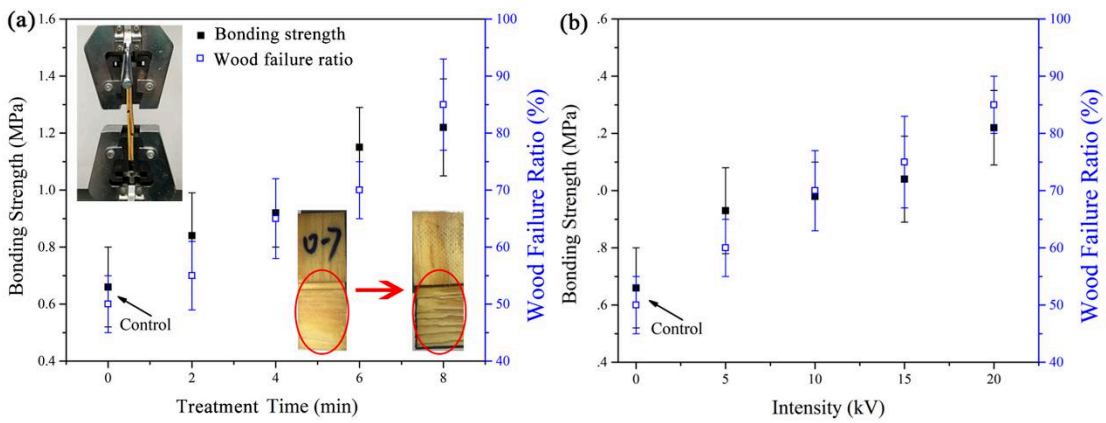

**Fig.0-10** Force d'adhérence et taux de défaillance du bois des échantillons traités par HVEF à des durées de traitement (a) et des intensités (b) variables.

**Chapitre 5** :

Le diagramme du dispositif de traitement HVEF, le diagramme du profil de densité verticale (VDP) obtenu à partir de l'interphase de collage du bois stratifié et le modèle RVE sont présentés dans la figure 0-11. L'ENI obtenu à partir de la mesure du nanoindenNI pour du bois stratifié de pin masson et de peuplier à 5 plis est présenté dans la figure 0-12. Selon le profil de densité verticale à l'interface de collage, le modèle de distribution de la rigidité et des contraintes du bois stratifié à l'interface de collage a été établi. Les résultats ont montré que l'erreur relative était inférieure à ±15%. Sur la base du modèle de distribution, les propriétés mécaniques macroscopiques du composite sont prédites en combinant la mécanique des composites et la théorie des plaques stratifiées, notamment le module d'élasticité, la résistance à la flexion, le module de cisaillement et la résistance au cisaillement. Les résultats montrent que l'erreur de prédiction des propriétés mécaniques est inférieure à 30%. Avec le modèle de distribution de la rigidité et de la résistance, l'effet du traitement HVEF peut être caractérisé quantitativement et les propriétés mécaniques des composites traités HVEF peuvent être prédites. En conséquence, le mécanisme de renforcement de l'interphase de liaison peut être révélé avec le modèle de distribution de la rigidité et de la résistance.

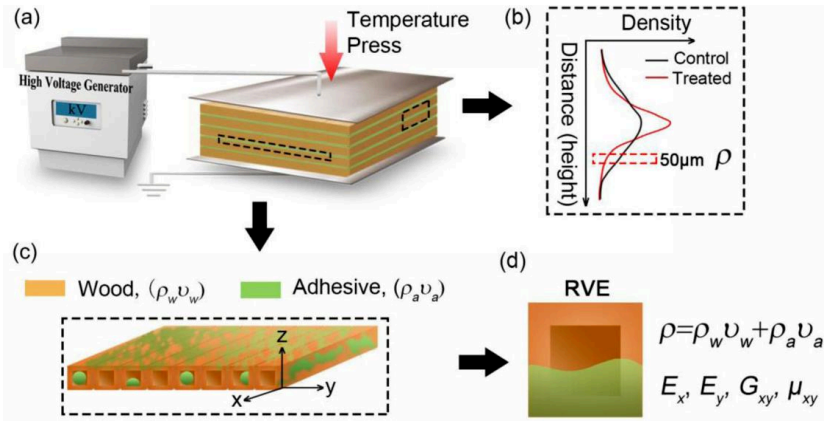


**Fig.0-11** Le diagramme pour (a) le dispositif de traitement HVEF. (b) Diagramme VDP obtenu à partir de l'interphase de collage du bois stratifié. (c) Répartition de l'adhésif entre les vaisseaux de bois. (d) Modèle RVE basé sur la fraction adhésive et la fraction de bois.

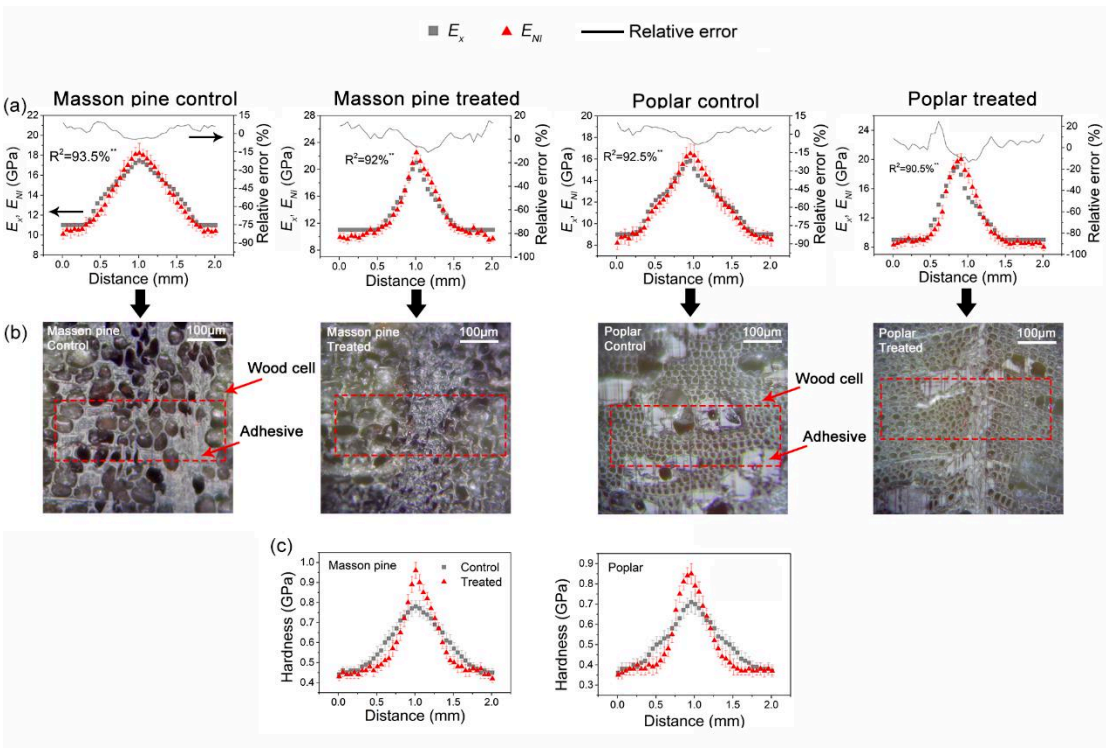


**Fig.0-12** (a) ENI obtenu à partir de la mesure NI pour du bois stratifié 5 plis en pin masson et en peuplier, comparé aux prédictions. Coefficient de corrélation (R2) et erreurs relatives obtenues entre Ex et ENI. (b) Micrographies de la surface d'indentation pour les échantillons de pin masson et de peuplier. (c) Dureté de la surface d'indentation pour les échantillons de pin masson et de peuplier. Erreurs relatives : [(Ex-ENI)/ENI]×100%.

# General introduction

In this study, the advanced equipments such as ESR (electron spin resonance), dynamic contact angle device, X-ray photoelectron spectrometer, rotational rheometer, fluorescence microscope and nano-indentation device were selected in order to investigate the effects of HVEF on the physicochemical properties of wood and bamboo, the effects of HVEF on the chemical structure and rheological properties of adhesives under a series of HVEF parameters. The aggregation effect of adhesive at bonding interface induced by HVEF has also been revealed and the micro-mechanical prediction model is established.

The main conclusions of this study are as follows:

1. After HVEF treatment, the surface activity of wood and bamboo increased significantly. Moreover, with the increase of voltage/time, the surface free radicals, O/C ratio and the number of oxygen groups increased significantly while the contact angle decreased. Under the condition of 60kV, the surface activity highly increased. The increment of free radicals was 26%, the decrease of initial contact angle was 22%, the decrease of equilibrium contact angle was 23%, the increment of free energy component was 43% ~ 75%, the increment of O/C ratio was 34%, the increment of oxygen-containing groups were 39% (C–OH), 149% (C–O or C=O) and 97% (O–C=O), respectively. Varied surface characteristics of different species and different sections were obtained under HVEF treatment. The change ratio was based on the surface characteristic parameters: cross section < tangential section < radial section; ayous < poplar < masson pine < Chinese fir. Under HVEF, the triggered silver particles reacted with wood functional groups with different oxidation forms of Ag (0), Ag (I) and Ag (III). The highest concentration of silver particles in wood samples was 10.71%. Nano-scale silver particles were obtained with a certain crystal morphology and the average particle size was less than 50 nm. For bamboo, the surface activity of treated bamboo skin was significantly higher than that of bamboo pith. Under the condition of 60kV, the free

radical, O/C ratio and oxygen-containing groups of bamboo skin increased by 35%, 32%, 33% (C–OH), 136% (C–O or C=O) and 71% (O–C=O) respectively. Therefore, under HVEF treatment, the physical and chemical properties of wood and bamboo can be significantly improved, which is conducive to improving the interphase properties of composite materials.

2. With the increase of voltage/time, significantly improved inter-molecular reactions of urea formaldehyde resin and phenol formaldehyde resin were obtained. After 60kV/8 min treatment, significant increment of the characteristic peaks of C–O groups were obtained. Under HVEF treatment, the temperature/frequency dependence of the rheological behaviors of the two resins changed significantly. In the temperature spectrum test, the viscosity, storage modulus and loss modulus of urea formaldehyde resin and phenol formaldehyde resin increased significantly after treatment. There was no significant difference in the increment of rheological property parameters between the two resins under various treatment conditions, but the reaction characteristics of the two adhesives were different with the water factor. In the frequency spectrum test, with the increase of temperature constant, the increment of viscosity, storage modulus and loss modulus of urea formaldehyde resin and phenol formaldehyde resin decreased. Therefore, the degree of inter-molecular polymerization of phenol formaldehyde and urea formaldehyde resin can be significantly improved and the viscoelasticity of the resin can be improved under HVEF treatment.

3. After HVEF treatment, the distribution of adhesive at the bonding interphase was continuous and uniform. The penetration depth was significantly reduced. The density and bonding strength at the bonding interphase were significantly increased, and the delamination rate was reduced. After treatment, the maximal density at interphase is 1081 kg/m$^3$, which was 32% higher than the control. The bonding strength increased from 0.66MPa to 1.25MPa and the wood breaking rate increased to 85%, and the delamination rate decreased to 5.97%. Varied effects of HVEF treatment on different sections (C, cross section, T, tangential section and R, radial section) and different species were achieved. According to the change

ratio of the interface characteristics, the sequence was: C-C < T-T < T-$T_{\perp}$ < R-T < R-R; ayous < poplar < masson pine < Chinese fir. The results showed that the improvement of the interphase properties of softwood induced by HVEF was higher than that of hardwood. According to the correlation analysis, the increase of lignin content significantly increased with the increment of free radicals, the decrease of penetration depth and the increment of bonding strength. However, there was a negative correlation between the content of extract, the diameter of cell cavity and the decrease of penetration depth and the increment of bonding strength. For bamboo material, the bonding strength was significantly improved after HVEF treatment. The bonding strength of bamboo skin and bamboo skin was 9.51MPa, and the bamboo failure ratio was 60%. In the combination of bamboo pith and bamboo pith, the maximum bamboo failure ratio was 85%, which was increased by 70%. Therefore, under HVEF treatment, the continuous and uniform distribution of bonding interphase adhesives can be obtained, which can significantly improve the bonding performance of wood bamboo composite, and is conducive to the efficient utilization of wood bamboo composite.

4. According to the vertical density profile at the bonding interface, the laminated stiffness and stress distribution model of the bonding interface has been established. The results showed that the relative error was less than ±15%. Based on the distribution model, the macroscopic mechanical properties of composite are predicted with the combination of composite mechanics and laminated plate theory, including elastic modulus, bending strength, shear modulus and shear strength. The results showed that the prediction error of mechanical properties is less than 30%. With the stiffness and strength distribution model, the effect of HVEF treatment can be quantitatively characterized and the mechanical properties of HVEF treated composites can be predicted. As a result, strengthening mechanism of bonding interphase can be revealed with the the stiffness and strength distribution model.

# Chapter I Literature review

## 1.1 Introduction

The mechanical properties of wood, bamboo and other biomass composites are closely related to the bonding interphase properties and bonding strength. It is of great significance to promote product upgrading and industrial development for the preparation of biomass composites with high adhesive strength. Biomass materials have complex structure and diverse components. For example, the penetration of adhesives on wood surface was ununiform because of multi-scale pore structure and anisotropy of wood; it is difficult for the adhesive to penetrate and extend on the surface of bamboo due to fat, wax and other substances existing on its surface. As a result, the bonding interphase of biomass composites is often unable to form a continuous and uniform adhesive layer, leading to the decrease of bonding strength. Therefore, it is of significance for enhancing the bonding strength of biomass composites to increase the surface activity of biomass materials and improve the penetration form of adhesives at the bonding interphase. It is also important to improve the bonding theory of biomass composites and then provide a theoretical basis for their industrial development. In this chapter, the bonding theory of biomass composites and the structural and mechanical properties of their interphase were introduced, the modification methods of wood and bamboo composite materials from domestic to abroad were summarized, and the shortcomings of these researches on the bonding interphase of biomass composites at present cwere analyzed. At the same time, the effect of high voltage electric field on the physicochemical performances of biomass materials, electrohydrodynamics, bonding interphase and other applications

were introduced; the advantages and disadvantages of the effect of high voltage electric field on the biomass materials and their composite materials were summarized in the study; finally, the research content of this paper, research objectives, research significance and innovative points were expounded.

## 1.2 Research on the bonding interphase of biomass composites

### 1.2.1 Overview of biomass composites

Biomass materials, such as wood and bamboo, are renewable, widely available and environmentally friendly polymer materials. The main chemical components of these materials include cellulose, hemicellulose and lignin. Through the reprocessing and recycling of wood or bamboo materials, new technologies and methods of rational preparation of biomass composite materials can be studied, so as to obtain a series of new biomass composite materials with high performance and high added value [1-3]. Composites are a kind of materials composed of two or more substrates with different physical and chemical properties, so that high performance or special functional composites can be obtained, which can further integrate the material performance advantages of each substrate, optimize the material configuration, and improve the application performance of composites [4-7]. The composite material generally contains two components, namely the matrix material and the reinforcing material. The reinforcing material generally determines the stiffness and strength performance of the composite material. The main function of the matrix material is to support and fix the fiber material and transfer the load. Therefore, the performance of composite materials depends not only on the stiffness and strength characteristics of each

substrate component, but also on the interphase characteristics between the two materials [8, 9].

### 1.2.2 Bonding theory for composite material

The interphase is one of the important factors in the property evaluation of composite materials. In the process of research and preparation of composite materials, the structure of the interphase and the physico-chemical reaction mechanism at the interphase should be analyzed in detail [10]. In composite materials, the interphase is a transitional region with complex structure. Its size generally calculated with nanometer to micron grade and its features mainly depends on the substrate material, the density of reinforced material, the surface free energy, surface features and the load and stress distribution in the material during manufacture process[11]. First of all, during the wetting process, the matrix material and the reinforcing material contact and wet each other to form an interphase under the molecular force; then, under certain temperature and pressure conditions, through a series of physical and chemical reactions, the interphase is formed with stable performance [12]. At present, based on the interaction between matrix phase and reinforcement phase. The formation mechanism has been widely studied. At the same time, the bonding theory related to composite materials has also been proposed. These theories mainly include adsorption theory, mechanical bonding theory, diffusion theory, electrostatic theory, chemical bond theory and so on since 1940s [13-15].

Adsorption theory was proposed by A. McLaren et al. It is based on the theory of intermolecular adsorption between surfaces. During the process of interphase

formation, adhesive molecules diffuse into the bonded material in the process of thermal movement, and generate adsorption force under certain conditions. Thus, the interphase layer was obtained. The main influencing factors include polarity, surface free energy and intermolecular force. However, the adsorption theory is not perfect and can not explain all the bonding phenomena.

Mechanical theory, material surface is not absolutely smooth, there is a certain roughness, including features such as cracks and sag. In the process of the interaction of reinforced material and matrix, adhesive can fill surface depressions. In the process of solidification, the mutual contact area of material improved through the meshing function, forming a solid interphase layer. The influencing factors mainly include surface roughness, friction and machining pressure of materials. Biomass materials such as wood, are porous materials. There are a lot of pores on the surface, which is conducive to the formation of glue force (glue nail) under the meshing action, so as to obtain a stable interphase layer. However, this theory cannot explain the bonding properties of non-porous materials.

Diffusion theory refers to the bonding strength at the interphase of materials formed by intermolecular entanglement and binding of polymer macromolecular chains under the interaction of diffusion. This theory is mainly applied to linear polymers or adhesives with low crosslinking degree.Adhesives and bonded materials contact each other, through swelling, mutual diffusion occurs at the interphase, forming the interphase layer. The diffusion is mainly affected by thermodynamic and kinetic conditions. However, this theory can not explain the bonding phenomenon between some inorganic substances.

According to the electrostatic theory, there is a double electric layer at the interphase of the bond, in which the electrostatic attraction forms the glue force in the interphase layer. From a quantum mechanical point of view, electrons can pass through the material and form a double electric layer at the interphase. It is mainly related to the energy loss of film stripping and the adhesion work in the double electric layer. This theory explains the phenomenon that the adsorption theory cannot explain, but it also cannot explain the bonding phenomenon of some conductive adhesives with a variety of high polymer.

According to the chemical bond theory, the formation of adhesive relay is mainly due to the effect of chemical bond force, and the intermolecular chemical reaction can be produced between the adhesive and the bonded material, so as to obtain a higher adhesive relay through the combination of the main chemical bonds such as ionic bond and covalent bond. Therefore, according to the chemical reaction mechanism of the chemical bonds, types of reaction can be divided into three categories, including adhesive and the cementing material in the chemical reactive group formed by chemical bond, coupling agent with the adhesives by chemical bond formed between the cementing materials and surface treatment methods for the chemical activity of group formation of chemical bonds between molecular and adhesives. The influencing factors of this theory mainly include the surface properties of the bonded material, the molecular structure characteristics of the adhesive and the preparation method of the adhesive. However, this theory still has some limitations.

To sum up, the formation process of composite material interphase is a very complex physical and chemical reaction process. Interphase depends not only on the surface of the material properties, such as wettability, and the size of the free energy of biomass materials, structure, chemical composition, fiber texture direction levels and types, and adhesive functional group structure, solid content, factors such as liquidity and viscoelasticity. At the same time, it also depends on the preparation method and technological parameters of the composite material. Therefore, the study of the interphase of composite materials involves a variety of related factors, and it is necessary to combine various theories to further explore the formation mechanism of the interphase at the same time to obtain better interphase properties of composite materials.

### 1.2.3 Interfacial structural characteristics of biomass composites

The interphase characteristics of biomass composites are mainly determined by the surface properties of materials, the properties of adhesives and the degree of crosslinking reaction between chemical functional groups on the surface of materials and adhesives. A large number of chemical groups (–OH, –CHO, etc.) on the surface of wood and bamboo play an important role in the crosslinking reaction with adhesives. In addition, wood and bamboo materials are considered to be typical porous materials. These pore structures are mainly composed of the cell lumina or tracheid structure in the wood material, the pore structure on the cell wall and the gap between the cellulose macromolecule chains. The microstructures of cells were different among three sections of wood. There were significant differences in the content of chemical components among different tree species. There are a lot of

vascular bundle cell structures in bamboo material, and the vascular bundle distribution of bamboo green is more dense, but the vascular bundle distribution of bamboo yellow is sparse. Meanwhile, the chemical composition of bamboo green and bamboo yellow is different. These factors, such as chemical groups, microstructure and composition content of biomass, will affect the adhesive permeability at the interphase of the composite material, thus further affecting the crosslinking reaction and mechanical properties of the interphase [16]. Previous studies have shown that adhesives enter structures such as cell walls through osmosis and interact with wood cell wall polymers at the molecular level. Therefore, the polymer and adhesive groups in the cell wall have important applications for osmosis and can change the physical and mechanical properties (thermal, swelling and mechanical properties) of the composite interphase [17,18]. In order to further characterize the structural characteristics of the penetration and distribution of adhesives at the bonding interphase, a series of testing methods were used to study the structural characteristics at the bonding interphase from a macro to a micro perspective, including: optical microscopy, environmental scanning electron microscopy, fluorescence microscopy, X-ray tomography microscopy, thermal scanning microscopy, confocal laser scanning microscopy and atomic force infrared microscopy, etc. Jakes et al. [19] using X-ray computed tomography (X-ct) scanning technology and X ray fluorescence microscope to study the phenolic resin of different molecular weight and the flow of adhesives at loblolly pine composites interphase and its penetration form. It is concluded that the relationship between the cell wall structure and the weight gain rate of adhesives among cell wall layers. After curing, the distribution form of different adhesives interphase was investigated as

well. These results are important for the further understanding and prediction of wood-adhesive interaction and permeability models. Peng et al. [20] systematically studied the microstructure characteristics of adhesives at the interphase of wood/bamboo composites by X-ray phase contrast microscopy (XCPM), and analyzed the effects of different processing parameters on the adhesives' penetration behavior at the interphase of wood/bamboo composites. The results showed that XPCM is one of the important methods to accurately detect the interphase structural characteristics of wood and adhesive composites. Modzel et al. [21] used fluorescence microscopy, scanning electron microscopy and X-ray microtomography to analyze the interphase structure between wood and adhesives, and quantitatively evaluated the permeability of adhesives to porous material networks. Based on the same interphase structure, different detection methods are used for comparative analysis. It is concluded that any of these techniques can better characterize the interphase structure characteristics, but they also have their own defects. Therefore, multiple methods can be used in combination according to the characteristics of samples for research. At the same time, many new techniques are applied to study the structural characteristics of the bonding interphase. Xu et al. [22] studied the permeability of phenolic resins modified by two different nanomaterials by scanning thermal microscopy (STHM). By studying and comparing the differences of thermal conductivity changes, the interaction between resin and cell wall and the form of penetration were revealed. For the permeability of adhesives in cell cavity, it was concluded that STHM is also an effective tool to accurately detect the permeability of adhesives at the micro level.

According to the review, the permeability of adhesives is affected by many factors, including the surface properties of the material to be bonded, the properties of adhesives themselves and environmental factors. These existing studies indicate that the studies on the permeability of adhesives and the structure characteristics of the bonding interphase are of great significance for the evaluation of the bonding strength and mechanical properties of biomass composites under different loads [23,24].

### 1.2.4 Interfacial mechanical properties of biomass composites

Composite materials are mainly composed of matrix materials and fiber reinforced materials, which are nonuniform and anisotropic. Therefore, the properties of composites are determined by the properties of their components. At the same time, the interphase properties between the components (matrix and reinforcement material) also have an important effect on the properties of composites. Interfacial bonding properties and mechanical properties are also important factors that determine the overall stiffness and strength of composites [8]. The permeability of adhesives is an important factor affecting the mechanical properties at the interphase of composites. Adhesive penetration, that is, the non-directional and non-uniform movement of adhesives in biomass microstructure, will cause uneven stress distribution in the bonding interphase during the bonding process. Therefore, under different preparation methods and modification methods, various permeability distribution forms of adhesives can be obtained, and these permeability and distribution forms of adhesives at the interphase under different conditions have a great influence on the bonding strength and mechanical properties of composites [25,26]. Previous studies have also summarized different test methods to characterize the interphase mechanical properties of different composites from the macro to micro perspectives.

Yuan et al. [27] used micro-CT to study the diffusion of polyvinyl acetate (PVAC) in different types of wood cell walls. In addition, compressive shear tests were carried out, and the effects of adhesive penetration on mechanical properties of composite materials with different tree species were obtained. Ivana et al. [28] studied the influence of pressure on the penetration forms of diameter section and chord section and the shear strength at the interphase of UF in poplar under different hot pressing pressures, and obtained the variation rule of the bonding strength between different types of wood section combinations and the penetration depth at the bonding interphase.

At the same time, in-situ nano-indentation (NI) test method was used to study the mechanical properties of the interphase between cell wall and adhesive. Konnerth et al. [29] measured the mechanical properties of cell walls at the interphase of wood composites and natural fiber reinforced composites by nanoindentation method, and compared the results with tensile tests. The results showed that the nanoindentation test method can effectively test the mechanical properties of material bonding interphase. There is a good correlation between the elastic modulus measured by tensile test and the elastic modulus measured by nano indentation method. The elastic modulus measured by nano indentation method is obviously higher than that by tensile method. Konnerth and Gindl et al. [30,31] used melamine, modified melamine and spruce to prepare composite materials. The nano indentation technology was also used to measure the change of mechanical properties in the middle layer of cell wall under the penetration of adhesive. Jakes et al. [32] quantitatively studied the permeation behavior, elastic modulus and hardness of phenolic resin (PF) in the cell wall of loblolly pines late wood using quasi-static nanoindentation technique and X-

ray fluorescence microscopy. Obersriebnig et al. [33] obtained the bonding properties and mechanical properties of the interphase of spruce cell wall and urea-formaldehyde resin adhesive.

Through these macroscopic and microscopic interphase mechanics test methods, we can better understand the interaction between different adhesives and biomass materials and the interphase mechanical properties from different scales. Moreover, we can further establish the penetration and mechanical model between adhesives and wood according to the existing interphase mechanical properties in order to improve the induction, prediction and research of interphase properties of different composite materials. Mendoza et al. [34] proposed an analysis model of wood tube hole network structure to predict and simulate the penetration depth of adhesives. In addition, different adhesives were selected to test the penetration form and penetration depth of adhesives in wood, which indicated that the measured value was highly consistent with the theoretical value. Koseki et al. [35] used the nonlinear least square method to predict and verify the shear strength distribution, elastic modulus and static flexural strength of laminated plates, and discussed the failure modes of composite materials under load, indicating the importance of the shear strength and stress distribution at the adhesive layer. Edward et al. [36] proposed a model for the stiffness of the adhesive layer of double-lap shear specimens, taking into account the interaction between the adhesive and wood, which effectively predicted and verified the overall stiffness of the sample and the stiffness performance of the adhesive layer. Corigliano et al. [37] tested the elastic modulus of wood laminates by using three-point bending and ultrasonic method, and compared it with the theoretical value obtained by classical laminates theory. It was also concluded that classical laminates theory

can quickly and accurately predict the distribution characteristics of stiffness and strength of laminates. In conclusion, the interfacial properties of composites can significantly affect the overall mechanical properties of the composites. By using mechanical analysis methods of different scales, including adhesive strength and mechanical properties at the macro level, nano-indentation test at the micro level, and the interphase microstructure test method combined with them, the penetration form of the interphase adhesive, the stress distribution at the macro and micro level and the mechanical properties of the adhesive layer can be characterized effectively. At the same time, by using the classical laminated plate theory, composite mechanics and numerical calculation methods, the mechanical model of composite materials is established, which can accurately predict the distribution of stiffness and strength at the bonding interphase of composite materials, so that various composite materials can be used effectively and reasonably, and the utilization rate of composite materials can be improved.

### 1.2.5 Research on modification of wood based composite bonding interphase

Wood is a common natural polymer material, which has a multi-scale pore structure, mainly composed of cellulose, hemicellulose and lignin, and has complex anatomical properties. The penetration path of adhesives in it varies from macroscopic cracks, tube pores, cell wall pores, and then to cell wall gaps [38]. Wooden composite material is generally made of wood material, or wood material and one or more non-wood materials, the use of adhesives, or glue-free bonding, through pressure heating and other conventional preparation methods of composite multiphase natural polymer composite material. Its main categories include: (1) veneer and veneer laminated materials, which are mainly veneer laminated materials

(LVL, made by splicing and gluing of veneer) and parallel strand laminated materials (PSL, made of narrow veneer as raw material and gluing of veneer laminated materials); (2) wood and non-wood particleboard, which mainly include cement, gypsum, slag particleboard and other non-wood particleboard; (3) wood and non-wood fiber composite materials, such as cement fiberboard; (4) wood-plastic composite materials; (5) Wood ceramics; (6) wood-metal composite materials, including metallized wood and metal-clad boards, etc.; (7) structural wood composite materials. Zhang et al. [39,40] added glass fiber to wood composite materials, and the results showed that the mechanical strength of wood particleboard was significantly improved. He et al. [41] pointed out that carbon fiber material can improve the stiffness and strength of wood composite material, and the bending modulus of the composite material obtained is 12 times higher than that of wood. Wang et al. [42] proposed a laminated wood of poplar veneer reinforced with metal mesh, which has better physical and mechanical properties compared with general boards. In addition, J.DColeman [43] prepared a kind of high strength wood composite material, that is, natural wood was dissociated to a certain extent and then recombined with each other, thus forming a composite material with obvious advantages in strength compared with ordinary wood.

Wood composite materials have been widely used in interior decoration, wood structure and transportation materials. At the same time, researchers have devoted themselves to the research of various new wood materials and achieved a lot of research results. Wood units and adhesives are the main components of the interphase of wood composite materials. At present, the modification methods of wood composite materials mainly include the surface modification of wood units and the

modification of adhesives. The modification methods for wood material units mainly include physical modification methods (plasma treatment, corona treatment and heat treatment, etc.) and chemical modification methods (acid-base treatment and coupling agent treatment), etc. In addition, the influence results of different modification methods on the change rate of wood material surface properties and adhesive properties are listed in Table 1-1.

Physical modification methods: use plasma to modify the surface of wood, which can etch the surface of the material and generate free radicals at the same time as the chemical bond, thereby improving the surface activity of the material. Tang et al. [44] studied the effect of cold plasma treatment on the surface properties of poplar wood, and showed that the surface morphology and wettability of the material will change significantly, improving the surface wettability of the material, indicating that the cold plasma modification can effectively improve the bonding performance of poplar wood interphase and further improve the cold plasma treatment process. At the same time, the timeliness of cold plasma modification was discussed. Novak [45] et al. studied the surface properties of beech wood veneer materials and the bonding properties of composite materials using low-temperature plasma in an air atmosphere. The results showed that after plasma treatment, the surface free energy of the material was significantly increased, which was mainly due to the increased oxygen-containing groups on the surface, thereby improving the wettability and hydrophilicity of the surface of the material, and promoting the cross-linking reaction between the surface of the material and the adhesive, and the bonding strength of the beech plywood is significantly improved. Menandro [46] et al. used a dielectric barrier discharge oxygen plasma treatment method to increase the surface free energy of

different tree species, and used phenolic resin and urea-formaldehyde resin to prepare composite materials, which showed that the bonding strength of eucalyptus composite materials was significantly improved. For the species with higher extract content, the bonding strength of the composite material did not increase significantly. Hünnekens et al. [47] studied the effects of three different plasma discharge methods on the surface properties of wood, which effectively improved the surface properties of wood and significantly improved the bonding properties of composite materials. Altgen et al. [48] studied the effect of atmospheric plasma on the surface properties of wood. After treatment, the activity and wettability of the wood surface were significantly improved. Uehara et al. [49, 50] studied the influence of corona treatment methods on the surface chemical properties of wood fibers, and used corona to generate a large number of free electrons on the surface of wood fibers and obtain more chemical reaction groups, thereby improving surface chemical activity and bonding strength of composite materials. Isao [51] studied the degree of oxidative activation of different wood surfaces by corona treatment. The results showed that the content of aldehyde groups on the surface of the material after treatment increased significantly, and as the treatment strength increased, the surface wettability increased significantly, and the bonding strength of the urea-formaldehyde resin plywood increased by 20 to 46%. Ruponen et al. [52] studied the surface properties and bonding properties of birch under corona conditions (125 W, 28 kV). The results showed that the surface contact angle of birch veneer was significantly reduced, and the wettability was significantly improved. The bonding strength of PF composite is increased by 10 ~ 45%. Haller et al. [53] used the influence of different laser types, treatment time and intensity on the surface characteristics of

wood. It was concluded that after laser sintering, a molten layer is formed on the wood surface, which reduces the active chemical groups on the wood surface and increases the contact angle. In addition, it inhibits the survival rate of microorganisms and plays a role in cleaning the surface. Miklečić et al. [54] studied the effect of heat treatment on the surface properties of beech wood, and showed that the contact angle of the treated wood was significantly increased, the surface free energy was significantly reduced, and the rate of change gradually increased with the increase of the treatment temperature. In addition, PETRIČ [55] et al. used vacuum heat treatment to treat spruce material, and concluded that vacuum heat treatment can increase the surface free energy of the material. At the same time, Sernek et al. [56] studied the heat treatment of different softwood and hardwood materials at 165 ~ 180°C, and prepared laminate composite materials using urea-formaldehyde resin, phenolic resin and polyurethane resin. The result showed that shear strength of urea-formaldehyde resin and phenol-formaldehyde resin composite was significantly reduced after heat treatment; for polyurethane composites, its shear strength is higher than that of untreated composites.

Chemical modification methods: Bekhta et al. [57] used different types of chemical reagents (hydrogen peroxide, aluminum persulfate, acetic acid and sodium carbonate) at different concentrations (1%, 2% and 3%) and usage amounts (10, 20 and 30g/m$^2$), the effects of chemical reagents on the surface characteristics of birch veneer and the mechanical properties of its plywood were studied. After surface treatment, the surface activity and wettability of the veneer were significantly improved, thereby enhancing the plywood bonding strength. Olakanmi et al. [58] pretreated lignocellulosic materials with alkali, which reduced the content of surface

extracts and increased the chemical activity of the fiber surface, so that the bonding strength and physical and mechanical properties of wood-plastic composites were effectively improved. Coupling agent treatment methods can also effectively improve the interphase characteristics of wood composite materials. Silane coupling agents can significantly improve the surface wettability of the material. At the same time, it can improve the permeability of the adhesive in the wood [59, 60]. Lu et al. [61] proposed that coupling agents can improve the compatibility and adhesion between polar wood fibers and non-polar polymer matrix. It comprehensively evaluated the performance of coupling agents such as cyanate esters, acid anhydrides, silanes, and acid anhydride modifications applied to wood fibers and polymers. At the same time, it was concluded that the usage of coating or grafting for the pretreatment of wood fiber and polymer could effectively improve the mechanical properties of wood composite materials. Yin [62] et al. comparatively studied the effects of silane, silane/tannin and other different modification methods on the bonding properties and mechanical properties of glass fiber/larch composites, indicating that the addition of coupling agents had a positive effect on the bonding properties and mechanical properties of wood composites.

Modification methods for adhesives mainly include: toughening modification methods, enhanced modification methods and preparation of new adhesives.

Toughening treatment methods: adhesive (such as phenolic resin and urea-formaldehyde resin), after curing, tends to form stress cracks on the interphase during the stress process, showing low toughness. Therefore, the toughening treatment is conducive to improving the ability of the resin to transfer loads and disperse stress [63].

At present, there are mainly two toughening methods: external toughening and internal toughening. External toughening refers to the addition of external toughening agents after phenolic resin synthesis, such as natural rubber, carboxylic acid-based polybutadiene, silicone, and thermoplastic resins [63, 64]. Internal toughening refers to the addition of internal toughening agents such as acrylic acid, tung oil, unsaturated fatty acids and other flexible groups during the synthesis of phenolic resins [65, 66]. Through toughening modification, the thermal stability of the adhesive can be improved. At the same time, it can also enhance the ability to transmit loads and disperse stress [63].

Reinforcement treatment methods: Cui Juqing et al. [67] studied the usage of nano-filler modified adhesives to prepare wood-plastic composites and nano-cellulose modified adhesives to prepare wood composites, thereby improving the interphase characteristics of the adhesive layer and improving the bonding and mechanical properties. Similarly, the usage of nano-silica and nano-cellulose and other nano-materials could also improve the mechanical properties of phenolic resin [68, 69]. In addition, nano-montmorillonite, ceramic fiber materials and nano-carbon materials were added to the adhesive resin to improve the thermal stability of the resin [70, 71].

New environmentally friendly wood adhesives: in order to reduce the consumption of petroleum resources, researchers have also proposed a variety of polyphenols and formaldehyde or glyoxal to replace phenolic resins, such as tannin adhesives, lignin adhesives and environmentally friendly, high-efficiency biomass-based adhesive. Pizzi et al. [72] studied different types of environmentally friendly adhesives such as

tannin adhesives, tannin-hexamethylenetetramine adhesives, etc., and showed that tannins have strong self-condensation ability, which can significantly improve, bonding strength and mechanical properties of plywood and particleboard. Mansouri et al. [73] studied the thermomechanical properties of natural lignin and tannin extract adhesives by using nuclear magnetic resonance and other methods to analyze the difference between the structure of lignin before and after purification. Dabbabi et al. [74] used different lignin separation conditions to prepare lignin tannin adhesives. As the ratio of tannins increased, the thermomechanical properties of the adhesive increased and a higher elastic modulus was obtained. At the same time, He et al. [75] studied steam-exposed lignin, which has lower molecular weight and higher phenolic hydroxyl content. After mixing glyoxalized lignin with tannins, high thermomechanical properties and elastic modulus lignin-based adhesive was obtained.

Tab.1-1 The effects of physicochemical modification methods on the change ratios of wood surface and bonding properties

| Methods | Parameters | Free radical (%) | Surface energy (%) | Contact angle (%) | O/C (%) | Bonding strength (%)/ Actual value |
|---|---|---|---|---|---|---|
| Low-temperature constant-pressure plasma [45] | Voltage: 2kV, Power: 300W, Duration: 0~3 min | / | 8 ~ 23 | 15 ~ 45 (water) | 83 | 8 ~ 60 (5.6 ~ 8.3Mpa) (beech composites, PU) |
| Low-temperature constant-pressure plasma [44] | Power: 200W, Duration: 7 min | 70 | 60 ~ 67 | 66 (UF) | 73 | 25 (0.95 Mpa) (poplar composites, UF) |

| | | | | | | |
|---|---|---|---|---|---|---|
| Oxygen plasma [44] | Power: 200W; Duration: 7 min | 50 ~ 75 | 70 ~ 75 | 65 ~ 72 (UF) | 104 ~ 304 | 31 ~ 38 (1.03 ~ 1.12 MPa) (poplar composites, UF) |
| Oxygen plasma [46] | Voltage: 28kV; Power: 58~465 W·min/$m^2$ | / | 86 ~ 114 | / | / | 60 (6.1 MPa) (eucalyptus composites，PF) （no significance in other species， G. *arborea*； *A. mangium*） |
| Corona [51] | Voltage: 16kV; Power: 0~2000 W·min/$m^2$ | / | / | 40 ~ 65 （UF） | / | 20 ~ 46 (7.2 ~ 7.9 Mpa) (cherry composites, UF) |
| Heat treatment [54] | Temperature: 190°C; 212°C | / | 7~11 （decrease） | 31 ~ 45 (increase, water) | / | Decrease or not significant Sernek[56] |
| Laser sintering [53] | Power: 25×$10^6$W | / | / | 94 (increase, water) | / | / |
| Chemical treatment [57] | $CH_3COOH$ | / | / | 12 ~ 33 (water) | / | 25 ~ 30 (1.9 ~ 2.1 MPa) (Birch composites, PF) |
| | $NaCO_3$ | / | / | 10 ~ 34 (water) | / | 16 ~ 31 (1.8 ~ 2.0 MPa) (Birch composites, PF) |

### 1.2.6 Research on modification of bamboo composite material interphase

Bamboo has the characteristics of high specific strength, renewable and abundant resources, and is one of the ideal processing materials to replace steel and wood. Because of its unique growth characteristics and high economic added value, it has been widely used in various industrial fields such as textiles, energy and chemical industries. The efficient use of bamboo and its bamboo composite materials is conducive to the promotion of sustainability and the development of circular economy[76, 77]. The main categories of bamboo composite materials include: bamboo plywood, bamboo strip laminated lumber, bamboo particle board, bamboo fiberboard, reconstituted bamboo and bamboo-based composite materials. In addition, bamboo is combined with wood, glass fiber, ceramics, carbon fiber, and non-woven fabrics to form functional bamboo-based composite materials [78, 79].

Although the chemical composition of bamboo and wood are similar, the microstructure of bamboo is quite different from that of wood. Due to this difference in microstructure, the surface characteristics of bamboo, including wettability, permeability, surface chemical composition, and wood are significantly different [80]. The surface of bamboo contains natural aliphatic and low reactive waxy layer, which is not conducive to the cross-linking reaction with general biomass material adhesives [81]. At the same time, there are a large number of vascular bundle cell structures in bamboo, the distribution of bamboo green vascular bundles is denser and the distribution of bamboo yellow vascular bundles is sparse. The chemical composition of bamboo green and bamboo yellow is also different. These biomass chemical groups, microstructure, and component content will affect the adhesive

penetration of the composite interphase, which will further affect the crosslinking reaction and mechanical properties of the interphase [82]. Researchers have conducted a lot of research on the performance modification of bamboo composite materials, the focus is mainly on the bonding of bamboo composite materials and the rational use of bamboo processing residues to reduce resource waste [83-85]. At this stage, the research on the modification of the bonding interphase of bamboo composite materials mainly includes the physical and chemical modification of the surface of the bamboo unit, new processes, new methods, and new equipment applications. In addition, different modifications are listed in Table 1-2. The result of the method on the change rate of bamboo material surface characteristics and bonding characteristics was obtained.

Physical modification methods: Rao et al. [86] used oxygen plasma treatment method with different treatment time, power and pressure and other parameters and studied the surface characteristics of bamboo green, bamboo yellow, and bamboo green and bamboo yellow after carbonization. The results showed that after plasma treatment, the wettability of the bamboo surface significantly improved and the change rate of the surface contact angle was significantly related to the treatment time and other parameters. At the same time, the elastic modulus and modulus of rupture of the composite material prepared by the phenolic resin significantly improved. Li et al. [87] studied the influence of atmospheric plasma treatment on the contact angle and free energy of bamboo green and bamboo yellow surfaces, and used scanning electron microscopy and X-ray photoelectron spectroscopy to study the changes in the surface microstructure and functional groups of bamboo. The results showed that the contact angle of the bamboo surface significantly reduced and the free energy significantly increased after treatment of 1kW. With the increase of

the treatment time, the rate of change increased. At the same time, the hydrophilic groups on the surface of the bamboo significantly increased. Thus, the cross-linking reaction and intermolecular interaction between the bamboo surface and the resin or coating were enhanced. Guan et al. [88] used modified phenolic resin to prepare carbonized and non-carbonized bamboo composites with different cross-section combinations. The results showed that the penetration depth of the bonding interphase of the carbonized bamboo composites increased, while the bonding strength decreased. In addition, the bonding strength of the composite material of the combination of bamboo and green noodles is greater than that of the combination of bamboo and yellow noodles. Meng et al. [89] studied the effect of heat treatment on the chemical composition and functional groups of bamboo. The results showed that after heat treatment at 180 ~ 200°C, the content of hemicellulose in bamboo reduced and the relative content of lignin increased, which was beneficial to improve the dimensional stability of the material. This result provided the reference data for the effective use of bamboo in the future. Li et al. [90] used vegetable oil to heat the bamboo and studied the changes in the contact angle of the bamboo surface and the bonding strength of the bamboo composite material. The results showed that after the treatment, the contact angle of the bamboo surface was significantly increased, and the bonding strength of the composite material reduced or not changed significantly. The failure ratio of the bamboo composite material increased significantly after treatment.

Chemical modification methods: Chen et al. [91] studied the effects of sodium hydroxide and sodium carbonate reagents on the surface characteristics of bamboo green and bamboo yellow, indicating that these modification methods could not

significantly improve the chemically active groups and surface properties of the bamboo. The bonding strength of the composite material composed of bamboo green and bamboo yellow did not significantly improve compared with untreated ones. Atanda et al. [92] studied that the content of surface extracts reduced and chemical activity improved, and the bonding strength and mechanical properties of their polyethylene composite materials were effectively improved after bamboo fiber treated with NaOH solution. Zhao et al.[88] formulated modifiers based on the chemical components of bamboo green and bamboo yellow. Through orthogonal experiments, the optimal process parameters were obtained, and the bonding strength of bamboo could be effectively improved. XBLi et al. [93] studied the wettability of urea-formaldehyde resin, phenolic resin, isocyanate adhesive and distilled water on the surface of bamboo green, bamboo yellow and bamboo flesh, and the wettability of bamboo surface changes after acid and alkali treatment. The results showed that different adhesives possessed different wettability on the bamboo surface. After treatment, the wettability of different bamboo surfaces had significant changes, and the contact angle rate of different surfaces was different. After acid-base treatment, there is no significant difference in the change rate of the contact angle of the bamboo surface compared with the untreated bamboo. Lee [94] used a coupling agent treating bamboo fibers to improve the surface wettability of the material, to increase the penetration capacity of the adhesive resin on the surface of the material, and to improve the bonding strength and mechanical properties of the prepared wood-plastic composite material. Ren et al. [95] used three silane coupling agents and one coupling agent HMR to treat the surface of bamboo, showing that the coupling agent could improve the surface free energy and wettability of bamboo. One of the silane

coupling agents induced a reduction of surface free energy and wettability of bamboo, but the four agents could improve the bonding strength of bamboo composites. Wang et al. [96] studied the usage of nano-calcium carbonate materials to modify bamboo fiber materials, thereby improving the interphase characteristics and mechanical properties of the composite material.

Applications of new technology and new equipment: Yu [97] discussed the influence of factors such as hot pressing pressure, sizing amount, bamboo age, blank assembly method, and different bamboo processing methods on the bonding performance of bamboo composite materials. Scanning electron microscope was used. The distribution and difference of bamboo adhesive layer adhesive were observed. Fu [98, 99] studied the influence of bamboo composite material assembly method on the bonding strength of bamboo curtain board. It concluded that when thick and thin bamboo veneers were alternately assembled, the thin veneer and phenolic resin could be combined with the formation of a "composite glue layer". It could significantly improve the bonding strength of the bamboo composites and reduce its variability. Deng et al. [100] studied the bonding performance and paint performance of the carbonized bamboo substrate. The results showed that the bonding and coating performance of the carbonized bamboo substrate were improved. Chang et al. [101] studied the preparation and the use of high-frequency hot pressing equipment to ensure the uniformity of heat conduction inside the reconstituted bamboo slab, thereby helping to improve the bonding strength and mechanical properties of the reconstituted bamboo. Zhang et al. [102] studied the effect of friction welding equipment on the gluing performance of bamboo green and bamboo yellow composites. It showed that the usage of glue-free friction welding equipment could

prepare bamboo composites with excellent properties. It was discussed the effect of process parameters on the bonding performance of composite materials.

Tab.1-2 The effects of physicochemical modification methods on the change ratios of bamboo surface and bonding properties

| Methods | Parameters | Free radical (%) | Surface energy (%) | Contact angle (%) | O/C (%) | Bonding strength (%)/ Actual value |
|---|---|---|---|---|---|---|
| Oxygen plasma [86] | Power: 60 ~ 180W<br>Duration: 60 ~ 90s | / | / | 28 (BS, PF)<br>13 (BP, PF) | / | 10 ~25 (10~13 GPa) (MOE，PF)<br>9 ~ 44 (125~167 MPa) (MOR, PF) |
| Oxygen plasma [87] | Power: 1kW<br>Duration: 0 ~ 60s | / | 10 ~ 85 (BS)<br>5 ~ 71 (BP) | 10 ~230 (BS, water)<br>5 ~ 200 (BP, water) | / | / |
| Heat treatment [88] | Temperature: 180°C | Bonding strength, decrease 10% (BP) ~14% (BS),<br>Average penetration depth, increase+17% (BS) ~22% (BP) | | | | |
| Hot-oil treatment [90] | Temperature: 180°C | / | / | 37 (BS, water)<br>54 (BP, water) | / | decrease/ no significance, increase bamboo failure ratio |
| Heat treatment | Temperature: 180°C, 200°C | / | / | / | 5 ~ 23 (decrease) | / |

| | | |
|---|---|---|
| [82] | | |
| Chemical treatment [91, 93] | HCl | No significance (PF) |
| | NaOH | No significance (PF) |
| | $Na_2CO_3$ | |

In summary, the current modification methods for the surface of biomass materials, adhesives and bonding interphases have improved the surface activity and interphase compatibility of the materials, and improved the chemical reaction between biomass materials and adhesives. However, during the treatment process, the chemical composition and surface morphology of the biomass material are often damaged. There is too much ineffective penetration of the adhesive in the biomass material. A continuous and uniform adhesive layer could not be formed at the bonding interphase. Therefore, the validity of enhancing the bonding performance of the biomass composite material is affected. At the same time, the durability of the biomass material and its bonding interphase reduced as well, thereby further reducing the bonding performance. During the bonding process, the porous structure of the material, the penetration form of the adhesive and the polymerization reaction of the cell wall functional group and the adhesive are involved. Therefore, to explore the characteristics of the bonding interphase of biomass materials and their composites, the structural characteristics of the materials, adhesive penetration form and cross-linking reaction between the material and the adhesive, and other influencing factors should be considered comprehensively.

## 1.3 Research on the influence of high voltage electric field (HVEF) induction on biomass and its composite materials

### 1.3.1 Influence of HVEF induction on the physical and chemical properties of materials

As a treatment method that has a unique impact on the physical and chemical properties of materials, HVEF (>1kV) are used in the process of material preparation and modification[103, 104]. Zhang et al. [105] studied the use of HVEF treatment methods to significantly increase the surface conductivity and charge density of poly(3,4-ethylenedioxythiophene): poly(styrene sulfonic acid) (PEDOT:PSS) film. After the treatment, the internal chemical structure of the material was not damaged. Arun[106] tested the variation of the surface microscopic morphology of the elastic film material under the action of an electric field. It showed that the variation was related to the strength and thickness of the material itself. Jankowiak et al.[107] studied the surface electrical behavior and microstructure changes of silicon carbide modified ceramic materials under high-voltage pulsed electric field conditions. The results showed that under the action of electric field, the degree of ionization in the air was significantly increased, and a large number of free charges were accumulated on the surface of the material. Moreover, the surface potential and conductivity of the material were significantly increased, while the surface morphology did not change significantly. Based on numerical simulation and experimental testing, Souza et al.[108] studied the surface potential distribution characteristics of polymer insulators in HVEF under dry and wet conditions. The results showed that the surface behavior characteristics obtained by finite element numerical simulation and the experimental

results are significant. Relevance, under certain humidity conditions, more accumulated charges and surface potential could be obtained. Under excitation corona conditions, the degree of ionization in the surrounding atmosphere could be increased, thereby obtaining more active groups and free radicals on the surface of the material. Wang et al.[109] studied the charge distribution and agglomeration characteristics of the polymer surface under a DC high voltage electric field, revealing the law of charge accumulation and dispersion on the surface of the medium, the viewpoint of bipolar charge accumulation on the surface of the medium was put forward, indicating that the surface of the medium was densely charged with positive and negative charges. It was due to gas ionization at high temperatures and more dotted particles generated on the surface of the material. Liu et al.[110] studied the surface characteristics of epoxy resin polymer under pulsed HVEF conditions. The results showed that a large number of dotted particles and ionized free electrons in the atmosphere accumulated on the surface of the material after treatment. At the same time, the contact angle of the material surface significantly reduced. Kilic[111] tested the surface potential of the fiber material in the electric field. The results showed that the surface energy of the fiber material increased and the resistivity decreased after the electric field treatment. With the change of time, the potential gradually decreased and showed a decay trend. Richman[112] tested the effect of the degree of ionization under the action of electric field energy on the surface activity and biological functions (catalysis, recognition and binding) of biological proteins. Astorga et al.[113] comparatively studied the characteristics of surface charge distribution and surface potential of resin polymer and ceramic composites in HVEFs. The results showed that the type of polymer is one of the main factors affecting their

surface characteristics under electric field conditions. Xie et al.[114] studied the surface charge accumulation characteristics of four different polymers of epoxy resin, silicone rubber, plexiglass and polytetrafluoroethylene under DC electric field conditions. The results showed that the surface of the material reflects Bipolar charge accumulation, and the material type; voltage application time and amplitude are the main influencing factors that affect the surface charge distribution and surface potential energy of the material under the plane finger electric field

Therefore, it can be concluded that under the action of the electric field, the free electrons in the excited state collide with the chemical groups on the surface of the material, thereby forming a large number of broken chemical bonds and new free electrons on the surface of the material. Therefore, the polarization degree and surface free energy of the material surface will be significantly increased, thereby improving the physical and chemical properties of the material, and providing a large number of chemical reaction sites for the chemical reaction between the material and other polymers after the treatment.

In addition, previous studies have shown that the use of electric field treatment methods can excite and release metal particles, that is, metal particles can interact with biomass materials, thereby improving the corrosion resistance of biomass materials[115]. Treu et al.[116] studied the application of an electric field in the wood material, which caused the metal particles triggered in the electrode in contact with the material to bind to the chemically active groups of cellulose and lignin in the wood. Hattori et al.[117] showed that, compared with alternating current and high frequency current, direct current electric field has better resistance to wood rot fungi.

In addition, Treu et al.[118] used a low-voltage and low-pulse mode to treat the wood samples. The results showed that the mass loss of the wood samples was significantly reduced after the wood rot fungi corroded under the action of an electric field, and the excited metal particles interacted with the wood structure. Wood corrosion resistance has a positive effect. Therefore, a higher voltage will excite more metal particles, which react with the chemical functional groups of the wood along the conduit, and trigger more free radicals between the wood components[119]. Moreover, according to previous studies, the chemical reaction between silver particles and wood chemical groups can increase the resistance of wood to wood-rot fungi, and therefore, is beneficial to improve the anti-corrosion performance of biomass materials[120].

Because the HVEF can improve the physical and chemical properties of substances, the physical and chemical properties of wood, bamboo and other biomass materials, adhesives, and the bonding interphase of the two are all affected by the HVEF. Biomass materials such as wood and bamboo hardly contain free electrons, so the conductivity of biomass materials is very weak. Studies have found that under the action of an electric field, biomass materials can produce weak ionization. This weak conductivity is caused by the movement of ions. In a DC electric field, the polarization phenomenon of biomass materials has the typical characteristics of ion ionization. In addition, according to the research of electrohydrodynamics, the transmission, convection and distribution of liquids will also be affected by HVEF. The flow pattern and internal structure of liquid droplets or fluids will continue to change with the introduction of electric fields[107]. According to the dynamic phenomenon and motion equation of the charged particles in the electric field, it can be concluded that the Coulomb force can cause the condensed movement of the

charged particles[118]. Therefore, the number of free electrons and chemical bonds between the material and the adhesive increased through polarization, providing conditions for adding more chemical reaction sites for the reaction between them by applying a HVEF to the hot pres process of composite materials.

At the same time, the electric field treatment method has the advantage that it does not require materials to interact with harmful solutions, does not produce waste liquid waste, and reduces the damage to the wood structure and chemical composition[118]. In this study, the output voltage of the high-voltage generator is in the range of 0 to 60kV, the output current is in the range of 0 to 1.5mA, the maximum output power is 100W, and the maximum input power is 200W. It is a low-power electrical appliance and will not increase economic costs.

### 1.3.2 Electrohydrodynamics

Electrohydrodynamics is a combination of electric field and fluid mechanics. Nowadays, humans have higher requirements for energy efficiency and energy consumption. Electrohydrodynamics can provide support for research in this area, so it is gradually being recognized by the academic community[122]. Under normal temperature and pressure, substances generally exist in three forms: solid, liquid and gas. The corresponding substances are called solid, liquid and gas. Liquid and gas are collectively referred to as fluid. Electrohydrodynamics (EHD) is a discipline involving these two fluids. Fluid contains free charge and bound charge, and electric field can interact with these two kinds of charges. This is the content of electrofluid dynamics research. At the same time, the subject also discusses the behavior of electrofluid or particles in the electric field. When the electric field interacts with the

fluid, it generates electromotive force. In fluids, there is a certain correlation between the motion of the medium and the electric field, and the interaction between the two will form an electrofluid phenomenon.

So far, the research of related electrofluid dynamics has been more in-depth. Melcher deeply studied the convection phenomenon of liquid in different electric fields, and then established the corresponding leakage dielectric model based on this. Many similar studies later adopted this model. On the basis of summing up the previous research experience, Saville studied the electrofluid dynamics of different types of topological structures in combination with the charge generation mechanism in the dielectric[104]. At the end of the 1990s, foreign scholar Castellanos wrote a special book, which mainly introduced the generation mechanism of electrohydrodynamics, which laid a good foundation for research in this field[123].

Based on Coulomb's law, the electrostatic force of the interaction between two point charges $q_1$ and $q_2$ [C] with a distance of $r$[m] is $F$[N]:

$$\mathbf{F} = \frac{1}{4\pi\pi}\frac{q_1 q_2}{r^2}\mathbf{r_0} \tag{1.1}$$

According to the dynamic phenomenon in the direct current electric field, the motion equation of the charged particle can be derived, and it is assumed that the charged particle is a spherical particle, a spherical particle with a mass of $M$ and a radius of $a$, and a quantity of electricity with $q$. The motion in the electric field $E$ is subject to the following formula:

$$M\frac{d^2\mathbf{r}}{dt^2} + 6\pi\eta a\frac{d\mathbf{r}}{dt} = q\mathbf{E} + \mathbf{F_1} + \mathbf{F_2} \tag{1.2}$$

Here $r$ is the position vector, $\eta$ is the medium viscosity coefficient, the first term on the left is the inertial force term, the second term is the viscous resistance term, the first term on the right is the Coulomb force, and the second term F1 is the gradient force other than the Coulomb force. , The third term F2 is gravity other than electricity. When the charged particles in the DC uniform electric field move, the two terms F1 and F2 in the formula (1.2) can be ignored. Coulomb force can cause the cohesive movement of charged particles. Two charged particles with masses of M1 and M2, radii of a1 and a2, charged quantities of q1, q2, air viscosity coefficient, and charged quantities are proportional to the surface area of the ball Proportional, then there is the equation:

$$\begin{cases} M_1 \dfrac{d\upsilon_1}{dt} + M_1 \dfrac{\upsilon_1}{\tau_1} = \dfrac{q_1 q_2}{4\pi\varepsilon_0 r^2}, \\ M_2 \dfrac{d\upsilon_2}{dt} + M_2 \dfrac{\upsilon_2}{\tau_2} = -\dfrac{q_1 q_2}{4\pi\varepsilon_0 r^2}, \end{cases} \tag{1.3}$$

The "-" indicates attractiveness.

(1) $a_1 = a_2 = a, M_1 = M_2 = M, \tau_1 = \tau_2 = \tau_v, |-q_1| = |q_2| = q$ When the particle diameter is small, the particle aggregation speed will decrease sharply; in addition, when the distance between the particles increases, the aggregation speed also decreases.

$$\left(\frac{dr}{dt}\right)_1 = 12\varepsilon_0 \left(\frac{\varepsilon_r}{2+\varepsilon_r}\right)^2 \left(\frac{C_m E_c^2}{\eta}\right)\left(\frac{a^3}{r^2}\right) \tag{1.4}$$

（2） When $a_1 >> a_2$, $M_1 >> M_2, \tau_1 >> \tau_2, q_1 >> q_2$ , if small charged particles are mixed with large particles of opposite polarity, the aggregation speed will increase.

$$\left(\frac{dr}{dt}\right)_2 = 6\varepsilon_0\left(\frac{\varepsilon_r}{2+\varepsilon_r}\right)^2\left(\frac{C_m E_c^2}{\eta}\right)\left(\frac{a_1^2 a_2}{r^2}\right) \quad (1.5)$$

### 1.3.3 Influencing factors of HVEF induction on biomass materials

Due to the particularity of the structure and composition of biomass, it lacks electrons that can effectively conduct electricity. Therefore, the conductivity of some biomass materials is often poor. Studies have found that under the action of an electric field, such substances will be ionized. Therefore, they believe that a certain degree of conductivity of substances is due to the dissociation of ions, which is not directly related to electrons. In some cases, biomass materials will also undergo polarization, and this phenomenon happens to have the characteristics of ion ionization, which can explain that the dissociation of ions makes the material conductive under certain conditions.

The ions present in biomass materials can exist in two forms, which can be divided into bound ions and free ions. Free ion are ions that can migrate. Generally, the migration of ions needs to meet certain conditions. Research results show that the conduction of biomass materials is related to free ions, and the ion dissociation usually occurs in the amorphous region of the cell wall. When the moisture content of the material is low, the conductivity of the material mainly depends on the concentration of free ions; when the moisture content in the material is high, the bound ions have a dissociation effect and the ion mobility is higher, which directly leads to enhanced conductivity of materials. The conductivity of biomass materials is closely related to ions. Therefore, changes in ion concentration, distribution, or both will affect the conductivity of biomass materials at the same time. In terms of the

direct current conductivity of such materials, there are many factors that can affect it, such as moisture content and temperature[124].

Moisture content: this element is closely related to the conductive activation energy E. Two important concepts are involved here, namely the dissociation capacity U and the migration energy S, which will have a decisive influence on the conductive activation energy E. With the participation of strongly polar water molecules, the binding effect of ions and adsorption sites is significantly reduced, so the moisture content is an important factor affecting the conductivity of biomass materials. Dry biomass materials have poor electrical conductivity, and when the moisture content increases, the electrical conductivity of the material gradually increases. When the moisture content reaches a certain threshold, the electrical conductivity of biomass will increase several million times[125].

Temperature: for metal materials, an increase in temperature will lead to an increase in its conductivity; on the contrary, for biomass materials, the resistivity decreases with the increase in temperature. This is because of the different conductive mechanisms of biomass materials and metals. As a result, metals conduct electricity through the migration of electrons, while biomass materials conduct electricity through the dissociation of ions. When the ambient temperature is low, the number of free ions in the biomass material is relatively stable; when the ambient temperature rises, the bound ions will become current-carrying ions and be freed. At this time, the conductivity of the material is stronger. According to the above discussion, temperature is an important factor affecting the conductivity of biomass

materials. It should be pointed out that when the moisture content increases, the temperature influence becomes smaller.

Texture direction: The texture direction is an important factor that affects the physical properties of biomass materials, and the electrical properties are also affected by it. The grain direction of biomass materials includes the horizontal grain direction and the normal grain direction. In comparison, the horizontal grain direction has a more obvious influence on the resistivity. In softwood, the resistivity in the cross-grain direction is significantly higher than the resistivity in the along-grain direction, while in hardwood, the difference between the two is more significant. There is no correlation between the influence of the texture direction on the resistivity of the material and the moisture content, and the influence is mainly caused by the anisotropy of the direction. There is a difference between the chordal resistivity and the radial resistivity of biomass materials, but this difference is not obvious.

Density, species and location: the density of different biomass materials is also related to the conductivity, but its impact on the conductivity is not significant and can even be ignored. Under the same conditions, the greater the density of the biomass material, the more substantial part of the biomass material, the fewer void parts, the greater the resistivity and the lower the electrical conductivity. The difference in resistivity between tree species and the influence of density on electrical conductivity are not all consistent. Compared with the density factor, the tree species has a more obvious impact on the electrical conductivity. This is because the electrical conductivity is related to the water-soluble electrolyte, and different tree

species have a certain difference in the internal water-soluble electrolyte content, which makes the tree species the main influence on the electrical resistivity factor. Compared with the density factor, its influence on the resistivity is more significant. In addition, there are also certain differences in the resistivity between the center and the edge of the biomass material. The resistivity of the former is lower. Some scholars believe that the reason for this phenomenon is that the center contains more extracts.

### 1.3.4 Influence of HVEF on the characteristics of the bonding interphase of biomass materials

Because the HVEF can improve the surface and interphase properties of the material, the physical and chemical properties of wood, bamboo, adhesives and their bonding interphase will all be affected by the HVEF. Due to the lack of free electrons that can effectively conduct electricity in the chemical structure of biomass materials, biomass materials are also weakly conductive materials. When there is an electric field, biomass materials will produce ionization and polarization. This phenomenon is a characteristic of ion ionization, indicating that under certain conditions, the ionization of ions makes the material conductive.

The equations of motion and kinetic phenomena of charged particles in an electric field, so as to obtain the Coulomb force can cause the movement of charged particles aggregation [121] . Thus, the high voltage electric field is applied to the composite through pressing process, by ionizing and polarizing effect, a large number of excited molecules in the air to form a fracture and the new group of electrons impinging material body surface, the adhesive surface of the material the number of free

electrons and breaking chemical bonds increased to facilitate adhesive bonding material more chemical reaction sites of the crosslinking reaction between the agents.

Qian et al. [126, 127] studied the gluing performance of polyvinyl acetate emulsion (PVAc ) poplar plywood using low-voltage electric field treatment methods. The results showed that the voltage value and the amount of glue are important factors affecting the bonding strength of composite materials. Voltage value or different glue amount will significantly affect the rate of change of the bonding performance of the composite material. Meanwhile, Qian [128] has investigated the (untreated and treated by electric field polyvinyl acetate emulsion of PVAc) bonding properties of lauan plywood. The influence of the voltage value on bonding properties of the composite was described and the voltage can significantly affect the rate of change of the bonding strength. Thus, more polar groups triggered in the atmosphere and more broken chemical groups occurred under HVEF treatment, providing more possibilities for chemical reaction of adhesive molecules and bomass materials. However, the induction mechanism of the electric field treatment method on the interphase of biomass materials and their composite materials has not yet been clear, and further research and exploration should be conducted.

### 1.3.5 Other applications of HVEF induction effects

The characteristics of HVEF-induced effects mainly include: dose uncertainty, parameter diversity, threshold and multi-directionality. Dose is a physical quantity, which is mainly closely related to two factors, namely voltage and time of action. When the added dose is different, the corresponding electric field effect is also different. Biomass material is a special field equipotential body, characteristic of

complex and its electric field effect s also different. This phenomenon is related to many factors, the most important factor is their biological, physiological, biochemical or electromagnetic property etc. In addition, environmental factors will also affect it. Therefore, the joint influence of multiple factors on materials should be considered in the research. There is a certain correlation between the electric field and organisms. This correlation is specifically presented in the following ways, including promotion, inhibition and no change. Under different thresholds, the induction effect is different, and the threshold area could be selected according to needs. At the same time, different organisms have different requirements for the directionality of the electric field.

The HVEF is closely related to the growth of plants. Applying a certain voltage to crops such as wheat, corn, sorghum, etc. will help improve the growth of crops and increase the rate of grain weight and root weight. The growth rate of tomatoes in an 18kV electrostatic field was significantly higher than that under natural conditions. After applying a 25kV electric field to soybeans and corn, the grain weight and growth were significantly increased [129, 130]. Seeds treated with a high-voltage electrostatic field can significantly increased their vitality. After soybean seeds treated with 30kV/m and 25kV/m HVEFs, the extravasation of inorganic ions, soluble sugars and soluble proteins were significantly lower when swelling at low temperatures. In the control group, the accumulation of malondialdehyde was reduced, the activity of seed amylase and dehydrogenase was promoted, and the germination rate of seeds was increased [131, 132] . High voltage electric field thaw, HVEF drying and osmotic dehydration can solve many practical problems for materials containing water. HVEF thawing test was conducted by using distilled

water, potatoes, pork, etc. as raw materials, and significantly improved efficiency of thawing was achieved [133]. At present, the dehydration technology, electro-osmotic dehydration technology have been mature, and they have been promoted in many fields [134-137]. The current stage segment, dewatered sludge, oil were used as environmentally friendly energy technology [138].There is a close correlation between the evaporation of water and the high-voltage field. Due to the influence of the electric field , the evaporation speed of water is faster. There is a significant positive correlation between parameters and evaporation speed. The energy consumption by the electric field is very low [139]. TRBajgai 's research on spinach leaves showed that the drying speed of spinach leaves in a HVEF was faster than that under natural conditions. This method can preserve chlorophyll a and b. At the same time, this method is also suitable for drying other materials and good results were achieved relatively [140-143].

In summary, we can get

(1) Nowadays, modification methods for the surface of biomass materials, adhesives and bonding interphase of composites was utilized to improve the compatibility, surface activity, the chemical reaction between the biomass material with adhesive and the bonding strength. However, in the process of fabrication, the chemical composition and surface morphology of biomass materials are often damaged. There is too much ineffective penetration of the adhesive in the biomass materials, and a continuous and uniform dense glue layer cannot be formed at the bonding interphase. Thus, the reinforcing effect of the bonding properties of the biomass composite material is affected, at the same time, redued durability material glued interphase is obtained, and poor bond performance is achieved. In the

bonding process, the porous structure of the material, penetration of adhesive and the polymerization reaction with the functional group of adhesive cell wall were involved. Thus, the material structure characteristics, the penetration form of the adhesive and the cross-linking reaction between the material and the adhesive and many other influencing factors should be considered to explore the biomass material and their bonding interphase properties.

(2) In a previous study, the researchers used only a low voltage electric field conditions for preparation plywood. The adhesive was poly vinyl acetate emulsion and did not involve the hot-pressing conditions of interphase characteristics. The induction effect of HVEF was not obtained. Since the HVEF has the effect of improving the surface and interphase materials. The physicochemical properties wood, bamboo, and adhesive bonding agent, and bonding interphase are affected by of HVEF treatment. When an electric field is present, the biomass material can produce ionization and polarization phenomena, affecting the surface charge distribution, the phase between chemically reactive groups and their interaction. In addition, according to the research of electrohydrodynamics, the transmission, convection and distribution of liquid will also be affected by HVEF, and the flow pattern and internal structure of liquid droplets or fluids will continue to change with the introduction of electric fields. When HVEF treatment is applied to the composite material during hot press, the activity surface of material, the adhesive, the chemical reaction at bonding interphase will be affected. However, the effect of HVEF treatment on the physical and chemical properties of biomass material, adhesives distribution and mechanical properties of composite materials has not yet been investigated in detail and it needs further in-depth study and exploration.

## 1.4 Research content and objectives

In order to clarify the influence mechanism of HVEF on the activation performance of wood and bamboo and the bonding characteristics of the interphase, this study uses coniferous wood (masson pine and fir), hardwood (poplar and white phoenix) and bamboo as the test materials, the adhesive of phenolic resins and urea-formaldehyde resin is selected. Under different HVEF conditions, the effect mechanisms of HVEF on the physical and chemical properties of wood amd bamboo, adhesive reaction, bonding interphase and aggregation performance were explored. On this basis, combined with the changes of mechanical properties of wood and bamboo composite materials, revealing the enhancing mechanisms of bonding interphase. The main research contents are as follows:

(1) The effect mechanism of HVEF treatment on the activation performance of wood and bamboo.

Testing the ion migration, radical concentration, wettability, free energy and oxygen-containing group changes of wood and bamboo induced by HVEF treatment, and to obtain the law of chemical and activation degree of wood and bamboo under the conditions of HVEF (electric field intensity, treatment time and temperature) amd to reveal the change mechanism and difference of physical and chemical properties of wood and bamboo (different tree species and different sections). Testing the interaction between the silver particles and the chemically reactive group of wood induced by HVEF treatment, to obtain the changes of chemical structure, the structure of the silver particles, the antibacterial properties of HVEF-treated wood.

The reaction mechanism of wood active groups and silver particles under the synergistic effect of HVEF treatment and silver.

(2) The action mechanism of HVEF treatment on the chemical composition and rheological behavior of the adhesive.

Testing the changes in the chemical bonds and rheological properties of the adhesive under HVEF treatment, studying the effects of HVEF conditions (electric field intensity, treatment time and temperature) on the rheological behavior of adhesives (UF and PF resins) at the temperature (30 ~180°C) and frequency ( 1~100Hz ), revealing the reaction mode and induction mechanism of the adhesive under HVEF treatment.

(3) The influence of HVEF on the aggregation effect and mechanical properties of wood-bamboo composite material bonding interphase

Testing the adhesive penetration depth and the vertical density profile of the cross-sectional wood and bamboo composite under HVEF treatment, exploring the law of HVEF conditions (electric field intensity, treatment time and temperature) on the adhesive penetration depth and distribution, to reveal the aggregation effect of adhesives at the bonding interphase of wood and bamboo (different tree species and different section combinations). Bonding strength, elastic modulus, bending strength and delamination rates for wood and bamboo composites were investigated under HVEF treatment, to obtain the law of changes of macroscopic mechanical properties for wood and bamboo composite material (different species and different combinations ) under HVEF treatment..

(4) the enhancing mechanism of the bonding interphase and the mechanical model of stiffness and strength distribution under HVEF treatment.

Based on the above contents (1), (2) and (3), constructing the correlation between micromechanics (elastic modulus and hardness) of bonding interphase and adhesive penetration depth and degree of homogeneity, analyzing the influence of the mechanical properties of bonding interphase from macro to micro multiscale under HVEF treatment, explaining the enhancing mechanism of the bonding interphase induced by HVEF treatment. 50μm equivalent volume element thickness (RVE) was proposed to establish the stiffness and strength distribution model under HVEF treatment, predicting elastic constants and strength parameters of RVE unit along the thickness, further predicting the mechanical properties (elastic modulus, bending strength, shear strength composite material and shear modulus).

Research objectives:

(1) To reveal the influence mechanism of HVEF treatment on the activation performance of wood and bamboo;

(2) To clarify the mechanism of HVEF treatment on the chemical composition and rheological behavior of the adhesive;

(3) To obtain the change law of the aggregation effect and mechanical properties of the interphase adhesive induced by HVEF treatment;

(4) To reveal the strengthening mechanism of wood and bamboo bonding interphase induced by HVEF and construct a mechanical prediction model.

## 1.5 Technical route

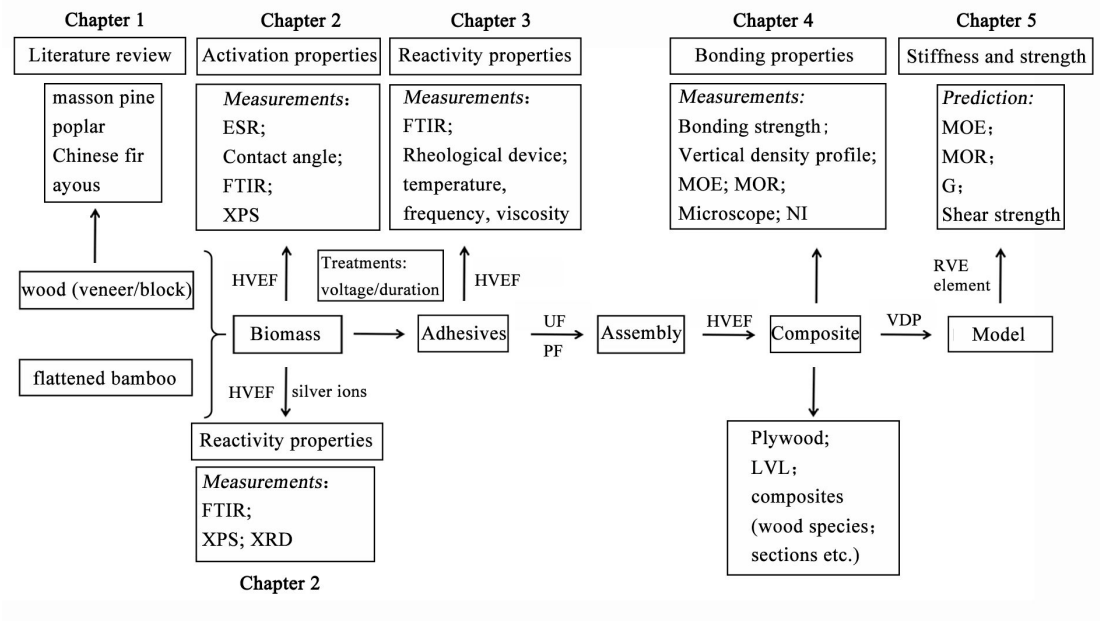


## 1.6 Research significance and innovation

In this study, the HVEF induction method was used to improve the physical and chemical properties of wood and bamboo and the chemical reaction sites. On the basis of optimizing the HVEF induction conditions, the adhesive was continuously, uniformly and densely distributed at bonding interphase. The bonding strength and mechanical properties of wood and bamboo composite materials were significantly improved. This research can not only solve the key scientific issues, but also further improve the enhancing mechanism of the bonding properties of wood and bamboo composites. This study provided a new way to improve the bonding strength and mechanical properties of wood and bamboo composites. It is of great significance for promoting wood and bamboo products upgrading and industrial development.

Innovation points :

(1) Clarifying the mechanism of HVEF-induced activation of wood, bamboo, and adhesive activation and the enhancement of bonding properties of composite materials, constructing the correlation between the penetration depth, uniformity of the adhesive and the micromechanics of the bonding interphase, revealing the strengthening mechanism the aggregation effect of the adhesive.

(2) Using the advantages of interdisciplinary, applying HVEF technology to the preparation of wood and bamboo composite materials, significantly improving the surface activity of wood and bamboo, the degree of intermolecular reaction of the adhesive, and achieving continuous, uniform and dense bonding layer, thus improving wood, bamboo mechanical properties of composite materials, for providing the basis theory for wood and bamboo composites efficient processing and industrial upgrading.

# Chapter II The influence mechanism of HVEF treatment on the activation performance of wood and bamboo

## 2.1 introduction

In wood, bamboo and other biomass materials, the main components of the fiber cell wall are cellulose, lignin and hemicellulose. The chemical group activities of these components (such as: –OH, –CHO) cross-link between the fibers. It plays an important role in the adhesion of fibers and polymers [144-149]. The microstructure of different sections of wood (tracheids or pores, pits, etc.) and different tree species contain different chemical components (such as lignin,extracts, etc.), which also have a significant impact on the surface chemical reaction activity of wood [150, 151]. In addition, the surface of bamboo contains natural aliphatic and low reactive waxy layer, which is not conducive to the cross-linking reaction with general biomass material adhesives [80]. The current surface modification research methods mainly include: plasma treatment, dielectric barrier discharge treatment, magnetic field treatment and corona discharge treatment, and the combination of these treatment methods to change the surface chemical properties of biomass materials [152-155]. However, the current modification research method belongs to the category of chemical pretreatment, which increases the bonding strength by improving the activity of the surface of the material and the compatibility of the interphase. The chemical pretreatment method improves the chemical reaction between the biomass material and the adhesive, and increases the penetration of the adhesive in the biomass material. However, the chemical composition and surface morphology of biomass materials are often damaged, and there is too much ineffective penetration of

adhesives in biomass materials, which in turn affects the bonding performance of composite materials.

As a processing method that has a unique impact on the physical and chemical properties of materials, HVEF are used in the process of material preparation and modification [104, 156]. Kilic [111] tested the surface potential of the fiber material in an electric field, and the results showed that after the electric field treatment, the surface free energy of the fiber material increased and the resistivity decreased. With the change of time, the potential gradually decreased and showed a decay trend. Richman [112] tested the effect of the degree of ionization under the action of electric field on the surface activity and biological functions (catalysis, recognition and binding) of biological proteins. In addition, the use of electric field treatment methods can excite and release metal particles, which can interact with biomass materials. Treu et al. [116] studied the application of an electric field in wood materials, which led to the triggering of metal particles in the electrode in contact with the material. Combines with the chemically active groups of cellulose and lignin in wood. Therefore, the researchers predict that the voltage will excite more metal particles, which react with the chemical functional groups of the wood along the ducts, and trigger more free radicals between the wood components [118].

Because HVEFs can improve the physical and chemical properties of materials, the physical and chemical properties of wood, bamboo, adhesives and their bonding interphases will all be affected by HVEFs. When there is an electric field, biomass materials will produce ionization and polarization phenomena, which will affect the charge distribution on the surface of the material and the interaction between active

groups and their chemical bonds. However, the research on the influence of HVEF treatment on the surface properties of biomass materials is not very sufficient, and its influence mechanism needs to be further explored.

In this chapter, four wood species and flattened bamboos are used as test materials: masson pine (*Pinus massoniana Lamb.*), Chinese fir (*Cunninghamia lanceolata Lamb.*), poplar (*Populus tomentosa Carr.*) and ayous (*Triplochiton scleroxylon K. Schum.*). Exploring the surface ion migration and free radical concentration of biomass materials induced by HVEF, to obtain the effects of HVEF treatment conditions (electric field intensity, treatment time and temperature) on the degree of ionization and activation of the surface of biomass materials. At the same time, the influence mechanism of HVEF treatment on the surface characteristics of different tree species and different wood sections, revealing the change mechanism and difference of the surface characteristics of different biomass materials.

## 2.2 Materials and Methods

### 2.2.1 Test materials

The materials were selected from four wood species: masson pine (*Pinus massoniana Lamb.*), Chinese fir (*Cunninghamia lanceolata Lamb.*), poplar (*Populus tomentosa Carr.*) and ayous (*Triplochiton scleroxylon K. Schum.*) (Xiashu Town, Jurong, Jiangsu, Nanjing Forestry University, Forest Farm). The dimension of sawn timber was: 850mm×50mm×20 mm (length×width×height), and all of them were radial-cut boards, with no defects and uniform materials. The dimension of the

prepared wood sample was selected as 200mm×50mm×20mm (length×width×height), dried in an oven at 50°C for 72 hours, and the moisture content was 8±3%. The poplar wood material (*populus canadensis moench'i- 72/58'*) was selected, which came from Siyang, Jiangsu (33°43'N, 118°36'E). The sample was cut from the fixed area of the sapwood. The size of the sample was 20 mm × 20 mm × 20 mm (longitudinal × radial × chord), and all samples were free of defects. The sawn samples were first immersed in absolute ethanol, and the wood samples were disinfected and cleaned with an ultrasonic cleaner for 2 hours, and then dried at 103°C for 48 hours. The moisture content was less than 5±1%, and the average drying density was 0.45g/cm$^3$.

The flattened moso bamboo (Dechang Bamboo and Wood Co., Ltd., Zhejiang Province, China) was selected in this study. The bamboo age was 4-year old, and the bamboo was cut at a distance of 3 m to 4 m from the root. The diameter at breast height was 13 cm. The dimension of sample was 500mm×100mm×6mm (length×width×height) without any defects. The bamboo samples were dried in an oven at 50°C for 72 hours, with a moisture content of 7±1% and a density of 658kg/m$^3$. The surface was sanded with a sander to remove surface stains (the amount of sanding was 0.3-0.5mm). The specific material details are as follows in Table 2-1:

Tab.2-1 The basic properties for samples.

| Species | Latin | Density ($g/cm^3$) | Years | Diameter（m） | Place |
|---|---|---|---|---|---|
| masson pine | *Pinus massoniana Lamb.* | 0.55 | 10 | 0.54 | Guangxi, China |
| Chinese fir | *Cunninghamia lanceolata Lamb.* | 0.37 | 15 | 0.61 | Jiangsu, China |
| poplar | *Populus tomentosa Carr.* | 0.42 | 4 | 0.42 | Jiangsu, China |
| ayous | *Triplochiton scleroxylon K. Schum.* | 0.52 | 120 | 1.28 | Gabon, Africa |
| poplar | *populus canadensis moench 'i- 72/58'* | 0.45 | 3 | 0.35 | Jiangsu, China |
| bamboo | *Phyllostachys heterocycla* | 0.66 | 4 | 0.13 | Zhejiang, China |

### 2.2.2 HVEF processing method

The HVEF generator used in this experiment was produced by Hangzhou Jingtong Co., Ltd. (JT207K-1, HC-JDGC-C), Zhejiang, China. The sample was placed in a flat electric field in a hot press. The average thickness of the aluminum plate is 3mm, the upper plate is connected to the high-voltage generator, and the lower plate is grounded, as shown in Figure 2-1. The material sample was placed between the two plates. After setting the temperature and adjusting the voltage value, the high-voltage generator was turned on. After the treatment time was reached, the generator was turned off. The samples were taken out and put in a ziplock bag. They were stored in a drying tank for 2 week.

The silver particle-HVEF treatment device consists of two pieces of silver electrode plates with the dimension of 150 mm×150 mm×1.5 mm (length×width×height). One of the electrode plates was connected to the high voltage

generator as the negative electrode, and the other electrode plate was connected to the ground as the positive electrode. The wooden block sample was placed between two silver electrodes, and the sample was subjected to a longitudinal pressure of 2 kPa. During the treatment, the voltage was 60kV, the temperature was set to 100°C, and the selected treatment durations were 6h, 12h, 24h, and 48h. After treatment, the treated sample was removed from the equipment and put it in a drying tank to equilibrate for about 4 weeks (temperature: 25°C, relative humidity: 10%). The test was repeated five times for each test condition. The test conditions selected for this test are shown in Table 2-2:

Tab.2-2 Materials and parameters selected for high voltage electric field.

| Types of materials | Species | Dimension | Density ($g/cm^3$) | Temperature (°C) | Voltage (kV) | Time (min) |
|---|---|---|---|---|---|---|
| Veneer | masson pine | 400 mm×400 mm×2.5 mm (length × width × thickness) | 0.55 | 120 | 0/5/10/20/60 (8min) | 0/2/4/6/8 (60kV) |
| Wood samples | masson pine | 200mm×50mm×20mm (length × width × thickness), radial board | 0.55 | 145 | 60 | 0, 40 |
| | | 200mm×50mm×20mm (length × width × thickness), tangential board | | 145 | 60 | 0, 40 |
| | | 200mm×50mm×20mm (length × width × thickness), cross-cut board | | 145 | 60 | 0, 40 |
| | Chinese fir | 200mm×50mm×20mm (length × width × thickness) | 0.37 | 145 | 60 | 0, 40 |
| | poplar | 200mm×50mm×20mm (length × width × thickness) | 0.42 | 145 | 60 | 0, 40 |
| | ayous | 200mm×50mm×20mm (length × width × thickness) | 0.52 | 145 | 60 | 0, 40 |
| Bamboo sample | Flattened bamboo | 200mm×50mm×20mm (length × width × thickness) | 0.66 | 145 | 60 | 0, 14 |

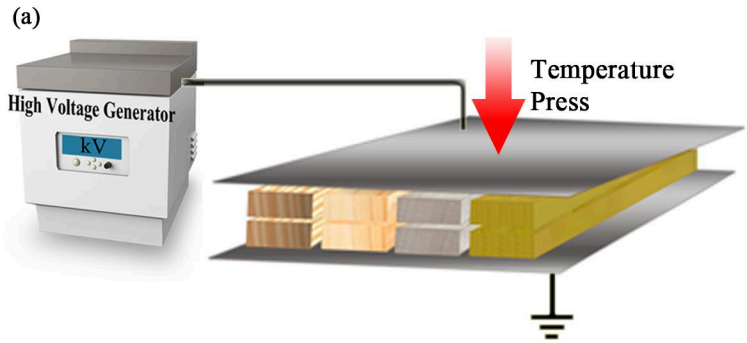


Fig.2-1 The diagram for high voltage electric field treatment device.

### 2.2.3 Electron spin resonance spectroscopy

The most effective and direct method to test free radicals at this stage is the electron spin resonance method. The generation of free radicals was due to the breaking of covalent bonds, forming groups or atoms without paired electrons. Such electrons not only surround the electron core Orbital motion, and spin motion [157]. Test method: in this experiment, an electron spin resonance (JES-FA200) instrument was used to measure the content of free radicals in solid wood. The sample was selected from the fixed area of the wood sample, and the dimension was 43mm×2mm×2mm (length×width×thickness), as shown in Figure 2-2. After the samples were dried in an oven at 103°C for 48 hours, they were placed in a drying dish containing $P_2O_5$ powder (≥98%) to equilibrate for 1 week to obtain a moisture content of less than 4%. After the HVEF treatment was completed, the free radical content test was carried out, and the repetition was ten. The test conditions was including center field: 326.550 mT, sweep width: 5 mT, sweep time: 2 min, amplitude: 50 mV, time constant: 0.3s.

### 2.2.4 Static and dynamic contact angle test method

When a droplet drops on the surface of a porous material, there will be two different phenomena, namely complete wetting and incomplete wetting. At the junction of gas, liquid, and solid phases, the contact angle is the angle between the liquid-solid interphase and the liquid-gas interphase through the liquid side [158]. Generally, the wettability of a solid surface is mainly reflected by the contact angle, and a small contact angle means good wettability. The Young formula reflects the tension balance between the three phase interphases, namely:

$$\gamma_{SV} - \gamma_{SL} = \gamma_{LV} \cos\theta \tag{2.1}$$

Where $\gamma_{SV}$ refers to the free energy between the solid phase and the gas phase interphase; $\gamma_{SL}$ refers to the free energy between the solid phase and the liquid interphase; $\gamma_{LV}$ refers to the surface tension of the liquid. The amount of free energy on the surface of a solid phase material is also related to the wettability of the material. Free energy is a manifestation of the interaction between molecules in the material, which can be expressed as isothermal reversible work per unit area [159].

This test uses an optical contact angle tester (OCA40Micro), and the test liquid includes deionized water, diiodomethane, polyethylene glycol, urea-formaldehyde resin and phenol formaldehyde resin. During the test, the initial contact angle and equilibrium contact angle were recorded. According to the Fowkes extended theory equation, the free energy data of the material surface was measured with three test liquids. The formula is as follows [160]:

$$\gamma_{LV}(1+\cos\theta) = 2\left[\left(\gamma_{LV}^{d}\gamma_{SV}^{d}\right)^{\frac{1}{2}} + \left(\gamma_{LV}^{p}\gamma_{SV}^{p}\right)^{\frac{1}{2}} + \left(\gamma_{LV}^{h}\gamma_{SV}^{h}\right)^{\frac{1}{2}}\right] \tag{2.2}$$

In the formula, γ LV、$\gamma d\ LV$、$\gamma p\ LV$ and $\gamma h\ LV$ respectively refer to the free energy and its components of the liquid phase, and γ SV 、$\gamma d\ SV$ 、$\gamma p\ SV$ and $\gamma h\ SV$ respectively refer to the free energy and its components of the solid phase surface. The parameter values of the test liquid (surface free energy and its components) are shown in the following Table 2-3:

Tab.2-3 Parameters for the test liquids

| Testing liquids | Surface energy（$mJ/m^2$） | | | |
|---|---|---|---|---|
| | γp | γd | γh | γtotal |
| Deionized water | 1.3 | 29.1 | 42.4 | 72.8 |
| Diiodomethane | 1.3 | 49.5 | 0.00 | 50.8 |
| Polyethyleneglycol | 0.1 | 29.9 | 13.5 | 43.5 |

The wettability of the adhesive on the surface of the material is a dynamic process that changes with time. In the experiment, the value of the contact angle of the adhesive on different wood species and bamboo materials with time is recorded. Test method: The sample is selected from the fixed area of the wood sample, the size is 10mm×10mm×2mm (length×width×thickness), as shown in Figure 2-2. After the samples were dried in an oven at 103°C for 48 hours, they were placed in a drying dish containing $P_2O_5$ powder (≥98%) to equilibrate for 1 week to obtain a moisture content of less than 4%. After the HVEF treatment was completed, the free radical content test was carried out, and the repetition was 10. The syringe specification is 1mL, and the droplet is dropped from a fixed thickness to the center of the material surface at a dosage of 10μL/drop.

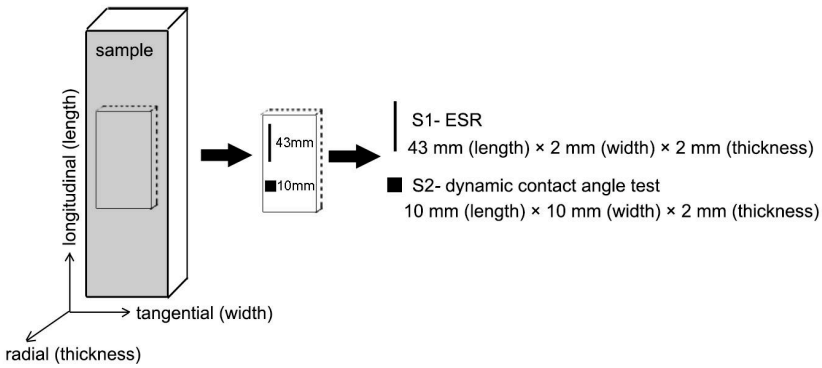


Fig.2-2 The diagram for the samples preparation.

### 2.2.5 X-ray photoelectron spectroscopy test

X-rays can be used to excite electrons in atoms and molecules. By testing the kinetic energy and chemical displacement of the excited electrons, the electron binding energy of each element in the sample (except hydrogen and helium) can be obtained. At the same time, based on the binding energy and characteristic spectrum, the composition of the solid surface elements and the chemical properties of the related valence states can be further obtained [161].

Wood and bamboo and other biomass materials are mainly composed of carbon C, hydrogen H, oxygen O, nitrogen N and silicon Si. The electron binding energy of the 1s layer of carbon atoms is approximately equal to 284.80 eV. The carbon atom and hydrogen atom or oxygen atom When it is combined with each other, the binding energy obtained will change and shift accordingly [162]. There are four different types of carbon atoms in biomass materials, including C1, C2, C3 and C4. At the same time, the characteristic peaks at 368eV are divided into Ag(0), Ag(I), Ag(III) and Ag(III). ) Four composition forms of sat to analyze Ag 3d elements as shown in Table 2-4:

Tab.2-4 The assignments for C1s binding energy and bond type in high resolution XPS spectra

| C1s | Binding energy （eV） | Formations |
|---|---|---|
| C1 | 284.8 | C–C or C–H |
| C2 | 286.5 | C–OH |
| C3 | 288.0-288.5 | C–O or C=O |
| C4 | 289.0-289.5 | O–C=O |

Test method: Grinding various samples into powder of 40~60 mesh, dried for 48 hours in an oven at 103°C, and equilibrating in a drying dish with $P_2O_5$ powder (≥98%) for 1 week to obtain less than 4% moisture content. After the HVEF treatment was completed, the test was carried out. The excitation source is AlKα (1486.6eV), and the vacuum degree is 7×10-8Pa. Two analytical methods are used in the test, broad peak and narrow peak, to accurately obtain the combination of carbon atoms and oxygen atoms.

### 2.2.6 Fourier infrared spectroscopy test method

Fourier infrared spectroscopy is mainly used to analyze the functional group components and structural characteristics of materials. The test method of this test: Grinding various samples into powder of 40~60 mesh, dried for 48 hours in an oven at 103°C, and equilibrating in a drying dish with $P_2O_5$ powder (≥98%) for 1 week to obtain less than 4% moisture content. After the HVEF treatment was completed, the test was carried out. The sample and KBr powder were mixed uniformly according to the mass ratio (1/1000) and then pressed into a transparent sheet. The infrared test

was performed on a VERTEX 80V instrument with a resolution of 2 $cm^{-1}$ and a test range of 400-3000 $cm^{-1}$.

### 2.2.7 Chemical composition analysis method

Soxhlet extractor and toluene/ethanol (volume ratio 2/1) solution was used to extract 2 g of wood flour (40 mesh), and the extraction time was 6 h. According to the standard TAPPI T222-om-02 standard and NREL/TP-510-42618~c42622 standard, the acid-insoluble lignin and monosaccharide content were determined. Using high performance anion exchange liquid chromatography detection method (Waters alliance e2695 and Waters 1525), the lignin hydrolyzed liquid monomer sugars were analyzed, so that the content of cellulose, hemicellulose and lignin can be calculated according to the formula. The test was repeated three times for each sample.

### 2.2.8 Crystallinity test method

X-ray diffraction analysis equipment (Ultima IV, Rigaku) was used to analyze the chemical composition and crystallinity changes of the treated wood samples. The X-ray diffractometer radiation source is composed of Cu-Kα, the wavelength is λ=1.5406Å, the accelerating voltage is 40kV, and the current is 30mA. The resolution of the test equipment is 0.02°, and the 2θ range is 5°~90°. The untreated and processed wood block samples were ground into 100 mesh powder, which was stored in a desiccator for later use. The Debye-Scherrer formula was used to calculate the average particle size of the silver particles.

## 2.3 Results and analysis

### 2.3.1 The influence of HVEF treatment conditions (voltage/time) on the surface characteristics of wood

As shown in Figure 2-3, the free radical change of masson pine materials after HVEF conditions was characterized. It described that the free radical content distribution curve during the test (Figure 2-3 (b)). From Figure 2-3 (a), it can be seen that after HVEF treatment, the free radical change rate of masson pine material was significantly increased under certain treatment time conditions. This is because excited state electrons collided with the chemical groups of water and oxygen molecules in the air under HVEF treatment, forming a large number of broken chemical bonds and gathering on the surface of wood, thus providing a large number of free electrons and chemical groups on the surface of the material (– OH and –CHO) [163]. It can be found from the figure that the higher the voltage of the HVEF, the higher change rate of the free radical content of the material was obtained under a certain condition. This was mainly because the higher the voltage, the greater the number of excited electrons was achieved under the conditions of HVEF treatment. For another, after colliding with each other and hitting a large number of molecular chemical groups in the air, more broken, free chemical bonds and ions acted on the surface of the material [164].

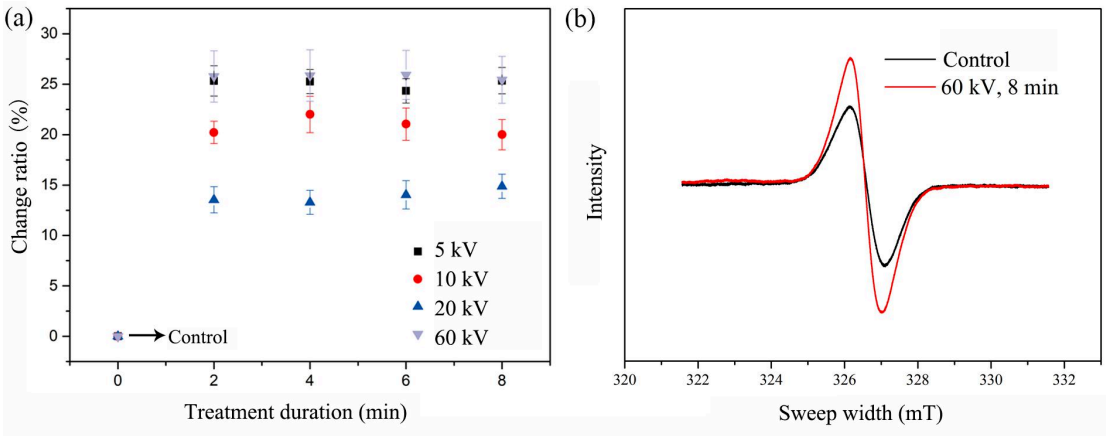


Fig.2-3 (a) Change ratio of free radicals as a function of treatment time and intensity, respectively. (b) Curve obtained by the electron spin resonance (ESR) measurement. Change ratio was calculated as ((valuetreated−valuecontrol)/valuecontrol)×100%.

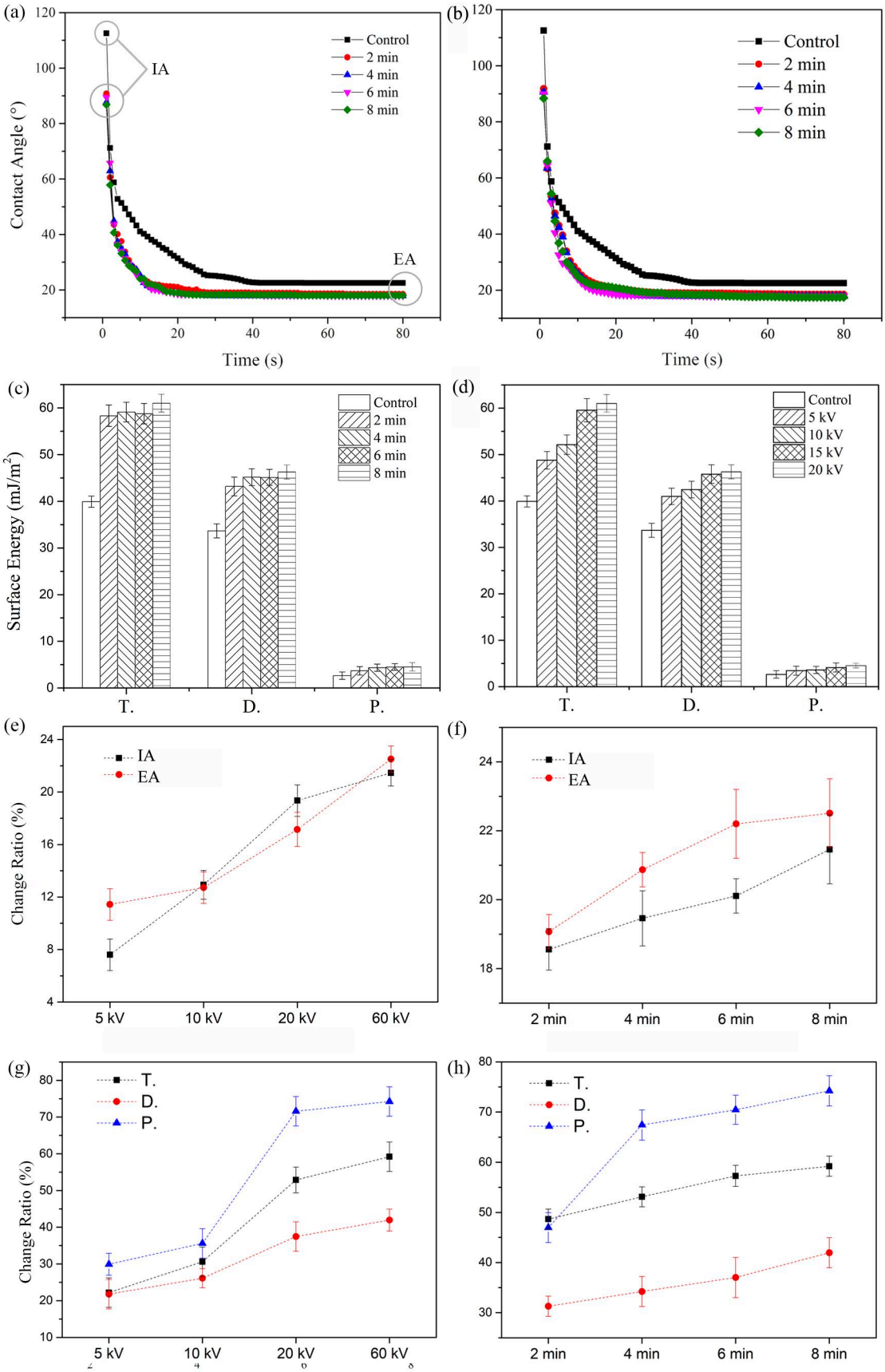
(a)
Contact Angle (°)
Time (s)
IA
EA
Control
2 min
4 min
6 min
8 min
(b)
Time (s)
Control
2 min
4 min
6 min
8 min
(c)
Surface Energy (mJ/m²)
T.
D.
P.
Control
2 min
4 min
6 min
8 min
(d)
T.
D.
P.
Control
5 kV
10 kV
15 kV
20 kV
(e)
Change Ratio (%)
IA
EA
5 kV
10 kV
20 kV
60 kV
(f)
IA
EA
2 min
4 min
6 min
8 min
(g)
Change Ratio (%)
T.
D.
P.
5 kV
10 kV
20 kV
60 kV
(h)
T.
D.
P.
2 min
4 min
6 min
8 min

Fig.2-4 Dynamic contact angles displayed for (a) different treatment times and (b) intensities. Surface energy displayed for (c) different treatment times and (d) intensities, consisting of IA initial contact angle, EA equilibrium contact angle, T surface total free energy, D surface free energy of dispersion components, and P surface free energy of polar components. The change ratios of (e), (f) contact angles and (g), (h) surface energy are also displayed.

After treated by the HVEF, the relationship of the contact angle with the treatment time and voltage was as shown in Figure 2-4. As shown in Figure 2-4 (a) and (e), the initial contact angle (IA) and equilibrium contact angle (EA) were significantly reduced after HVEF treatment. As the treatment time increased, the change rate of the equilibrium contact angle did not change significantly. Under different voltage conditions (Figure 2-4(b)), the initial contact angle and equilibrium contact angle were significantly reduced, and the change rate increased significantly with the increase of voltage (Figure 2-4(f)). Under the treatment condition of 60kV/8 min, the most decrements for the initial contact angle and equilibrium contact angle were obtained. At the same time, as shown in Figure 2-4(c)(d), after HVEF treatment, the overall free energy (T), dispersed component (D) and polar component (P) of the material surface were significantly increased. Under different treatment conditions, as the voltage and time increased, the respective energy components increased significantly, but as the voltage increased, the change rate decreased. This was mainly because there is a limit value during the HVEF treatment effect [165]. It can be seen from the figure that the HVEF has a significant influence on the change of the contact angle of the material surface. Under HVEF treatment, a large number of excited state electrons, broken chemical bonds and new ions, such as –OH and –CHO, were generated on the surface of the wood, which significantly increased the surface energy of the material and reduced the IA and EA. More reaction sites were provided for the cross-linking reaction between the resin and wood.

X-ray photoelectron spectroscopy was used to quantitatively analyze the changes of chemical elements such as oxygen and carbon on the surface of the material. As shown in Figure 2-5 (a) and (b), from the overall spectrum, the oxygen element ratio has increased significantly. At the same time, the carbon/oxygen (O/C) element ratio before and after the HVEF treatment were also analyzed. The O/C ratio was calculated in Table 2-5. After HVEF treatment, the O/C ratio increased significantly, with an increase rate of 34%. This result showed that under the HVEF treatment, the surface of the material contained more oxidative groups. This result was attributed to the fact that the excited electrons destroyed a large number of molecular chemical groups in the air, and the broken chemical groups were concentrated on the surface of the material, so that a higher degree of oxidation was obtained around the surface of the material [166, 167]. In the C1 sub-peak spectra of Figure 2-5 (c) and (d), the C1, C2, C3 and C4 sub-peaks were all marked. C1 represented the change of the C–H group. The components of C2, C3 and C4 represented chemical groups containing oxygen. According to the image and area integral calculation in Figure 2-5(c)(d), the calculation results of C1s peak content and change rate were listed in Table 2-5. The results showed that C1, C2, C3 and C4 sub-peaks had significant changes after HVEF treatment. The C2, C3 and C4 components were significantly increased by 39%, 149%, and 97% (60kV/8min), respectively, and the C1 component was relatively significantly reduced. These results were due to the large number of broken oxygen-containing groups obtained after the HVEF treatment. The reaction with the groups on the surface of the material significantly increased the degree of polarization and oxidation on the surface of the material. As the voltage and time increased, the C2, C3, and C4 components

increased significantly, and the C1 component decreased. This was mainly because the excited chemical groups increased with the increase of voltage and time, resulting in a large number of electrons, ions, and other cleavage groups. The impact of clusters on the surface of the material improved the oxygen-containing groups and reactivity on the surface of the material, but as the voltage increased, the change rate of components decreased. It was mainly because there was a limit value in the process of the electric field treatment [165].

Tab.2-5 O/C ratio and C1s assignments in X-ray photoelectron spectra under HVEF treatment and compared with the control.

| | Untreated | 5 kV | Δ(%) | 10 kV | Δ(%) | 20 kV | Δ(%) | 60 kV | Δ(%) |
|---|---|---|---|---|---|---|---|---|---|
| $C1_S$(%) | 71.06 | 67.63 | / | 65.43 | / | 65.93 | / | 65.70 | / |
| $O1_S$(%) | 22.94 | 24.65 | / | 25.98 | / | 27.85 | / | 28.30 | / |
| O/C | 0.32 | 0.36 | 14% | 0.40 | 24% | 0.42 | 32% | 0.43 | 34% |
| C1(%) | 64.46 | 56.01 | -13% | 49.28 | -24% | 43.04 | -33% | 41.43 | -36% |
| C2(%) | 22.76 | 24.13 | 6% | 27.99 | 23% | 30.95 | 36% | 31.54 | 39% |
| C3(%) | 3.53 | 5.79 | 64% | 7.17 | 103% | 8.51 | 141% | 8.78 | 149% |
| C4(%) | 9.26 | 14.08 | 52% | 15.56 | 68% | 17.50 | 89% | 18.25 | 97% |

| | Untreated | 2 min | Δ(%) | 4 min | Δ(%) | 6 min | Δ(%) | 8 min | Δ(%) |
|---|---|---|---|---|---|---|---|---|---|
| $C1_S$(%) | 71.06 | 66.24 | / | 66.64 | / | 66.75 | / | 65.70 | / |
| $O1_S$(%) | 22.94 | 25.65 | / | 26.87 | / | 27.98 | / | 28.30 | / |
| O/C | 0.32 | 0.39 | 21% | 0.40 | 26% | 0.42 | 31% | 0.43 | 34% |
| C1(%) | 64.46 | 51.11 | -21% | 46.76 | -27% | 43.83 | -32% | 41.43 | -36% |
| C2(%) | 22.76 | 27.15 | 19% | 29.36 | 29% | 30.73 | 35% | 31.54 | 39% |
| C3(%) | 3.53 | 6.57 | 86% | 8.08 | 129% | 8.30 | 135% | 8.78 | 149% |
| C4(%) | 9.26 | 15.17 | 64% | 15.80 | 71% | 17.15 | 85% | 18.25 | 97% |

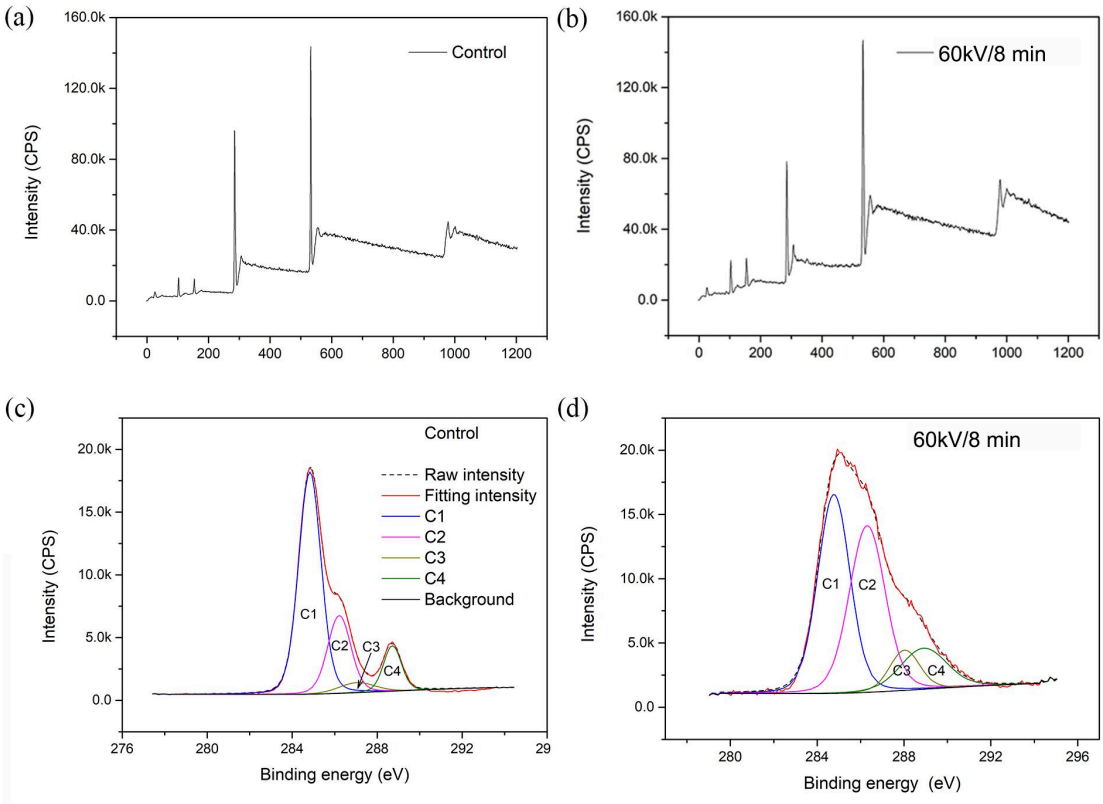


Fig.2-5 X-ray photoelectron spectra for C1s and O1s (a) control, (b) treated; C1-C4 components under HVEF treatment (c) control, (d) treated

In Figure 2-6, the effect of HVEF on the chemical groups on the surface of the material under different treatment times and voltages was characterized. The change of functional groups on the wood surface was analyzed by FTIR spectroscopy. According to Table 2-6, the main functional groups on the surface of the material before and after the HVEF treatment could be compared [168]. The O–H band at 3333cm$^{-1}$ and C–H at 2900cm$^{-1}$ are tensile vibration absorption peaks, and C=O at 1732cm$^{-1}$ is the tensile vibration peak, which belongs to the xylan acetyl group CH3C=O , C=O at 1646cm$^{-1}$ is the stretching vibration peak, which belongs to the conjugated carbonyl group in lignin. After HVEF treatment, the chemical bond functional groups of oxygen-containing groups increased. As the voltage value

increased, such oxidized chemical bonds increased significantly. Regardless of the treatment time, such chemical groups would increase significantly compared to untreated materials. This was because the electrons triggered by the HVEF formed a large number of free radicals on the surface of the material, thereby increasing the degree of polarization. The broken oxygen-containing bonds gathered on the surface of the material, increasing the O/C ratio and the content of C2, C3 and C4. Therefore, the results of FTIR were consistent with those of X-ray photoelectron spectroscopy, which further demonstrated that HVEF treatment can significantly increase the free radical content and oxygen-containing groups on the surface of the material, and increase the degree of polarization, making it compatible with other polymers. More reaction sites were provided during the reaction [169].

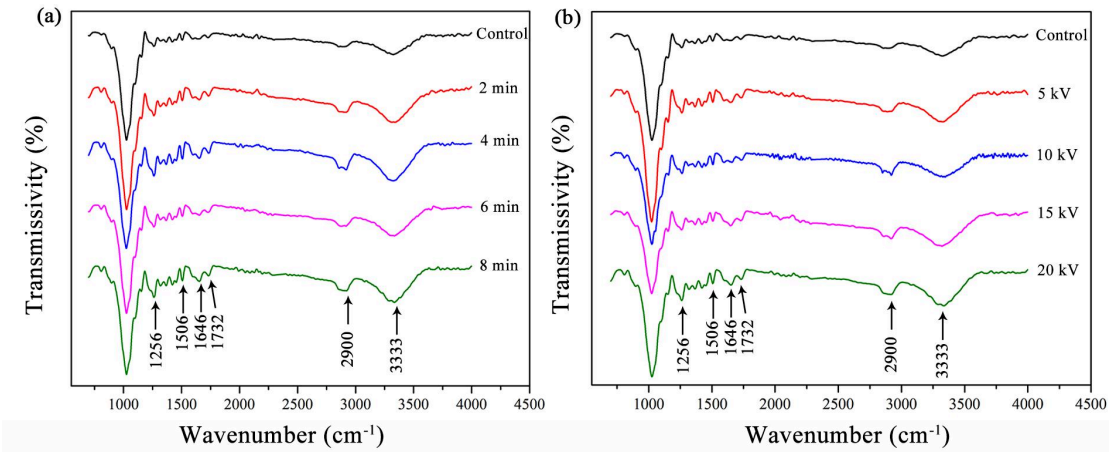


Fig.2-6 (a) Fourier transform infrared spectroscopy for wood samples under (a) different voltages and (b) different durations with the comparison of the control.

Tab.2-6 Chemical groups assignments for Masson pine Fourier transform infrared spectroscopy

| Wavenumber ($cm^{-1}$) | Chemical groups | Attributions |
|---|---|---|
| 3333 | O–H | O-H stretching vibration |
| 2900 | C–H | C–H stretching vibration |
| 1732 | C=O | C=O stretching vibration ($CH_3C=O$) |
| 1646 | C=O | C=O stretching vibration |
| 1506 | C=C | Carbon skeleton vibration of benzene rings (lignin) |
| 1460 | C–H, C=C | C–H bending vibration ($CH_2$)<br>Carbon skeleton vibration of benzene rings (lignin) |
| 1424 | C–C | Benzoal ring skeleton, C–H stretching vibration |
| 1376 | C–H | CH bending vibration (cellulose and hemi-cellulose) |
| 1256 | C–O–C | C–O–C stretching vibration (cellulose and hemi-cellulose) |
| 1055 | C–O | C–O stretching vibration |
| 895 | C–H | C–H bending vibration (cellulose) |

### 2.3.2 The effect of HVEF treatment on the surface characteristics of different sections of wood

Wood is an anisotropic material, that is, a natural polymer composed of countless cells of different shapes, sizes, and arrangements, as shown in Figure 2-7. From the macroscopic structure of wood, wood has three different sections, namely, cross section, radial section and tangential section. On the transverse section, you can see the distribution of tracheids and lumina and gradual change of wood from earlywood to latewood. The different structural characteristics of holes or channels,

pits and wood rays can be observed on the radial and tangential sections [170]. Because of the different structural characteristics from wood three sections, different effects on the adhesive distribution and the chemical reaction of wood and other polymers could be observed [171-173].

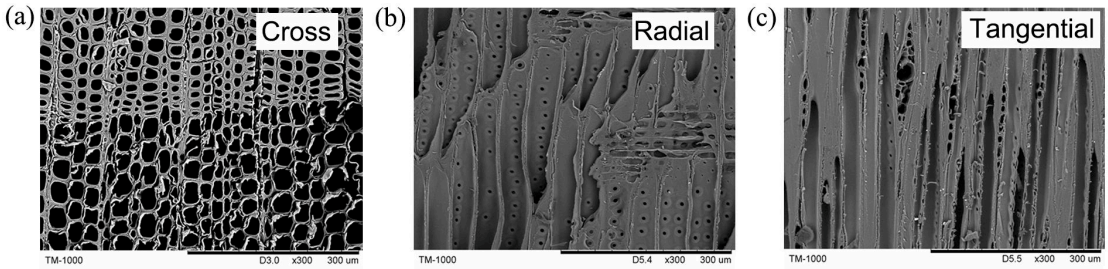


Fig.2-7 Microscopy for wood different sections. (a) cross section, (b) radial section and (c) tangential section.

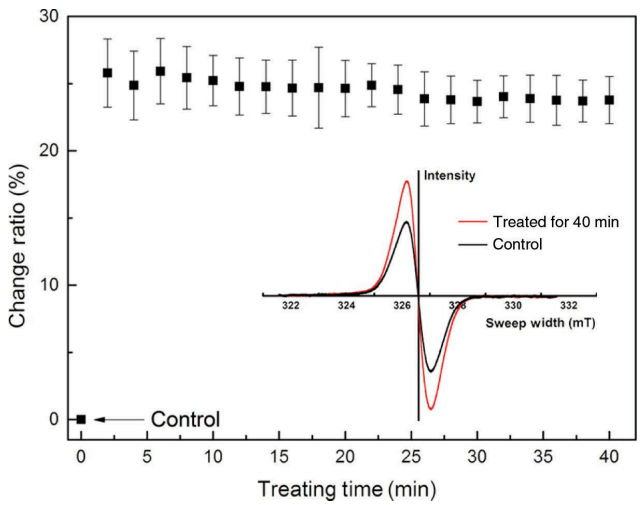


Fig.2-8 Change of content of the free radical ratio of wood samples under HVEF treatment. Change ratio was calculated as [(Valuetreated − Valuecontrol)/Valuecontrol] × 100%.

As shown in Figure 2-8, the change rates of the free radical content of the masson pine material before and after the HVEF treatment were characterized. After HVEF treatment, the free radical content of the material increased significantly. With the increment of treatment time, the change rate of free radical content did not change significantly [174]. In order to further explore the surface characteristics of different wood sections induced by HVEF, as shown in Figure 2-9, the contact angle change

rates of three different wood sections before and after treated by HVEF were characterized. After the HVEF treatment, the contact angle of the cut surface was significantly reduced. For different wood sections, different decrements for the initial contact angle and the equilibrium contact angle were obtained (Figure 2-9 (a) ~ (c)). In the radial section, the largest change rates were obtained for the initial contact angle and the equilibrium contact angle, followed by the tangential section and the cross section (Figure 2-9(g)). After the HVEF treatment, the surface free energy of the three-section surface of the material also significantly increased, including the total surface free energy (T.), the surface free energy of the dispersed components (D.) and the surface free energy of the polar components (P.) (Figure 2-9 (d) ~ (f)). After comparing and analyzing the contact angle and surface energy of the untreated material, it could be found that the influence of HVEF on different sections was different, the order of the change rate was: cross section < tangential section < radial section. After HVEF treatment, a large number of broken chemical bonds hit and accumulated on the surface of the wood. Chemical groups in large numbers such as –OH and –CHO appeared on the surface of the wood. For the radial section and the tangential section, a large number of chemical functional groups were exposed on the longitudinal section. At the same time, the tracheid channels (cell inner wall) are closely arranged on the longitudinal section, and there are a large number of tracheid pores on the cross section. Therefore, the excited electrons and broken chemical groups could not fully react with the chemical groups of the cell wall, and there are similar descriptions in the previous literature [175-177]. In addition, there are a large number of pit structures on the radial section, which will affect the ion exchange

between tracheids, and some aspirated pit membranes will also affect the change of contact angle after HVEF treatment [178, 179].

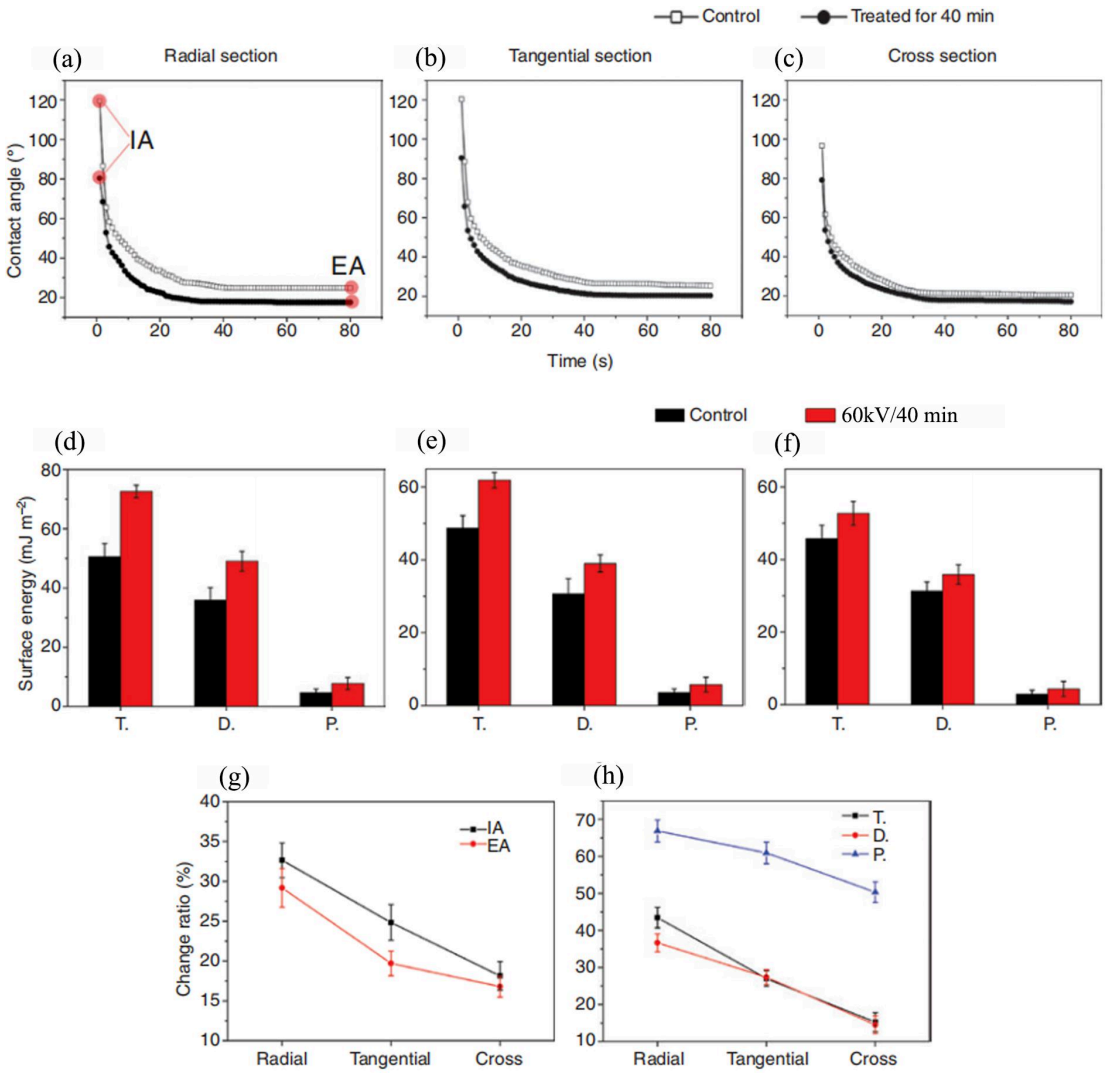


Fig.2-9 Contact angle measurement for different wood sections treated by HVEF and compared with the control. Contact angles displayed for (a) radial, (b) tangential and (c) cross sections. The surface energy displayed for (d) radial, (e) tangential and (f) cross sections, consisting of IA, initial contact angle; EA,equilibrium contact angle; T., surface total free energy; D., surface free energy of dispersion components and P., surface free energy of polar components and the change ratios of (g) contact angles and (h) surface energy.

### 2.3.3 The effect of HVEF treatment on the surface characteristics of different wood species

In previous studies, the microstructure characteristics of wood of different species (softwood and hardwood), including pore size and pore structure of tracheid or lumina, have a significant impact on the cross-linking reaction between wood and adhesives [180- 182]. In this study, two types of softwood and two types of hardwood species were selected. Under HVEF treatment, the influence of HVEF on the free radical content, dynamic contact angle and O/C ratio of different tree species was explored.

The chemical compositions of the four wood species were summarized as shown in Table 2-7. The results of their chemical composition were in the same range as the chemical composition obtained by Poletto et al. [183]. The highest and lowest lignin content were observed for Chinese fir and ayous. The extract content of ayous was higher than other species. In Table 2-8, the diameters of tracheids and lumina were characterized, and their order was as follows: Chinese fir < masson pine < poplar < ayous. At the same time, the double wall thickness of different species were measured in this research. It could be observed that compared with the two hardwood of poplar and ayous, masson pine and fir have thicker cell walls.

Tab. 2-7 Wood chemical components.

| Species | Air-dried Density (g/cm$^3$) | Holo-cellulose (%) | Lignin (%) | Extract (%) |
|---|---|---|---|---|
| masson pine | 0.53±0.04 | 64.8±1.2 | 27.5±0.5 | 2.5±0.3 |
| Chinese fir | 0.42±0.03 | 62.5±0.9 | 32.2±0.4 | 1.7±0.2 |
| poplar | 0.45±0.05 | 69.4±1.0 | 23.5±0.8 | 2.0±0.5 |
| ayous | 0.52±0.05 | 68.5±1.4 | 20.6±0.8 | 7.6±1.1 |

Tab. 2-8 Wood anatomical properties.

| | Lumen diameter (μm) | | Double cell wall thickness (μm) | |
|---|---|---|---|---|
| | Tracheids | | Tracheids | |
| | earlywood | latewood | earlywood | latewood |
| masson pine | 39.5±5.21 | 28.8±6.40 | 9.5±0.55 | 12.9±0.75 |
| Chinese fir | 35.8±4.05 | 26.55±4.85 | 6.3±0.40 | 8.2±0.50 |
| | Trachees | | Trachees | |
| poplar | 62.4±18.38 | | 4.75±0.35 | |
| ayous | 155.3±22.21 | | 8.0±0.50 | |

As shown in Figure 2-10, the change rates of free radical content of different species before and after HVEF treatment were characterized. After HVEF treatment, the free radical content of each species increased significantly. However, the change rate did not increase significantly with the increase of treatment time. This result was consistent with previous studies [174]. Through further comparison, it could be observed that the change rate of softwood free radical content was greater than the that of hardwood. The order of increments were as follows: ayous < poplar < masson pine < Chinese fir. This result can be attributed to the difference in the lignin content of different species. From Table 2-7, the Chinese fir possessed the highest lignin content and the lowest was for ayous. It has also been found from previous studies that lignin has a significant contribution to the content of free radicals in materials. Therefore, under HVEF treatment, the content of lignin significantly affected the change rate of free radical content of various species [163, 184].

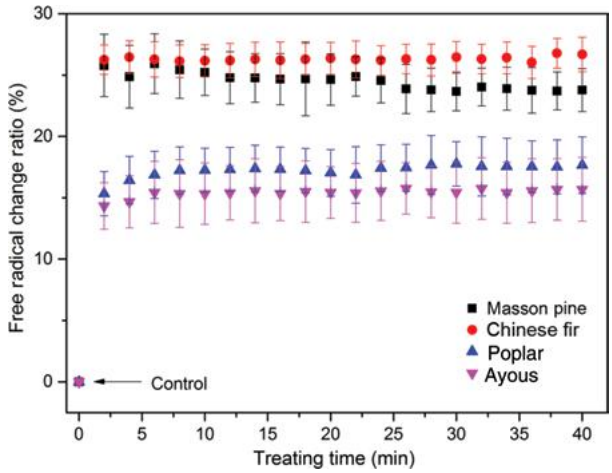


Fig.2-10 Changing ratio of free radical for different wood species under HVEF treatment. Change ratio was calculated as [(Valuetreated − Valuecontrol)/Valuecontrol] × 100%.

From Figure 2-11, it could be observed that the initial contact angle and equilibrium contact angle of the radial section of masson pine, Chinese fir, poplar and ayous were significantly reduced after HVEF treatment (Figure 2-11(a)~(d)). The reduction of the contact angle of the radial surface of the softwood was greater than that of the hardwood. In addition, from Figure 2-12 (a) ~ (b), it could be observed that after HVEF treatment, free energy including total free energy content (T.), dispersed free energy content (D.) and polar free energy content (P.) increased significantly for different species. Through analysis and comparison, after HVEF treatment, for the four different species, the change rate of free radical content, contact angle, and free energy have the same order of: ayous < poplar < masson pine < Chinese fir (Figure 2-13). These results indicated that lignin content, extract content and cell diameter are important parameters that have great effect on HVEF treatment for different species. After HVEF treatment, a large amount of extract components migrated for ayous with high extract content, thereby affecting the wetting properties [185]. In addition, in hardwood, the larger the cell diameter, the

smaller the flow resistance of the liquid. Therefore, after the HVEF treatment, the change rate of each parameter is smaller, which affected the reactivity of the wood and the adhesive.

Using X-ray photoelectron spectroscopy, the changes of surface oxygen, carbon and other chemical elements of different species were quantitatively analyzed. As shown in Figure 2-14 to Figure 2-17 (a) and (b), the percentage of oxygen element is significantly increased after HVEF treatment. At the same time, the carbon/oxygen (O/C) before and after the HVEF treatment was also analyzed. Element ratio and O/C ratio were calculated in Table 2-9. After HVEF treatment, the O/C ratio increased significantly, the order of change rates were as follows: ayous (19%) < poplar (25%) < masson pine (34%) < Chinese fir (43%). This result showed that the surface of the material contained more oxidative groups under HVEF treatment. Different species have different chemical composition content, resulting in different change rates, which was consistent with the change law of free radicals. This result was also attributed to the fact that the excited electrons destroyed a large number of molecular chemical groups in the air and the broken chemical groups were concentrated on the surface of the material, so that a higher degree of oxidation was obtained from the surface of the material [166, 167]. According to Figure 2-14 to Figure 2-17 (c) and (d), the calculation results of C1s peak content and change rates were listed in Table 2-9. The results showed that the C1, C2, C3 and C4 sub-peaks of different tree species had significant changes after HVEF treatment. The C2, C3, and C4 components significantly increased, and the C1 component relatively significantly decreased. For the C1s component, the largest change rate was involved in Chinese fir while the the smallest was for ayous. These results were attributed to the fact that a large number

of broken oxygen-containing groups reacted with the groups on the surface of the material after HVEF treatment, which significantly increased the degree of polarization and oxidation on the surface of the material. Due to the variation of free radical content between different species, the variation of C1, C2, C3 and C4 components of different species was obtained, which was consistent with the variation of free radical content.

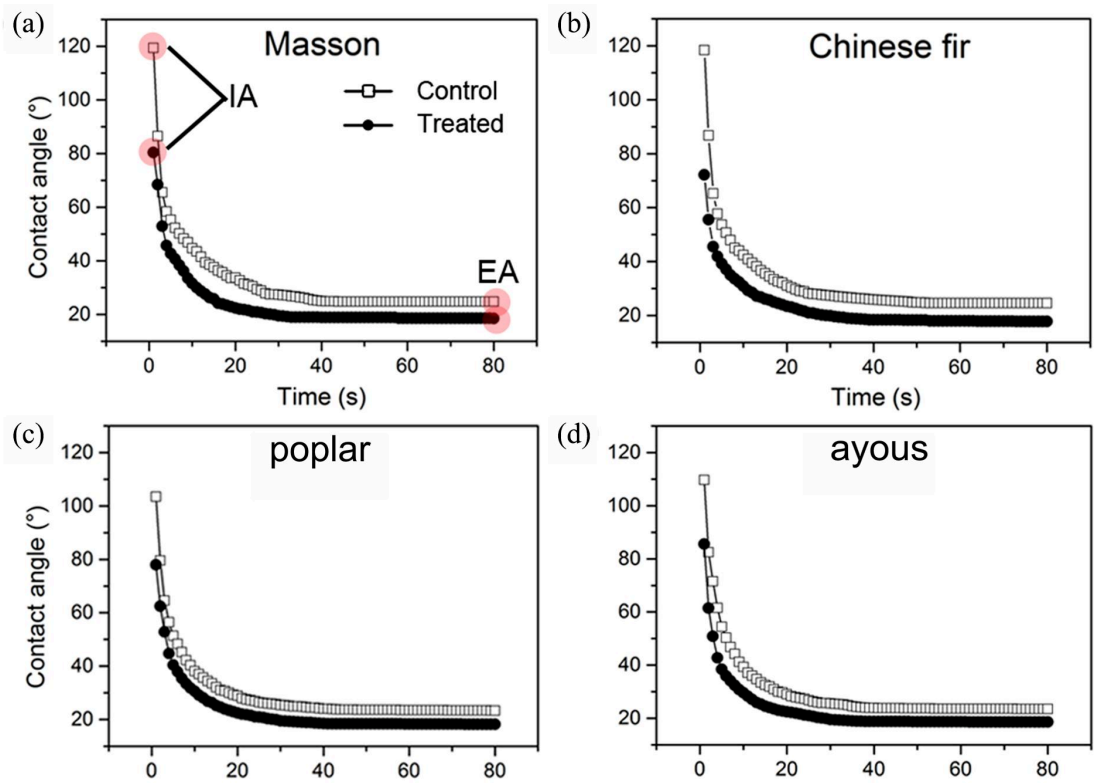


Fig.2-11 Dynamic contact angle measurement for different wood species treated by HVEF and compared with the control. Contact angles displayed for (a) masson pine, (b) Chinese fir, (c) poplar and (d) ayous.

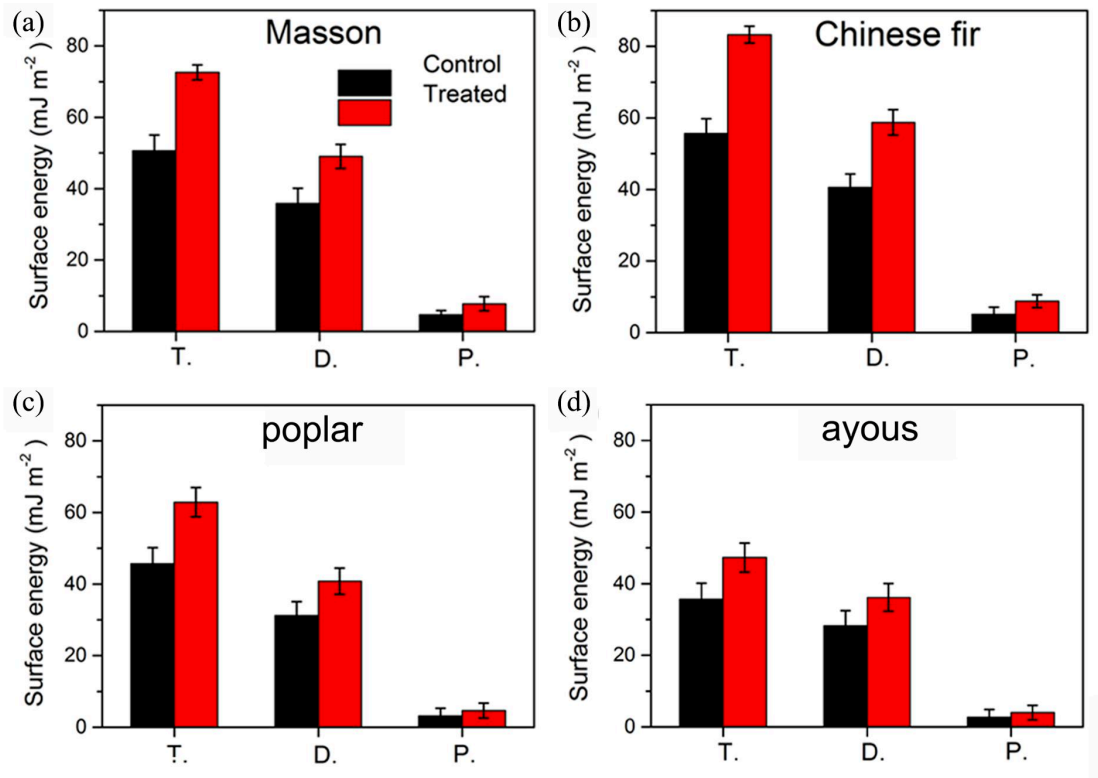


Fig.2-12 The surface energy displayed for different wood species treated by HVEF and compared with the control, for (a) masson pine, (b) Chinese fir, (c) poplar and (d) ayous, consisting of IA, initial contact angle; EA, equilibrium contact angle; T., surface total free energy; D., surface free energy of dispersion components and P., surface free energy of polar components.

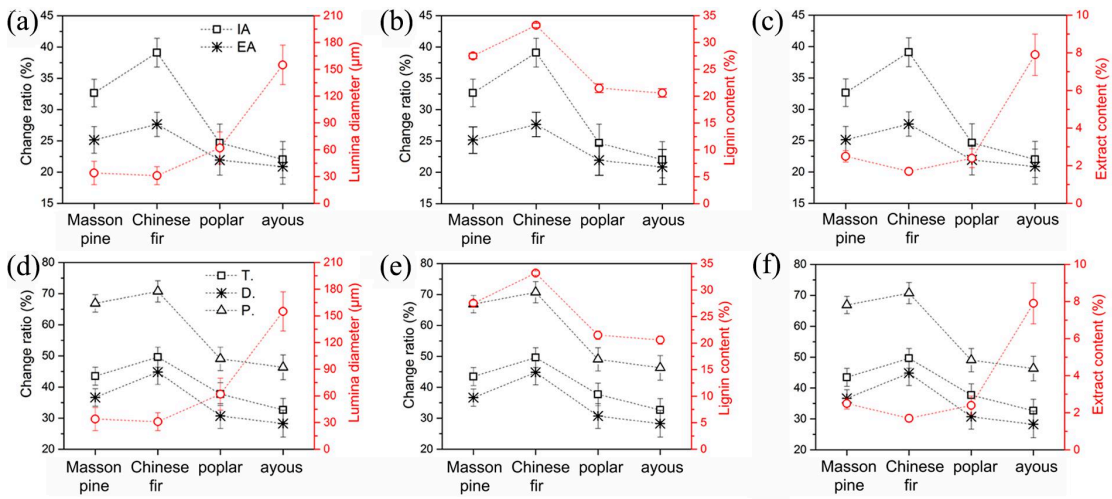


Fig.2-13 The relationship of contact angles change ratio and (a) lumina diameter, (b) lignin content and (c) extract contact, respectively, with four species. The relationship of surface energy change ratio and (d) lumina diameter, (e) lignin content and (f) extract contact, respectively, with four species.

Tab.2-9 O/C ratio and C1s assignments in X-ray photoelectron spectra under HVEF treatment and compared with the control.

| | masson pine | | | Chinese fir | | |
|---|---|---|---|---|---|---|
| | Untreated | 60 kV | Δ(%) | Untreated | 60 kV | Δ(%) |
| $C1_S$(%) | 71.06 | 65.70 | / | 64.09 | 55.44 | / |
| $O1_S$(%) | 22.94 | 28.30 | / | 35.91 | 44.56 | / |
| O/C | 0.32 | 0.43 | 34% | 0.56 | 0.80 | 43% |
| C1(%) | 64.46 | 41.43 | -36% | 60.21 | 23.6 | -60% |
| C2(%) | 22.76 | 31.54 | 39% | 21.99 | 32.4557 | 48% |
| C3(%) | 3.53 | 8.78 | 149% | 13.84 | 35.195 | 154% |
| C4(%) | 9.26 | 18.25 | 97% | 4.47 | 9.3885 | 110% |
| | poplar | | | ayous | | |
| | Untreated | 60 kV | Δ(%) | Untreated | 60 kV | Δ(%) |
| $C1_S$(%) | 71.38 | 66.51 | / | 70.95 | 67.28 | / |
| $O1_S$(%) | 28.82 | 33.65 | / | 29.05 | 32.72 | / |
| O/C | 0.40 | 0.51 | 25% | 0.41 | 0.49 | 19% |
| C1(%) | 50.16 | 29.5 | -41% | 73.33 | 67 | -9% |
| C2(%) | 29.61 | 36.3813 | 23% | 18.19 | 21.2832 | 17% |
| C3(%) | 9.7 | 19.845 | 105% | 0.8 | 1.54 | 93% |
| C4(%) | 9.52 | 14.2784 | 50% | 7.68 | 10.3616 | 35% |

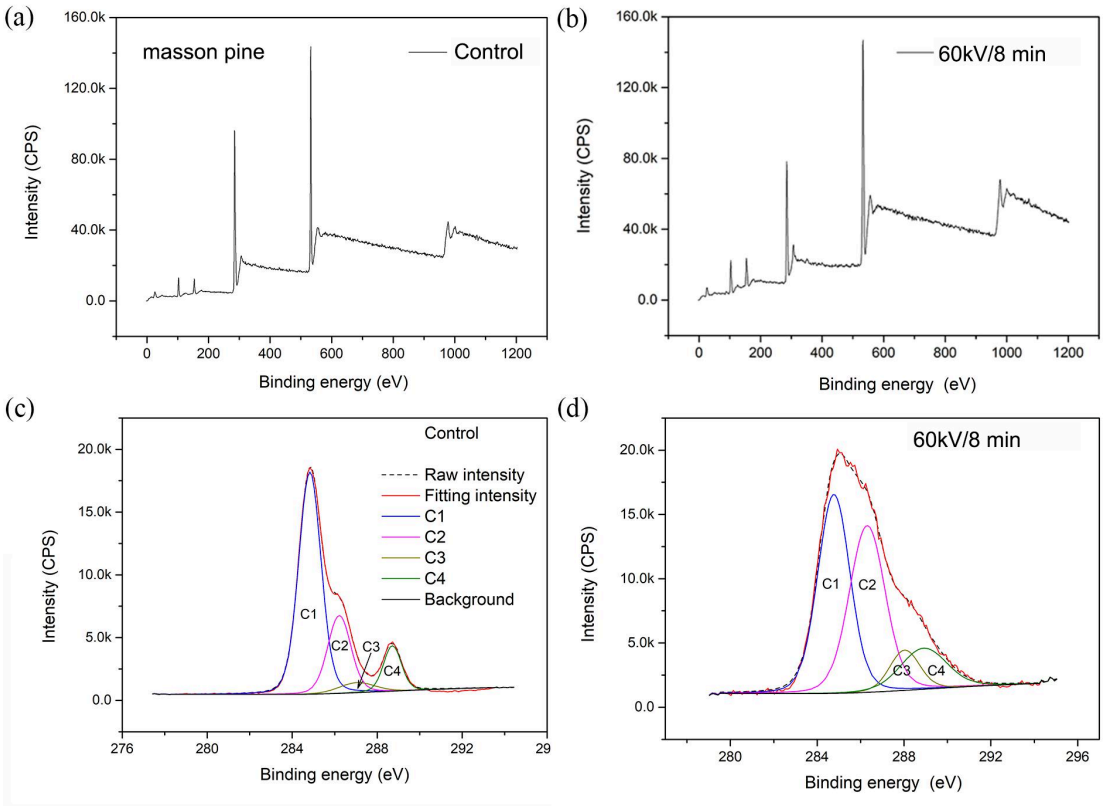


Fig.2-14 X-ray photoelectron spectra for C1s and O1s (a) control, (b) treated; C1-C4 components under HVEF treatment (c) control, (d) treated

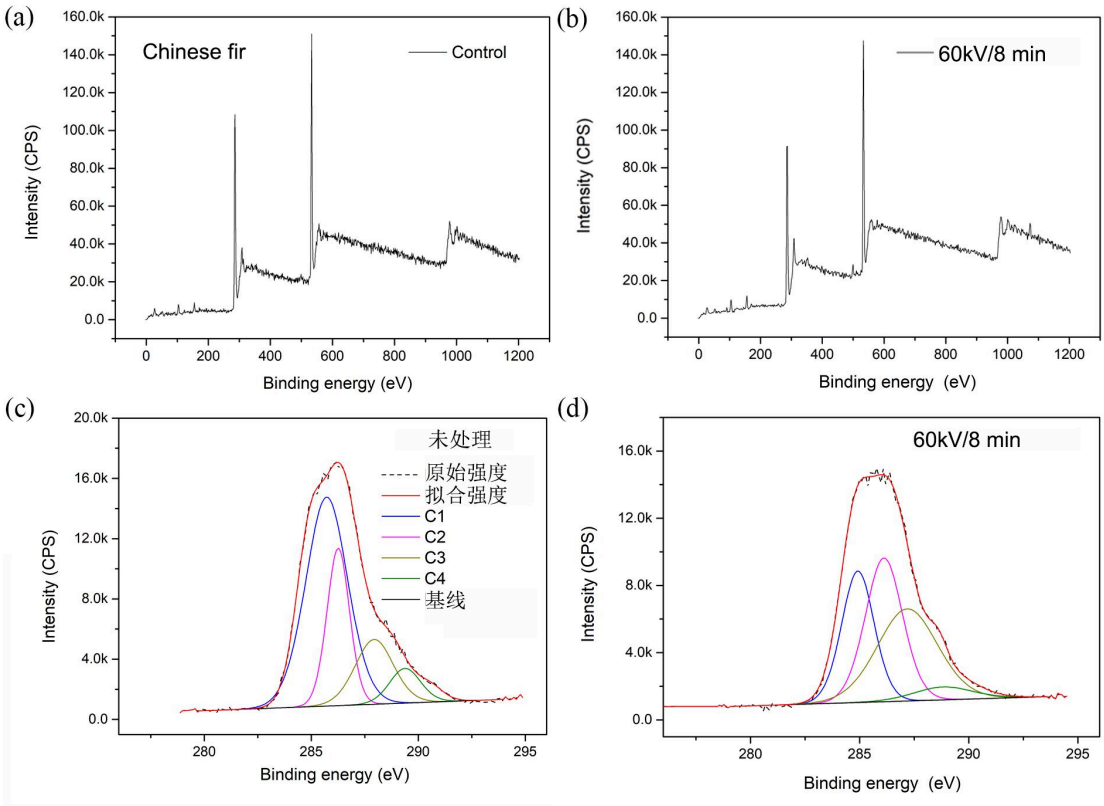


Fig.2-15 X-ray photoelectron spectra for Chinese fir C1s and O1s (a) control, (b) treated; C1-C4 components under HVEF treatment (c) control, (d) treated.

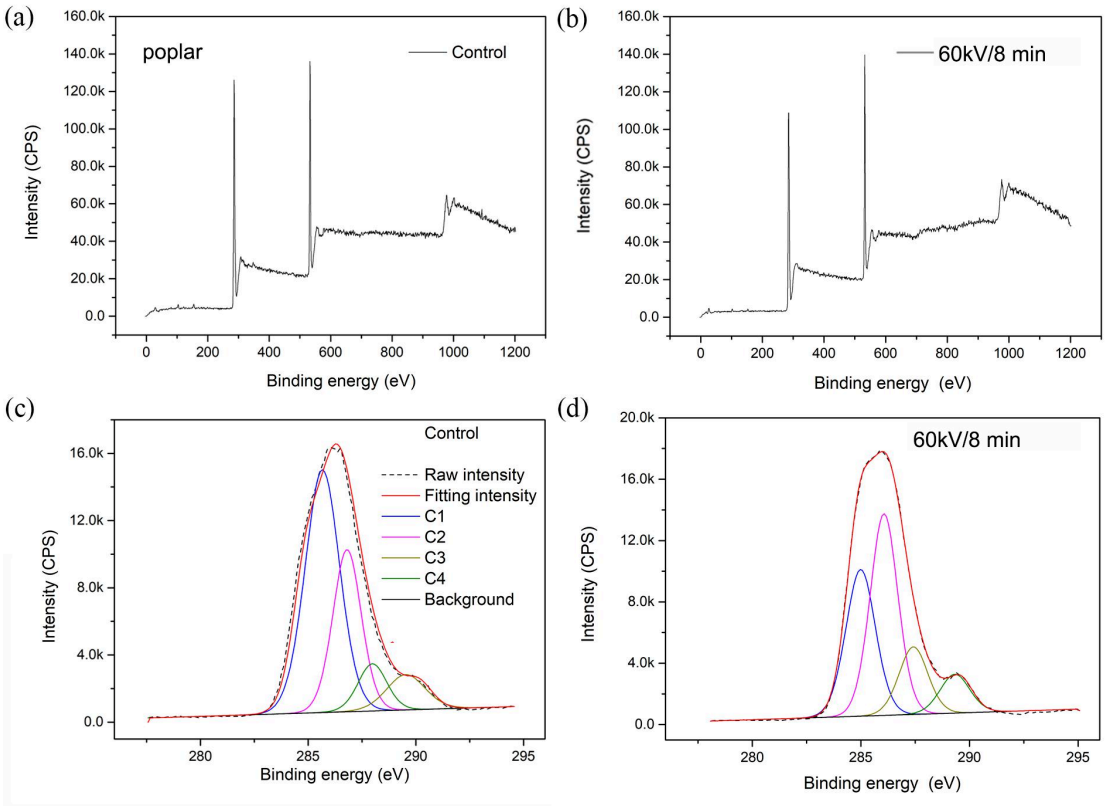


Fig.2-16 X-ray photoelectron spectra for poplar C1s and O1s (a) control, (b) treated; C1-C4 components under HVEF treatment (c) control, (d) treated

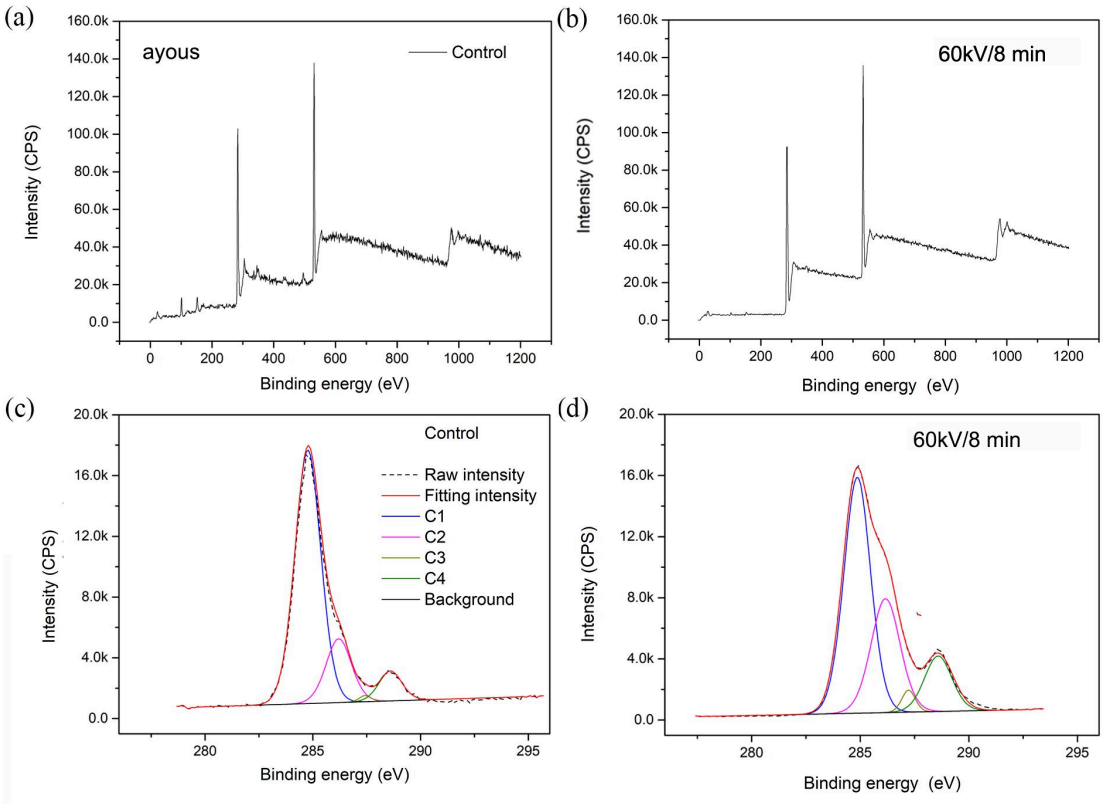


Fig.2-17 X-ray photoelectron spectra for ayous C1s and O1s (a) control, (b) treated; C1-C4 components under HVEF treatment (c) control, (d) treated

### 2.3.4 The effect of HVEF on the reaction characteristics of wood and silver particles

As shown in Figure 2-18, the X-ray photoelectron spectroscopy analysis chart of wood samples under different treatment time was achieved. The characteristic peaks at 285.8mV, 368.8/373.8mV and 532.8mV were shown in the broad peak spectrum, which indicated the positions of C1s, Ag 3d5/2, Ag 3d3/2 and O1s elements, respectively. It could be observed from the figure that the silver particles in the sample have increased significantly after treatment. As the treatment time increased, the concentration of silver particles increased significantly. These results could be mainly attributed to more excited silver particles and electrons colliding with the

wood surface and, the particle concentration would reach a saturated state under a certain voltage [165].

In addition, it could be concluded from Table 2-10 that the O/C element ratio of the sample significantly reduced after treatment with the increase of the treatment time, which could be mainly attributed to the reactions between silver particles and wood chemical groups ( –OH and –CHO, etc.), and significantly increased the excited silver particles covering the wood surface [186]. As shown in Table 2-10, the distribution of the four components of the narrow C1s peak in the X-ray photoelectron spectroscopy has been further studied. It could be observed that the C2 component in the sample significantly reduced and C1 relatively increased after treatment. This result was consistent with the that of the O/C ratio. This was mainly because the silver particles reacted with the chemical groups (–OH and –CHO) in the wood, which were largely covered on the wood chemical groups of the lignin and cellulose components [187]. At the same time, it could be concluded that the C3 and C4 components in the treated wood sample increased significantly, indicating that the silver particles have in-situ reactions with the C=O or C–O groups. The characteristic peaks of the reaction between silver particles and wood sample groups were explained in detail in FTIR. In addition, the largest change rate of the C1s component and the highest concentration of silver particles were observed for the sample treated for 48 hours.

In order to analyze the structure and chemical composition of Ag3d, X-ray photoelectron spectroscopy was used for the samples under different conditions. As shown in Table 2-10, no silver signal was observed in the untreated wood samples.

For the treated wood sample, the characteristic peak at 368.8 mV was divided into four components, namely Ag(0), Ag(I), Ag(III) and Ag(III)SAT, indicating that the phenomenon of oxidation occurred in an oxidizing atmosphere (O2, O3 (generated in a HVEF)) for the silver element and silver oxide was produced. Under HVEF treatment, the silver particles in the oxide interacted with the wood and a chemical combination reaction was found [188]. The sample treated for 48h contained higher Ag(III), which was mainly due to the increase in the treatment time leading to more silver oxide produced with more Ag(III) component. Therefore, the change of the Ag(III) composition in the sample depended on the change of the treatment time. A longer treatment time will increase the degree of silver oxidation. Previous studies have shown that the higher the Ag(III) concentration in silver oxide has a positive effect on improving the anti-corrosion performance of wood samples [189].

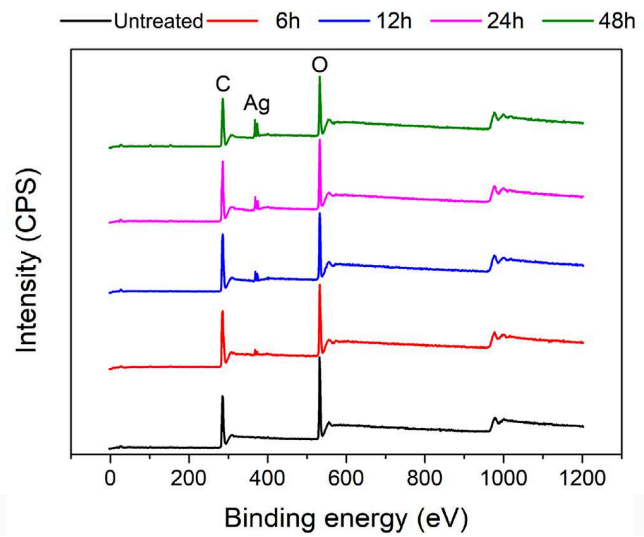


Fig.2-18 X-ray photoelectron spectra with detected elements of C, O and Ag for (a) untreated

Tab.2-10 Ag 3d, C1s and O1s concentration and components for C1s and Ag 3d.

| | Untreated | Treated | | | |
|---|---|---|---|---|---|
| | | 6h | 12h | 24h | 48h |
| Ag 3d (%) | 0 | 1.85 | 3.80 | 10.12 | 10.71 |
| $C1_S$ (%) | 66.64 | 66.72 | 68.75 | 65.56 | 66.04 |
| $O1_S$ (%) | 33.36 | 31.43 | 27.45 | 24.32 | 23.25 |
| O/C | 0.50 | 0.47 | 0.40 | 0.37 | 0.35 |
| C1 (%) | 39.67 | 43.37 | 48.36 | 50.71 | 51.86 |
| C2 (%) | 39.03 | 33.33 | 27.15 | 24.97 | 20.68 |
| C3 (%) | 10.59 | 11.86 | 12.32 | 12.99 | 13.33 |
| C4 (%) | 10.71 | 11.44 | 12.17 | 13.33 | 14.13 |
| Ag (0) | 0 | 30.01 | 23.39 | 22.76 | 21.08 |
| Ag (I) | 0 | 52.87 | 53.57 | 50.31 | 51.17 |
| Ag(III) | 0 | 8.28 | 10.71 | 12.69 | 13.15 |
| Ag(III) sat | 0 | 8.84 | 12.33 | 14.24 | 14.60 |

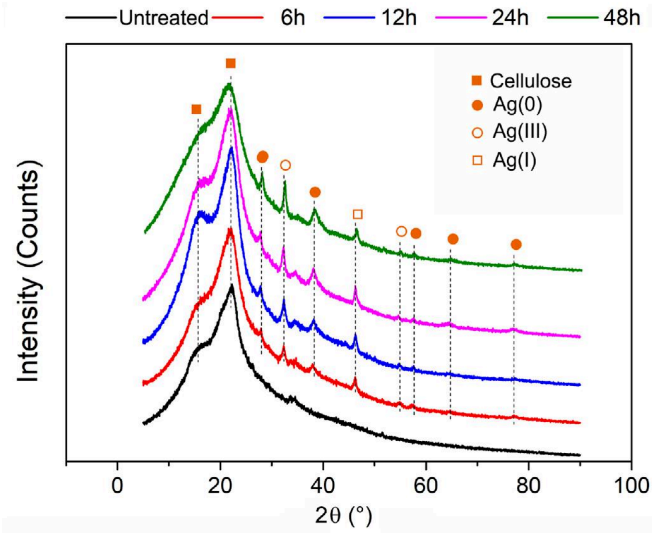


Fig.2-19 X-ray diffraction patterns of treated wood samples with different treatment durations compared with untreated sample.

As shown in Figure 2-19, it characterized the changes in the X-ray diffraction spectrum of the untreated sample and the treated wood sample. According to previous studies, the diffraction peaks at 15° and 21° are attributed to the crystalline region of wood cellulose [190]. After the silver particle-HVEF synergistic treatment, according to the powder diffraction peak standard (JCPDS, No. 5-2272, 84-108 and 42-084), some new diffraction peaks were discovered and marked in the figure. They are Ag(0) (2θ=28°, 38°, 64°, 58° and 78°), Ag(III) (2θ=33° and 55°) and Ag(I) (2θ=46°). At the same time, no diffraction peaks of any other impurities were detected. Compared with other treatment conditions, after 48h treatment, the diffraction peaks of silver particles in the sample were higher. In addition, the treated wood sample showed that the silver particles contained in the treated wood sample were nanometer-sized crystalline with an average particle size of less than 50 nm from the X-ray diffraction pattern. According to previous literature, it was shown that silver particles of this size were more likely to enter the internal microstructure of

wood pipe pores and interacted with the active chemical groups in cellulose and lignin. At the same time, it has the possibility of reducing leaching[187].

As shown in Figure 2-20, FTIR spectra of untreated samples and treated wood samples were characterized. It could be observed from the figure that the characteristic peak at 3405 $cm^{-1}$ significantly reduced under the treatment of HVEF (attributed to the functional group −OH, tensile vibration). In the treated sample, the characteristic peak at 3405 $cm^{-1}$.moved to 3430 $cm^{-1}$. As the treatment time increased, the characteristic peak at 3405 $cm^{-1}$ droped significantly, especially for the treatment time of 48h. This result showed that HVEF treatment promoted the accumulation of silver particles on the surface of wood cell walls and the in-situ reaction with the active groups (hydroxyl groups, etc.) on the wood surface [191]. In addition, the characteristic peak at 2928$cm^{-1}$ was attributed to the tensile vibration of the C–H functional group; it is a newly generated characteristic peak at 1625$cm^{-1}$, attributed to the vibration peak of C=O bond [192]. After HVEF treatment, these characteristic peaks in the treated sample increased significantly. the highest increments for these characteristic peaks were found in the wood sample treated for 48 hours. These results indicated that the silver particles in silver oxide were tightly bound to wood chemical groups [193]. This was consistent with the decrease of O/C ratio and the change of C1-C4 composition obtained in X-ray photoelectron spectroscopy.

After 4 weeks of exposure to wood rot fungi, the mass loss of the sample reached to ≈5% for the HVEF treatment time of 6h and 12h; after the sample was exposed to white rot fungus and brown rot fungus for 16 weeks, the mass loss was less than 1% for the treatment time of 24h. These results were mainly due to the in-

situ chemical binding between silver particles and oxygen-containing groups in the wood cell wall (obtained from X-ray photoelectron spectroscopy and infrared spectroscopy). The silver particles had significant resistance to wood rot fungi. The higher the concentration of silver particles, the higher the degree of destruction and dissociation of wood-rot fungus cells [194]. At the same time, after HVEF treatment, the leaching rate of silver particles of the sample was between 1.22% and 3.94%.

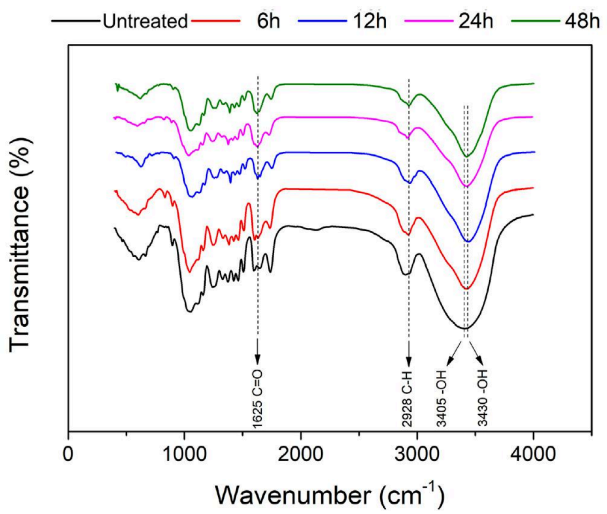


Fig.2-20 Fourier transform infrared spectroscopy of treated wood samples with different treatment durations compared with untreated sample

### 2.3.5 The effect of HVEF treatment on the surface characteristics of bamboo

Bamboo is considered a renewable biomass material. Because of its wide range of sources, fast growth, high strength, and low cost, it is one of the ideal processing materials to replace steel and wood. Bamboo composite materials are widely used in decoration, construction and transportation fields, such as bamboo flooring, bamboo building templates and bamboo laminate materials [195-198]. However, in the application of these bamboo composite materials, many bonding problems have occurred, including poor weather resistance, cracking of the adhesive layer, and low mechanical properties. These problems are mainly attributed to the special surface

and processing technology of bamboo [199]. The surface of bamboo green naturally contains aliphatic and low-oxygen wax skin, which has a negative impact on wettability. Bamboo is a complex heterogeneous material composed of bamboo green, bamboo meat and bamboo yellow. The two parts of bamboo green and bamboo yellow have completely different morphological and chemical characteristics. The cellulose and lignin content of bamboo green are higher than that of bamboo yellow. With the decrease of the number of vascular bundles from the bamboo green surface to the bamboo yellow surface, the density gradually decreased. The bamboo yellow surface presents a lower density and fewer chemically active groups, which will affect the surface characteristics of bamboo composites, the degree of polymer reaction and other factors. [200].

As shown in Figure 2-21, the free radical content of the bamboo sample increased significantly after treated by HVEF. The bamboo green part has a higher increment of free radical than that of bamboo yellow part. When the treatment condition is 60kV/14min, the highest change rate of bamboo green was 35%, and the highest change rate of bamboo yellow was 28%. These results can be explained by the fact that triggered electrons collided with oxygen and water molecules in the atmosphere under HVEF treatment, resulting in an increase in the chemical bonds that broken on the surface of the bamboo [201]. With the increase of the treatment time, the surface free radical content increased slightly. In previous studies, it was also found that the free radical change rate of wood did not significantly increase with the increment of treatment time [174]. In addition, as shown in Table 2-11, a comparative analysis of the cellulose, lignin, and hemicellulose content of bamboo was conducted, it could be found that the cellulose content and lignin content of bamboo green were greater than

those of bamboo yellow. In addition, it was found that the change rate of free radicals in bamboo green was higher than that in bamboo yellow. This could be mainly attributed to the fact that the content of lignin in bamboo green is more than that in bamboo yellow. The chemical groups have a positive effect on the change rate of free radicals [163].

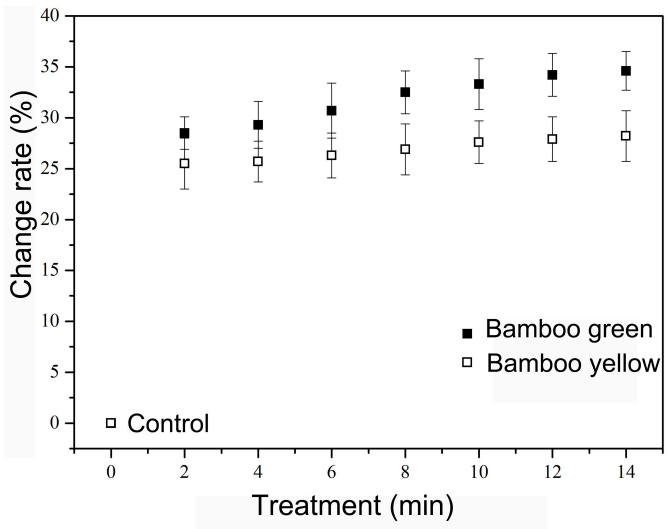


Fig. 2-21. Free radicals for BS and BP surfaces with the relationship of treating times.

Tab.2-11 Chemical components for bamboo skin and bamboo pith

| | Cellulose (%) | Hemi-celluloase (%) | Lignin (%) | Extracts (%) |
|---|---|---|---|---|
| bamboo skin | 44.20 (0.50) | 20.37 (0.40) | 32.56 (0.37) | 2.50 |
| bamboo pith | 35.87 (0.41) | 26.15 (0.42) | 27.88 (0.40) | 3.92 |

The changes in the contact angle and free energy of the bamboo green and bamboo yellow surfaces before and after the HVEF treatment were showed Figure 2-22. It

could be observed from the figure that the initial contact angle and equilibrium contact angle of bamboo green and bamboo yellow are significantly reduced after HVEF treatment (Figure 2-22 (a) ~ (b)). The reduction rate of the contact angle for bamboo green was greater than that of bamboo yellow. In addition, it could be observed from Fig. 2-22(c)~(d) that for bamboo green and bamboo yellow, the free energy including the total free energy content (T.) and the dispersed free energy content (D .) and the content of polar free energy (P.) increased significantly after HVEF treatment. After analysis and comparison, it was observed that after the HVEF treatment, the change rate of the free radical content and the change rate of contact angle for bamboo green were greater than that of bamboo yellow. These results indicated that lignin content, extract content and vascular bundle cell distribution are some important conditions have great influence on the treatment of HVEF. After HVEF treatment, a large amount of extract components migrated, which affected the wetting of the adhesive on the substrate [185]. In addition, the vascular bundles in bamboo green are closely arranged and the surface density is high, so their contact angles are greater than that of bamboo yellow. However, after HVEF treatment, due to the high lignin content of bamboo green, the free radical content was greater than that of bamboo yellow, so the change rates of the initial contact angle and equilibrium contact angle of bamboo green were greater than that of bamboo yellow.

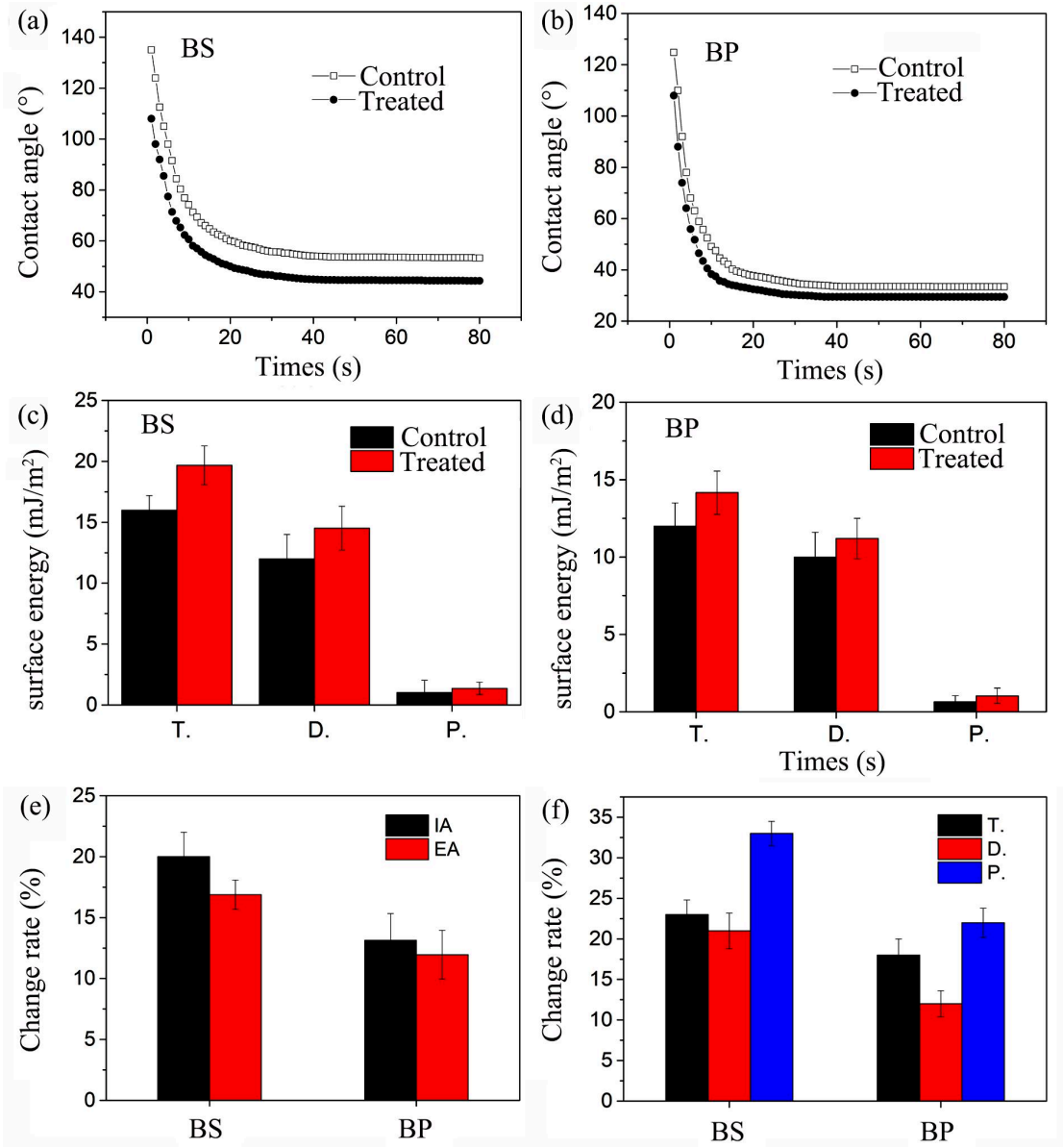


Fig.2-22 Dynamic contact angle measurement for (a) bamboo skin, (b) bamboo pith treated by HVEF and compared with the control. The surface energy displayed for (c) bamboo skin, (d) bamboo pith treated by HVEF and compared with the control, consisting of IA, initial contact angle; EA, equilibrium contact angle;T., surface total free energy; D., surface free energy of dispersion components and P., surface free energy of polar components. The change ratios of (e) contact angles and (f) surface energy were also displayed.

In order to further explain the changes of the chemical groups on the surface of bamboo materials induced by HVEF. X-ray photoelectron spectroscopy was used to qualitatively analyze the distribution of chemical groups and elements on the surface

of bamboo. As shown in Figure 2-23, the changes in the oxygen and carbon concentrations and chemical groups of the bamboo samples after treated by HVEF were characterized. From the broad peak diagram of the X-ray photoelectron spectrum, it showed that carbon and oxygen were located at about 284eV and 532eV of binding energy, respectively (Figure 2-23 (a). In the bamboo green, some silicon elements were observed at 98eV, which was mainly due to the waxy and siliceous layers on the surface of the bamboo green [202, 203]. As shown in Table 2-12, after the HVEF treatment, the relative changes of the oxygen and carbon elements were obtained. In the untreated sample, the oxygen/carbon element (O/C) of bamboo yellow was higher than that of bamboo green. This was because some silicon elements covered the surface of bamboo green, and some oxygen elements could not be accurately detected. After HVEF treatment, the O/C ratio of bamboo green and bamboo yellow increased significantly. The degree of polarization and oxidation of the bamboo surface increased as well. At the same time, higher change rate of the O/C ratio was obtained in bamboo green than that of bamboo yellow. This result was attributed to the fact that a higher content of free radicals on the surface of the bamboo and more broken chemical bonds (oxygen atoms and ions) were found for the bamboo green. At the same time, the content of cellulose and lignin in the bamboo green component were higher, leading to higher degree of polarization and oxidation than that of bamboo yellow [204, 205].

The C1s peak spectrum in X-ray photoelectron spectroscopy was shown in Figure 2-24. The C1s peak of biomass materials consists of four types of carbon atoms, consisting of C1, C2, C3, and C4. The C1 component mainly represents the content of lignin and extracts. C2, C3, and C4 mainly represent cellulose and semi-fibrous

components, and the C2 component is a carbon-oxygen combination, mainly connected to a single non-carbonyl oxygen atom. The C3 component mainly refers to the group connected to the carbonyl oxygen or non-carbonyl oxygen atom, and the C 4 component mainly refers to the group connected to the non-carbonyl oxygen and carbonyl oxygen atom [206]. The changes in the integrated areas of the four sub-peaks before and after the HVEF treatment were characterized in Table 2-12. For the components of bamboo green and bamboo yellow, the C1 component decreased while the C2, C3 and C4 components increased significantly. This result was consistent with the increase in breaking chemical bonds (containing oxidative bond groups or ions), free radical content, and the O/C ratio. This result also showed that oxygen-containing functional groups including –OH, C–O, and C=O were significantly increased after HVEF treatment, leading to increased C2-C4 component and decreased C1 component. In addition, the increase of C2, C3 and C4 components in bamboo green was higher than that of bamboo yellow. These results were mainly due to the higher content of lignin and cellulose in bamboo green than that in bamboo yellow (as shown in Table 2-11). After the treatment of HVEF, more broken chemical bonds, oxygen-containing functional groups, and free radicals were induced on the bamboo surface, thereby the C2, C3, and C4 components and the O/C ratio significantly increased, leading to the increase of surface energy and wetting ability [207-209].

Tab.2-12 C1s components and O/C ratios for BS and BP surfaces investigated by X-ray photoelectron spectra.

| | BS | | | BP | | |
|---|---|---|---|---|---|---|
| | Untreated | Treated | Δ (%) | Untreated | Treated | Δ (%) |
| $C1_S$ (%) | 69.50 | 66.40 | / | 70.40 | 66.30 | / |
| $O1_S$ (%) | 23.70 | 30.01 | / | 25.45 | 27.80 | / |
| O/C | 0.34 | 0.45 | 32% | 0.36 | 0.42 | 17% |
| C1(%) | 59.20 | 34.16 | -42% | 46.36 | 35.91 | -23% |
| C2(%) | 23.01 | 30.70 | 33% | 30.45 | 34.19 | 12% |
| C3(%) | 7.28 | 17.21 | 136% | 12.74 | 15.41 | 21% |
| C4(%) | 10.51 | 17.93 | 71% | 10.45 | 14.49 | 39% |

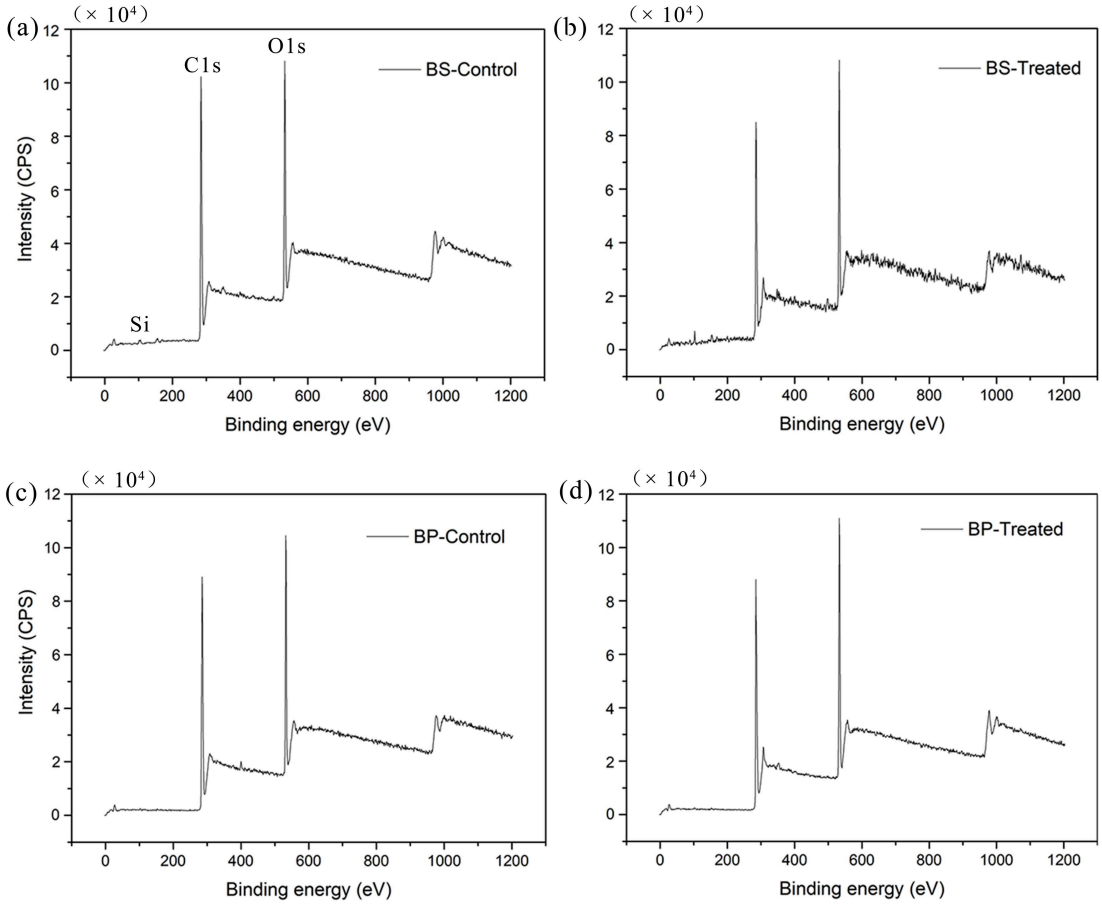


Fig.2-23 Carbon and oxygen elements in X-ray photoelectron spectra for (a) untreated bamboo skin and (b) treated bamboo skin; for (c) untreated bamboo pith and (d) treated bamboo pith.

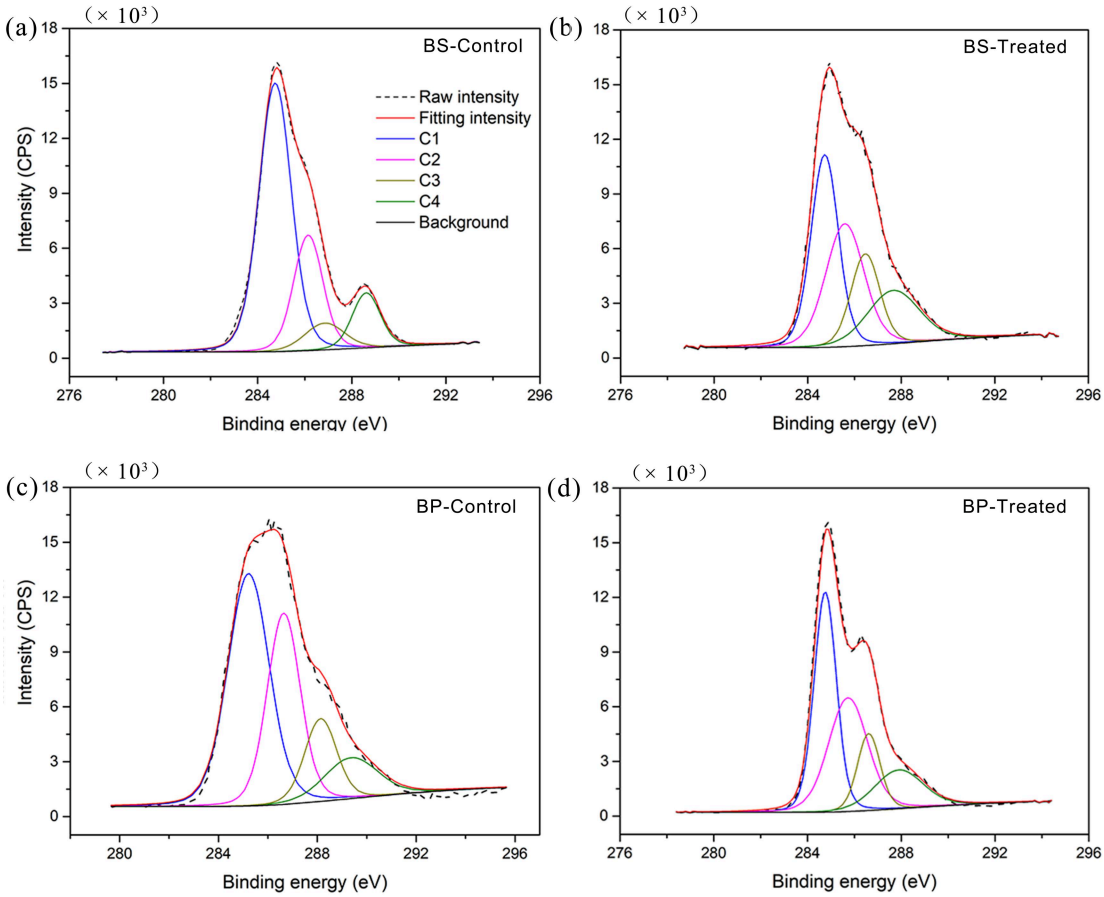


Fig.2-24 (a) C1s components in X-ray photoelectron spectra for (a) untreated bamboo skin and (b) treated bamboo skin; for (c) untreated bamboo pith and (d) treated bamboo pith.

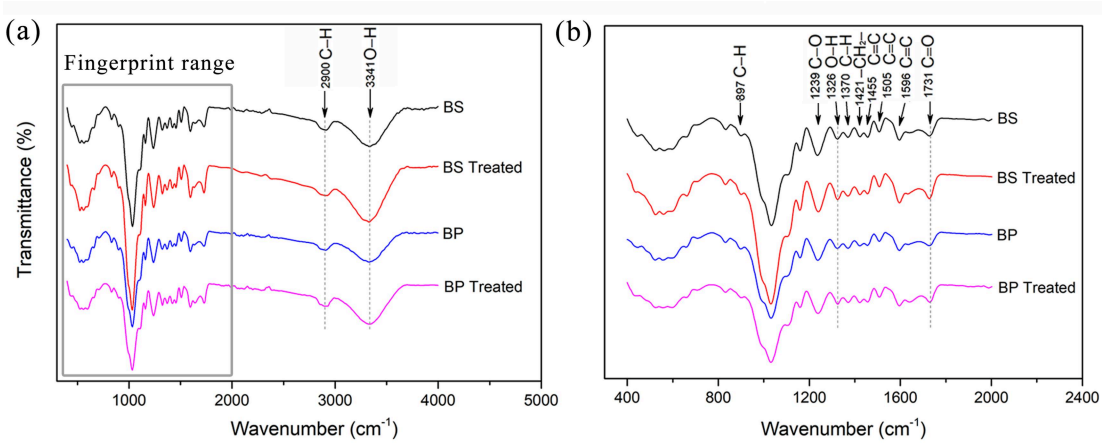


Fig.2-25 Fourier transform infrared spectroscopy for HVEF treated BS and BP samples compared with the controls, (a) the range from 400~4000cm-1 (b) 400~2000cm$^{-1}$

In order to further study the formation of chemical bonds and the mechanism of chemical changes, FTIR spectra of bamboo samples before and after HVEF treatment were measured. As shown in Figure 2-25, the testing range of the bamboo surface is 400~4000cm$^{-1}$, and the fingerprint spectrum range is 400~2000 cm$^{-1}$ [202]. As shown in Table 2-13, the spectral values corresponding to the main characteristics of bamboo were characterized. It could be observed from the FTIR spectra that the chemical groups on the surface of the bamboo have changed significantly. The stretching vibration peak at 3341cm$^{-1}$ (–OH, water molecules and wood chemical groups) increased significantly. The free carbonyl, acetyl or carboxylic acid tensile vibration peaks at 1326cm$^{-1}$ (–OH, cellulose) and 1731cm$^{-1}$ (C=O, C–O cellulose and hemicellulose) increased significantly as well. After HVEF treatment, the change rates of these oxygen-containing chemical groups in the bamboo green sample were greater than that in the bamboo yellow. These results were consistent with the above-mentioned surface characteristics. This was due to the high content of lignin and cellulose in bamboo green, as shown in Table 2-11. The peaks at 1421cm$^{-1}$ (C-H, aromatic ring skeleton vibration), 1505cm$^{-1}$ and 1596cm$^{-1}$ (C=C, aromatic ring) have no significant changes. The peaks at 897 cm$^{-1}$ and 1370 cm$^{-1}$ caused by the C–H bond of cellulose and hemicellulose also showed no significant changes. These results can further explain the changes in the O/C ratio and C2-C4 components of the bamboo-green and bamboo-yellow materials before and after HVEF treatment in the X-ray photoelectron spectroscopy.

Tab.2-13 Chemical groups assignments for bamboo Fourier transform infrared spectroscopy

| Wavenumber ($cm^{-1}$) | Chemical groups | Attributions |
|---|---|---|
| 3341 | O–H | O–H stretching vibration |
| 2900 | C–H | C–H stretching vibration |
| 1731 | C=O | C=O stretching vibration ($CH_3C=O$) |
| 1646 | C=O | C=O stretching vibration (lignin) |
| 1596 | C=C | Carbon skeleton vibration of benzene rings (lignin) |
| 1505 | C=C | Carbon skeleton vibration of benzene rings (lignin) |
| 1455 | C–H, C=C | C–H bending vibration（$CH_2$ in lignin and xylan); carbon skeleton vibration of benzene rings (lignin) |
| 1421 | C–H | benzene rings, C–H stretching vibration |
| 1370 | C–H | C–H, bending vibration (cellulose and hemi-cellulose) |
| 1326 | –OH | phenolic group (cellulose) |
| 1239 | C–O–C | C–O–C stretching vibration (cellulose and hemi-cellulose)；(guaiacyl, lignin) |
| 1055 | C–O | C–O stretching vibration |
| 897 | C–H | C–H bending vibration (cellulose) |

## 2.4 Summary

(1) After HVEF treatment, the free radical content of wood increased significantly, the initial contact angle and equilibrium contact angle decreased, the O/C ratio and the C2~C4 peak components increased significantly. In addition, in FTIR spectrum, the characteristic peak at the oxygen group significantly improved. With the increase of the treatment voltage (0~60kV), the free radicals, contact angle, O/C ratio and the change rates of characteristic peaks at oxygen-containing groups all increased significantly. As the voltage and time increased, more electrons were in the excited

state. After colliding with each other and hitting a large number of molecular chemical groups in the air, more broken free chemical bonds and ions would act on the surface of the materials. The change rate of free radicals content was in dynamic equilibrium.

(2) Varied results for the surface characteristics of wood different sections were obtained under the treatment of HVEF. The change rates of the surface chemical property parameters (free base, contact angle) were in the order as follows: cross section < tangential section < radial section. This was mainly due to the fact that a large number of chemical functional groups were exposed on the longitudinal section for the radial and tangential section. At the same time, tracheid channels (cell inner walls) were closely arranged on the longitudinal section while a large number of pores on the transverse section. The excited electrons and broken chemical groups could not fully react with the chemical groups on the cell wall. In addition, a large number of pit structures were on the radial section, which had a great effect on the ion exchanging between tracheids. The aspirated pits had negative effects on the change of contact angles after HVEF treatment.

(3) The influence of HVEF on the surface properties of different species were different. According to the change rates of the surface chemical properties parameters (free radicals, contact angle), the order was as follows: ayous < poplar < masson pine < Chinese fir. This was mainly because of the tracheid structure of softwood and the higher content of lignin. The chemical groups in lignin could significantly affect the content of free radicals on the surface of the material.

(4) Under the treatment of HVEF, the excited silver particles chemically combined with wood functional groups in different oxidation forms, Ag(0), Ag(I) and Ag(III). The highest concentration of silver particles in the sample after 48h treatment was 10.71%. The particle size of silve was of nanometer range (average particle size is less than 50nm), which has a certain crystal morphology. After the treatment exceeding 24h, the treated sample has high anti-corrosion performance with the mass loss less than 1%, and the leaching rate less than 4%.

(5) The effect of HVEF on the surface characteristics of bamboo was also significant. After HVEF treatment, the content of free radicals in the bamboo material increased significantly, the initial contact angle and equilibrium contact angle decreased, the O/C ratio and the C2~C4 peak components increased significantly. The characteristic peaks at the oxygen-containing groups increased significantly. However, the effect of HVEF on the surface chemical properties of bamboo green and bamboo yellow was different. The change rate of surface characteristic parameters in bamboo green was greater than that of bamboo yellow. This was mainly due to varied chemical properties of bamboo green and bamboo yellow and microstructures of vascular bundles.

Therefore, under the treatment of HVEF, the physical and chemical properties of wood and bamboo can be significantly improved, which is beneficial to improve the interphase properties of composite materials.

# Chapter III The influence of HVEF treatment on the chemical composition and rheological behavior of the adhesive

## 3.1 Introduction

Adhesives play an important role in the preparation process of composite materials and determine various performance of composite materials. In order to prepare composite materials with high mechanical strength and durability, the modification of adhesives generally includes toughening and strengthening treatments. Toughening the resin is an effective method to improve the characteristics of the adhesive performance [63, 65]. Toughening agents are added during or after the resin synthesis to improve the thermal stability of the adhesive and enhance the ability to transfer and disperse stress. For strengthening treatment, the usage of nano-silica and nano-cellulose and other nano-materials could improve the mechanical properties of the adhesives. In addition, the addition of nano-montmorillonite, ceramic fiber materials and nano-carbon materials to the adhesives can improve their performance of thermal stability [70, 71]. However, the modification methods for the surface, adhesive and bonding interphase of biomass materials at this stage belong to the category of chemical pretreatment, and the penetration form of the adhesive in the material during the preparation of composite materials is not considered. At the same time, whether a continuous, uniform and dense adhesive layer is formed at the interphase of composite materials also has an important effect on the properties of composite materials such as mechanics and durability.

HVEF treatment used in material preparation and modification process that has a unique effect on the surface and interphase of the substance [104, 156]. Under the treatment of the electric field, the excited free electrons and the broken chemical bonds collided with the chemical groups on the surface of the material, thereby increasing the free radical content and free energy on the surface. In addition, according to the research of electrohydrodynamics, the distribution form and molecular flow behavior of the liquid will also be affected by HVEF treatment. Its flow pattern and internal chemical structure will continue to change with the treatment of HVEF [121-123]. The physical and chemical properties of wood, adhesives and the bonding interphase are all affected by HVEF because of the improvement surface and interphase properties of composites. However, the impact of HVEF treatment methods on the properties of adhesives has not yet been clear.

Based on HVEF treatment, two commonly used adhesives, urea-formaldehyde resin and phenol-formaldehyde resin, were selected in this study. The influence of different HVEF conditions (treatment time and voltage) on the rheology and chemical group changes of the adhesive was explored. The induction mechanism of HVEF on the reaction mode of the adhesive is analyzed.

## 3.2 Materials and methods

### 3.2.1 Materials

Adhesives include urea-formaldehyde resin (UF) and phenolic resin (PF), both of which are self-made in the laboratory.

Preparation method of urea-formaldehyde resin: 213g of formaldehyde (37%), adding it to a 500ml four-necked flask, starting the stirrer, and adjusting the pH concentration to 7.5-8.0 with 30% NaOH solution. Adding 80g of urea for the first time and slowly increasing the temperature to 90°C within 30-40 minutes. Keeping at 90°C for 40 minutes, measuring the pH value three times at this stage to observe the trend of pH changes. After that, adjusting the pH to 4.6-5.1 with 20% $NH_4CI$ solution, and reacting at 90-94°C. After a period of time, taking a drop of the reaction solution and dropping it into the water at room temperature of 20°C. The end point is when white clouds appear. At this time, alkali should be added immediately (30% NaOH solution), neutralizing to 7.0-7.5. Adding 20g of urea for the second time and keeping it warm for 15 minutes. Pumping water to cool to 45°C and adjusting the pH to 7.0-7.5 with 30% NaOH. After cooling to room temperature, storing in a refrigerator at 6°C. Parameters: the molar ratio of formaldehyde to urea is 1.5, the solid content is 50%, and the viscosity is 109mPa·s (rotating viscosity instrument, DV-79+Pro), 1% ammonium chloride (according to solid content) is mixed with adhesive when applied. All chemical reagents were purchased from Jiangsu Nanjing Chemical Pharmaceutical Company.

Phenol formaldehyde resin preparation method: adding 470 g of phenol, 200 g of sodium hydroxide solution (40%) and 1258 g of distilled water to a 3-necked flask (5000 ml). After mixing, keeping it at 40°C for 25 minutes. Next, adding 649 g of formaldehyde solution (37%). After that, the temperature rose to 85°C within 30 minutes, and the heating continued for 30 minutes. Then, the temperature was lowered to below 70°C and 162 g of formaldehyde solution was added. The mixture was heated to 90°C for 90 minutes. Finally, cooling the temperature to 25°C. After

preparation, the resin is stored in a refrigerator at 6°C. Parameters: the molar ratio of formaldehyde to phenol is 2:1, the viscosity is 346mPa·s, and the solid content is 45%.

### 3.2.2 HVEF method

The HVEF generator used in this experiment was produced by Hangzhou Jingtong Co., Ltd. (JT207K-1, HC-JDGC-C), Zhejiang, China. The sample was placed in a flat electric field within a hot press. The average thickness of the aluminum plate is 3mm. As shown in Figure 2-1, the upper plate is connected to the high-voltage generator and the lower plate is grounded. 2mL resin was put into a polytetrafluoroethylene container and the container was placed between the two plates. After setting the temperature, the voltage value was adjusted and the high-voltage generator was turned on. After the treatment time was reached, the generator was turned off and the test material was taken out. The resin was put into a 5mL glass bottle and set aside. The test conditions selected for this test are shown in Table 3-1:

Tab.3-1 The parameters selected for high voltage electric field

| Temperature(°C) | Voltage (kV) | Time (min) |
|---|---|---|
| 120, 145 | 0 | 0, 2, 4, 6, 8 |
| 120, 145 | 5 | |
| 120, 145 | 10 | |
| 120, 145 | 20 | |
| 120, 145 | 60 | |

### 3.2.3 FTIR spectroscopy analysis method

FTIR spectroscopy is mainly used to analyze the functional group components and structural characteristics of materials. The resins were dried in an oven at 100°C. The solid sample was ground into the powder of 40~60 mesh and dried in an oven at 50°C for 48h. Then, they were put in a drying dish for 1 week with the $P_2O_5$ powder (≥98 %). The sample and KBr powder were mixed uniformly with the mass ratio of (1/1000) and then pressed into a transparent sheet. The test was performed on a VERTEX 80V instrument with a resolution of $2cm^{-1}$ and a test range of $400\text{-}3000cm^{-1}$.

### 3.2.4 Rheological performance analysis method

In this experiment, a modular rotating rheometer workstation (MARS60) was used to test the molecular rheological behavior of the adhesive. This workstation selects two modes of controlled stress (CS) and controlled strain (CD) to switch freely. The oscillation test was including: frequency scan, temperature scan, time scan tes. A Peltier flat lamina temperature control system was used in the equipment. The parameters of a plate fixture with a diameter of 20mm and a gap of 0.5mm was selected. The setting parameters are shown in Table 3-2:

Tab.3-2 The parameters selected for rotary rheometer

| Test steps | Temperature (°C) | Operating mode | Oscillation test |
|---|---|---|---|
| 1 | 30 | CD（Control strainγ=0.01） | Frequency sweep（1~100Hz） |
| 2 | 30~50 | CS（Control stressτ=1.00Pa） | Temperature sweep |
| 3 | 50 | CD（Control strainγ=0.01） | Frequency sweep（1~100Hz） |
| 4 | 50~70 | CS（Control stressτ=1.00Pa） | Temperature sweep |
| 5 | 70 | CD（Control strainγ=0.01） | Frequency sweep（1~100Hz） |
| | 70~140 | CS（Control stressτ=1.00Pa） | Temperature sweep |

## 3.3 Results and analysis

### 3.3.1 The influence of HVEF conditions (voltage/time) on the chemical components in the adhesiv

As shown in Figure 3-1, the changes in FTIR spectrum of the urea-formaldehyde resin before and after HVEF treatment were obtained. Table 3-3 summarized the characteristic peak range of the main chemical bonds in urea-formaldehyde resin. The characteristic peak at 1606cm$^{-1}$ is attributed to C–N stretching vibration, the characteristic peak at 1506cm$^{-1}$ is attributed to the functional group of $CH_2$ and $CH_3$, the characteristic peak at 1161cm$^{-1}$ is attributed to C–N stretching vibration and the characteristic peak of 1112cm$^{-1}$ is attributed to the C–O stretching vibration. It could be observed from the figure that after HVEF treatment, the characteristic peaks at C–O and other functional groups increased significantly. The increase of these characteristic peaks indicated that after HVEF treatment, a large number of water molecules, oxygen molecules and free formaldehyde in the air

were strongly ionized, and chemical groups such as new electrons, hydrogen ions, oxygen ions, and hydroxyl groups significantly increased. These chemical groups collided with the adhesive and increased polarity, charge density and chemical group activity of the adhesive were obtained. The methylol content in the adhesive improved, and the polycondensation reaction of the adhesive was promoted under certain temperature conditions. Then, the methylene bond in the treated resin increased and the intermolecular chemical reaction ability and crosslinking degree of the resin were improved [169, 210]. At the same time, the literature showed that the increase of C–O functional group in the adhesive is beneficial to improve the cross-linking reaction between the adhesive and wood chemical groups [211]. As the voltage/treatment time increased, the number of excited chemical groups and the intensity of characteristic peak increased significantly, thereby further promoting the degree of polycondensation reaction of the adhesive and increasing the crosslinking reaction. The change rate increased with the increase of voltage or treatment time. In addition, under the treatment condition of 60kV/8 min, the highest intensity of each characteristic peak is obtained compared with the spectrum of the untreated resin.

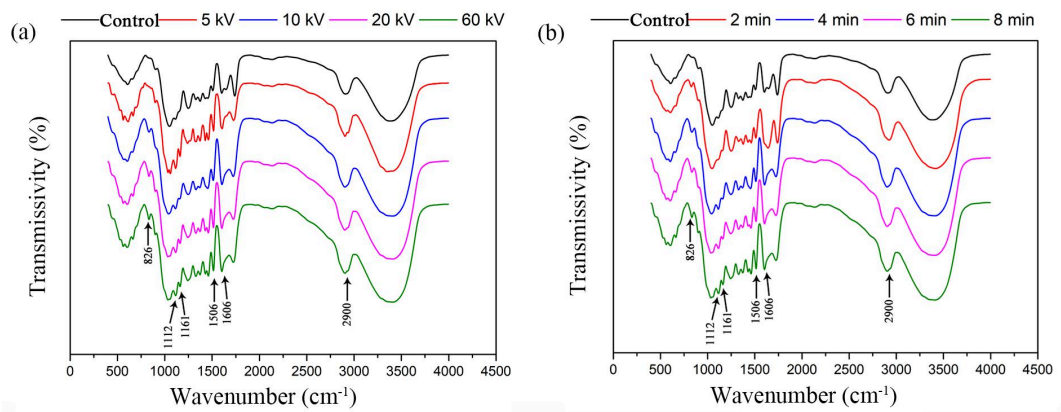


Fig.3-1 Fourier transform infrared spectroscopy for HVEF treated UF samples compared with the controls, under varied voltages and (b) under varied treatment durations.

Tab.3-3 Chemical groups assignments for UF Fourier transform infrared spectroscopy

| Wave number（$cm^{-1}$） | Functional group | Attribution |
|---|---|---|
| 3375 | N–H | NH Stretching vibration（Primary fatty amine） |
| 2900 | O–$CH_3$ | O–$CH_3$ Fatty ether |
| 1750 | C=O | C=O Stretching vibration（Primary amide） |
| 1606 | C–N | C–N Stretching vibration（Secondary amine） |
| 1506 | C–H | $CH_2$，$CH_3$ |
| 1480 | C–N | C–N Stretching vibration |
| 1460 | =C–N | C–N Tertiary cyclic amide |
| 1355 | C–N/N–H | C–N/N–H Stretching vibration（Tertiary amines） |
| 1250 | C–O | C–O Stretching vibration（Fatty ether） |
| 1161 | C–N | C–N Stretching vibration（Methylene bond） |
| 1112 | C–O | C–O Stretching vibration（Hydroxymethyl） |
| 826 | N–H | N–H Flexural vibration (primary fatty amine) |

As shown in Figure 3-2, the changes in FTIR spectrum of the PF resin before and after the HVEF treatment were characterized. Table 3-4 summarized the characteristic peak of the main chemical bonds in PF resin. The characteristic peak at 3433$m^{-1}$ belongs to O–H stretching vibration, the characteristic peak at 2921$m^{-1}$ belongs to C–H stretching vibration, the characteristic peak at 1450$cm^{-1}$ belongs to the $CH_2$ shear vibration, the characteristic peak of 1213$cm^{-1}$ belongs to the C–O stretching vibration, the O–H bending vibration and the characteristic peak of 1017$cm^{-1}$ belong to the C–O stretching vibration. It could be observed from the figure that after HVEF treatment, the characteristic peaks at the O–H and C–O functional groups both increased significantly. At the same time, as the treatment

voltage or treatment time increased, the intensity of these characteristic peaks increased significantly. The change rate of increased varing with different treatment voltages or different times. Under the treatment of 60kV/8 min, the highest intensity was obtained for each characteristic peak compared with the spectrum of untreated resin. These results were mainly because a large number of water molecules, oxygen molecules and free formaldehyde molecules in the air were strongly ionized after treated by HVEF and the formation of new electrons, hydrogen ions, oxygen ions, hydroxyl groups and other chemical groups significantly increased. These chemical groups improved the polarity and charge density of the adhesive with the voltage/processing time increased. The excited chemical groups increased, and the methylol content in the adhesive increased. Under certain temperature conditions, the polycondensation reaction of the adhesive increased, the number of methylene bond in the treated resin and the intermolecular chemical reaction improved. At the same time, a large number of excited electrons and broken chemical bonds (oxygen-containing groups) hit the resin and reacted with each other and the cross-linking reaction of the resin increased. In order to further explore the reaction mode of the resin after HVEF treatment, the rheological properties of urea-formaldehyde and phenol-formaldehyde resin were tested.

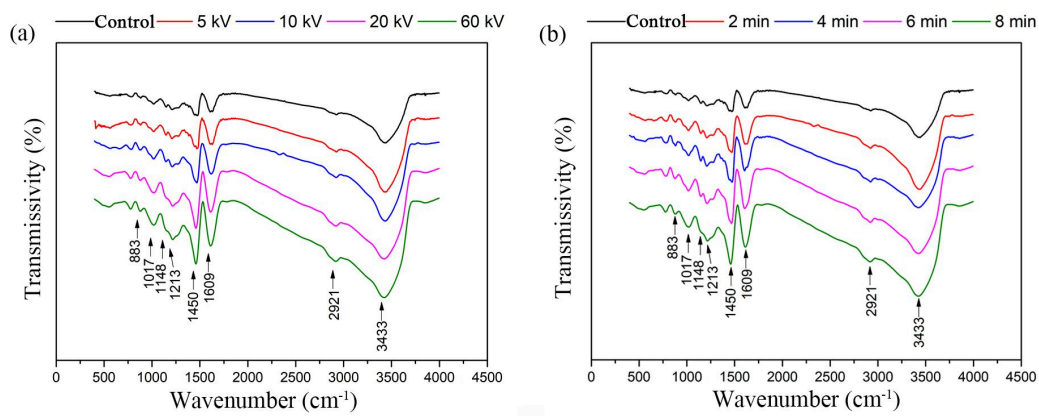

Fig.3-2 Fourier transform infrared spectroscopy for HVEF treated PF samples compared with the controls, (a) under varied voltages and (b) under varied treatment durations

Tab.3-4 Chemical groups assignments for PF Fourier transform infrared spectroscopy

| Wave number（$cm^{-1}$） | Functional group | Attribution |
|---|---|---|
| 3433 | O–H | O–H Stretching vibration（Phenolic hydroxyl） |
| 2921 | C–H | C–H Stretching vibration(Methylene) |
| 1609 | C=C | C=C Stretching vibration(Aromatic ring) |
| 1450 | C–H | CH2 Scissor vibration (methylene) |
| 1213 | C–O，O–H | C–O Stretching vibration，O–H Bending vibration |
| 1148 | C–H | Aromatic ring C–H in-plane bending vibration |
| 1017 | C–O | C–O Stretching vibration(Hydroxymethyl） |
| 883 | C–H | C–H bending vibration (aromatic ring) |

### 3.3.2 The relationship between the rheological behavior of the adhesive and the temperature under the conditions of HVEF induction

In this experiment, a rotating rheometer was used to test the rheological behavior of urea-formaldehyde resin and phenol-formaldehyde resin before and after HVEF treatment. As shown in Figure 3-3, the relationship between the viscosity of the urea-formaldehyde and phenol-formaldehyde resin and the temperature before and after HVEF treatment was characterized. It could be observed from the figure (Figure 3-3(a) and (b)) that the viscosity of the adhesive increased rapidly as the temperature increased within the range of 30°C to 50°C for urea-formaldehyde resin. It was mainly due to the fact that the addition of the curing agent increased the polycondensation reaction of the resin and the cross-linking reaction occurred

quickly between the molecules. The viscosity changed smoothly between 40°C and 80°C, the viscosity decreased significantly after 100°C and then increased with the increment of temperature. This was mainly because the evaporation of water during heating process reduced the heat of reaction, thereby reducing the degree of interaction between the molecules and the viscosity. After heating, the water content decreased and the intensity of chemical reaction increased. As the reaction duration increased, the degree of cross-linking reaction of the adhesive and the viscosity of the adhesive increased [212, 213]. For PF resin, during the heating process, the viscosity of PF resin will continue to decrease at 100°C due to the swelling between molecules and its high molecular weight. After the minimum value appeared, the degree of intermolecular reaction increased as the water evaporated, resulting in significantly increased viscosity (Figure 3-3 (b) and (c)).

After HVEF treatment, the viscosity of urea-formaldehyde resin and phenol-formaldehyde resin both increased. The average change rate under different conditions could be ranked as follows: UF resin under different voltage conditions, 48.65%±5.44% (5 kV) < 152.34%±35.45% (10 kV) < 492.61%±40.53% (20 kV) < 660.98%±53.76% (60 kV); urea-formaldehyde resin under different treatment times, 225.54%±20.43% (2 min) < 297.39%±52.77% (4 min) < 530.87%±45.80% (6 min) < 660.98%±63.76% (8 min); phenol-formaldehyde resin under different voltage conditions, 50.22%±10.23% (5 kV) < 150.89%±31.03% (10 kV) < 501.84%±43.22% (20 kV) < 650.69%±43.64% (60 kV); phenol-formaldehyde resin is treated at different time conditions, 226.49%±18.76% (2 min) < 316.39%±40.55% (4 min) < 525.55%±54.45% (6 min) < 650.69%±43.64% (8 min). This was mainly due to the fact that a large number of water and oxygen molecules in the air were strongly

ionized, and chemical groups such as new electrons, hydrogen ions, oxygen ions, and hydroxyl groups significantly increased. These chemical groups increased the polarity and charge density of the adhesive. The excited chemical groups increased with the increase of voltage/treatment time. It was beneficial to increase the methylol content. They participated in the polycondensation reaction of the adhesive under certain temperature conditions. At the same time, it could be observed that the methylene content also increased significantly in the polycondensation reaction, which was beneficial to improve the viscosity of the adhesive after treatment from FTIR spectrum.

At the same time, the changes in the rheological behavior of the adhesive before and after HVEF treatment during the heating process were characterized in Figure 3-4 and Figure 3-5, including the storage (elastic) modulus and loss modulus. It could be observed from the figure that the change trend of storage modulus and loss modulus was similar to the change trend of viscosity, which reflected that the evaporation of water during the heating process had a significant effect on viscosity, storage modulus and loss modulus. From Figure 3-4, it was stated that the storage modulus of both urea-formaldehyde and phenol-formaldehyde resin increased significantly after treated by HVEF . This was mainly due to the formation of new electrons, hydrogen ions, oxygen ions, and hydroxyl groups during the HVEF treatment. The significant increase of other chemical groups improved the polycondensation reaction capacity of the adhesive. As the viscosity of the adhesive increased, the storage elasticity between molecules and the storage modulus of the adhesive increased. Under different conditions, the average change rate could be ranked as follows: urea-formaldehyde resin under different voltage conditions,

62.32%±8.45% (5 kV) < 185.48%±40.43% (10 kV) < 681.56%±40.53% (20 kV) < 840.22%±67.41% (60 kV); urea-formaldehyde resin under different treatment times, 217.49%±11.68% (2 min) < 369.62%±39.76% (4 min) < 601.69%±56.30% (6 min) < 840.22%±67.41% (8 min); phenolic resin under different voltages, 65.78%±12.42% (5 kV) < 180.82%±35.89% (10 kV) < 702.37%±46.92% (20 kV) < 835.58%±70.88% (60 kV); phenolic resin under different treatment times, 233.43%±18.76% (2 min) < 373.74%±32.16% (4 min) < 592.49%±67.33%(6 min) < 835.58%±50.88% (8 min). From Figure 3-5, after HVEF treatment, the storage modulus of urea-formaldehyde resin and phenol-formaldehyde resin both increased significantly. Due to the impact of a large number of chemical groups and participation in the polycondensation reaction, the viscosity and elastic modulus of the adhesive increased. It promoted the interaction and relative movement of molecules and further improved the loss modulus of the adhesive. The average increment rate under different voltages and treatment times could be ranked as follows: urea-formaldehyde resin under different voltages, 50.22%±18.45% (5 kV) < 224.92%±36.69% (10 kV) < 785.98%±63.39% ( 20 kV) < 1012.49%±77.65% (60 kV); urea-formaldehyde resin under different times, 370.89%±23.88% (2 min) < 494.18%±63.61%(4 min) < 789.29%±68.79%(6 min) < 1012.49%±77.65% (8 min); phenol-formaldehyde resin under different voltages, 54.71%±10.54% (5 kV) < 220.92%±41.92% (10 kV) < 801.28%±59.61% (20 kV) < 1002.38%±67.40% (60 kV); phenol-formaldehyde resin under different treatment times, 375.90%±18.59% (2 min) < 511.85%±55.83% (4 min) < 783.50 %±52.98% (6 min) < 1002%±67.40% (8 min).

During the heating process, the average increment rate of the viscosity of the urea-formaldehyde resin obtained under different voltage/time treatment was not

significantly different from that of the viscosity, storage modulus and loss modulus of the phenol-formaldehyde resin (Figure 3-6). From 5kV to 20kV, the increment of the resin viscosity, storage modulus, and loss modulusare significantly increased, while decreased at 60kV, mainly because the effect of HVEF treatment on the material had a certain limit voltage value [165]. The increment rate of adhesive viscosity, storage modulus and loss modulus under different treatment conditions was relatively small. As the treatment time increased, the increment rate of adhesive viscosity, storage modulus and loss modulus increased significantly. This was mainly due to the fact that the treatment time of HVEF increased, and the ions and oxygen-containing groups excited in the electric field with the reaction time increased, which promoting the polycondensation reaction of the adhesive.

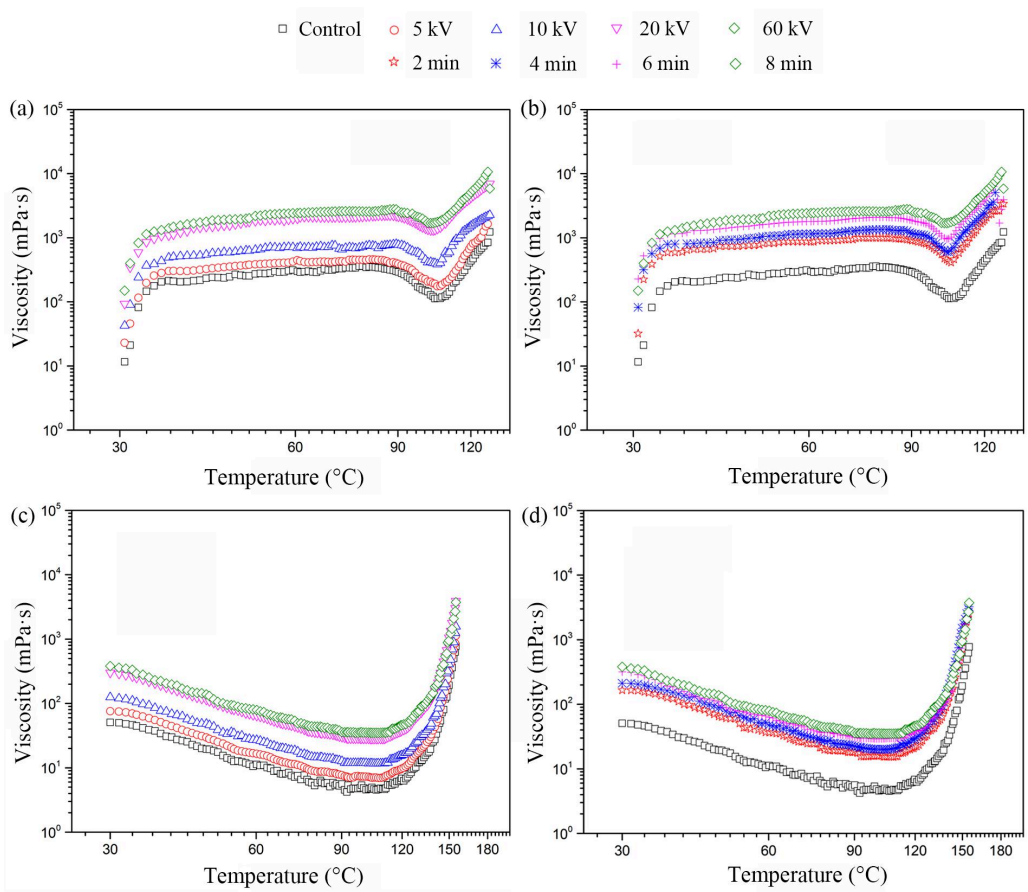

Fig.3-3 The relationship between adhesive viscosity and temperature for treated adhesive and compared with the control, (a) UF treated under varied voltages, (b) UF treated under varied durations, (c) PF treated under varied voltages and (d) PF treated under varied durations.

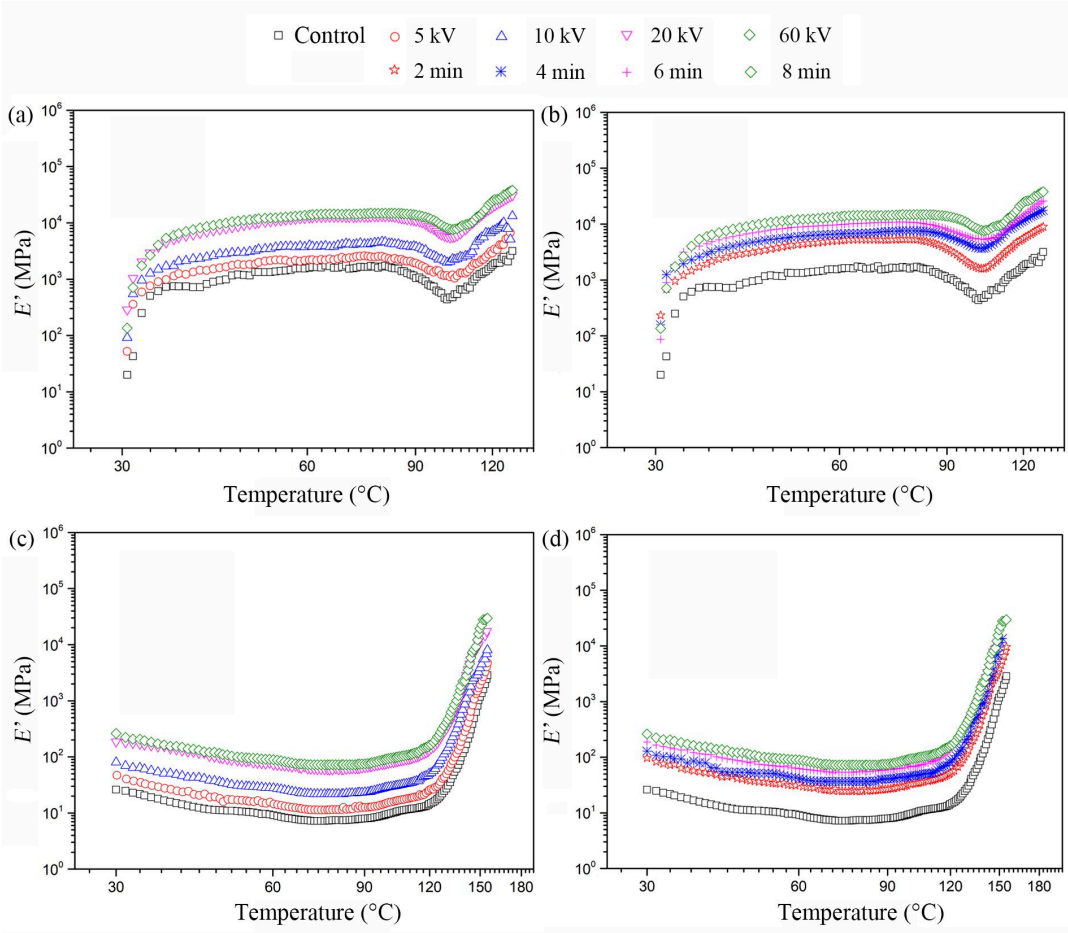


Fig.3-4 The relationship between storage modulus and temperature for treated adhesive and compared with the control, (a) UF treated under varied voltages, (b) UF treated under varied durations, (c) PF treated under varied voltages and (d) PF treated under varied durations.

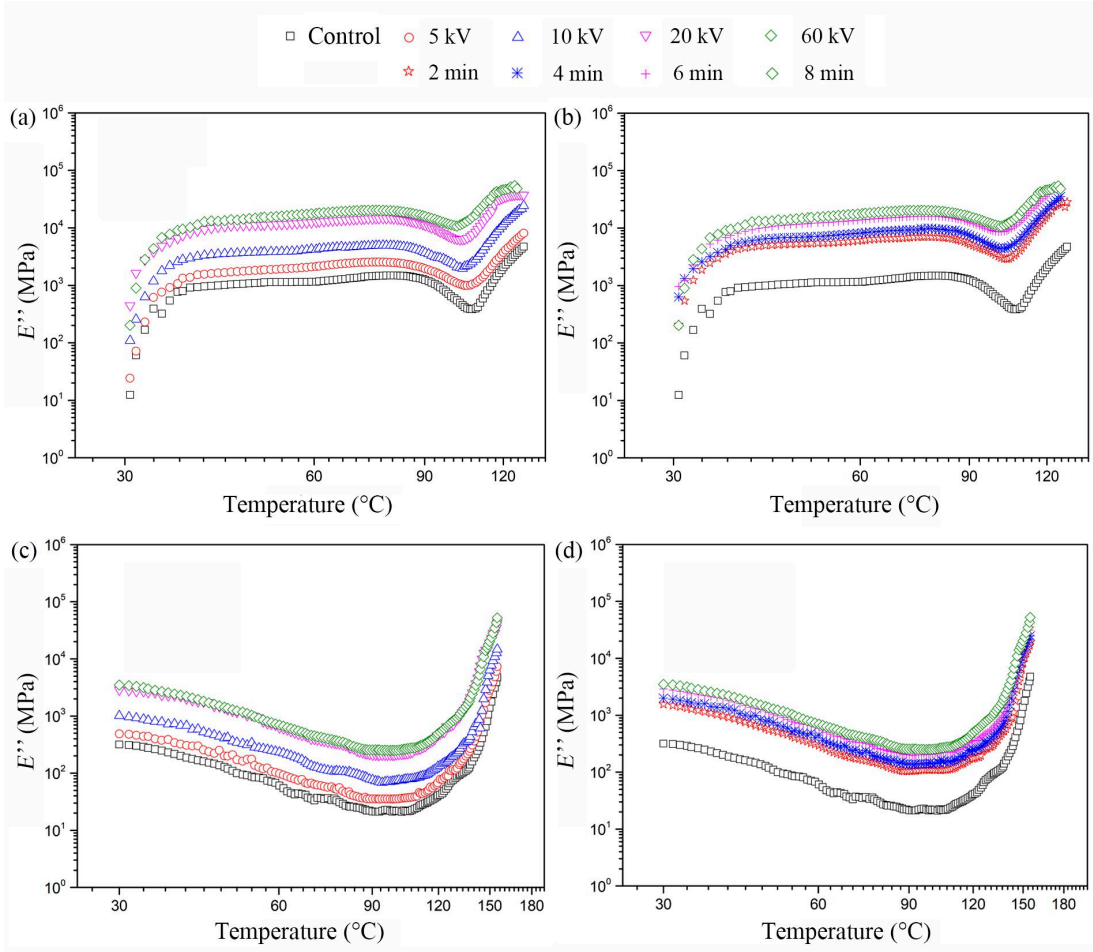


Fig.3-5 The relationship between loss modulus and temperature for treated adhesive and compared with the control, (a) UF treated under varied voltages, (b) UF treated under varied durations, (c) PF treated under varied voltages and (d) PF treated under varied durations

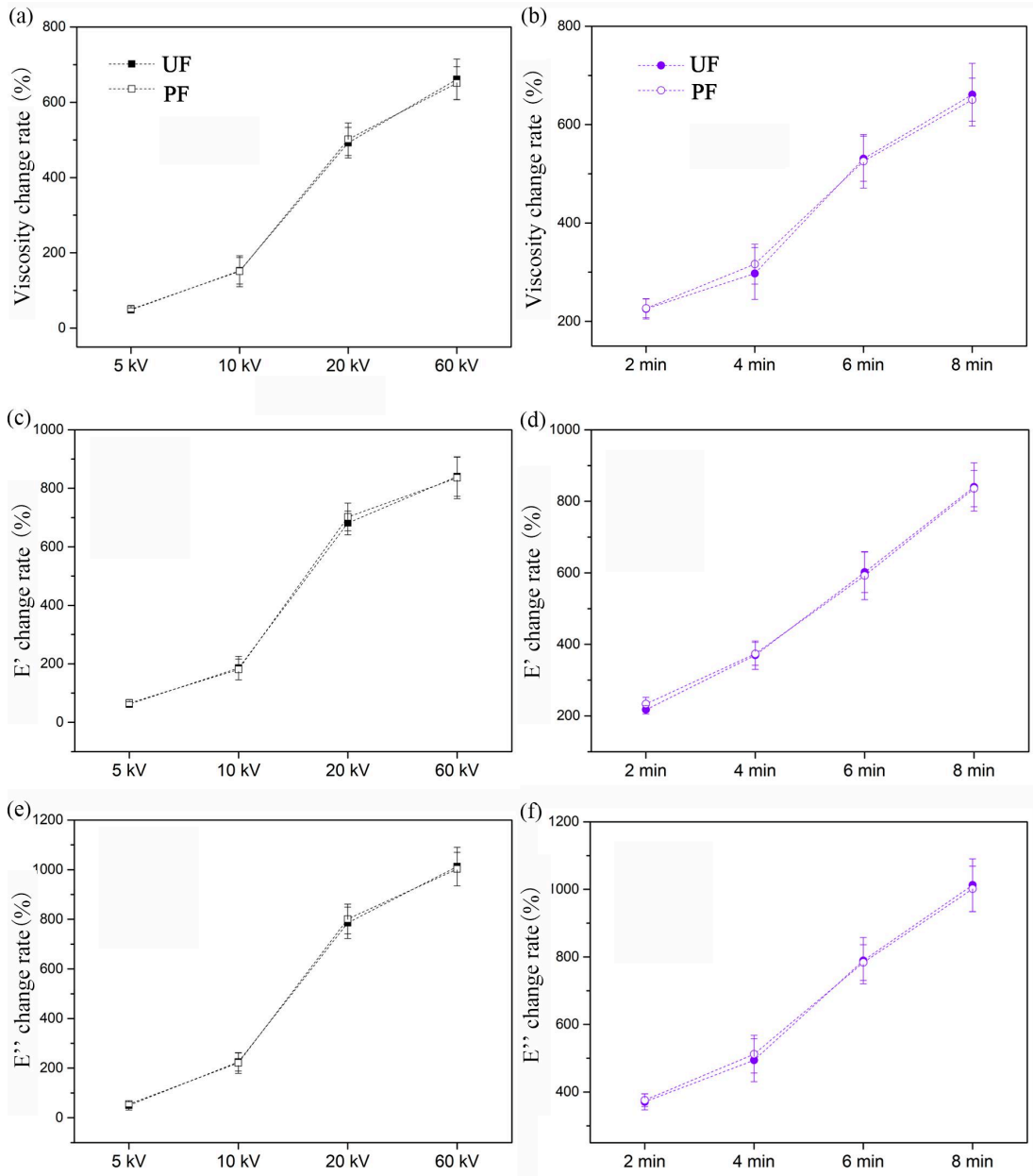


Fig.3-6 The relationship between change ratio of viscosity, storage modulus and loss modulus and varied voltages/durations for treated adhesive under increased temperature condition, (a) change ratio of adhesive viscosity under varied voltages, (b) change ratio of adhesive viscosity under varied durations, (c) change ratio of adhesive storage modulus under varied voltages, (d) change ratio of adhesive storage modulus under varied durations, (e) change ratio of adhesive loss modulus under varied voltages, (f) change ratio of adhesive loss modulus under varied durations.

### 3.3.3 The relationship between the rheological behavior of the adhesive and the frequency under the conditions of HVEF induction

Oscillatory shearing flow was to apply sinusoidal shearing strain acting on the material and to measure the stress to characterize the dynamic response of the material. Viscoelasticity is to indicate the two characteristics of viscous and elasticity that the material exhibits when subjected to external stress. In this experiment, the changes of rheological behavior of urea-formaldehyde and phenol-formaldehyde resin in the frequency range of 1 to 100 Hz before and after HVEF treatment were obtained (the constant temperature conditions of the test are 30°C, 50°C and 70°C).

As shown in Figure 3-7, Figure 3-8 and Figure 3-9, it characterized the viscosity, storage modulus, loss modulus and frequency of urea-formaldehyde resin and phenolic resin before and after HVEF treatment at a constant temperature of 30°C. From Figure 3-7, it could be observed that the viscosity increased significantly with the increase of frequency at a constant temperature of 30°C. For PF resin, there was a sudden change point at 10Hz, which was related to the inherent characteristics of the material [214]. This was mainly due to the elastic properties of the macromolecular increasing during the deformation process under the action of external force. The better the elasticity of the adhesive, the more increase in the amount of work done between molecules and higher the viscosity of the adhesive were obtained [215]. After HVEF treatment, the viscosity of urea-formaldehyde resin and phenol-formaldehyde resin increased significantly within the frequency range, and increased significantly with the increase of voltage and time as well. This was mainly due to the large amount of water in the air during HVEF treatment. Molecules and oxygen molecules were strongly ionized, and chemical groups such as new electrons, hydrogen ions, oxygen ions, and hydroxyl groups significantly increased. Moreover, as the voltage or processing time increased, the excited groups and these chemical groups colliding

with the adhesive improved. The polarity and charge density of the adhesive were beneficial to increase the methylol content and participated in the polycondensation reaction of the adhesive under certain temperature conditions. At the same time, the methylene content also increased significantly in the polycondensation reaction. It is beneficial to increase the viscosity of the adhesive after treatment. From Figure 3-8 and Figure 3-9, it could be observed that after HVEF treatment, the storage modulus and loss modulus of urea-formaldehyde resin and phenol-formaldehyde resin both increased significantly with the increase of treatment voltage and time. The increase was mainly because the more ions and oxygen-containing chemical groups were excited under the action of HVEF, the viscosity of the glue increased and the degree of intermolecular reaction improved.

As shown in Figure 3-10, Figure 3-11 and Figure 3-12, the relationship between the viscosity, storage modulus, loss modulus and frequency of resins before and after HVEF treatment at a constant temperature of 50°C was characterized. It could be observed from Figure 3-10 that the viscosity of the urea-formaldehyde resin decreased with the increase of frequency. This was mainly because the evaporation of water reduced the heat required for the intermolecular reaction in the resin and the degree of the intermolecular interaction was reduced as well. As the external force increased, the molecules were prone to deformation and thus the viscosity decreased. At a constant temperature of 50°C, the relationship between the viscosity and frequency of the PF resin was similar to that at a constant temperature of 30°C. This was mainly because the PF resin had a larger molecular weight and was not easily deformed under external force. The viscosity varied with the increase of frequency and a sudden change point appeared at 10 Hz. After HVEF treatment, the viscosity of

urea-formaldehyde resin and phenol-formaldehyde resin increased significantly within the frequency range and it increased significantly with the increase of voltage and time as well. This was mainly due to the formation of new electrons during HVEF treatment. The chemical groups such as hydrogen ion, oxygen ion and hydroxyl group and the excited groups increased significantly with the voltage or treatment time increased. These chemical groups collided with the adhesive and increase the polarity and charge density of the adhesive. It was beneficial for the adhesive to increase the methylol content and to participate in the polycondensation reaction under certain temperature. At the same time, the methylene content also increased significantly in the polycondensation reaction, thereby helping to increase the viscosity of the adhesive after treatment. From Fig. 3-11 and Fig. 3-12, for urea-formaldehyde resin, the relative changes of storage modulus and loss modulus at 1 Hz and 100 Hz were significantly lower than the change at a constant temperature of 30°C.

The main reason was that the viscosity of urea-formaldehyde resin decreased with the increasing frequency. After HVEF treatment, the storage modulus and loss modulus of urea-formaldehyde resin and phenol-formaldehyde resin both increased significantly, and increase significantly with the increase of processing voltage and processing time. This was mainly due to the excited ions under the action of HVEF. The more oxidative groups, the higher viscosity of the adhesive increased. Then, the degree of intermolecular reaction improved.

At a constant temperature of 70°C, as shown in Figure 3-13, Figure 3-14 and Figure 3-15,,the changes in the relationship between the viscosity, storage modulus,

loss modulus and frequency of PF and UF resins before and after HVEF treatment were characterized. Before and after HVEF treatment, the viscosity, storage modulus, and loss modulus of urea-formaldehyde resin and phenol-formaldehyde resin have similar changes within the frequency range measured at a constant temperature of 50°C.

Under the three constant temperature conditions, by calculating the increase rate of the viscosity, storage modulus and loss modulus of urea-formaldehyde resin and phenol-formaldehyde resin under different voltage/time treatment conditions (Figure 3-16), there was no significant difference in the increase rate of rheological performance parameters under various treatment conditions obtained. From 5kV to 20kV, the change rate of resin viscosity, storage modulus and loss modulus significantly increased, while the increase at 60kV slowed down. It was mainly due to a certain limit voltage involved in the effect of HVEF [165]. The increase rates of adhesive viscosity, storage modulus and loss modulus under different treatment conditions were relatively small. With the increase of treatment time, the increase rate of adhesive viscosity, storage modulus and loss modulus increased significantly. This was mainly due to the increased HVEF treatment time and excited ions and oxygen-containing groups in the electric field with increased reaction time, which promoting the polycondensation reaction of adhesive. With the increase of the constant temperature during test, the increase rates of the viscosity, storage modulus and loss modulus of urea-formaldehyde resin and phenolic resin under different voltage/time conditions decreased. This was mainly because the water moved vigorously in the adhesive and evaporated with the increased constant temperature, reducing the heat required in the reaction process, thereby weakening the degree of

intermolecular reaction and reducing the viscosity, storage modulus and loss modulus of the adhesive.

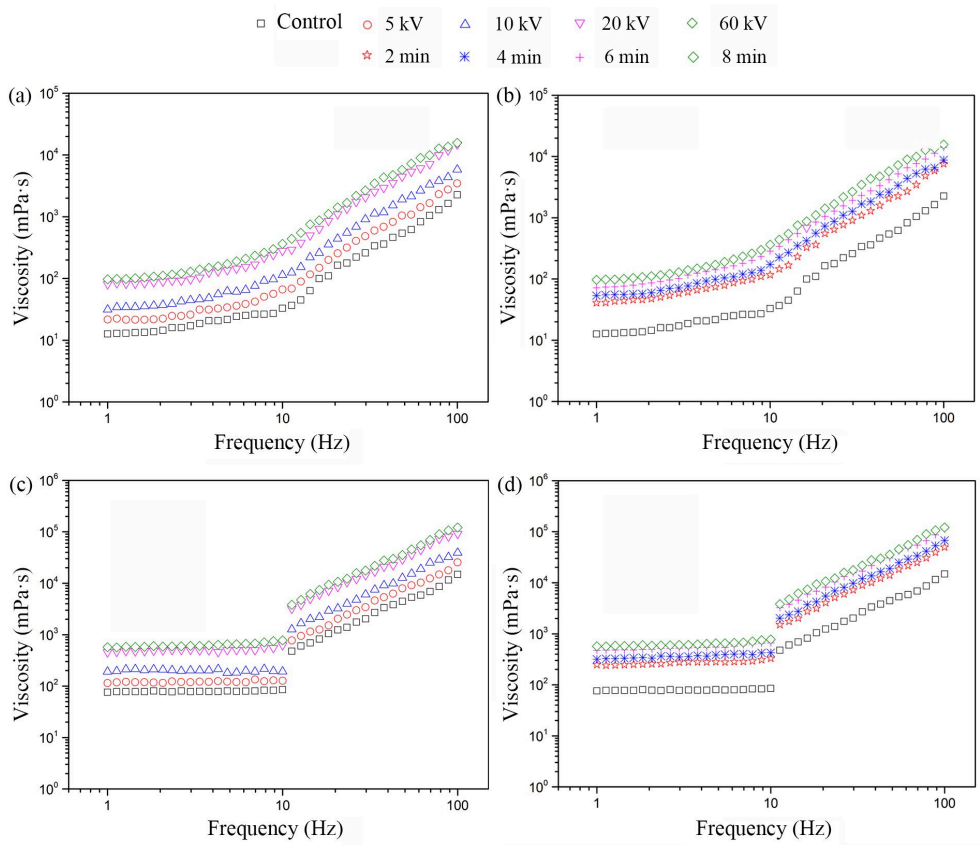


Fig.3-7 The relationship between adhesive viscosity and frequency for treated adhesive and compared with the control under 30°C, (a) UF treated under varied voltages, (b) UF treated under varied durations, (c) PF treated under varied voltages and (d) PF treated under varied durations

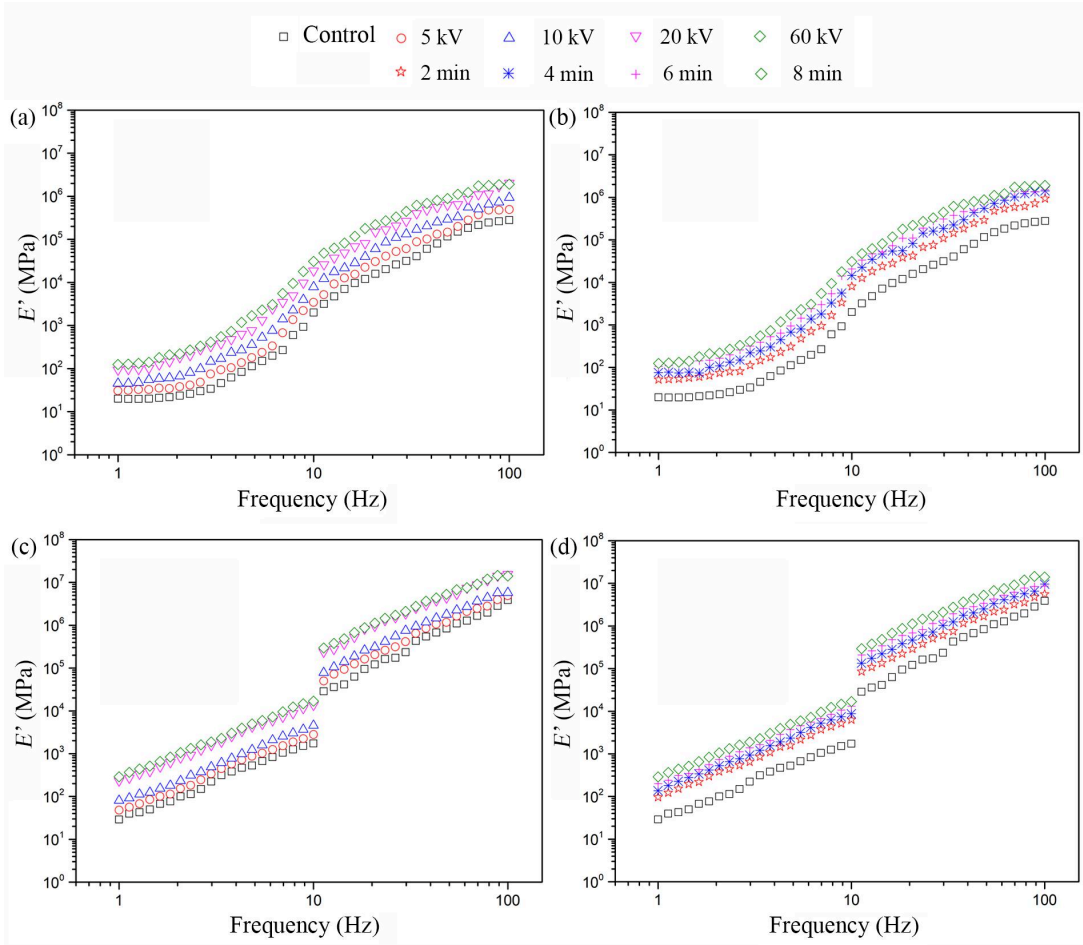


Fig.3-8 The relationship between storage modulus and frequency for treated adhesive and compared with the control under 30°C, (a) UF treated under varied voltages, (b) UF treated under varied durations, (c) PF treated under varied voltages and (d) PF treated under varied durations

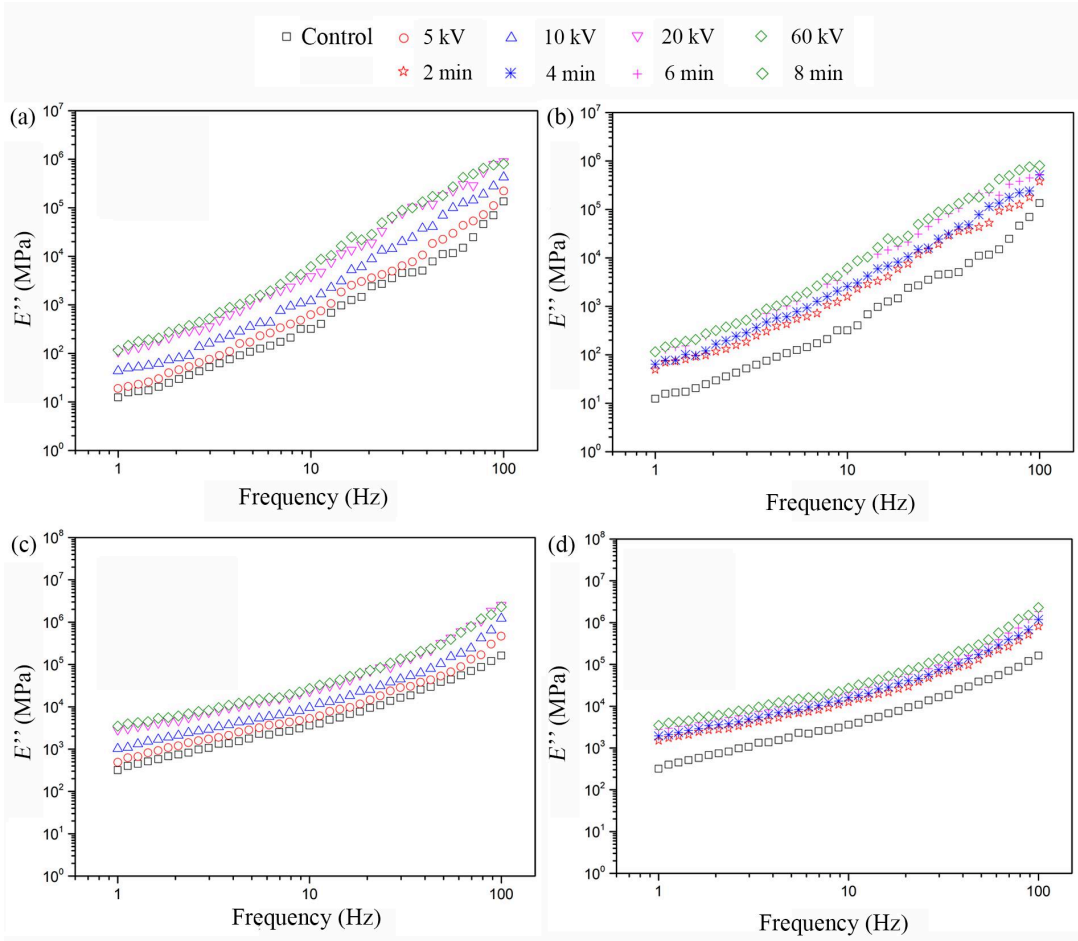


Fig.3-9 The relationship between loss modulus and frequency for treated adhesive and compared with the control under 30°C, (a) UF treated under varied voltages, (b) UF treated under varied durations, (c) PF treated under varied voltages and (d) PF treated under varied durations

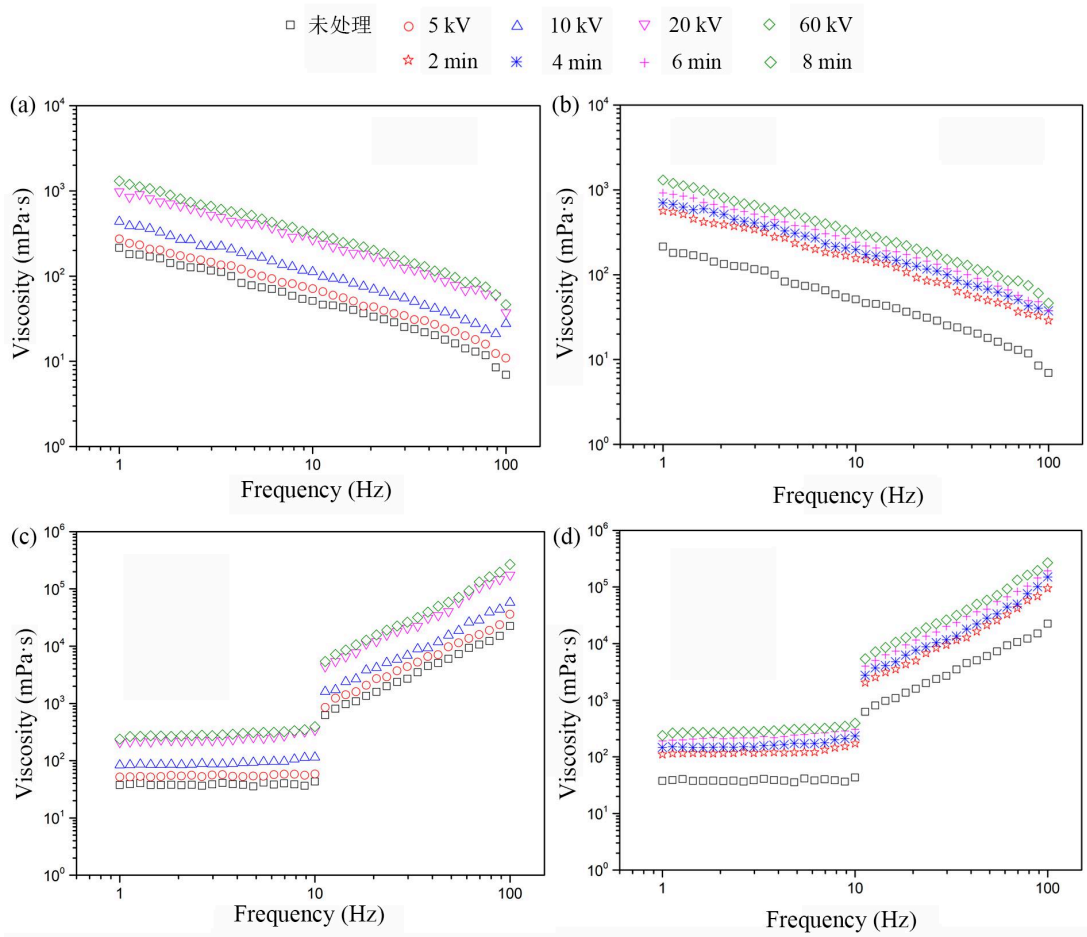


Fig.3-10 The relationship between adhesive viscosity and frequency for treated adhesive and compared with the control under 50°C, (a) UF treated under varied voltages, (b) UF treated under varied durations, (c) PF treated under varied voltages and (d) PF treated under varied durations

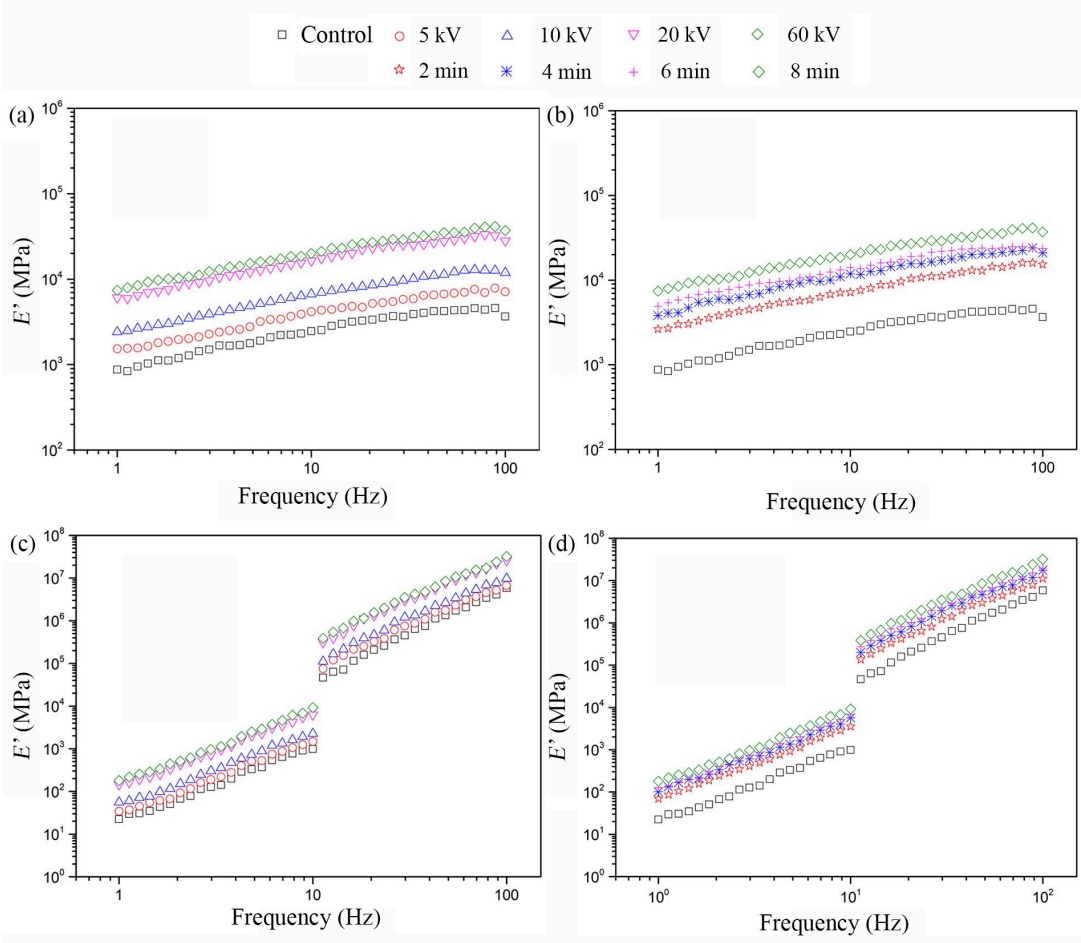


Fig.3-11 The relationship between storage modulus and frequency for treated adhesive and compared with the control under 50°C, (a) UF treated under varied voltages, (b) UF treated under varied durations, (c) PF treated under varied voltages and (d) PF treated under varied durations.

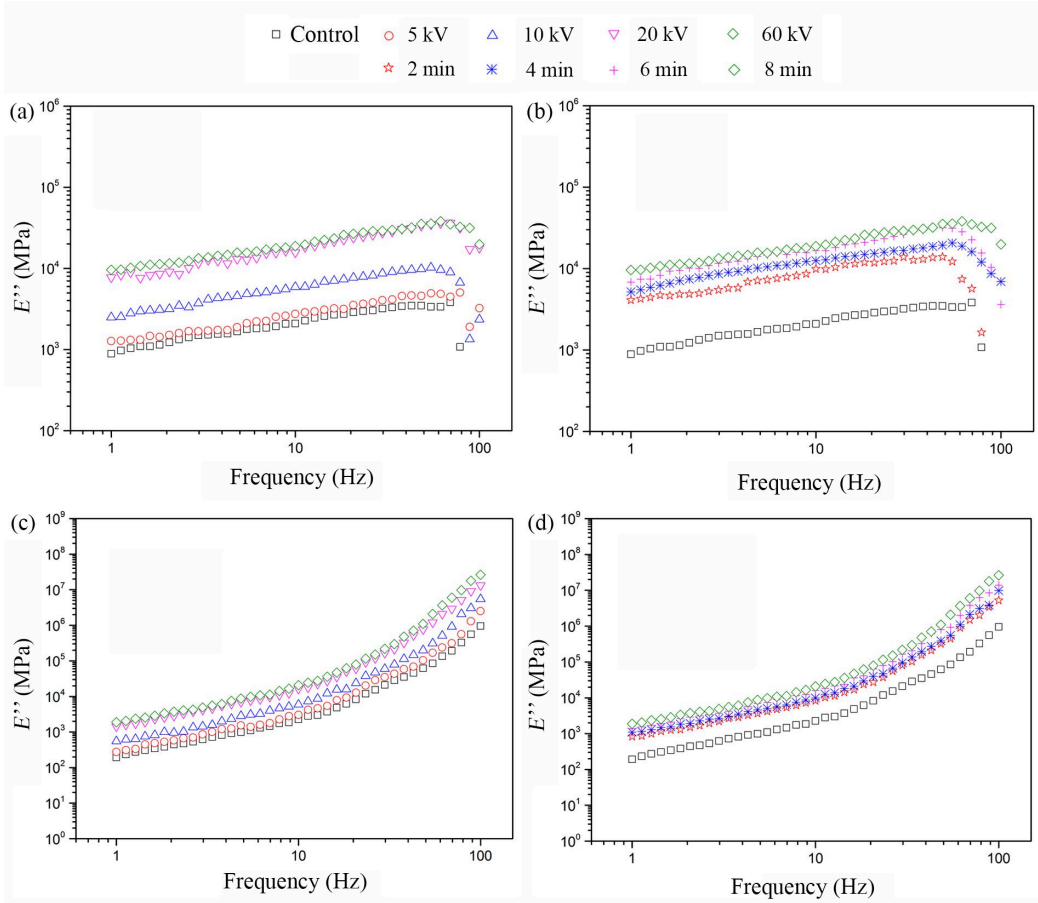


Fig.3-12 The relationship between loss modulus and frequency for treated adhesive and compared with the control under 50°C, (a) UF treated under varied voltages, (b) UF treated under varied durations, (c) PF treated under varied voltages and (d) PF treated under varied durations

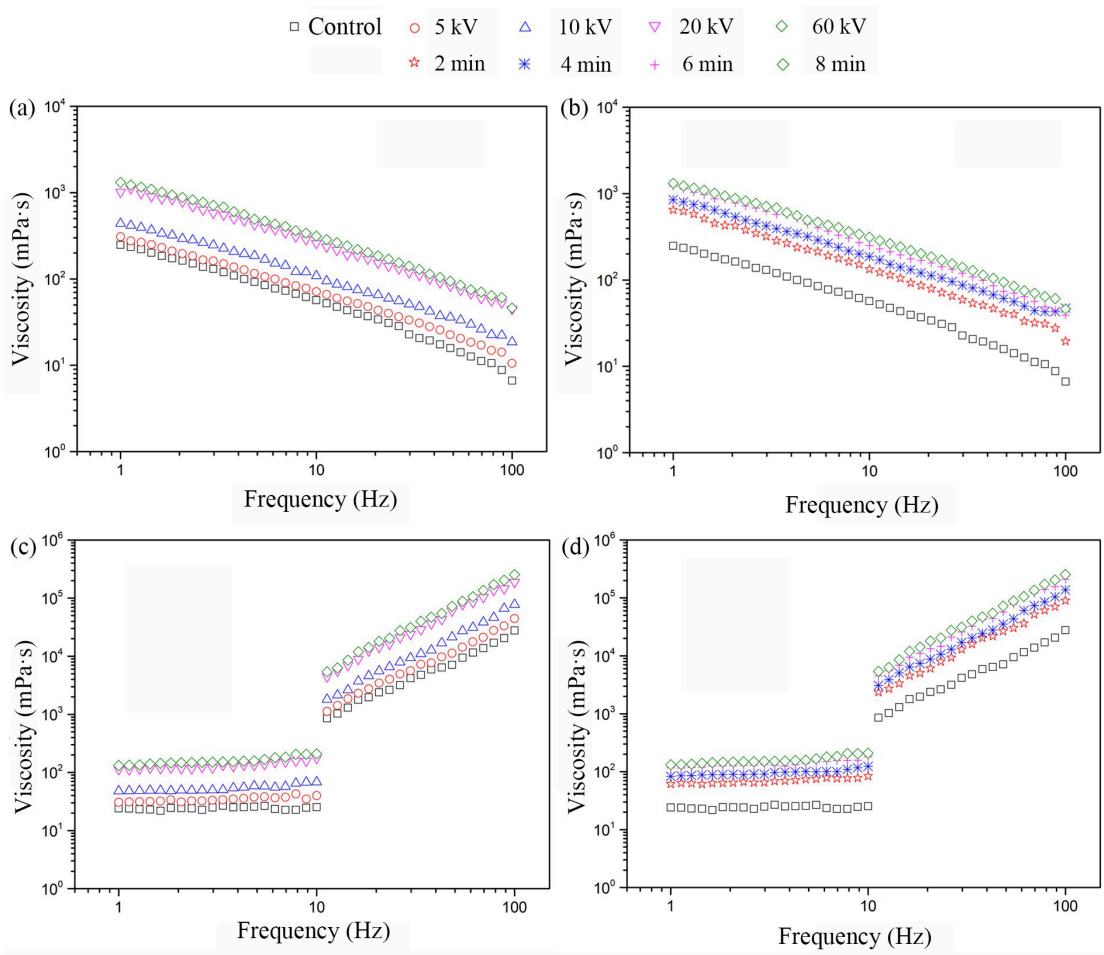


Fig.3-13 The relationship between adhesive viscosity and frequency for treated adhesive and compared with the control under 70°C, (a) UF treated under varied voltages, (b) UF treated under varied durations, (c) PF treated under varied voltages and (d) PF treated under varied durations

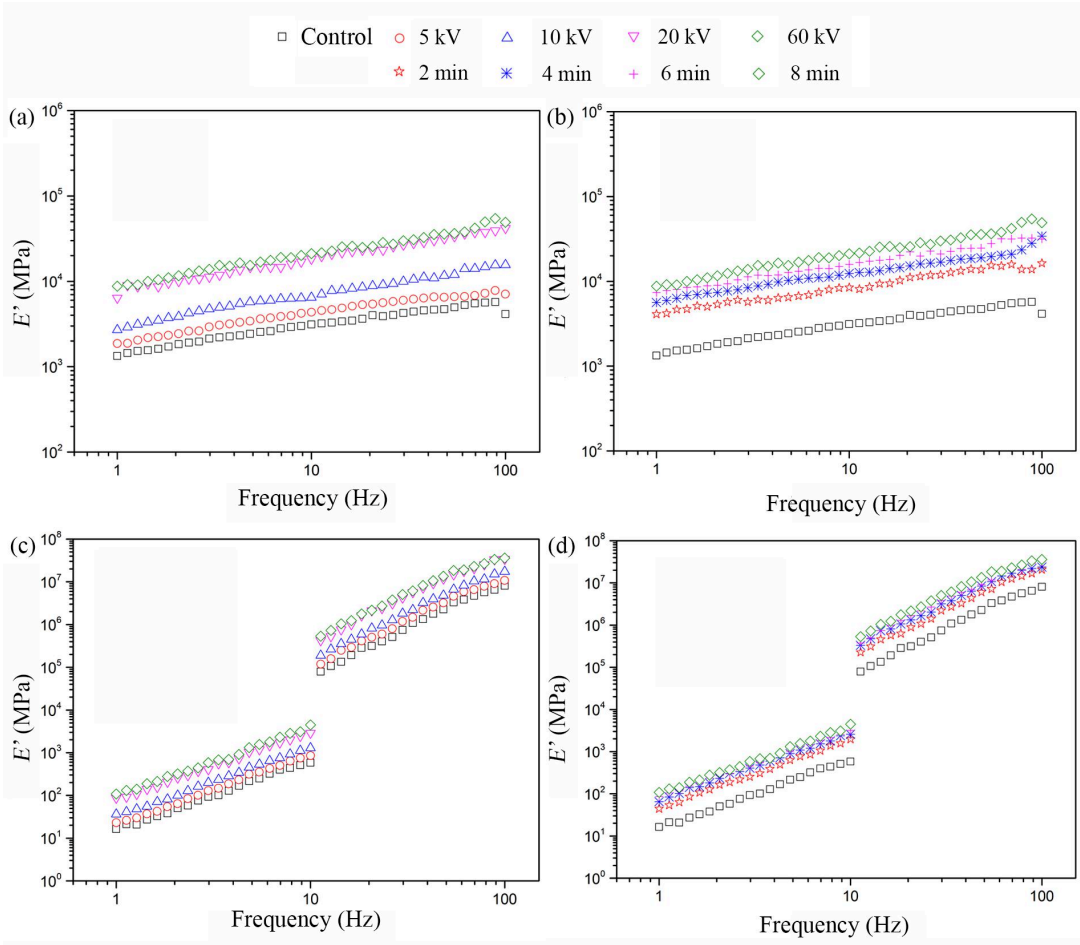


Fig.3-14 The relationship between storage modulus and frequency for treated adhesive and compared with the control under 70°C, (a) UF treated under varied voltages, (b) UF treated under varied durations, (c) PF treated under varied voltages and (d) PF treated under varied durations

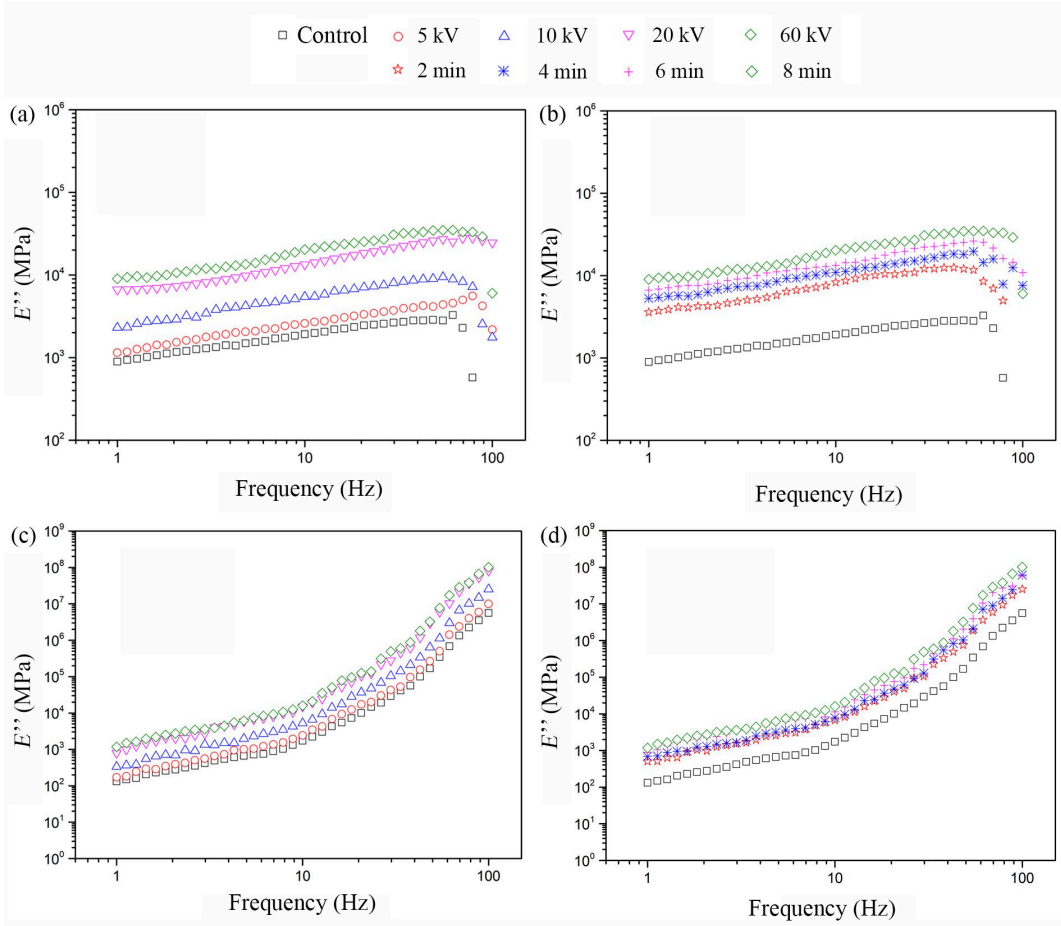


Fig.3-15 The relationship between loss modulus and frequency for treated adhesive and compared with the control under 70°C, (a) UF treated under varied voltages, (b) UF treated under varied durations, (c) PF treated under varied voltages and (d) PF treated under varied durations

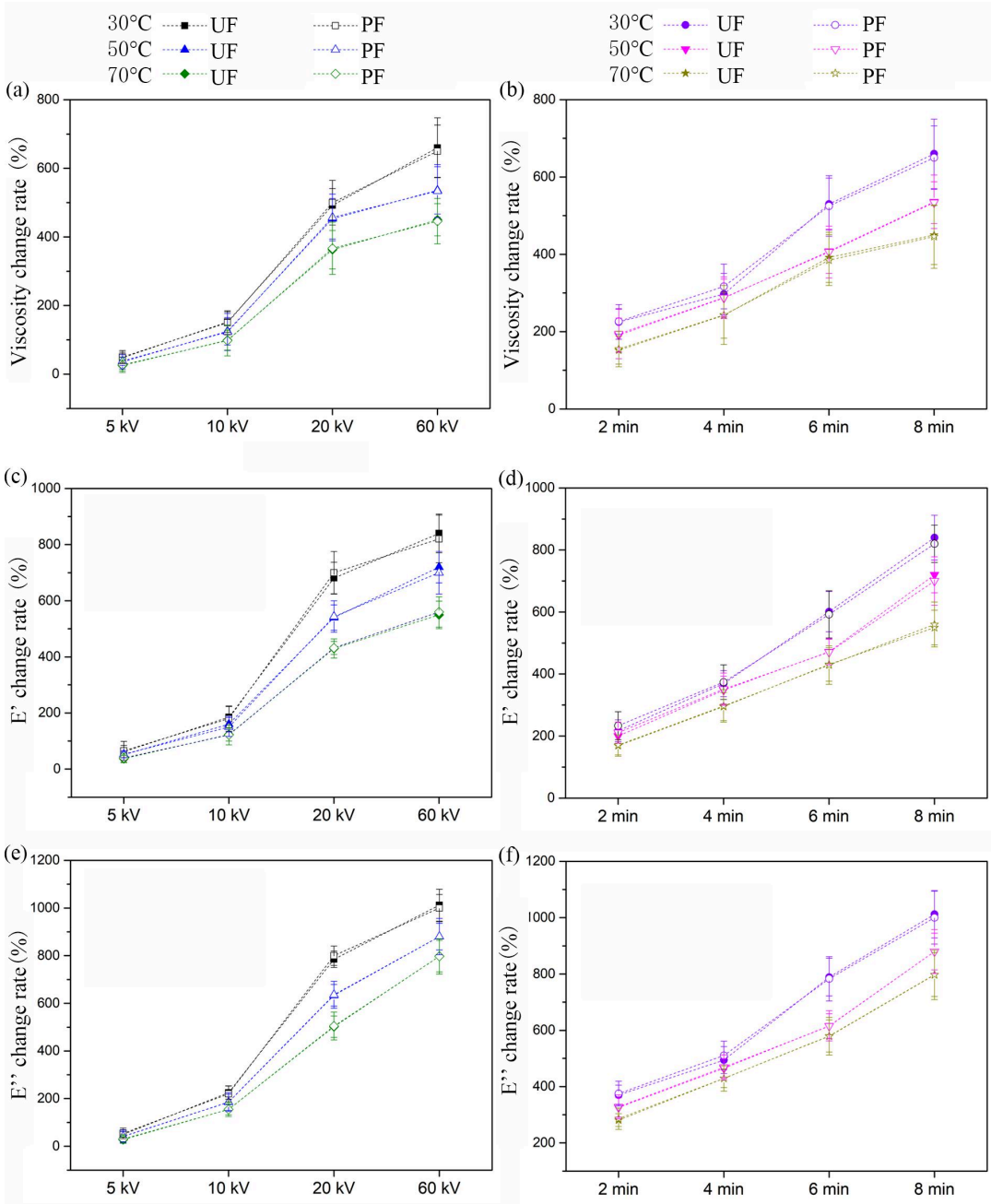


Fig.3-16 The relationship between change ratio of viscosity, storage modulus and loss modulus and varied voltages/durations for treated adhesive under 30°C, 50°C and 70°C from 1 to 100Hz, (a) change ratio of adhesive viscosity under varied voltages, (b) change ratio of adhesive viscosity under varied durations, (c) change ratio of adhesive storage modulus under varied voltages, (d) change ratio of adhesive storage modulus under varied durations, (e) change ratio of adhesive loss modulus under varied voltages, (f) change ratio of adhesive loss modulus under varied durations

## 3.4 Summary

This chapter mainly explored the effects of HVEF treatment conditions (voltage/time) on the rheological behavior and chemical group changes of urea-formaldehyde resin and phenol-formaldehyde resin. The induction mechanism of HVEF on the reaction characteristics of adhesives were analyzed.

(1) After HVEF treatment, the degree of intermolecular reaction in urea-formaldehyde resin and phenol-formaldehyde resin increased. After 60kV/8 min treatment, the characteristic peak intensity of C–O and other functional groups were the largest, indicating that the polarity, charge density and chemical group activity of the adhesive improved. The intermolecular chemical reaction ability improved as the voltage/treatment time increased.

(2) During the heating process, the evaporation of water in the resin has a significant effect on viscosity, storage modulus and loss modulus. After treated by HVEF, the viscosity, storage modulus and loss modulus of urea-formaldehyde resin and phenol-formaldehyde resin significantly increased compared with untreated resin. This was mainly due to the strong ionization of a large number of water molecules and oxygen molecules in the air, which increased oxidative groups, the polarity and charge density of the adhesive. As the voltage/treatment time increased, the excited chemical groups increased. It was beneficial to improve the polycondensation reaction of the adhesive. There was no significant difference in the increase rate of the rheological parameters of the two resins under various treatment conditions. From

5kV to 20kV, the viscosity, storage modulus and loss modulus of the resin increased significantly, while the increase rate of the resin at 60kV slowed down. It was because the inductive effect of HVEF on the material had a certain limit voltage value. With the increase of treatment time, the increase rate of adhesive viscosity, storage modulus and loss modulus increased significantly. This was mainly due to the fact that the ions and oxygen-containing groups excited in the electric field as the treatment time of HVEF increased, which promoted the polycondensation reaction of the adhesive.

(3) Under the condition of a constant temperature of 30°C, the viscosity increased significantly with the increase of frequency. For phenolic resin, there was a sudden change point at 10Hz, which was related to the inherent characteristics of the material. At a constant temperature of 50°C and 70°C, the viscosity of urea-formaldehyde resin decreased with increasing frequency, and it was greatly affected by moisture content. The change trend of PF resin was similar to that of a constant temperature of 30°C. After HVEF treatment, the viscosity, storage modulus and loss modulus of urea-formaldehyde resin and phenol-formaldehyde resin significantly increased in the frequency range compared with untreated resin. There was no significant difference in the increase rate of the rheological parameters of the two resins under various treatment conditions. From 5kV to 20kV, the increase rate of resin viscosity, storage modulus and loss modulus all increased significantly, while the increase rate at 60kV slowed down. After HVEF treatment, with the constant test temperature increased, the increase rate of the viscosity, storage modulus and loss modulus of resins decreased.

# Chapter IV Influence mechanism of HVEF induction on interfacial properties of wood/bamboo composites

## 4.1 Introduction

Biomass (wood, bamboo, etc.) is a green, renewable, natural polymer material from a wide range of sources, which has been widely used in new energy and new material based composite materials. However, cracking, degumming and peeling at the interphase of composite materials often occur in the process of usage. At present, in order to improve the bonding interphase properties of biomass materials and their composites, researchers have proposed modification methods, including chemical modification, plasma modification, corona modification and adhesive toughening and strengthening modification methods [58,49,216]. These modification methods of the surface, adhesives and bonding interphase of biomass materials all belong to the category of pretreatment, which can increase the bonding strength by improving the activity of the material surface and the compatibility of the interphase [46,47]. The interphase characteristics of biomass composites are mainly determined by the surface properties of materials, the properties of adhesives and the degree of crosslinking reaction between chemical functional groups on the surface of materials and adhesives.A large number of chemical groups (−OH, −CHO, etc.) on the surface of wood and bamboo play an important role in the crosslinking reaction with adhesives. In addition, wood/bamboo materials are considered to be typical porous materials. In wood materials, there are cell or tracheid structures, cellular wall pore structures and gaps between cellulose macromolecular chains, etc. [38]. The microstructures of cells

were different in different sections of wood. There were significant differences in the content of chemical components among different tree species. Bamboo material has a large number of vascular bundle cell structure. The vascular bundle distribution of bamboo green is more dense, while the vascular bundle distribution of bamboo yellow is sparse. Meanwhile, the chemical composition of bamboo green and bamboo yellow is different [80]. These factors, such as chemical groups, microstructure and composition content of biomass, will affect the adhesive permeability at the interphase of composite materials, thus further affecting the crosslinking reaction and mechanical properties of the interphase [81,82].

HVEF could improve the surface and interphase of materials and the physical and chemical properties of wood, bamboo, adhesives and their adhesive interphase will be affected by HVEF. In the presence of HVEF, biomass materials will produce ionization and polarization phenomena, which will affect the surface charge distribution of the material, the interaction between active groups and their chemical bonds. In addition, according to the research of electrodynamics, the transmission, convection and distribution patterns of liquid will also be affected by HVEF, and the flow pattern and internal structure of droplets or fluids will constantly change with the introduction of HVEF. The influence mechanism of HVEF induction on the surface properties and adhesives of various biomaterials has been described in detail in Chapter 2 and Chapter 3. However, the influence mechanism of HVEF treatment on the interphase and their composites are not clear yet and need to be further studied and explored.

In this chapter, four kinds of wood materials (*Populus tomentosa Carr.*, *Triplochiton scleroxylon K. Schum.*, *Pinus massoniana Lamb*, *Cunninghamia lanceolata Lamb*) and flattened bamboo (*Phyllostachys puercens*) were used as experimental materials. To explore the influence mechanism of HVEF on interphase properties of different kinds of composite materials.

## 4.2 Materials and methods

### 4.2.1 Test materials

In this experiment, the materials were selected: Masson's pine, Chinese fir, poplar and ayous (Forest Farm, Nanjing Forestry University, Xiashu Town, Jurong City, Jiangsu Province) and flatten bamboo (Dechang Bamboo Co., Ltd., Zhejiang Province, China). The basic information such as the size of material is shown in Table 4-1. The selected wood, bamboo and other materials were dried in the oven at 50°C for 72h with a moisture content of 8±3%. After drying, the samples were put into the constant temperature and humidity box for storage.

Preparation method of urea-formaldehyde resin: 213g formaldehyde (37%) was weighed and added into a 500ml four-mouth bottle, the agitator was started, and the pH concentration was adjusted to 7.5-8.0 with 30%NaOH solution. Adding 80g of urea for the first time and slowly heating up to 90°C within 30-40 minutes. The temperature was kept at 90°C for 40min, and the pH value was measured three times during this period to observe the change trend of pH. After the heat preservation,

adjusting pH = 4.6-5.1 with 20% $NH_4Cl$ solution and continuing the reaction at 90-94°C. After a period of time, a drop of reaction liquid was dropped into room temperature water at 20°C when white clouds appeared as the end point. At this time, alkali (30%NaOH solution) should be added immediately to neutralize it to 7.0-7.5. Adding 20g of urea for the second time, keeping the temperature for 15 minutes, pumping water to cool to 45°C, adjusting pH to 7.0-7.5 with 30%NaOH, cooling to room temperature, storing it in a refrigerator at 6°C.Parameters: molar ratio of formaldehyde and urea is 1.5, solid content is 50%, viscosity is 109MPa·s (rotary viscosity tester, DV-79+ PRO), 1% ammonium chloride (according to solid content) mixed with the glue solution. All reagents were purchased from Jiangsu Nanjing Chemical Pharmaceutical Company.

Tab.4-1 The basic properties for samples.

| Types of materials | Species | Dimension | Density ($g/cm^3$) |
|---|---|---|---|
| Veneer | masson pine | 400 mm×400 mm×2.5 mm (length × width × height) | 0.55 |
| Wood samples | masson pine | 200mm×50mm×20mm (length × width × height), radial cutting plate | 0.55 |
| | | 200mm×50mm×20mm (length × width × height), tangential cutting plate | |
| | | 200mm×50mm×20mm (length × width × height), cross-cutting plate | |
| | Chinese fir | 200mm×50mm×20mm (length × width × height) | 0.37 |
| | poplar | 200mm×50mm×20mm | 0.42 |

| | | | |
|---|---|---|---|
| | | (length × width × height) | |
| | ayous | 200mm×50mm×20mm (length × width × height) | 0.52 |
| Bamboo sample | Flattened bamboo | 200mm×50mm×20mm (length × width × height) | 0.66 |

### 4.2.2 Preparation of composite materials and HVEF treatment methods

Preparation of plywood and HVEF treatment method (as shown in Figure 4-1) the amount of glue applied on the single side of three-ply plywood is 150g·m$^2$ (urea formaldehyde resin). After forming the plywood, it was put into the plate electric field inside the hot press. The upper plate was connected with the high voltage generator, the lower plate was grounded, and the material sample was placed between the two plates. Treatment conditions for different voltages, including 5kV (8min), 10kV (8min), 15kV (8min) and 20kV (8min), and treatment conditions for different treatment times, including 2min (20kV), 4min (20kV), 6min (20kV) and 8min (20kV). The hot pressing temperature was set at 120°C, the hot pressing pressure of the composite material was 1MPa, the whole hot pressing time last for 8min, and the ambient humidity was 60%. Both hot pressing and HVEF treatment started at the same time. After treatment time was reached, the high voltage generator was shut down. At the end of the hot pressing process, the composite material was removed, cooled to room temperature, and balanced in a constant temperature and humidity box for 2 weeks. The experiment was repeated 10 times for each treatment condition.

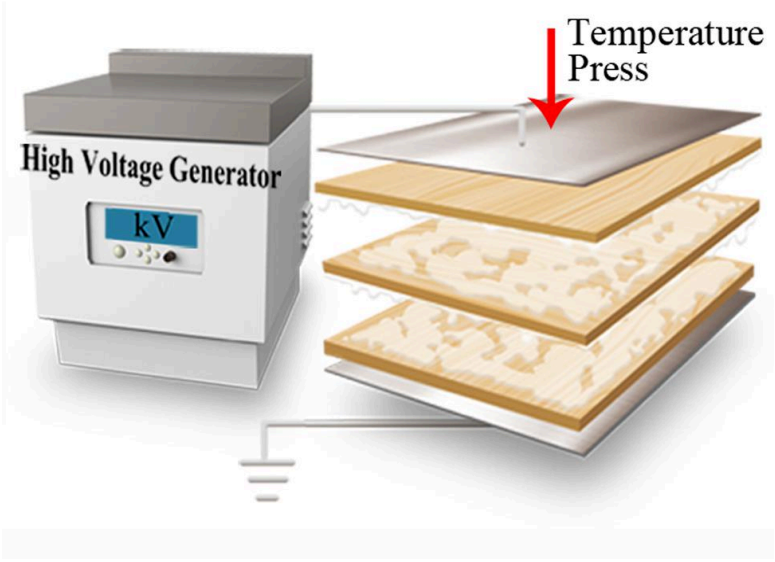


Fig.4-1 Schematic diagram for Masson pine-UF plywood preparation under HVEF treatment.

Preparation method of wood composites: including composite materials with different sectional combinations (as shown in Fig. 4-2) and composite materials composed of different tree species (as shown in Fig. 4-3). The amount of glue was 150g·m$^2$ (single side glue, phenolic resin). The composite materials were put into the plate electric field inside the hot press. Hot pressing time and HVEF treatment time were 40min, the treatment voltage was 60kV, the hot pressing pressure was 1MPa, the hot pressing temperature was 145°C, the environmental humidity was 60%. The experiment was repeated 10 times.

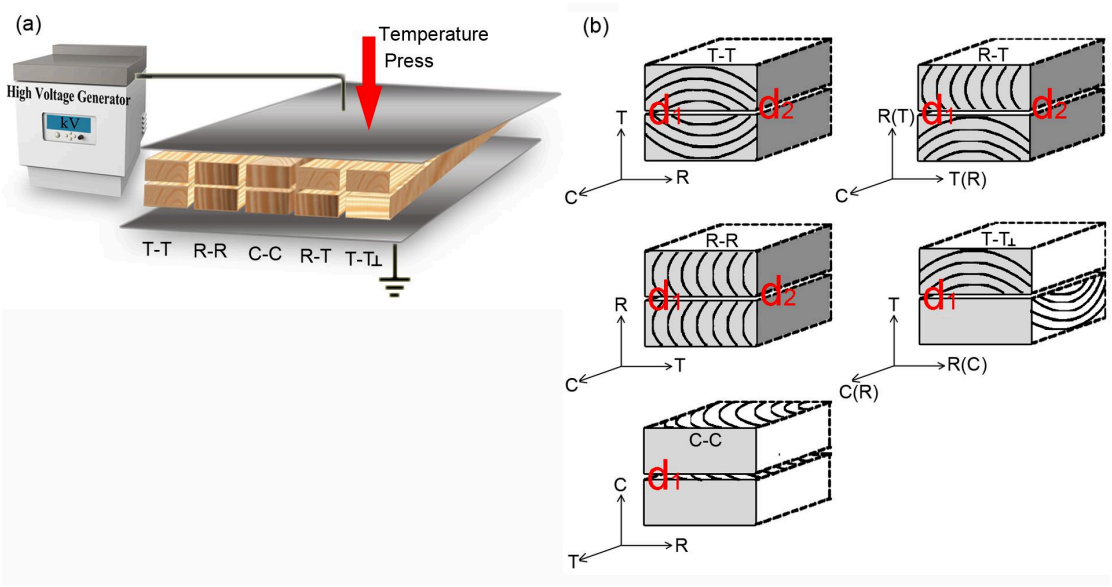


Fig.4-2 Schematic diagram for different cut combinations composites under HVEF treatment. (a) HVEF device, (b) five different cut combinations composites.

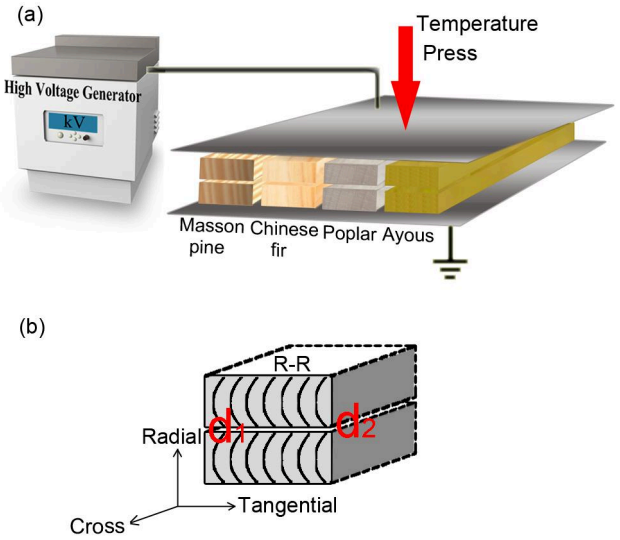


Fig.4-3 Schematic diagram for different wood species composites under HVEF treatment. (a) HVEF device, (b) R-R wood composite.

Preparation method of bamboo composite material (as shown in Figure 4-4) : bamboo composite material was glued with 250g·m$^2$ (double-sided adhesive, phenolic resin). The assembled composite material was put into HVEF inside the hot press.The hot pressing and electric field treatment started at the same time. The hot pressing time and the HVEF treatment time were both 14min, the treatment voltage was 60kV,

the hot pressing pressure was 1MPa, the hot pressing temperature was 145°C, and the ambient humidity was 60%.The experiment was repeated 10 times.

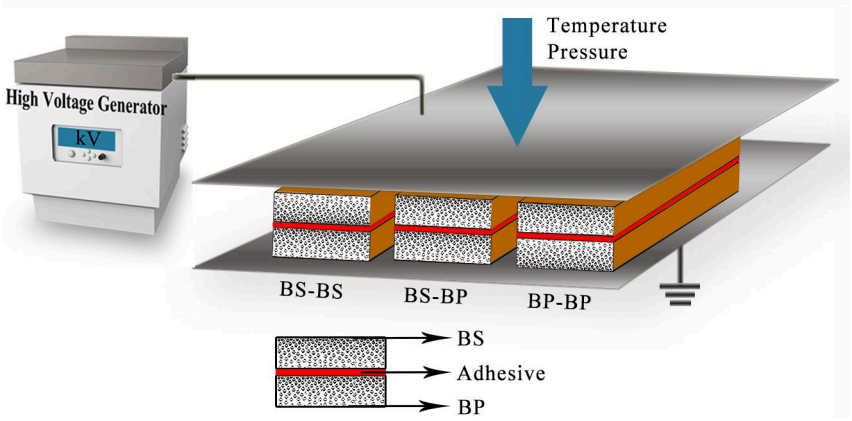


Fig.4-4 Schematic diagram for different combinations bamboo composites under HVEF treatment.

The HVEF generator selected for this test was produced in Hangzhou Jingtong Co., Ltd. (JT207K-1, HC-JDGC-C), Zhejiang, China. The sample was placed in the flat electric field in the hot press. The average thickness of the aluminum plate was 3mm. The upper plate was connected with a high voltage generator and the lower plate was grounded, as shown in Fig. 4-1. The sample was placed between the two plates. After setting the temperature, the voltage value was adjusted and the high voltage generator was turned on. After reaching the treatment time, the generator was turned off. The test material was taken out, cooled to room temperature, and put into the constant temperature and humidity box for balance for 2 weeks. The composite materials and HVEF parameters prepared in this experiment were shown in Table 4-2:

Tab.4-2 The parameters selected for high voltage electric field.

| Types of materials | Species | Adhesive | Composite material/layer number | Temperature (°C) | Voltage (kV) | Time (min) |
|---|---|---|---|---|---|---|
| Veneer | masson pine | UF | Plywood, three layers | 120 | 0/5/10/20/60 (8min) | 0/2/4/6/8 (60kV) |
| Wood samples | masson pine | PF | Double, Cross section - Cross section (C-C) | 145 | 60 | 0, 40 |
| | | | Radial section - Radial section (R-R) | | | |
| | | | Radial section - Tangential section (R-T) | | | |
| | | | Tangential section - Tangential section (Parallel, T-T), | | | |
| | | | Tangential section - Tangential section (Vertical, T-$T_{Vertical}$) | | | |
| | Chinese fir | PF | Double layer, radial section - radial section (R-R) | 145 | 60 | 0, 40 |
| | poplar | PF | Double layer, radial section - radial section (R-R) | 145 | 60 | 0, 40 |
| | ayous | PF | Double layer, radial section - radial section (R-R) | 145 | 60 | 0, 40 |

| | | | | | | |
|---|---|---|---|---|---|---|
| Bamboo sample | Flattened bamboo | PF | Double, BS-BS<br>BS-BP<br>BS-BP | 145 | 60 | 0, 14 |

### 4.2.3 Fluorescence microscopy analysis

A point light source is prepared in the fluorescence microscope, which has the characteristics of high luminescence rate, and can emit ultraviolet light after the light source is processed by the filter color system, so as to excite the fluorescence substances existing in the biological samples and produce different fluorescence colors in the biological samples. Conventional fluorescence microscopes consist of ordinary optical microscopes with light source accessories, including high pressure mercury lamp, excitation filter, blocking filter and beam separator. The fluorescence excited by the mercury lamp is passed through the excitation filter (UV, etc.), so that the excitation light of a certain broken length irradiates to the surface of the biological specimen, thus the internal characteristics of the specimen can be distinguished.

Sample preparation and test method: Samples were taken from the fixed position of the interphase of the composite material adhesive layer, and the obtained samples were fixed on the sliding slicer with the slice size of 5mm×5mm× 30μm (length × width × thickness) (as shown in Fig. 4-5). The slices were heated in a baking machine for 24h (50°C). After cooling, the slices were soaked with 1% saffron staining (Safraninet) for 20 min. The stained slices were then dehydrated and the ethanol solution (concentrations ranged from 55%, 65%, 75%, 85% to 100%) was changed

every 10 min. After dehydration, the slices are immersed in xylene/anhydrous ethanol (volume ratio 1/1) mixture (10 min), and then immersed in pure xylene solution for 10 min. After the slices were removed, the slices were sealed with gum and set aside. Fluorescence microscopy with ultraviolet light source (OLYMPUSBX51) was used in this experiment.

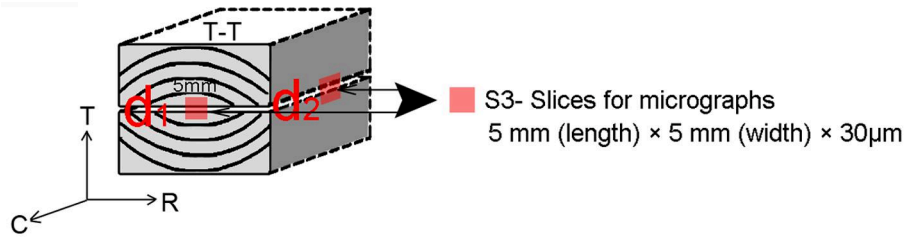


Fig.4-5 Schematic diagram for fluorescence microscope slices Preparation.

### 4.2.4 X-ray vertical density profile

X-ray vertical density profile is an effective nondestructive testing technology for testing the density distribution of the interphase of composite materials, which is beneficial to analyzing the adhesive distribution of the interphase of composite materials, and evaluating the quality and properties of the bonding materials. The sample was selected from the fixed area of the composite material, the size was 5mm×5mm (length × width). In this test, Grecondax-5000 test instrument was used, the test accuracy was 0.02mm, the test ambient temperature was 25℃, and the humidity was 60%. The density of wood was mainly calculated according to this formula:

$$\rho = \frac{1}{\mu t} \ln \frac{I_0}{I} \tag{4-1}$$

Where, $I_0$ was the initial intensity (X-ray), $I$ was the test intensity, $t$ was the thickness of the sample, and $\mu$ was the wavelength and the correlation constant (μ= 7).

### 4.2.5 Test method of mechanical properties

In this paper, Siswan mechanical testing machine equipment was used to test the mechanical properties of composite materials such as adhesive strength, elastic modulus and static bending strength. The load loading speed was 2mm/min. The test method was as follows.

Plywood adhesive strength test: the test samples were selected from the fixed area of the composite material and tested according to standard GB/T8617657-2013 (class II plywood). The sample size was 100mm×25mm×6mm (length × width × height), and each test condition was repeated for 10 times.

Laminate compression shear strength test: the size of the test sample was 50mm×50mm×40mm (length × width × height), according to the standard ASTMD905-98 test. The repetition was10 times for each test condition.

Test method for elastic modulus and static bending strength: The test sample was sawed from the fixed area of the composite material, the size of the sample was 300mm×50mm (length × width), the thickness was determined according to the thickness of the composite material, and the test was conducted in accordance with the standard EN-310-1993. Each condition was repeated for 10 times.

### 4.2.6 Impregnation delamination test method

In accordance with GB/T17657 of class II impregnation delamination test (urea formaldehyde resin), the test pieces were placed in hot water at (35±3) ℃ for 2h, and then placed in a drying oven at (63±3) ℃ for 3h. When dipping the test pieces, all the specimens were immersed in hot water. The total delamination rate was calculated by dividing the total delamination length by the length of the total adhesive line. Cracks in the wood caused by the drying process and natural environment were not counted. Each condition was repeated 10 times.

In accordance with the standard JAS-1980(I) test (phenolic resin), the delamination rate of the adhesive layer of the composite material was measured. The sample size was 75mm×75mm (length × width), and the thickness is determined by the actual thickness of the composite material. The sample was immersed in boiling water for 4h, and then immersed in water at 10℃~25℃ for 1h. After that, they were placed in a drying oven at (70±3) ℃. During the drying process, the distance between the samples was fixed to at least 50mm, and the mass of the dried samples increased by 0% to 10% compared with that of the unsoaked samples.The total delamination rate was calculated by dividing the total delamination length by the total glue line length. Cracks in the wood caused by the drying process and natural environment are not counted. Each condition was repeated 10 times.

## 4.3 Results and analysis

### 4.3.1 Influence of HVEF induction (voltage/time) on interfacial properties of wood plywood

In order to investigate the inductive mechanism of HVEF on the bonding interphase properties of composite materials. Firstly, the penetration of UF resin at the bonding interphase was observed by fluorescence microscope. In this experiment, serine T was used as a stain for wood tissue (Figure 4-6). Under a fluorescence microscope, the wood appears orange and the UF resin blue. It could be seen from the diagram that (figure 4-6 (a)), without HVEF, most of the resin penetrated into the framework of internal structure by tracheid, intercellular space and pit, a small amount of adhesive distributed along the interphase, especially on the bonding interphase with a small amount of adhesive in tracheid cavity and even not filling up. The distribution of UF resin on the bonding interphase of untreated composites is dispersed and disordered [217]. Equation 4-2 was used to calculate the average penetration length of the five adhesives with the longest resin penetration depth on the bonding interphase:

$$D = \sum_{i=1}^{5} l_i / 5 \tag{4-2}$$

Among them, *D* is the average resin penetration depth, and *li* is one of the longest penetration depth (μm) in the adhesive interphase.

The results of fluorescence microscopy showed that the average penetration depth of the resin at the untreated interphase was 1250μm. After HVEF treatment, the penetration depth of the adhesive on both sides of the adhesive interphase was significantly reduced, especially at the interphase, the tracheid cavity was filled with more UF resin. Meanwhile, it could be seen that the distribution of UF resin at the adhesive interphase was more continuous and regular than that without the treatment. Under the conditions of different treatment times and treatment voltage of 60kV, the average penetration depth of urea-formaldehyde resin at the bonding interphase was calculated as 851μm (2min), 698μm (4min), 535 μm (6min) and 257μm (8min), respectively (as shown in Figure 4-6 (b) ~ (e)). Under the treatment of different voltages and treatment time of 8min, the average penetration depth of urea-formaldehyde resin at the bonding interphase of the samples was 655μm (5kV), 564μm (10kV), 262μm (20kV) and 257μm (60kV), respectively (as shown in Figure 4-6 (E) ~ (H)). These results indicated that with the increase of treatment time and voltage, the penetration depth of the adhesive decreases, and the amount of UF resin at the bonding interphase of the composites increases. These results could be attributed to the fact that after HVEF treatment, the surface polarization and oxidation degree of the material improved, and the reactive groups increased, so that more chemical functional groups of resin and wood surface active groups involved in in-situ cross-linking reactions. Therefore, after treated by HVEF, the penetration of the adhesive into tracheid cavity, grain pore and gap to the internal structure deep at the

interphase could be restricted, and the chemical cross-linking reaction between the adhesive and wood at the interphase could be improved [218,219].

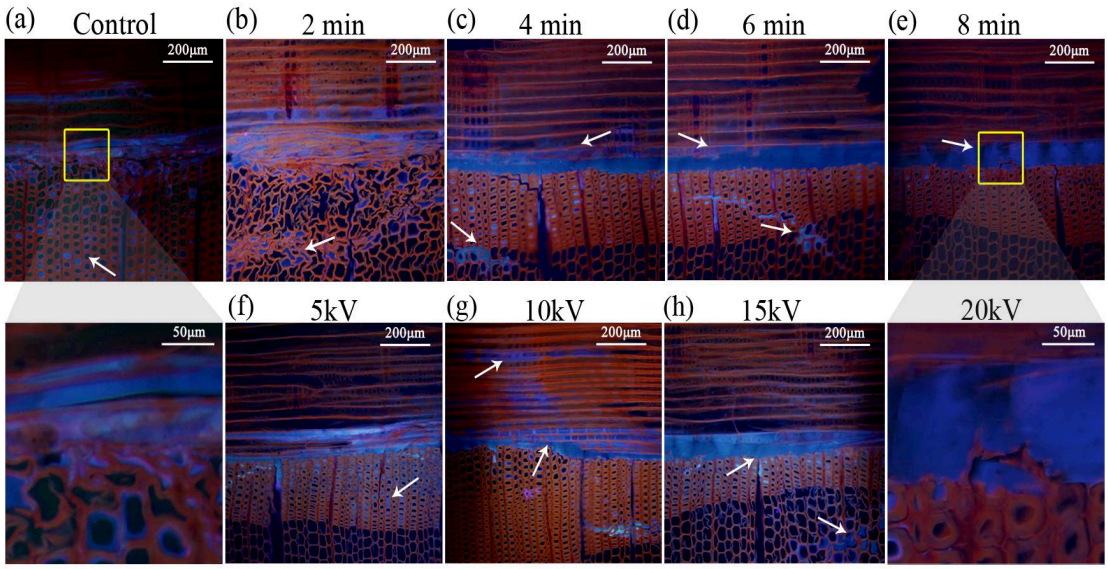


Fig.4-6 Micrographs of HVEF treated samples obtained by fluorescence microscope using UV light under different treating times and intensities respectively compared with the control. (a) Micrographs for the control samples. Micrographs for samples treated under 60 kV during (b) 2 min, (c) 4 min, (d) 6 min, (e) 8 min. Micrographs for samples treated during 8min under (f) 5 kV, (g) 10 kV, (h) 20 kV, (e) 60 kV.

As shown in Figure 4-7, in order to further study the distribution form of adhesives at the interphase of composite materials after HVEF treatment, the X-ray vertical density profile was used in this experiment to analyze the density distribution diagram of composite materials. As defined in Fig. 4-7 (a), the distribution range of resin in the density profile is beyond the range of the maximum wood density. As can be seen from the density distribution diagram of untreated composites, the average distribution length of UF resin within a single interphase range was 1905μm, and the average maximum density was 848kg/m$^3$. After the treatment of HVEF, the distribution range of adhesives within a single interphase decreased, and the maximum density at the interphase increased significantly (peak value). The average

value of the maximum density was 1081kg/m$^3$. After treated with HVEF (60kV, 8min), the resin distribution range at a single interphase was about 1000μm in length. Combined with the fluorescence micrographs at the interphase, the penetration depth of most resins during the bonding process was concentrated in the range of 250μm to 300μm. The longer the treatment time of the HVEF was, the higher the voltage was, and the maximum density value at the interphase of the composite material increased significantly. According to the results, under different treatment times, the average increase of maximum density could be sorted as follows: 16.21% (2min), 22.78% (4min), 27.45% (6min) and 32.12% (8min); under different voltages, the average increase of maximum density could be sorted as 21.16% (5kV), 22.43% (10kV), 31.05% (20kV) and 32.12% (60kV). These results were due to the significant increase of free radical contents, the decrease of initial contact angle and equilibrium contact angle, the increase of O/C ratio and the significant increase of C2~C4 peak components, and the significant increase of characteristic peak at the oxygen-containing group after the treatment of HVEF (Chapter 2). The increase of wood surface polarization, oxidation degree and active group provides more binding sites for the cross-linking reaction between wood surface and resin. At the same time, as mentioned in Chapter 3, the viscosity, storage modulus and loss modulus of adhesives induced by HVEF increased significantly. Therefore, the amount of resin at the interphase of composites increased, the density increased and the range of resin penetration depth decreased, which could affect the bonding strength of composites and the mechanical properties at the interphase [220,221].

Before and after HVEF treatment, the changes of the bonding strength and wood failure ratio (the ratio of wood damage area to the whole bonding area) of the composite were studied and analyzed, so as to evaluate the bonding performance of the composite interphase (as shown in Figure 4-8). The results showed that the bonding strength and wood failure ratio of the composites were significantly improved after HVEF treatment. Compared with the untreated composite, the bonding strength of the composite after HVEF treatment increased from 0.66MPa to 1.25MPa, and the wood failure ratio increased to 85%. At the same time, under the treatment voltage of 60kV, within a certain range, with the increase of treatment time, the change rate of bonding strength and wood failure ratio also increased significantly (as shown in Fig. 4-8 (a)). When the treatment time was 8min and within a certain range, the higher the treatment voltage was, the higher the bonding strength and wood failure ratio will be (as shown in Fig. 4-8 (b)). These results could be attributed to the fact that more adhesives were concentrated at the interphase (a significant increase in the density at the adhesive interphase and a decrease in the resin penetration depth, as described above).

At the same time, the changes of the impregnation delamination properties before and after HVEF treatment were further studied. As shown in Figure 4-9, it could be seen that the delamination rate of plywood after HVEF treatment significantly reduced. Under the condition of certain voltage, with the increase of treatment time, the delamination rate decreased significantly, and according to its change rate, it could be sorted as: 22.90% (2min) < 34.61% (4min) < 44.23% (6min)

< 48.22% (8min); under the condition of a certain time, with the increase of voltage, the impregnation delamination rate also decreased significantly, which could be classified as 15.35% (5kV), 26.80% (10kV), 44.15% (20kV) and 48.22% (60kV) according to the change rate. Therefore, these results further illustrated the positive effects of HVEF treatment on the interfacial properties, bonding strength and durability of plywood.

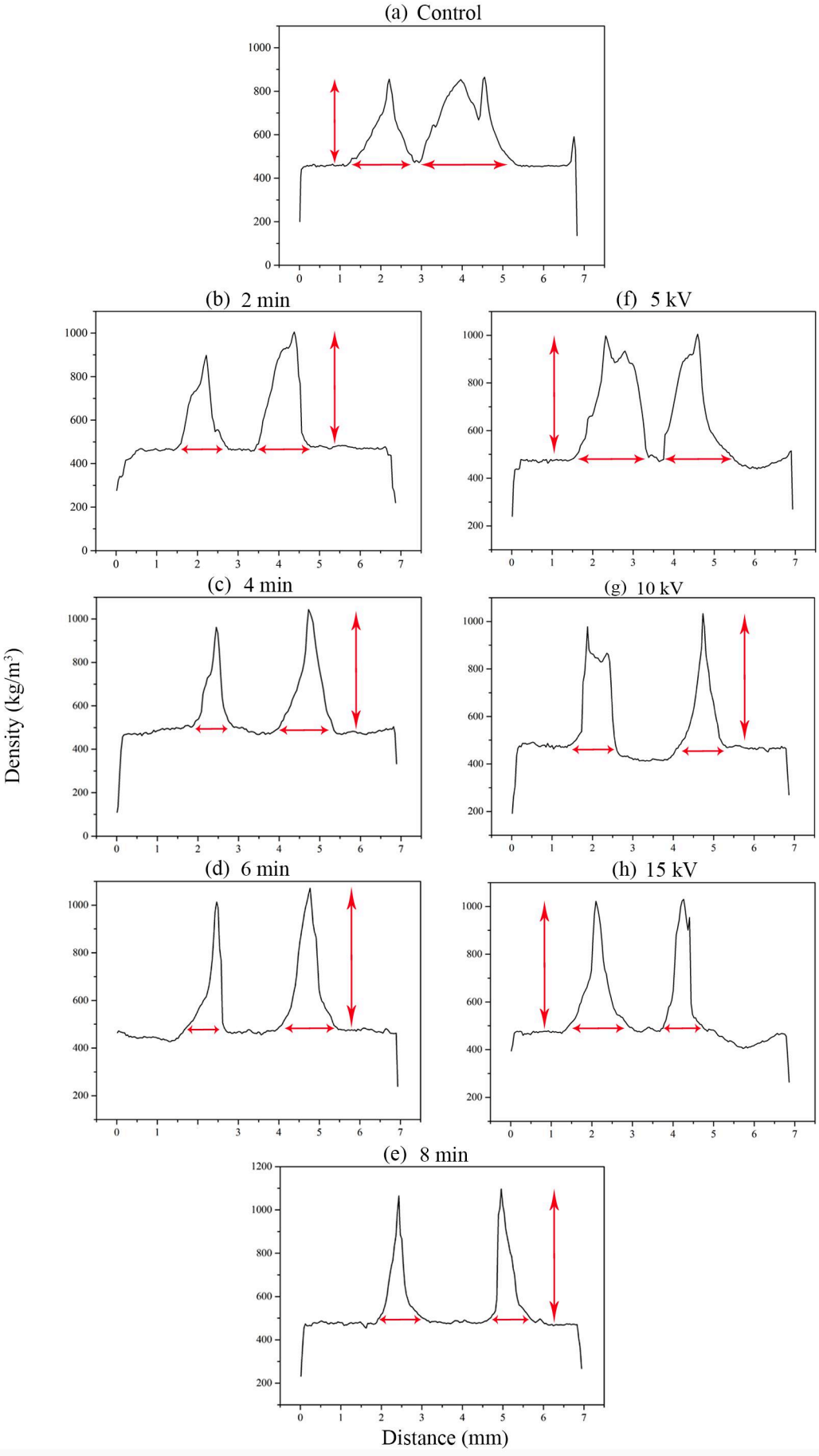
(a) Control
(b) 2 min
(c) 4 min
(d) 6 min
(e) 8 min
(f) 5 kV
(g) 10 kV
(h) 15 kV
Density (kg/m³)
Distance (mm)

Fig. 4-7 X-ray vertical density profile graphs of HVEF-treated samples at varying treatment times and voltages and compared with the control. (a) control, (b) 2 min (20 kV), (c) 4 min (20 kV), (d) 6 min (20 kV), (e) 8 min (20 kV), (f) 5kV (8min), (g) 10kV (8min), (h) 15kV (8min).

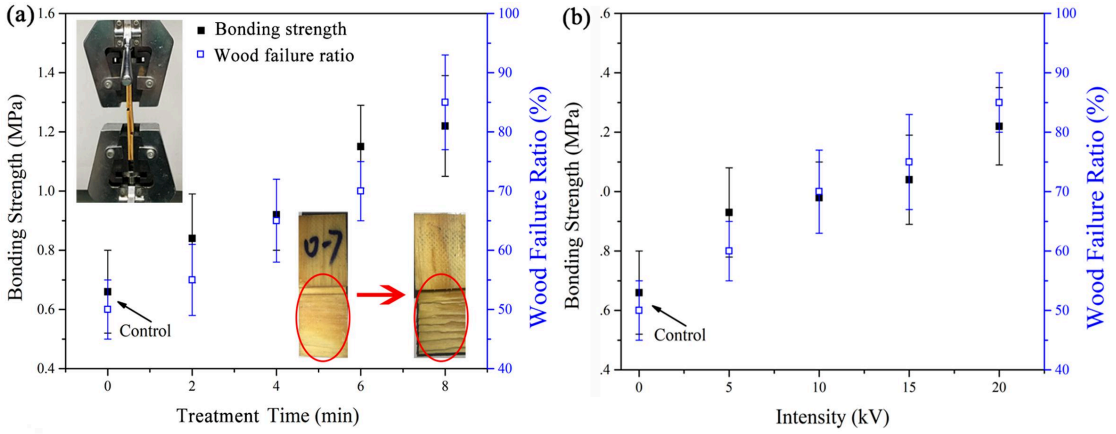


Fig. 4-8 Bonding strength and wood failure ratio of HVEF-treated samples at varying (a) treatment times and (b) intensities.

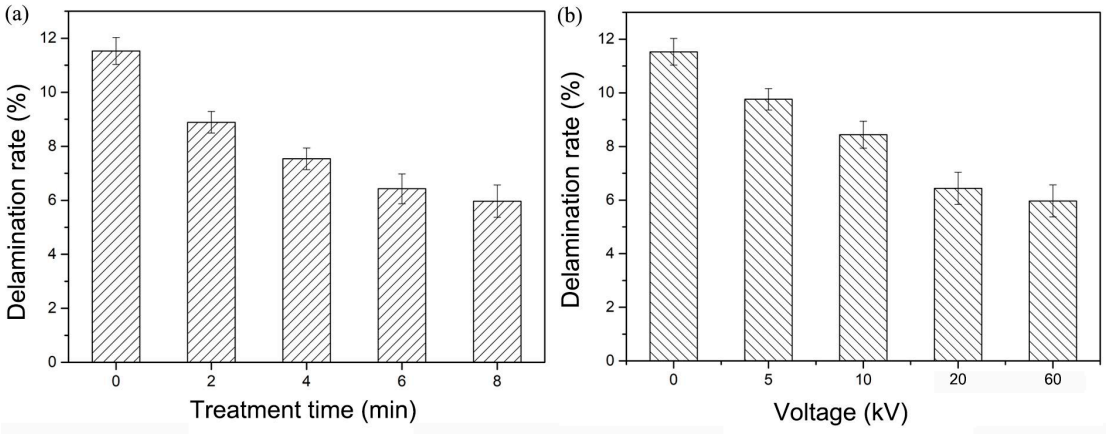


Fig. 4-9 Delamination rates of HVEF-treated samples at varying (a) treatment times and (b) intensities.

### 4.3.2 Influence of HVEF induction on interfacial properties of wood composite materials with different sections

After HVEF treatment, the content of wood free radical increased significantly, the initial contact angle and equilibrium contact angle decreased, the O/C ratio

increased and the peak fraction of C2~C4 increased significantly. The HVEF treatment can significantly improve the degree of wood surface polarity, increase the active group, and thus improve the chemical reaction ability of wood surface. Because of varied effect of HVEF treatment on the sections of wood surface, further study on the effect of HVEF on interphase properties of the composites are needed. The interphase characteristics of wood composite with different section combinations were explored under HVEF treatment.

As shown in Fig. 4-10, the changes of adhesive penetration forms at the interphase of composite materials with different combinations observed by fluorescence microscopy before and after the treatment of HVEF were characterized. In the fluorescent micrographs, wood was shown in orange and the phenolic resin in green. In the untreated condition, phenolic resin penetrated into the internal structure of wood mainly through tracheid cavity, intercellular space and grain pore structure, resulting in longer penetration depth, discontinuous and irregular distribution of adhesives at the interphase. As could be seen from the R-R untreated section in Figure 4-10 (a), most adhesives penetrated to both sides along the interphase through wood rays, grain holes and other structures, and the direction of wood rays was parallel to the direction of the interphase. In the T-T untreated samples (Figure 4-10 (c)), a large amount of adhesives permeated to both sides of the interphase along wood rays, tracellular lumen and cellular space. The direction of wood rays was perpendicular to the direction of the interphase, resulting in a smaller adhesive dose at the adhesive interphase than at the R-R interphase. In the microscopic section diagram of T-T

orthogonal complement (Fig. 4-10 (h)), it could be seen that the adhesive distribution pattern was similar to that of the medium T-T sample. In the R-T section diagram, the adhesive on one side of the interphase penetrated along the interphase through wood rays, grain holes and other structures, and the direction of wood rays was parallel to the direction of the interphase (R). On the other side of the interphase (T), the adhesive penetrated along the direction of the wood rays, which were perpendicular to the direction of the interphase. Compared with the R-section, there was more adhesive penetration on the T-side, and only a small amount of adhesive remained at the interphase. In C-C sample sections, most of the adhesives infiltrated along the tracheids. As the direction of tracheids was perpendicular to the direction of interphase, a large number of adhesives penetrated into the interior of the wood, and the distribution of adhesives at the interphase was discontinuous and the glue solution was insufficient.

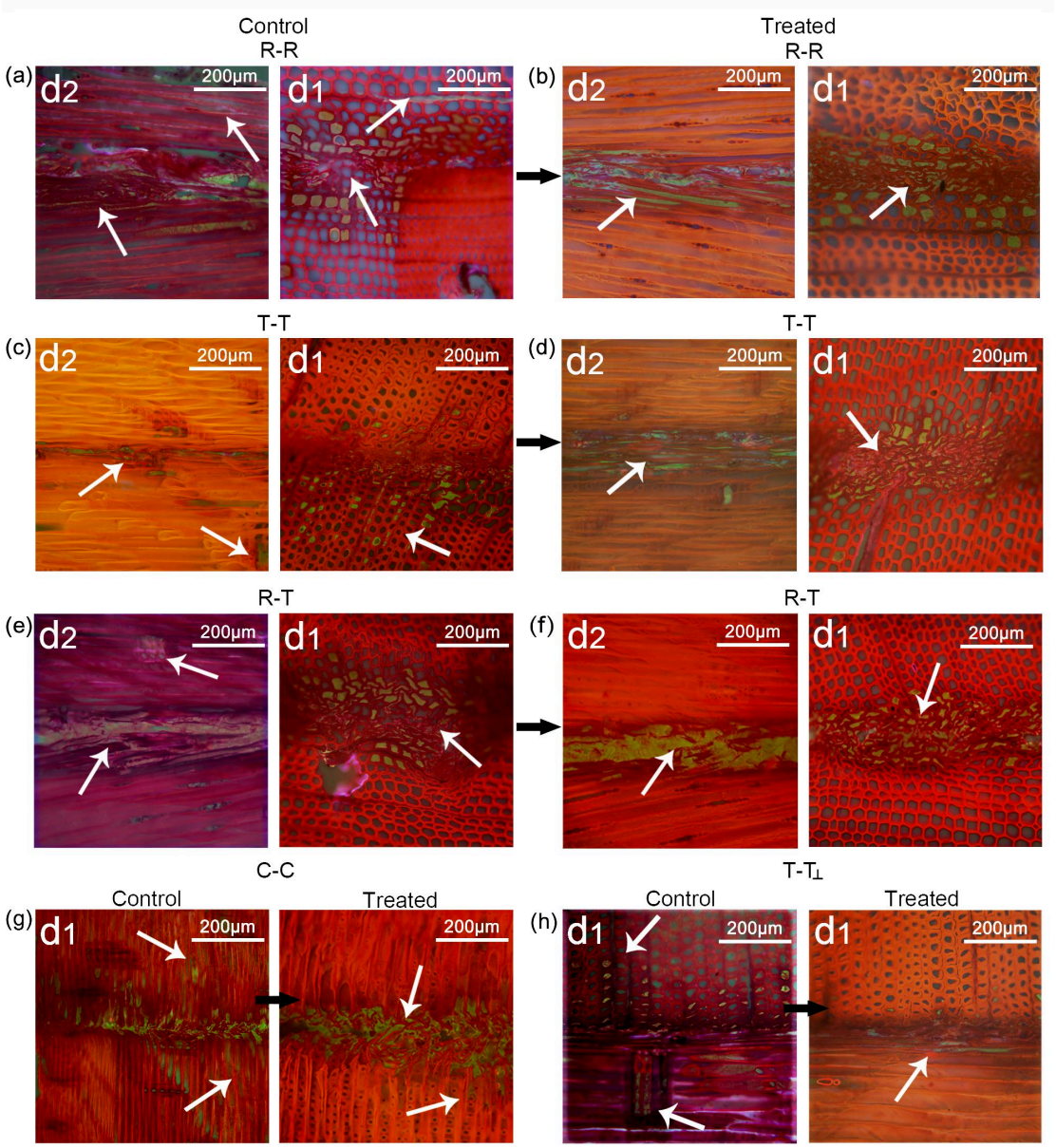


Fig. 4-10 Micrographs obtained by fluorescence microscope for different sample combinations treated by HVEF and compared with the control. Micrographs for the control ones including (a) R-R, (c) T-T, (e) R-T, (g) (left) C-C and (h) (left) T-T⊥. Micrographs for treated ones including (b) R-R, (d) T-T, (f) R-T, (g) (right) C-C, (h) (right) T-T.

According to the formula 4-2, the average penetration depth of the adhesive can be calculated. According to the penetration depth of composite materials with different sections without HVEF treatment, the order of penetration depth could be as follows: R-R (850μm) < R-T (950μm) < T-T (1150μm) < T-T (1160μm) < C-C (1250μm). Previous studies have also shown that both grain pore and wood ray tissue could

affect the permeation form of glue, especially in different sections, due to the difference of wood cell structure and different permeation form of glue will be caused [222,223]. After HVEF treatment, the penetration depth of composites with different section combinations was as follows: R-R (220μm) < R-T (230μm) < T-$T_{vertical}$ (242μm) < T-T (245μm) < C-C (310μm). As a result, the average penetration depth of the adhesive was significantly lower than that of the untreated composite, and the adhesive was continuously and uniformly distributed at the interphase. This result could be attributed to the fact that after HVEF treatment, the surface activity of the material improved and the degree of polarization increased, so that more chemical groups in the wood could cross-link with the adhesive. After HVEF treatment, in R-R slices, the direction of wood ray was parallel to the direction of interphase, and a large amount of adhesives were distributed at the interphase and filled with tracheids at the interphase (Figure 4-10 (b)). For the T-T and T-T orthogonal section diagrams, it could be seen that the direction of wood ray was perpendicular to the direction of the interphase, and the adhesive filled the tracheid lumen on both sides along the direction of the interphase, and concentrated in large quantities at the interphase (as shown in Figure 4-10 (d) and (h)). In R-T sections, one side had wood rays parallel to the interphase, and the other side had wood rays perpendicular to the interphase. Tracheids on both sides of the interphase were filled with a large amount of adhesive compared with untreated ones (Figure 4-10 (f)). For C-C sections, some of the adhesive still penetrated into the interior of the wood. The difference of the penetration depth of the composites with five cross-section combinations was mainly

caused by the different micro-structures of the pores on each cross-section, including the direction of wood rays, the distribution of grain pores and the morphology of tracheids.

At the same time, for the composite materials with different section combinations, the distribution of sectional density, and compared the changes of sectional density distribution of various composites before and after treated by HVEF (as shown in Fig. 4-11). In the untreated composites, the distribution of adhesives ranged from 2mm to 4mm, and the maximum density at the interphase did not exceed 850kg/m$^3$. After HVEF treatment, the maximum density at the interphase of various composites increased significantly, and the distribution range of adhesives was narrow. According to the density increment, it could be sorted as C-C (13%) < T-T (24%) < T-T$_{vertical}$ (25%) < R-T (28%) < R-R (30%). The distribution range of the adhesives in the composites treated by the HVEF was about 1mm, and most of the adhesives were distributed at the bonding interphase in the range of 200 to 250μm. Therefore, the effect of the adhesives at the interphase of the composites after HVEF treatment could be explained as the decrease of the permeability of the adhesives and the increase of the maximum density at the interphase. The interphase properties of composites, including the distribution of adhesives, density distribution, etc., could affect the mechanical properties of composites to some extent [220,221].

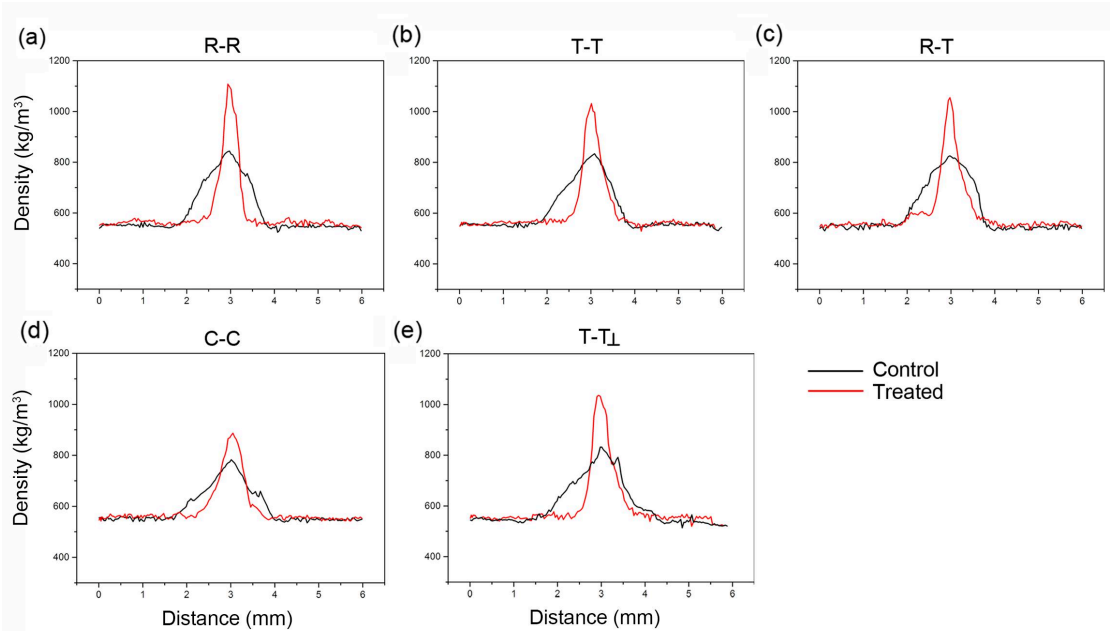


Fig. 4-11 VDP of different sample combinations treated by HVEF and compared with the control. Including (a) R-R, (b) T-T, (c) R-T, (d) C-C,(e) T-T.

Fig. 4-12 showed the change of compressive shear strength and wood failure rate of composites before and after treated by HVEF. For the samples treated by HVEF, the compressive shear strength and wood failure rate of the composites combined with the five sections significantly improved. The increment of shear strength at the interphase of composites with five combinations of sections could be sorted as follows: 18% (C-C) < 24% (T-T) < 26% (T-$T_{vertical}$) < 31% (R-T) < 42% (R-R). According to the increment size of wood failure rate, it could be sorted as 12% (C-C) < 13% (T-T) < 15% (T-$T_{orthogonal}$) < 19% (R-T) < 23% (R-R). The change rate of shear strength and wood failure rate of the composites with the highest in R-R composite, while the change rate of the composites with C-C composite was the lowest. This was because the penetration depth of the adhesive at the interphase and the density at the

interphase of the R-R composite material were the least and the maximum after treated by the HVEF. The compressive shear strength and wood failure rate of T-$T_{vertical}$ combination were higher than that of T-T combination, which was mainly because the macroscopic interweaving of fibers in the vertical textured combination further promoted the cross-linking reaction between wood and adhesive during the treatment. In addition, in Fig. 4-13, the impregnation delamination rates of composites with different combinations. After HVEF treatment, the impregnation delamination rate of the composite material significantly reduced, which could be ranked as 28.39% (C-C) < 51.78% (T-T) < 57.52% (T-$T_{vertical}$) < 62.91% (R-T) < 69.12% (R-R) according to the reduction rate. Obviously, R-R combination has the lowest impregnation delamination rate, while C-C section combination has the highest delamination rate. Therefore, this result was related to the penetration depth of the adhesive and the density at the interphase. The aggregation effect of the adhesive after HVEF treatment has a positive effect on the bonding strength and impregnation delamination rate of the composites.

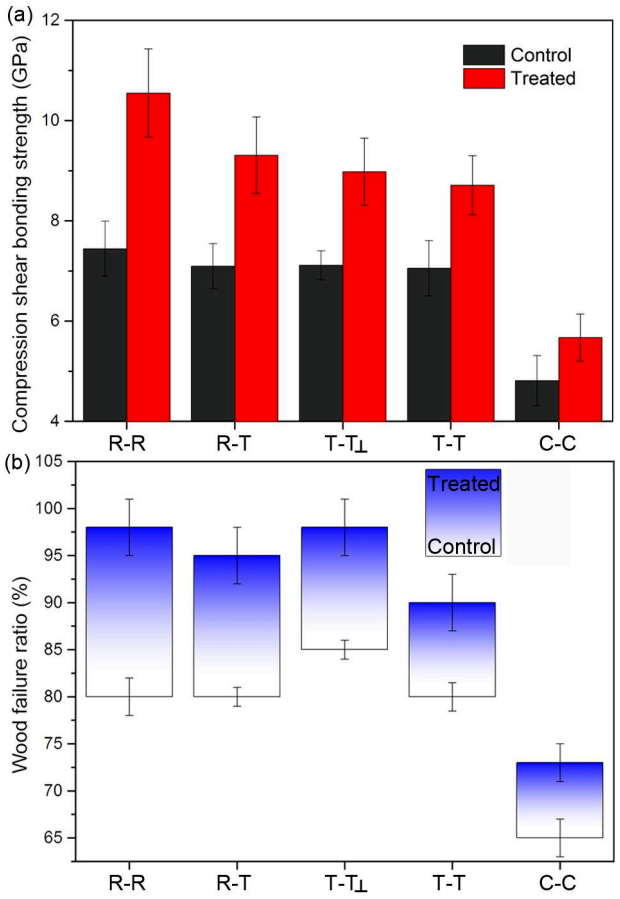


Fig.4-12 Compression shear bonding strength measurement for five cut combinations treated by HVEF compared with the control. (a) shear strength for different combinations, (b) Wood failure ratio for different combinations.

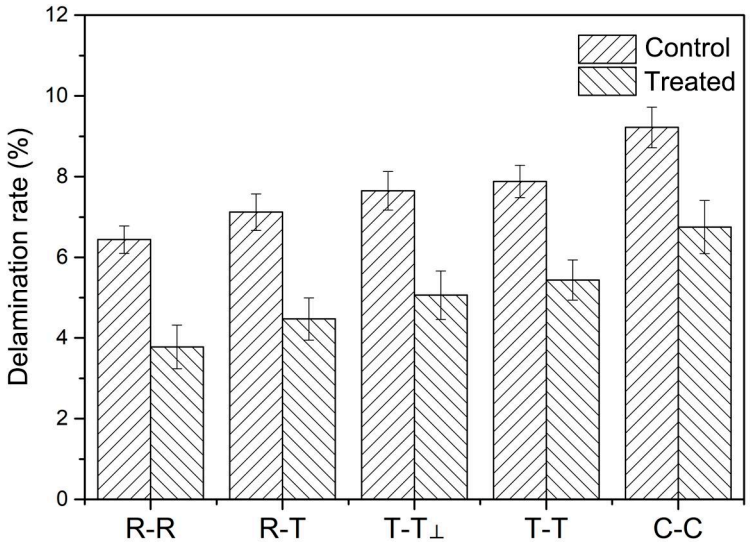


Fig.4-13 Delamination rate measurement for five cut combinations treated by HVEF compared with the control.

### 4.3.3 Influence of HVEF induction on interphase properties of composite materials with different tree species

In the second chapter, the effect of HVEF treatment on the surface characteristics of different tree species was studied. It was concluded that the influence of HVEF treatment on the surface characteristics of different tree species was significantly different, which was mainly due to the differences in chemical composition, tracheids or tubular pore microstructure among wood species. In this chapter, in order to obtain the effect of HVEF on the surface and interphase characteristics of different tree speciesthe influence of HVEF treatment on the interphase characteristics of composite materials of different tree species was further explored, and the correlation among various factors affecting the interphase characteristics was statistically analyzed.

In the fluorescent micrographs (Figure 4-14), wood section showed orange and the PF adhesive in green. As could be seen from all sections, the adhesive penetrated into the interior of the wood along the interphase and laterally through structures such as wood ray cells, pits, tracheids and tubules. As could be seen from the untreated sections (Fig. 4-14 (a), (c), (e) and (g)), the penetration form of the adhesive at the interphase was discontinuous and irregular, and the penetration depth of the adhesive on the longitudinal section (D2) and the cross section (D1) was relatively long. In softwoods, most of the adhesives were dispersed in various tracheids and ray cells far from the interphase. At the same time, longer adhesive penetration depth (through tube holes and other structures) was also observed in hardwood. Especially for the composite materials of poplar and Chinese sycamore species, a large amount of

adhesives penetrated into the tube holes and wood ray cells, resulting in longer penetration depth, more penetration volume and less adhesives near the interphase. In addition, it was also observed in micrographs that the diameter of tubules or tracheids of tree species also significantly affected the distribution uniformity and continuity of adhesives. The larger the diameter, the more uneven the distribution at the interphase of adhesives. According to the formula proposed by Modzel et al.[21], the average penetration length of the adhesive was calculated as: masson pine (850μm) < Chinese fir (866μm) < ayous (1035μm) < poplar (1180μm). After HVEF treatment, the section micrographs of the sample were shown in Fig. 4-14 (b), (d), (f) and (h). It could be seen from the figure that a large amount of adhesive existed and were filled in the tracheids at the interphase of the composite material. According to the average penetration depth, the order could be as follows: masson pine (220μm) < Chinese fir (223μm) < ayous (420μm) < poplar (448μm). Therefore, after HVEF treatment, the average penetration depth of the composite of different tree species significantly reduced, and the distribution of the adhesives was continuity and uniformity. The penetration depth of the adhesives at the interphase of hardwood composites was significantly greater than that of softwood whether or not treated. Among them, Chinese fir had the highest change rate of penetration depth, while ayous had the lowest change rate. This difference was mainly due to the highest lignin content of Chinese fir and the lowest lignin content of ayous. In addition, the tracheid diameter of softwood measured in Chapter 2 was smaller and the cell wall was thicker. However, in softwood and hardwood composites, the difference of adhesive

penetration depth of different tree species was small. Therefore, it was necessary to further explore the variation law of penetration depth of other tree species in future research, so as to improve the influence law of HVEF induction on surface interphase characteristics of different tree species.

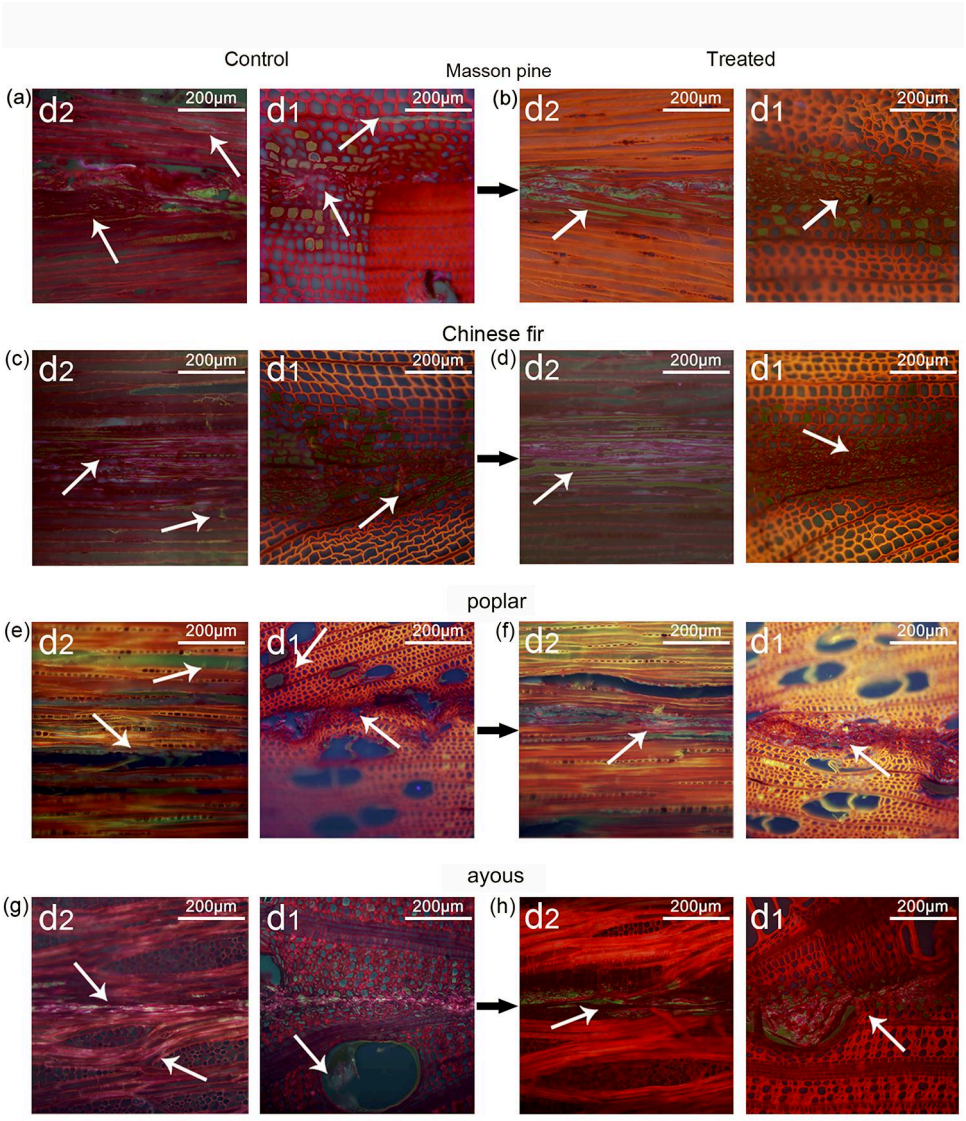


Fig.4-14 Micrographs for different treated bonding samples compared with the control. Micrographs for the control samples including (a) Masson pine, (c) Chinese fir, (e) poplar, (g) ayous. Micrographs for treated samples including (b) Masson pine, (d) Chinese fir, (f) poplar, (h) ayous.

As shown in Fig. 4-15, the change of X-ray density distribution of composite materials with different tree species combinations before and after treated by HVEF was represented. It could be seen from the figure that, after HVEF treatment, the distribution range of adhesives at the interphase significantly narrowed, and the density at the interphase significantly increased. The order of the increase at the interphase of different tree species obtained by calculation: ayous (+23%) < poplar (+25%) < masson pine (+31%) < Chinese fir (+32%). The difference of the results was mainly due to the different lignin content and the diameter of the tube hole in different tree species. In previous related studies, it was also found that the density at the interphase of the composite material increased significantly after treated by HVEF [169,174]. This was mainly because the increased surface energy and free radicals provided more reaction sites for the crosslinking reaction between wood chemical groups and adhesives. In addition, as shown in Fig. 4-16, the changes of the compression shear performance for composite materials with different tree species before and after treated by HVEF were measured. For composite materials with different tree species combinations, the compressive shear strength significantly improved after treated by HVEF. According to its change rate, it could be sorted as follows: ayous (+31%) < poplar (+38%) < masson pine (+42%) < Chinese fir (+46%). At the same time, the change of wood failure rate of composite materials before and after HVEF treatment was also measured. As could be seen from the figure, after HVEF treatment, wood failure rate of composite materials significantly improved, and the order of its change rate could be as follows: ayous (+15%) < poplar (+18%) <

masson pine (+23%) < Chinese fir (+27%). These results were mainly due to the aggregation effect of the adhesives at the interphase of the composites after HVEF treatment (that is, the density at the interphase increased and the penetration depth decreased), and the adhesives were continuously and uniformly distributed at the interphase. Therefore, the HVEF treatment improved the adhesive distribution form and interphase bonding properties of the composites [119].

In Figure 4-17, the impregnation delamination rates of composite materials with different tree species combinations were represented. After HVEF treatment, the impregnation delamination rate of the composites decreased significantly. Obviously, the impregnation delamination rate of Chinese fir composite was the lowest and the highest delamination rate was ayous composite, which could be ranked as follows: ayous (35%) < poplar (55%) < masson pine (69%) < Chinese fir (74%) according to its change rate. Therefore, this result was related to the penetration depth and density of the interphase of biomass composites. The aggregation effect of the adhesives after HVEF treatment has a positive effect on the bonding strength and impregnation peel rate of the composites.

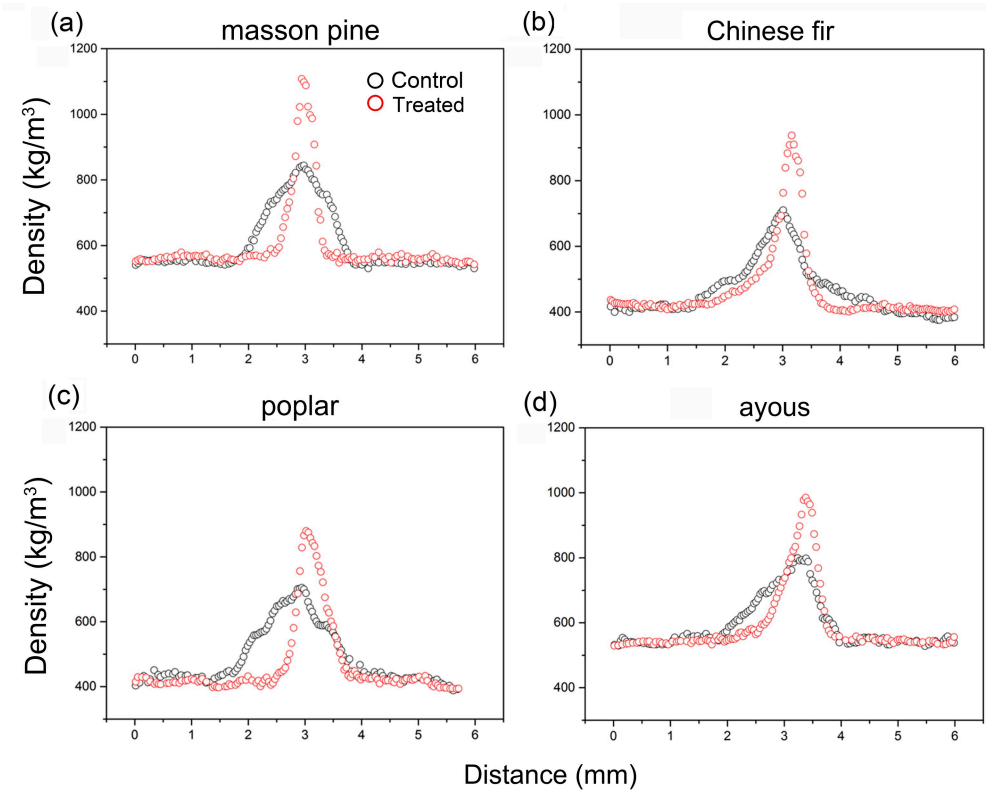


Fig.4-15 VDPs for different treated samples compared with the control including (a) masson pine, (b) Chinese fir, (c) poplar, (d) ayous.

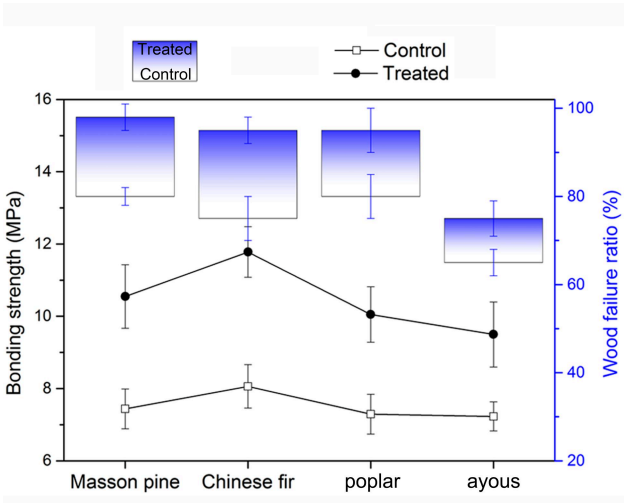


Fig.4-16 Compression shear bonding strength measurement for different bonding samples under HVEF compared with the control.

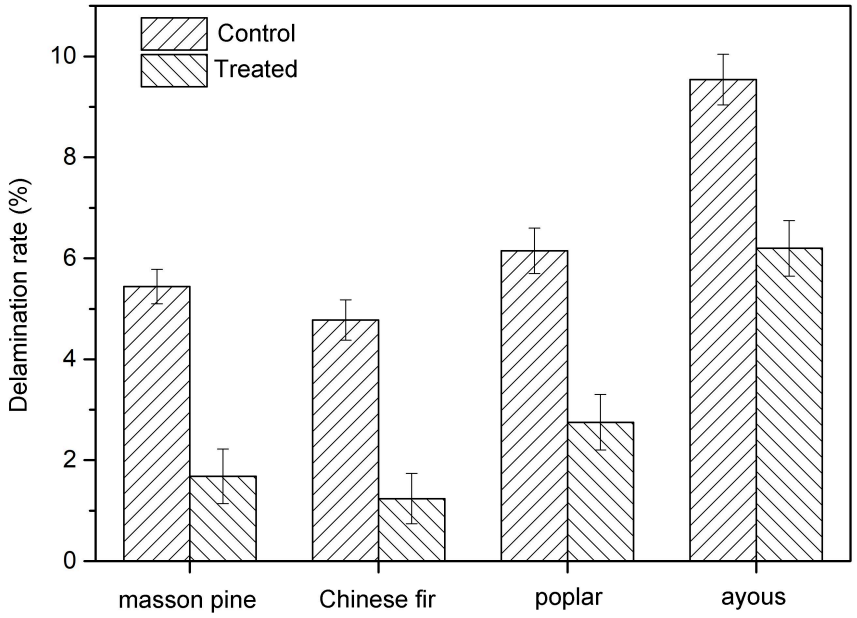


Fig.4-17 Delamination rate for different bonding samples under HVEF compared with the control.

In order to further study the inductive effect and influence mechanism of HVEF treatment on material surface and interphase characteristics, this test also analyzed the correlation between characteristic parameters affecting material surface and interphase under the condition of HVEF treatment, and made correlation analysis and statistical analysis of these parameters (as shown in Fig. 4-18). In the figure, these seven parameters include: lignin content, extract content, tubehole or tracheid diameter, rate of free radical increase, rate of penetration depth decrease, rate of maximum density increase and rate of shear strength increase. A 7×7 correlation analysis matrix was formed by using these parameters.Among them, formula 4-3 for calculating the rate of change is as follows:

Change rate (%) = ((treated parameter value - untreated parameter value)/untreated parameter value) ×100% (4-3). In the matrix, each element represented the correlation analysis results of parameters on the horizontal and vertical axes. The background color in the matrix represented the size of the different correlations (including red: $0.8 < R^2 < 1$, green: $0.7 < R^2 < 0.8$, blue: $0.6 < R^2 < 0.7$, and white: $R^2 < 0.6$). Elements on the diagonal represented the correlation of the same parameters; therefore, their correlation $R^2=1$. As could be seen from the whole matrix, the correlation of each element was symmetrically distributed along the diagonal. In the first line of the correlation matrix, the characterization of the seven parameters with the size of the correlation of lignin content analysis. It could be concluded that the lignin content, free radical change rate, the change rate of penetration depth, maximum density increment and the shear strength increment was positive correlated. The correlation between lignin, free radical change rate and the rate of penetration depth was $R^2 > 0.8$. Previous studies have also shown that materials with high lignin content have higher free radical content [224]. In this experiment, it was also found that the increase of free radical content was proportional to the lignin content. It was also found from the matrix that the change rate of free radical content was positively correlated with the penetration depth reduction rate, the maximum density improvement rate and the shear strength improvement rate. At the same time, the decreasing rate of penetration depth was positively correlated with the increasing rate of maximum density and shear strength, and $R^2 > 0.73$.

On the other hand, some negative correlation results were found between extract content and other parameters. For example, high extract content could have a negative effect on bonding strength. In the process of HVEF treatment, under the influence of temperature, the extract will migrate to the surface of the material, thus reducing the reactivity of the chemical groups on the surface of the material. Similar results have also been found in previous studies [225,226]. The extract content of ayous and masson pine was higher, which resulted in lower increase of free radicals (compared with poplar and Chinese fir, respectively). At the same time, the tracheid or pore diameter was negatively correlated with the rate of change of penetration depth ($R^2$=0.68), the maximum density improvement rate ($R^2$=0.63) and the shear strength improvement rate ($R^2$=0.69), which was mainly due to the fact that a higher diameter would more easily lead to a large amount of penetration of adhesive and the discontinuity and inhomogeneity of adhesive distribution at the interphase.

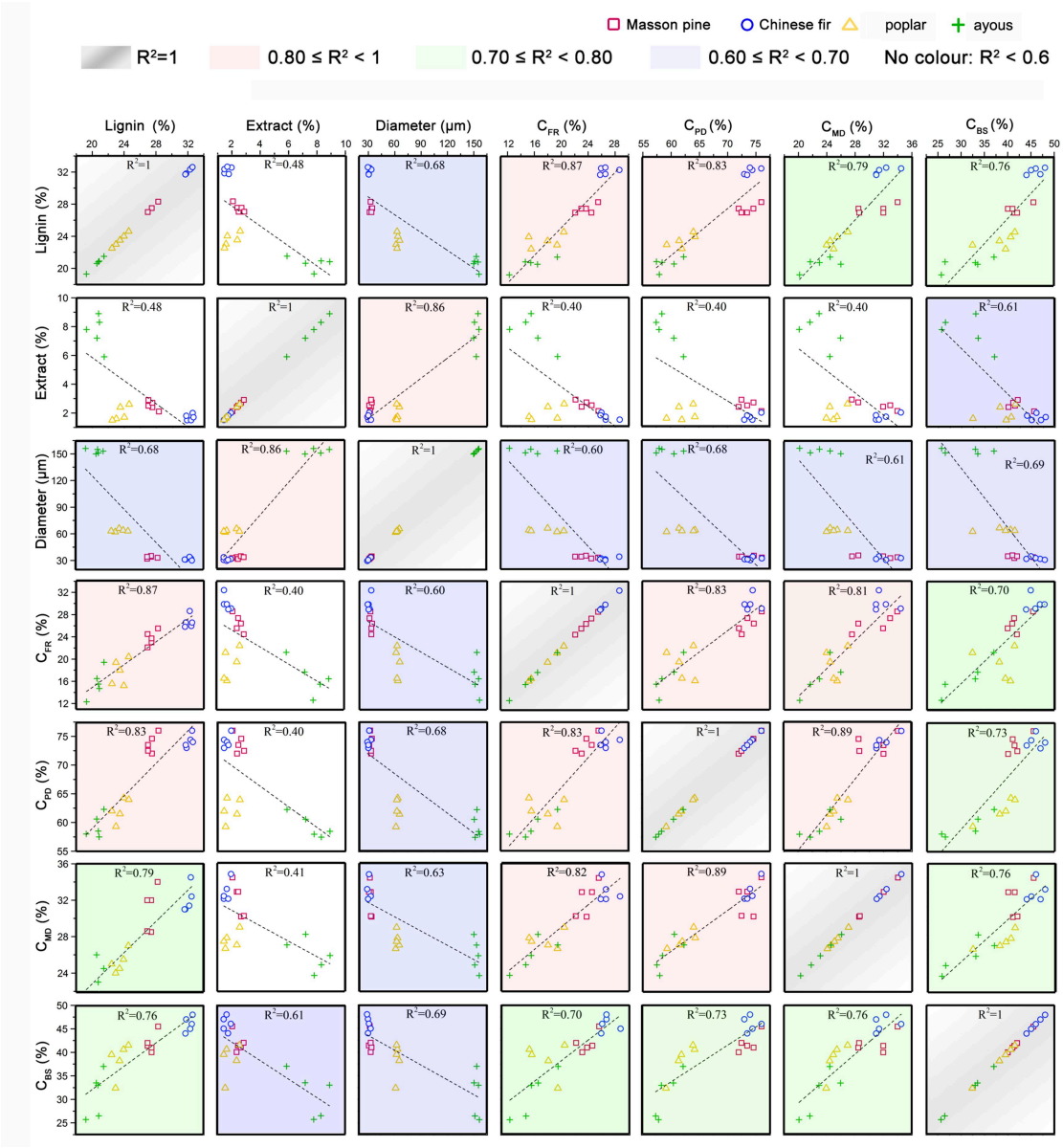


Fig.4-18 Correlations among lignin content, extract content, lumina diameter, change ratio of free radicals, penetration depth, maximum density and bonding strength in a 7 × 7 matric.

### 4.3.4 Influence of HVEF induction on interfacial properties of bamboo composites

In the second chapter, it was concluded that the effect of HVEF treatment on bamboo surface characteristics was significant. After HVEF treatment, the content of

wood free radical increased significantly, the initial contact angle and equilibrium contact angle decreased, the O/C ratio increased and the peak fraction of C2~C4 increased significantly, and the characteristic peak at the oxygen-containing group increased significantly. Moreover, the effect of HVEF on the surface chemical properties of bamboo green and bamboo yellow were different, and the change rate of surface chemical properties parameters of bamboo green was higher than that of bamboo yellow. In order to further study on the influence of HVEF on the features of bamboo composite interphase, this test was prepared by different combination forms of bamboo composite, the bond strength of bamboo composite interphase, adhesive distribution, vertical density distribution and analysis of the differences between different combination interphase features were conducted.

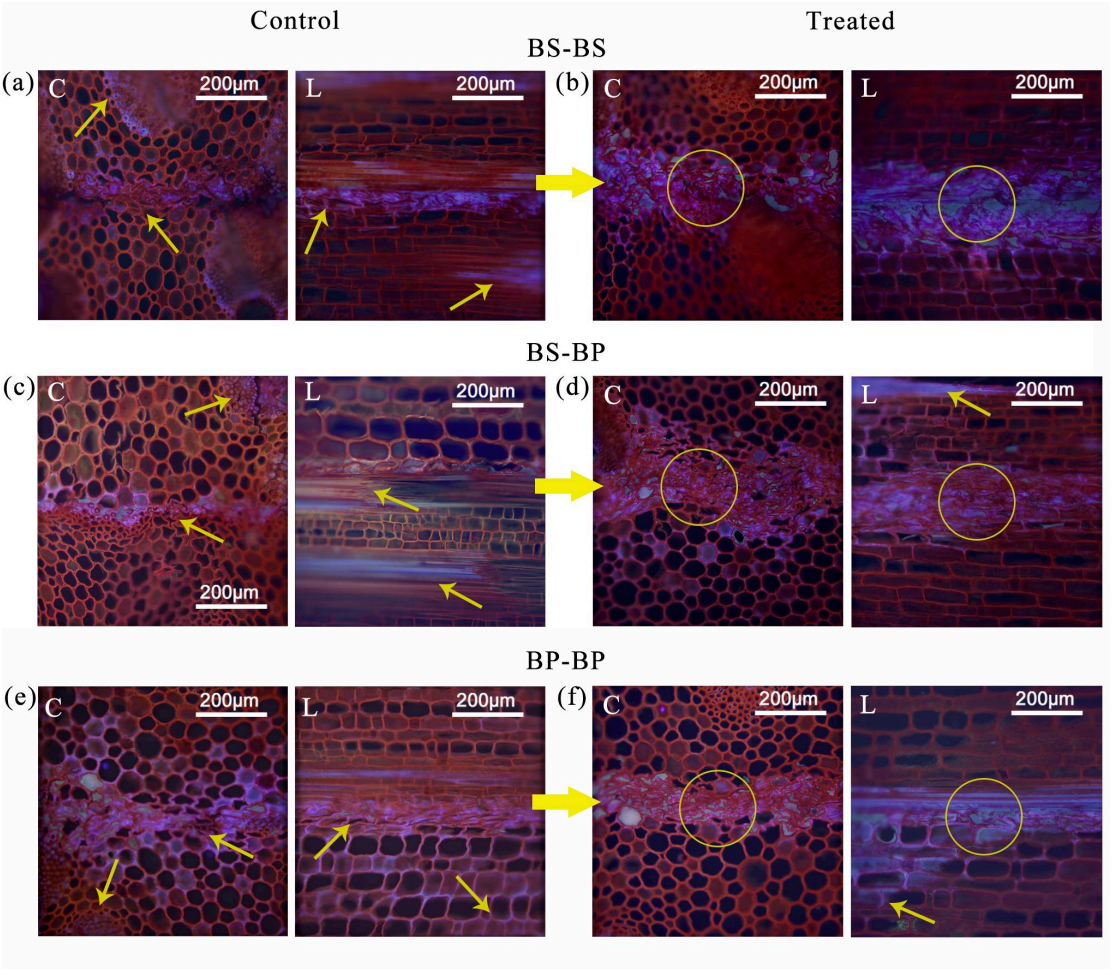


Fig.4-19 Micrographs for different treated bamboo bonding samples compared with the control. Micrographs for the control samples including (a) BS-BS, (c) BS-BP, (e) BP-BP. Micrographs for treated samples including (b) BS-BS, (d) BS-BP, (f) BP-BP.

As shown in Fig. 4-19, fluorescence diagrams of bamboo composite materials with different combinations were presented. The bamboo fiber structure was orange, and the phenolic resin was blue. In the untreated slices (figure 4-19 (a), (c), (e)), it could be seen that adhesive penetration into the bamboo structure through the bamboo fiber cells, vascular bundle and microscopic structure. A large amount of adhesives penetrated into both sides of bamboo structure, adhesive distribution at the interphase was scattered, discontinuous and uneven. The transverse and longitudinal sections showed that there was insufficient adhesive in the cell lumens at the interphase

(yellow arrow). The average penetration depth of adhesives was calculated according to formula 4-2 [21], and the average penetration depth of adhesives for composite materials with different combinations of bamboo sections was obtained as 950μm (BS-BS) < 1055μm (BS-BP) < 1280μm (BP-BP). It could be seen that the penetration depth of bamboo green was the least, which could be mainly attributed to the presence of dense vascular bundle cells in the bamboo green part, which was more dense than the bamboo yellow part and the presence of some waxy layers on the surface of the bamboo green layer [227,228]. After treated by HVEF, the distribution pattern of the adhesive at the interphase of the composite material changed significantly (Fig. 4-19 (b), (d) and (f)). For the treated BS-BS combination, the transverse and longitudinal sections showed that more adhesives gathered and there were a large number of adhesives in the cell cavity at the interphase. Their distribution was continuous and uniform. These results could be interpreted as the increase of oxygen-containing active chemical groups and free radical content on bamboo surface after HVEF treatment, which provided more reaction sites for bamboo surface to react with adhesives. In addition, for BS-BP and BP-BP composite materials, the same result existed, that is, after treated by HVEF, more adhesives concentrated at the interphase, and the distribution of adhesives at the interphase was continuous and uniform, which could be sorted according to the change rate: 386μm (BS-BS) < 570μm (BS-BP) < 720μm (BP-BP). However, for BS-BP and BP-BP composite materials (Fig. 4-19 (d) and (f)), both transverse and longitudinal sections, showed that some of adhesive still penetrated into the internal structure of bamboo after treated by HVEF. This result

was mainly due to the lower cellulose and lignin content in bamboo yellow than those of bamboo green. In the second chapter, the free radical, surface free energy change rate for bamboo yellow were lower than the bamboo green. The effect of HVEF on the surface activity and the degree of polarization properties played an important role on the combination of composite interphase [201].

In addition, the density distribution changes of various composites were tested by X-ray vertical density profile equipment (as shown in Fig. 4-20). In the figure, the dotted line represented the mean value of bamboo yellow and bamboo green. In bamboo, the density increased gradually from yellow to green, due to a gradual increase in the number of vascular bundle cells from yellow to green. From BS-BS, BS-BP and BP-BP of composite materials with different combinations. It could be concluded that the maximum density at the interphase increased significantly after the treatment of HVEF, and the distribution range of adhesive at the interphase became narrower, which was mainly because the penetration depth of adhesives at the interphase decreased after the treatment of HVEF. By comparison, it could be concluded that the order of maximum density was 923kg/$m^3$ (BP-BP) < 1039kg/$m^3$ (BS-BP) < 1087kg/$m^3$ (BS-BS). This result was mainly because the content of free radicals and free energy on the surface of bamboo green after treatment was higher than that on the surface of bamboo yellow, which provided more cross-linking reactions between the adhesive and the oxygen-containing active chemical groups on the surface of bamboo green. At the same time, according to previous studies, for wood and bamboo, after HVEF treatment, the penetration depth of the adhesive at the

interphase of the composite material was reduced and the distribution was continuous and uniform. The maximum density at the interphase was significantly increased. HVEF treatment has positive effect on the surface and interphase properties of bamboo and wood. However, bamboo and wood have different microscopic anatomical structures and chemical composition contents, so the effects of HVEF treatment on the surface and interphase properties of bamboo and wood are different. The microscopic anatomical structure of wood, including tracheid or pore structure, striated pore and wood ray, etc., can significantly affect the induced effect of HVEF on wood surface and interphase properties. There are also different chemical compositions and vascular bundle distribution patterns for bamboo green and bamboo yellow. Therefore, the differences in chemical compositions and microstructure have important reference significance for the application of HVEF treatment methods.

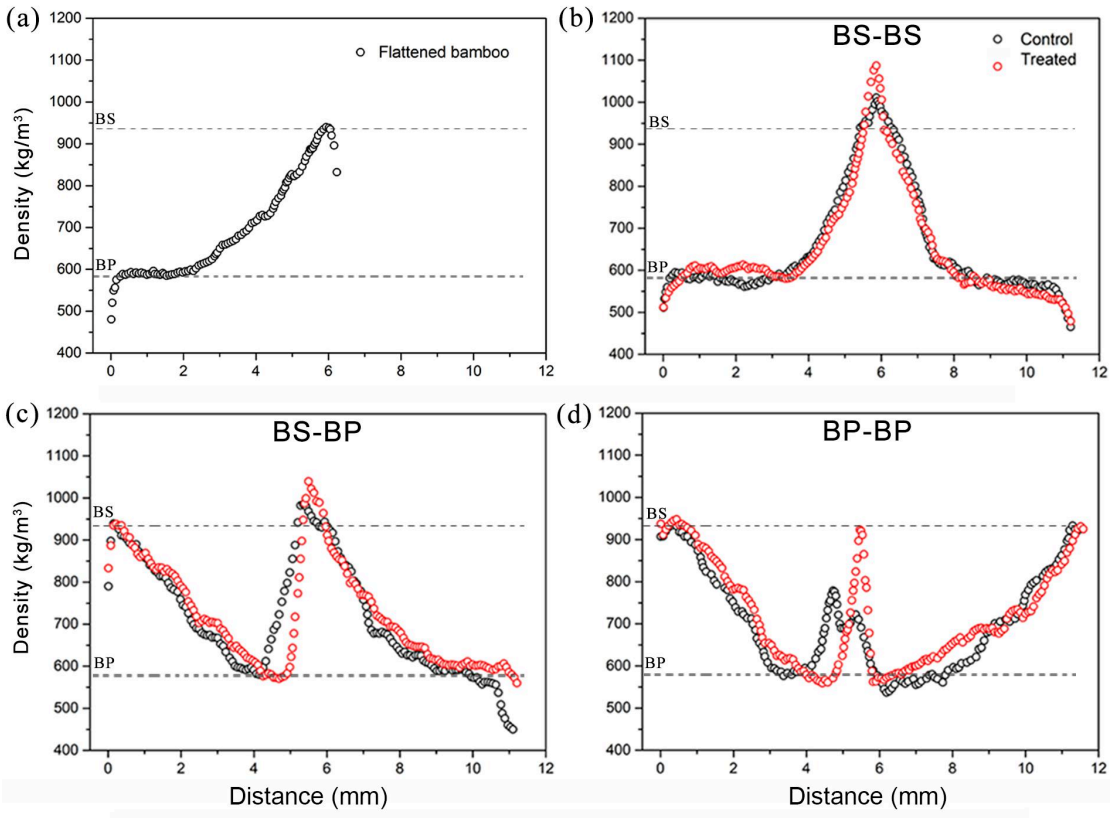

Fig.4-20 VDPs for different treated bamboo samples compared with the control including (a) flattened bamboo, (b) BS-BS, (c) BS-BP and (d) BP-BP.

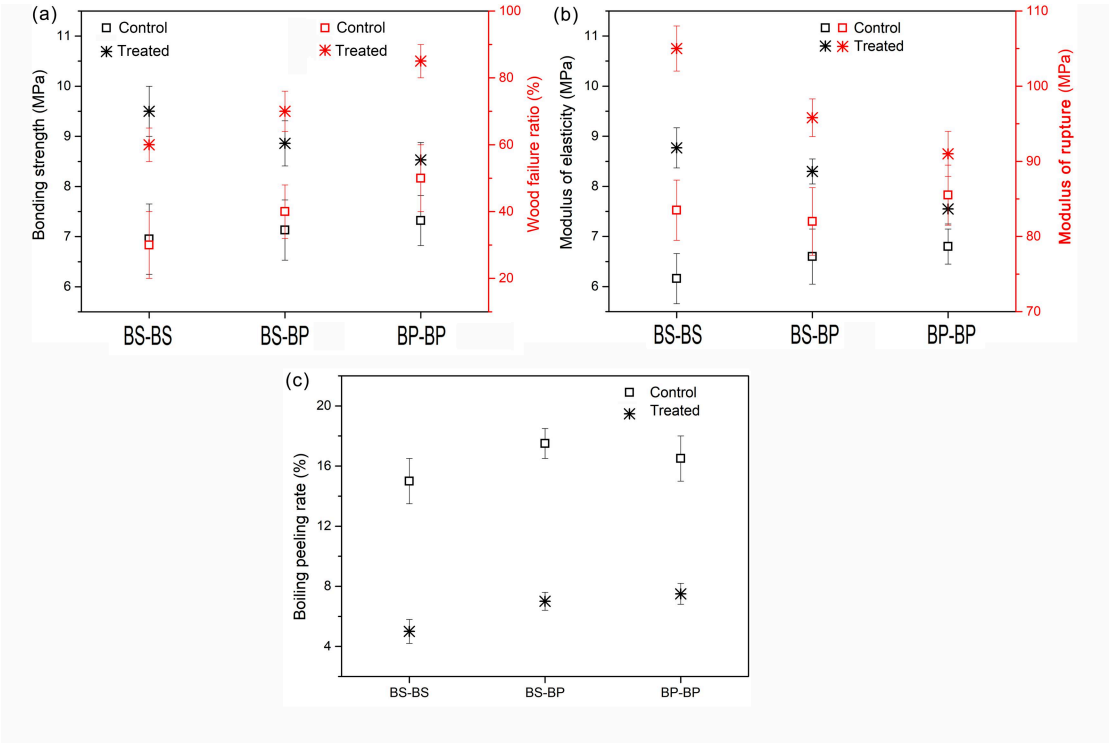


Fig.4-21 Bonding strength, wood failure ratio, MOE, MOR and boiling peeling rate for BS-BS, BS-BP and BP-BP bonding types treated by HVEF and the control ones.

As shown in Fig. 4-21, the bonding properties and mechanical properties of the three composites were further studied, including bonding strength, elastic modulus and static bending strength. As shown in Fig. 4-21 (a), for untreated condition, the bonding strength of BP-BP was higher than that of BS-BS and BS-BP composites. This was because the BP surface has a higher O/C ratio than the bamboo surface (as shown in Table 2-12). The bonding strength of various composites was significantly improved after HVEF treatment, and the bonding strength of BS-BS composites was the highest, with the improvement rate of 17% (BP-BP) < 24% (BS-BP) < 37% (BS-

BS), respectively. This result was mainly attributed to the highest density at the bonding interphase of BS-BS composites, continuous and uniform distribution of adhesives, and small penetration depth. After HVEF treatment, the bamboo failure rate of the composite material with three kinds of section combinations increased significantly, and the largest increase was in the BS-BS composite material. In addition, BP-BP composite material has higher bamboo failure rate.

The modulus of elastic (MOE) and modulus of rupture (MOR) results of the three bamboo composites have the same trend. As shown in Figure 8 (b), under untreated conditions, BP-BP composites have higher MOE and MOR. This was because the O/C ratio of BP surface was higher and the outer surface in BP-BP composites has a higher density. After HVEF treatment, the mechanical properties of the three kinds of composites significantly improved, among which, the mechanical properties of BS-BS composites have the highest improvement rate with the percentage of 42% for MOE and the MOR of 24%. These results were due to the fact that the improvement rate of the adhesive strength of BS-BS composites was the largest, and the improvement of the adhesive strength has a certain positive influence on other mechanical properties of the composite [229]. In addition, when bamboo composite material was used outdoors, the influence of water and heat on bamboo composite material was also very important. As shown in Fig. 4-21 (c), the boiling delamination rate was also studied in this experiment. As could be seen from the figure, after the treatment of HVEF, the impregnation delamination rate of bamboo composites with

three different sections significantly reduced, and the decrease rate of impregnation and delamination rate of BS-BS composites was the highest (67%).

At the same time, in order to analyze the effect of HVEF treatment on the wood, bamboo and its composite material interphase. The differences of lignin content, free radicals content rate, bond strength, maximum density change rate, penetration depth change rate and delamination rate among different tree species and bamboo as shown in figure 4-22. From the main surface factors of different tree species and the main interphase parameters of composite materials, it could be concluded that the change rate of free radical content was an important parameter that affected the surface and interphase properties. In Figure (b), the relationship between the content of lignin and the change of free radical content of different tree species, bamboo green and bamboo yellow was characterized, and the correlation coefficient was 87%. However, no significant correlation coefficients was calculated in the relationship between the change rate of free radical content and the interphase parameters of different tree species and bamboo green, bamboo yellow, the maximum density at the interphase, the penetration depth, the bonding strength and the impregnation peel rate (Fig. (c) to (f)). It was mainly due to the different arrangement and distribution patterns of vascular bundles in bamboo green and yellow (pores, pore size) and tracheids in wood. Moreover, the surface density of bamboo green was significantly higher than that of other wood materials [163,200,202,203]. So, for wood and bamboo composite material, the interphase penetration depth and the maximum density was not entirely measured according to the variation rule of free radicals, therefore, which further caused the

variation rule of HVEF induction on the bond strength and delamination rate of wood and bamboo composites.

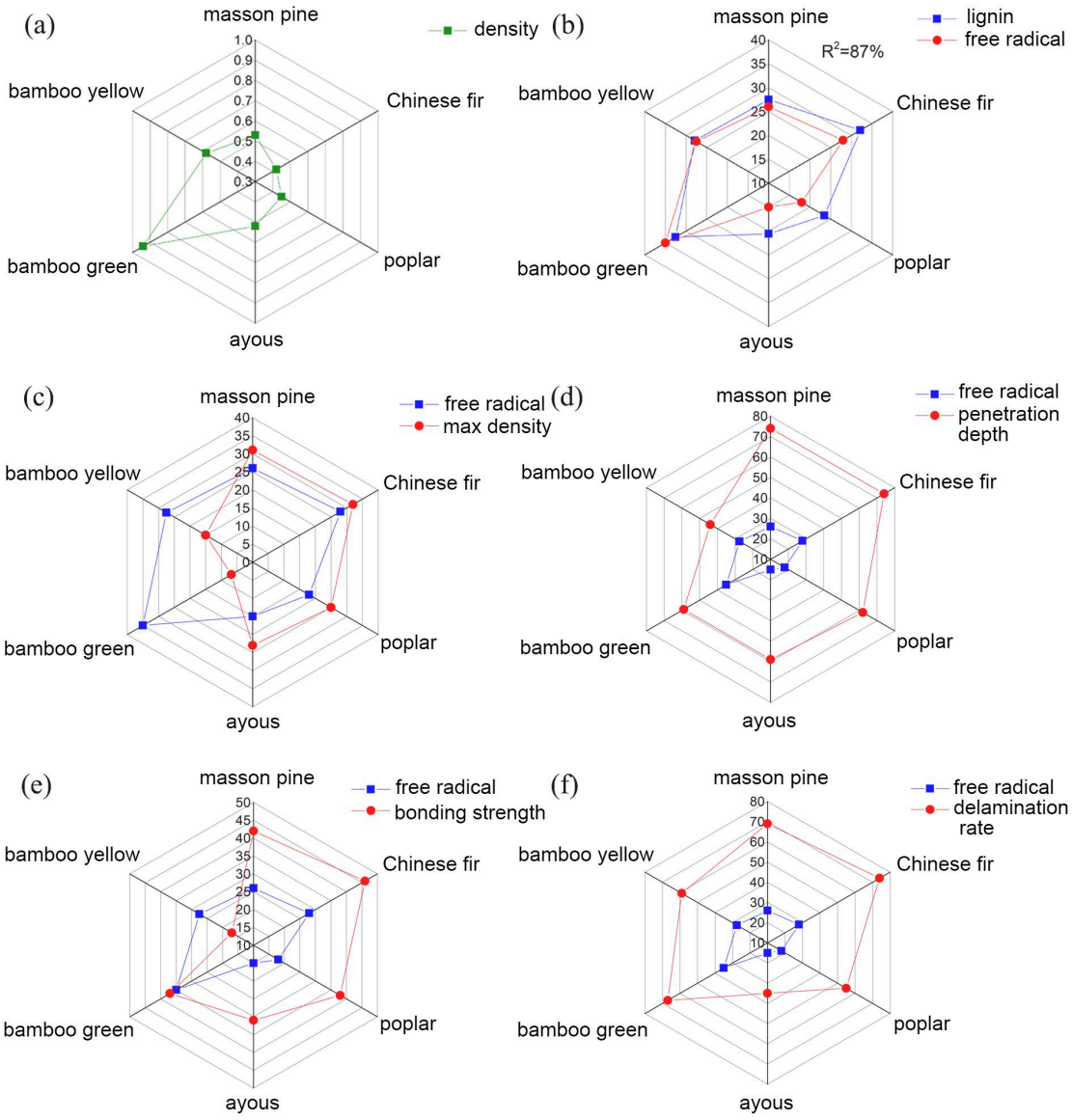


Fig.4-22 For different wood species and bamboo materials, (a) the density, (b) the relationship between free radicals change ratio and lignin contents, (c) the relationship between change ratios of free radicals and maximum density, (d) the relationship between change ratios of free radicals and penetration depth, (e) the relationship between change ratio of free radicals and bonding strength and (f) the relationship between change ratios of free radicals and delamination rates.

## 4.4 summary

Distribution form of adhesives, penetration depth and density distribution and bonding strength were investigated for wood and bamboo composites with different combinations under HVEF treatment by using fluorescence microscope, X-ray vertical density profile and mechanical device. The variation of interfacial characteristic parameters of various composites and its influencing factors were investigated.

(1) HVEF treatment could significantly affect the interphase properties of masson pine plywood. After HVEF treatment, the penetration depth at the interphase of the adhesive layer was significantly reduced, the distribution of the adhesive was continuous and uniform, the density and bonding strength at the interphase were significantly increased (the aggregation effect of the adhesive), and the impregnation delamination rate was decreased. With the increase of the treatment time/voltage of the HVEF, the maximum density change rate at the interphase of the composite material increased significantly. For the sample treated by the HVEF (60kV, 8min), the average maximum density at the interphase was 1081kg/$m^3$, and the average increase of the maximum density was 32.12%. The penetration depth of most resins in the bonding process was concentrated in the range of 250μm to 300μm. After HVEF treatment, the bonding strength of composites was 1.25MPa, which increased by 86%, the wood breaking rate was 85%, which increased by 71%, and the impregnation peeling rate was reduced to 5.97%, which decreased by 48%. Therefore, these results

further demonstrated the positive effects of HVEF on the interfacial properties, bonding strength and durability of plywood.

(2) HVEF treatment could significantly improve the interfacial properties of composite materials with different sections, that was, the penetration depth of the adhesive reduced and the density of the interphase increased. The distribution of the adhesive at the interphase was continuous and uniform, and the bonding strength significantly improved. However, the induced effect of HVEF treatment on the interphase properties of different section combinations was significantly different. For the change rates of adhesive penetration depth, maximum density, bonding strength and wood failure rate of composite materials with different section combinations, the order could be as follows:C-C < T-T < T-$T_{vertical}$ < R-T < R-R, in which the penetration depth of the adhesive of the R-R composite material was 220μm, reduced by 74%. The maximum density was 1095kg/$m^3$, increased by 30%. The compressive shear strength was 10.63MPa, increased by 42%. The wood failure rate was 98%, increased by 23%. The impregnation delamination rate was reduced to 1.68% with a decrease of 69%. The difference of these interphase properties was mainly due to the different arrangement and morphology of cell cavity, porosity and wood ray on different sections. In the C-C combination, some adhesives still penetrate into the interior wood structure, weaken the aggregation effect of adhesives at the interphase. Therefore, the micro-structure of wood, which has a significant effect on the interphase properties of the composites induced by HVF treatment.

(3) HVEF treatment can significantly improve the interphase of the composite material performance of different tree species combination, however, the effect of HVEF treatment on the interphase of the composite properties of different tree species combination had significant difference. After treated by HVEF, the adhesive penetration depth of different tree species composites, compression shear strength and the change rate of wood failure rate significantly improved. It could be sorted as: the penetration depth of the adhesive was 223μm, decreased by 74%, the maximum density was 968kg/$m^3$, increased by 32%, the compressive shear strength was 11.94MPa, increased by 46%, the wood failure rate was 95%, increased by 27%, and the impregnation delamination rate was reduced to 1.24% with a reduction of 74%. The differences of these parameters were mainly attributed to the differences in chemical composition and microstructure (cell wall thickness, diameter, etc.) of tree species. According to the correlation analysis of seven main parameters, the lignin content was the important parameter, and the lignin content was positively correlated with the change rate of free radicals ($R^2 > 0.8$), the decrease rate of penetration depth ($R^2 > 0.8$), the increase rate of maximum density and bonding strength. However, the extract content and cell diameter were negatively correlated with the decreasing rate of penetration depth, increase rate of maximum density and increase rate of shear strength. In addition, the improvement of interfacial properties of softwood by HVEF is better than that of hardwood composites.

(4) HVEF treatment has a significant effect on the interfacial properties of bamboo composites. The penetration depth of adhesives at the interphase significantly

reduced, the density increased and the adhesives continuously distributed, and the bonding strength and mechanical properties also significantly increased. According to the change rate of these parameters, BP-BP < BS-BP < BS-BS, in the BS-BS composite, the penetration depth of adhesive was 386μm, decreased by 59%, the maximum density was 1087kg/m3, increased by 5%, the adhesive strength was 9.51MPa, increased by 37%, the bamboo break rate was 60%, increased by 50%, and the penetration depth of adhesive was 386μm, decreased by 59%, the maximum density was 1087kg/$m^3$, increased by 5%. The elastic modulus was 10.75GPa, increased by 42%, the static bending strength was 104.68MPa, increased by 24%, and the impregnation delamination rate reduced to 5.37%, decreased by 67%. This was mainly due to the difference of chemical composition and structure between bamboo green and bamboo yellow. After HVEF treatment, the maximum mechanical properties were the highest and the impregnation delamination rate was the lowest. In the BP-BP composite, the maximum bamboo failure rate was 85%, which improved by 70%. Therefore, the study showed that the HVEF treatment method was an effective method to improve the interphase performance and durability of bamboo composite materials.

# Chapter V: Laminated stiffness and stress distribution model under HVEF treatment

## 5.1 Introduction

At present, the mechanical properties and mechanical model design of biomass composites, including structural plywood, laminated veneer lumber and cross-laminated structural materials, are of great significance for their applications in new materials, construction and transportation industries [230-232]. Foschi developed a model to predict the bending and tensile strength of bonded beams [233]. Takeuchi verified the modulus of rupture (MOR) of the glued beam based on the rigid body spring model (RBSM) simulation [234]. Ogawa proposed a model to predict the tensile strength of cross-laminated composites [235]. In these models, the predicted values and experimental values are in good agreement and correlation. However, these design models mainly considered the stiffness and strength of wood components, and do not take into account the influence factors related to interphase characteristics.

In composites, the properties of interphase also have an important effect on the mechanical properties of biomaterial composites [236]. Adhesives enter the internal microstructure of wood through wetting and osmotic action, and the adhesives interact with biomass materials under cross-link reaction, thus forming the bonding interphase. In a previous study, Mendoza proposed a structural analysis model for wood tubular hole networks to predict and simulate the penetration depth of adhesives [34]. Yuan studied the influence of distribution forms of adhesive permeated into different tree species on mechanical properties of composites [27]. Ivana obtained the variation rule

of adhesive strength and adhesive penetration depth between different types of wood combinations [28]. Therefore, the study of mechanical model based on the permeability of adhesives at the interphase of composites is of great significance for the evaluation of the bonding strength and mechanical properties of wood composites under different loads [23,24]. However, the distribution of the adhesive at the bonding interphase of the composites is significantly different from that of the untreated composites due to the treatment of HVEF. Therefore, some models for predicting the permeability of adhesives could not be directly applied to composites treated by HVEF.

Based on the previous study on the surface and bonding interphase of the HVEF treatment, it was concluded that the decreased penetration depth at the interphase of the composite material after HVEF treatment, the increased density, and the improved bonding strength and durability were obtained. In order to fully understand the influence of HVEF treatment on the stiffness and strength at the interphase of composite materials, it is necessary to quantitatively study the influence of HVEF treatment on the mechanical properties of composite materials. In this study, the laminated-woods of poplar and masson pine with different layers were treated by hot pressing and HVEF simultaneously. The interfacial mechanical properties of the composites were characterized from macroscopic and microscopic (cell wall), and the distribution of density of laminated materials and the distribution of adhesives along the thickness direction were also investigated. Based on the composite mechanics and classical laminated plate theory, the representative volume element (RVE) with a thickness of 50μm was proposed to establish the mechanical model of the stiffness

and strength of the composite material treated by HVEF. The theoretical distribution values of the elastic constants and strength parameters along the thickness direction of the RVE were predicted, and macro-mechanical properties [modulus of elasticity (MOE), modulus of rupture (MOR), shear modulus (G), shear strength (SS)] of laminated-woods were predicted.

## 5.2 Design Theory

### 5.2.1 Basic mechanical properties of wood

In order to facilitate design and simulation, the principle of orthogonal symmetry was applied to explain the anisotropy of wood. According to the three sections of wood, the three directions are defined, which are the axis parallel to the fiber direction (X), the axis parallel to the tangential direction (Y) and the axis parallel to the radial direction (Z) respectively, so that the wood structure can be regarded as orthotropic material. In the wood structure, the elastic properties can be characterized by 12 elastic constants, including $E_L, E_R, E_T$ (elastic modulus), $G_{RT}, G_{TL}, G_L$ (shear modulus) and$\mu_{RT}, \mu_{TR}, \mu_{TL}, \mu_{LT}, \mu_{LR}, \mu_{RL}$ (Poisson's ratio). According to the reciprocal theorem of work and the symmetry of the flexibility matrix, we can get:

$$\frac{\mu_{ij}}{E_i} = \frac{\mu_{ji}}{E_j}, \quad i, j = L, R, T \tag{5-1}$$

Among them, there are 6 independent constants, and the elastic modulus values of wood in tension and compression bending are similar, which are collectively referred to as $E_x$. Therefore, 4 independent constants can be obtained finally. However, the elastic modulus in the three spindle directions is different due to the difference in

the microstructure of wood. In general wood materials, the longitudinal elastic modulus is far greater than the transverse elastic modulus of wood, the radial modulus is greater than the tangential modulus. It can be obtained:

$$E_L >> E_R > E_T \tag{5-2}$$

When wood is subjected to a (longitudinal) load parallel to the fiber direction, its tensile and compression properties are not the same. According to the stress-strain curve of wood under tension, it can be shown that wood does not have a significant stage of plastic deformation (brittle failure) [237]. When the wood is subjected to the compression load parallel to the fiber direction (longitudinal), and the compression load is close to the ultimate load, the wood showed the plastic deformation characteristics (elastoplastic body).

When wood is subjected to shear load, it can be divided into three different forms according to different direction of cutting plane and shear direction, namely, longitudinal grain shear, transverse grain shear and transverse grain cutting. According to previous studies, the longitudinal shear strength is 25% of the longitudinal compressive strength and the transverse shear strength is 4 times of the longitudinal shear strength, while the difference between the radial shear strength and the tangential shear strength is not significant. Before subjected to the ultimate load of shear failure, wood still has the law of elastic deformation characteristics of orthotropic materials [238].

The compressive strength, bending strength and tensile strength along grain of wood increase successively, and the empirical formula is as follows:

$$\frac{f_m^s}{f_c^s} = \frac{3 \cdot \frac{f_t^s}{f_c^s} - 1}{\frac{f_t^s}{f_c^s} + 1} \tag{5-3}$$

In the formula, $f_m^s$, $f_t^s$, $f_c^s$ are respectively the bending strength, tensile strength and compressive strength of the material along the grain.

In addition, the defects of wood (cracks, twill, joints, etc.) have a significant effect on the tensile strength along the grain, which is easy to reduce the tensile strength along the grain.When the material is subjected to compression loading, due to the plastic deformation characteristics of the wood, the damage of stress concentration can be reduced, so the compression loading of the component does not have to consider the impact of stress concentration, in addition, the impact of joints compared to the tension condition is smaller.

### 5.2.2 Design theory of elastic constants of single-layer plates

The stiffness and strength properties of the composite materials, such as plywood and laminated veneer lumber, mainly depend on the stiffness and strength of the composite, as well as the processing method of the single-layer plate.

(1) Prediction of elastic modulus along grain of single-layer plate

According to the elastic constants of wood and adhesives and the mechanics theory of composite materials, the elastic modulus of single-layer plate in line with grain can be obtained as follows:

$$E_L = v_f E_f + v_g E_g \tag{5-4}$$

Where, $E_f$ is the tensile elastic modulus of the wood substance in the longitudinal direction of the veneer; $E_g$ is the tensile modulus of the adhesive; $v_f$ is the actual volume of veneer; $v_g$ is the volume of the adhesive.

By comprehensively considering factors such as density, mass, glue amount, compression rate during processing and substantial elastic modulus of wood [239], the elastic modulus $E_L$ of single-layer board along grain can be calculated as:

$$E_L = \frac{1}{(1 - T_V / 100)} \left( \frac{D_0}{D_f} E_f + \frac{A_g}{1000 t_0 D_g} E_g \right) \tag{5-5}$$

Where, $D_0$ (g/cm$^3$) is the density of single-layer, $D_f$ (g/cm$^3$) is the actual density of wood, $t_0$ (mm) is the initial thickness of layer, $T_V$(%) is the thickness change rate of layer, $E_f$ (MPa) is the actual longitudinal tensile elastic modulus of wood in layer, $E_g$ (MPa) is the elastic modulus of adhesive. $A_g$ (g/m$^2$) is the amount of adhesive per square meter (the amount of adhesive), and $D_g$ (g/cm$^3$) is the density of adhesive.

(2) Prediction of transverse elastic modulus of single-layer plate

Longitudinal tensile elastic modulus of wood is about transverse elastic modulus of the 23-26 times, in order to predict horizontal stripes elastic modulus [240], the prediction model, the single-layer plate as orthotropic material, and the material

fracture, density, size and thickness variation are considered. It is concluded that the transverse elastic modulus on the single $E_T$ as follows:

$$E_T = \frac{D_0}{D_f(1-T_v/100)}E_{Tf} + \left[\frac{A_g - A_{gp}}{1000t_0(1-T_v/100)D_g} + kk_2(1-T_v/100)\right]E_{\mathrm{m}} \qquad (5\text{-}6)$$

In the formula, $k$ (%) is the fissure degree of single-layer, $k_2$ is the ratio of fissure width to fissure spacing, $D_0$ (g/cm$^3$) is the density of single-layer, $D_f$ (g/cm$^3$) is the actual density of wood, $t_0$ (mm) is the initial thickness of single-layer, and $T_V$ (%) is the thickness change rate of single-layer. $E_{Tf}$ (Mpa) is the actual transverse tensile elastic modulus of wood in single-layer board, $E_m$ (Mpa) is the elastic modulus of adhesive, $A_g$ (g/m$^2$) is the amount of adhesive per square meter (the amount of adhesive), $A_{gp}$ (g/m$^2$) is the content of adhesive in cracks, and $D_g$ (g/cm$^3$) is the density of adhesive.

(3) Prediction of shear elastic modulus of single-layer plate

According to the elastic constant of wood under plane stress state and the prediction model in (2) and (3), and considering comprehensively the factors such as crack, density and compression rate of single-layer plate [4], the longitudinal and transverse shear elastic modulus ($G_{LT}$) of single-layer plate under load condition is further analyzed:

$$G_{LT} = \frac{D_0}{D_f(1-T_v/100)}G_{LTf} + \left[\frac{A_g - A_{gp}}{1000t_0(1-T_v/100)D_g} + kk_2(1-T_v/100)\right]G_{\mathrm{m}} \qquad (5\text{-}7)$$

In the formula, $k$ (%) is the fissure degree of single-layer slab, $k_2$ is the ratio of fissure width to fissure spacing, $D_0$ (g/cm$^3$) is the density of single-layer, $D_f$ (g/cm$^3$) is the actual density of wood, $t_0$ (mm) is the initial thickness of single-layer, and $T_V$ (%) is the thickness change rate of single-layer. $G_{LTf}$ (MPa) is the actual shear modulus of wood in single-laye, $G_m$ (MPa) is the elastic modulus of adhesive, $A_g$ (g/m$^2$) is the amount of adhesive per square meter (the amount of adhesive), $A_{gp}$ (g/m$^2$) is the content of adhesive in cracks, and $D_g$ (g/cm$^3$) is the density of adhesive.

(4) Poisson's ratio of single-layer plate

According to the elastic constants of wood and adhesives and the mechanics theory of composite materials, the Poisson's ratio of single-layer plate can be obtained as:

$$\mu_{LT} = v_f \mu_{LTf} + v_m \mu_{LTm} \tag{5-8}$$

In the formula, $\mu_{LTf}$is the transverse and longitudinal Poisson's ratio of wood in veneer, $\mu_{LTm}$ is the Poisson's ratio of adhesive, $v_f$ is the volume of veneer, and $v_g$ is the volume of adhesive.

### 5.2.3 Stiffness design theory of laminates

Laminates are made up of single layers stacked in a certain order and angle. The stiffness performance of laminates is closely related to the properties of single-layer laminates and the way of lamination.

In order to analyze the stiffness of laminates, the basic assumptions are as follows:

(1)The deformation of composite material is small, and the material conforms to Hooke's law.

(2) The laminates of the composite material are ideal gluing without gaps, and there is no mutual dislocation between the laminates and the deformation along the thickness direction is continuous.

(3) In the laminated plate, the straight line segment is still perpendicular to the middle plane after deformation, and its length remains unchanged.

The strain of the laminate varies linearly along the direction of the laminate thickness (Z). The stress expression of K layer in the laminated plate can be obtained from the stress-strain relation of the composite material:

$$\begin{bmatrix}\sigma_x\\ \sigma_y\\ \tau_{xy}\end{bmatrix}=\begin{bmatrix}\overline{Q_{11}} & \overline{Q_{12}} & \overline{Q_{16}}\\ & \overline{Q_{22}} & \overline{Q_{26}}\\ sym. & & \overline{Q_{66}}\end{bmatrix}\begin{bmatrix}\varepsilon_x\\ \varepsilon_y\\ \gamma_{xy}\end{bmatrix} \tag{5-9}$$

$$\begin{bmatrix}\sigma_x\\ \sigma_y\\ \tau_{xy}\end{bmatrix}=\begin{bmatrix}\overline{Q_{11}} & \overline{Q_{12}} & \overline{Q_{16}}\\ & \overline{Q_{22}} & \overline{Q_{26}}\\ sym. & & \overline{Q_{66}}\end{bmatrix}_k\left\{\begin{bmatrix}\varepsilon_x\\ \varepsilon_y\\ \gamma_{xy}\end{bmatrix}+z\begin{bmatrix}K_x\\ K_y\\ K_{xy}\end{bmatrix}\right\} \tag{5-10}$$

In the matrix, $\overline{Q}_{ij}$ is the transformation stiffness coefficient in the laminated plate; ($\varepsilon 0\,x$，$\varepsilon 0\,y$，$\gamma 0\,xy$) is the positive or shear strain of the midplane of the laminated plate; ($K_x$，$K_y$，$K_{xy}$) is the torsion rate or bending deflection rate of the midplane of the laminated plate. Thus, the integral form of the combined internal force and

internal force matrix of each single-layer plate in the direction of thickness (Z) can be obtained:

$$\begin{Bmatrix} N_x \\ N_y \\ N_{xy} \end{Bmatrix} = \int_{-h/2}^{h/2} \begin{Bmatrix} \sigma_x \\ \sigma_y \\ \tau_{xy} \end{Bmatrix} dz = \sum_{k=1}^{n} \int_{z_{k-1}}^{z_k} \begin{Bmatrix} \sigma_x^{(\kappa)} \\ \sigma_y^{(\kappa)} \\ \tau_{xy}^{(\kappa)} \end{Bmatrix} dz \tag{5-11}$$

$$\begin{Bmatrix} M_x \\ M_y \\ M_{xy} \end{Bmatrix} = \int_{-h/2}^{h/2} \begin{Bmatrix} \sigma_x \\ \sigma_y \\ \tau_{xy} \end{Bmatrix} z dz = \sum_{k=1}^{n} \int_{z_{k-1}}^{z_k} \begin{Bmatrix} \sigma_x^{(\kappa)} \\ \sigma_y^{(\kappa)} \\ \tau_{xy}^{(\kappa)} \end{Bmatrix} z dz \tag{5-12}$$

After sorting and merging, the following matrix expression is obtained:

$$\begin{Bmatrix} N \\ \cdots \\ M \end{Bmatrix} = \begin{bmatrix} \sum_{k=1}^{n} \left[\overline{Q}^{(k)}\right] \left(z_k - z_{k-1}\right) & \vdots & \frac{1}{2} \sum_{k=1}^{n} \left[\overline{Q}^{(k)}\right] \left(z_k^2 - z_{k-1}^2\right) \\ \cdots & \vdots & \cdots \\ \frac{1}{2} \sum_{k=1}^{n} \left[\overline{Q}^{(k)}\right] \left(z_k^2 - z_{k-1}^2\right) & \vdots & \frac{1}{3} \sum_{k=1}^{n} \left[\overline{Q}^{(k)}\right] \left(z_k^3 - z_{k-1}^3\right) \end{bmatrix} \begin{Bmatrix} \varepsilon^0 \\ \cdots \\ k \end{Bmatrix} \tag{5-13}$$

Therefore, the stress-strain relationship of the laminated plate can be expressed as:

$$\begin{Bmatrix} N_x \\ N_y \\ N_{xy} \\ \hdashline M_x \\ M_y \\ M_{xy} \end{Bmatrix} = \left[\begin{array}{ccc:ccc} A_{11} & A_{12} & A_{16} & B_{11} & B_{12} & B_{16} \\ A_{12} & A_{22} & A_{26} & B_{12} & B_{22} & B_{26} \\ A_{16} & A_{26} & A_{66} & B_{16} & B_{26} & B_{66} \\ \hdashline B_{11} & B_{12} & B_{16} & D_{11} & D_{12} & D_{16} \\ B_{12} & B_{22} & B_{26} & D_{12} & D_{22} & D_{26} \\ B_{16} & B_{26} & B_{66} & D_{16} & D_{26} & D_{66} \end{array}\right] \begin{Bmatrix} \varepsilon_x^0 \\ \varepsilon_y^0 \\ \gamma_{xy}^0 \\ \hdashline \kappa_x \\ \kappa_y \\ \kappa_{xy} \end{Bmatrix} \tag{5-14}$$

The above expression is the constitutive equation of laminated plates.($N_x$, $N_y$, $N_{xy}$) is the closing internal force per unit width in the laminated plate, and ($M_x$, $M_y$, $M_{xy}$) is the closing internal torque per unit width in the laminated plate. $A_{ij}$ is the tensile stiffness, $D_{ij}$ is the bending stiffness, $B_{ij}$ is the coupling stiffness, and $(\overline{Q})_k$ is the transformation stiffness coefficient of the K-layer in laminated plates. When the composite form of the laminated plate is determined, the stiffness calculation formula can be obtained, in which, the coordinates of each single layer of the laminated plate are defined as $z_k$, and the classical laminated plate theory can be calculated according to the integral results:

$$\left.\begin{aligned} A_{ij} &= \sum_{k=1}^{n}\int_{z_{k-1}}^{z_k}\overline{Q}_{ij}^{(k)}dz = \sum_{k=1}^{n}\overline{Q}_{ij}^{(k)}\left(z_k - z_{k-1}\right) \\ B_{ij} &= \sum_{k=1}^{n}\int_{z_{k-1}}^{z_k}\overline{Q}_{ij}^{(k)}zdz = \frac{1}{2}\sum_{k=1}^{n}\overline{Q}_{ij}^{(k)}\left(z_k^2 - z_{k-1}^2\right) \\ D_{ij} &= \sum_{k=1}^{n}\int_{z_{k-1}}^{z_k}\overline{Q}_{ij}^{(k)}z^2dz = \frac{1}{3}\sum_{k=1}^{n}\overline{Q}_{ij}^{(k)}\left(z_k^3 - z_{k-1}^3\right) \end{aligned}\right\}(i,j=1,2,6) \quad (5\text{-}15)$$

In symmetric laminated plates, there is no coupling effect between inside and outside the plane, so $B_{ij}$=**0**. Only the relationship between tensile stiffness and bending stiffness and elastic constant is studied.

### 5.2.4 Strength design theory of laminates

#### (1) the strength index of laminates

The strength of orthotropic laminates is different in different principal axis directions. For orthotropic laminates, five strength indexes are needed to predict the strength performance analysis of single-layer laminates under complex stress

conditions, including: $X_t$ (ultimate tensile strength along grain), $X_c$ (ultimate compressive strength along grain, absolute value); $Y_t$ (transverse tensile ultimate strength); $Y_c$ (transverse compression ultimate strength, absolute value) and $S$ (in-plane shear ultimate strength). After five strength indexes are obtained through the experimental measurement, the strength analysis of single-layer plate can be carried out after selecting the appropriate strength criterion for calculation.

**(2) Strength criterion**

1. Maximum stress theory

Maximum stress theory is a simple and commonly used theory of strength criteria. The maximum stress criterion refers to that the component of any stress in the main direction of the laminated plate material must be less than the corresponding strength.

Tensile stress:

$$\sigma_1 < X_T, \sigma_2 < Y_T, |\tau_{12}| < S \tag{5-16}$$

Compression stress:

$$\sigma_1 > -X_C, \sigma_2 > -Y_C \tag{5-17}$$

where $\sigma_1$ and $\sigma_2$ refer to stresses in 1, 2 principal directions. If any one of the above five inequalities is not satisfied, the laminate will be damaged, and the failure forms will not affect each other.

2. Maximum strain theory

The maximum strain theory regards the value of the ultimate strain as the basis for the failure of the single-layer plate. The tensile and compressive strengths are as follows:

$$\varepsilon_1 < \varepsilon_{X_T}, \varepsilon_1 > -\varepsilon_{X_C}, \varepsilon_2 < \varepsilon_{Y_T}, \varepsilon_2 > -\varepsilon_{Y_C}, |\gamma_{12}| < \gamma_S \tag{5-18}$$

where $\varepsilon\ XT$ and $\varepsilon\ XC$ are the maximum tensile and compression linear strains in direction 1 respectively. $\varepsilon\ YT$ and $\varepsilon\ YC$ are the maximum tensile and compression linear strains in 2 directions respectively. $\gamma\ S$ is the maximum shear strain in 1,2 planes. Any one of the 5 inequalities does not satisfy the composite material and it would be failure. Maximum stress/strain criterion, in most cases, is used to determine the failure of composite materials under uniaxial stress.

3. Tsai-Hill theory

For anisotropic unidirectional plates, Tsai-Hill puts forward the corresponding strength conditions as follows:

$$F(\sigma_2 - \sigma_3)^2 + G(\sigma_3 - \sigma_1)^2 + H(\sigma_1 - \sigma_2)^2 + 2L\tau_{23}^2 + 2M\tau_{31}^2 + 2N\tau_{12}^2 = 1 \tag{5-19}$$

In the formula, the stresses are all the stresses in the main axis direction, and F, G, H, L, M and N are all the coefficients, which are determined by uniaxial tensile (compression) and pure shear tests of single-layer plates. This theory is mainly applicable to single-layer plates with the same ultimate tensile and compressive strength.

4. Hoffman theory

$$\frac{\sigma_1^2}{X_t X_c} - \frac{\sigma_1 \sigma_2}{X_t X_c} + \frac{\sigma_1^2}{Y_t Y_c} + \frac{X_c - X_t}{X_t X_c}\sigma_1 + \frac{Y_c - Y_t}{Y_t Y_c}\sigma_2 + \frac{\tau_{12}^2}{S^2} = 1 \tag{5-20}$$

In the formula, the criterion takes into account the factors of different tensile and compressive strength. For single-layer plates with the same tensile and compressive ultimate strength under uniaxial conditions, the Tsai-Hill theory can be used.

5. Tsai-Wu theory

The failure characteristics of orthotropic composites can also be evaluated and determined by Tsai-Wu criterion, which is one of the most classical strength criterion theories in composite mechanics:

$$F_{11}\sigma_1^2 + 2F_{11}\sigma_1\sigma_2 + F_{22}\sigma_2^2 + F_{66}\sigma_6^2 + F_1\sigma_1 + F_2\sigma_2 = 1 \tag{5-21}$$

Under stable conditions:

$$F_{11}F_{22} - F_{12}^2 > 0 \tag{5-22}$$

$$F_1 = \frac{1}{X_t} - \frac{1}{X_c}, \quad F_2 = \frac{1}{Y_t} - \frac{1}{Y_c}, \quad F_{11} = \frac{1}{X_t X_c}, \quad F_{22} = \frac{1}{Y_t Y_c}, \quad F_{66} = \frac{1}{S^2} \tag{5-23}$$

In the formula, Tsai-Wu theory considers different situations of tension and compression, and obtains a good agreement with the experimental results. Therefore, this criterion can predict the failure determination of composite materials under complex stress conditions.

(3) stress and strength analysis of laminated plates

When the laminated plate is subjected to external load, complex stresses in and out of plane will occur between the single layer plate and the adhesive layer. When

the stress reaches a certain value, it will lead to the failure of laminated plates. There are two methods for calculating the strength of laminated plates. The first method is the assumption of initial layer failure. If any layer of laminated plates is destroyed, it is the failure of laminated plates. The second method is the assumption of failure of the final layer, that is, after the failure of a single layer in the laminated plate, the loading continues, and when all the single layers are destroyed, it is the failure of the laminated plate.

For laminated plate composite structures, the steps to determine the initial layer failure strength are as follows:

1. Calculate the stiffness $A_{ij}$, $B_{ij}$ and $D_{ij}$ of laminates.

2. Calculate the inverse matrix of the stiffness matrix, including: $a_{ij}$, $b_{ij}$, $d_{ij}$.

Constitutive equation:

$$\begin{bmatrix} N \\ M \end{bmatrix} = \begin{bmatrix} A & B \\ B & D \end{bmatrix} \begin{bmatrix} \varepsilon^0 \\ K \end{bmatrix} \quad (5\text{-}24)$$

Where, [N]=[$N_x$ $N_y$ $N_{xy}$]$^T$ represents in-plane resultant force per unit width, [M]=[$M_x$ $M_y$ $M_{xy}$]$^T$ represents bending moment per unit width, [$\boldsymbol{\varepsilon 0}$ ]=[$\varepsilon 0\ x\ \varepsilon 0\ y\ \gamma 0\ xy$]$^T$ represents midplane strain, [$\boldsymbol{K}$]=[$K_x$ $K_y$ $K_{xy}$]$^T$ represents bending rate of midplane. According to the stiffness calculation formula of laminated plate (classical laminated plate theory), the characteristics of symmetrical laminated plate and the expression of strain matrix of any point of laminated plate, the stress expression of any single layer of laminated plate can be obtained:

$$\begin{bmatrix}\sigma_1\\ \sigma_2\\ \tau_{12}\end{bmatrix}=\begin{bmatrix}Q_{11} & Q_{12} & \\ Q_{12} & Q_{22} & \\ & & Q_{66}\end{bmatrix}\begin{bmatrix}\varepsilon_1\\ \varepsilon_2\\ \gamma_{12}\end{bmatrix} \quad (5\text{-}25)$$

Where, $Q_{ij}$ is the retreat stiffness matrix of any single-layer plate and is composed of its elastic constants.

Thus, the failure index (F.I.) of any single layer of laminates is calculated accordingly, and the initial failure strength is determined final breakdown strength for laminated plates. The initial damage of structure strength analysis is in the first place, the distribution of stress occurs again. After calculating the residual stiffness of laminated plates, the stress inside the single board is determined. As load increases, laminated plates within a single board to limit stress and failure happens again. As continuing to increase the load, the failure strength of the final laminate can be determined by recalculating the laminated plate stiffness.

## 5.3 Mechanical model of stiffness and strength distribution of bonding interphase induced by HVEF

### 5.3.1 Basic Assumptions

The laminated plate material is regarded as an orthotropic material, and its three mutually perpendicular principal axes are shown in Fig. 5-1 (c). Fig. 5-1 (a), (b) and (d) also represented the process of HVEF treatment, the variation of laminated plate density after treatment and the components of equivalent volume elements (RVE) (Fig. 5-1).The distribution of RVE elastic constant and strength index parameters

along the main axis of thickness direction depended on the properties of wood, the properties of adhesives and the permeability distribution of adhesives at the interphase.

(1) In the laminated composite material simulated by RVE, the laminated-wood material is uniform, continuous, without voids and defects, and the stress-strain relationship can be calculated by using a continuous function.

(2) In the RVE simulation of laminated plate composites, adhesives are ideal void free matrix materials, and the stress-strain relationship can be calculated using a continuous function.

(3) Wood is a linear elastomer material, and the stress-strain relationship conforms to Hooke's law.

(4) Laminated-wood are orthotropic materials with three mutually perpendicular principal axes: X axis (longitudinal), Y axis (radial) and Z axis (tangential).

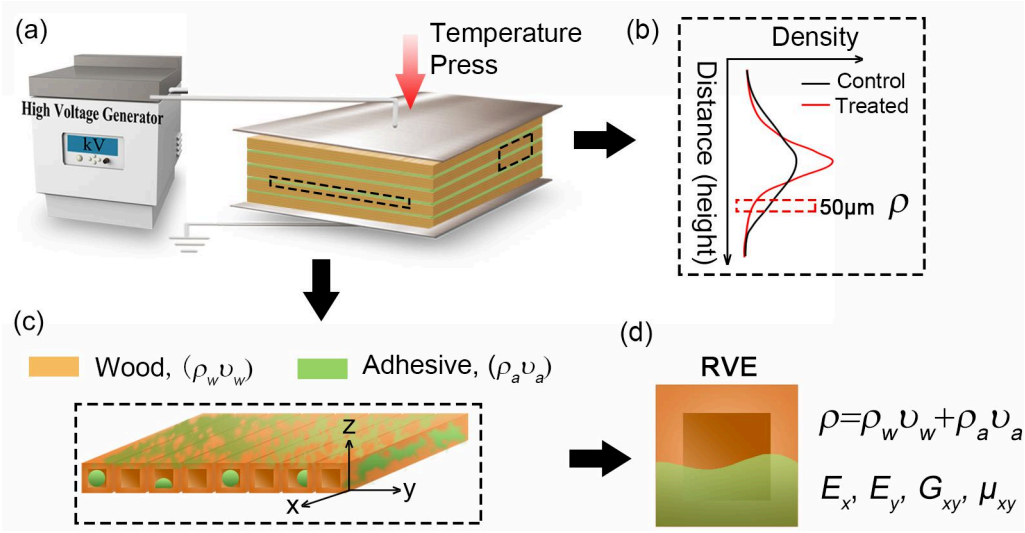


Fig.5-1 The diagram for (a) HVEF treatment device. (b) VDP diagram obtained from bonding interphase of aminated-wood. (c) Adhesive distribution among wood vessels. (d) RVE model based on adhesive fraction and wood fraction.

### 5.3.2 Prediction of elastic constants and strength indexes in RVE

Considering the variations of mechanical properties between pure wood and glued wood, the stiffness and strength of laminated-wood were largely depending on the adhesive fraction and wood fraction. RVE with a thickness of 50 μm was proposed to model stiffness and strength distributions in laminated-wood (Fig. 1) by considering the resolution of VDP. The adhesive fraction of RVE was calculated according to the VDP of laminated-wood, wood density and adhesive density as shown in the Eq. (5-26):

$$\rho = \frac{\rho_w V_w + \rho_a V_a}{V} = \rho_w v_w + \rho_a v_a \tag{5-26}$$

Where $\rho$ (kg/m$^3$ ) and $V$ (m$^3$ ) were the density and volume for RVE, $\rho_w$ and $V_w$ were the wood density and volume of RVE, $\rho_a$ and $V_a$ were the adhesive density and volume of RVE, $v_a$ and $v_w$ were the fraction of adhesive and wood of RVE.

Based on the density and adhesive fraction, the elastic constants of RVE were calculated. The elastic constants in principal directions for each RVE were predicted including modulus of elasticity (E), shear modulus (G) and Poisson ratio (μ) with the compression ratio considered as shown in the Eqs.:

$$E_x = \frac{E_{x-w} v_w}{(1 - c/100)} + \frac{E_{x-a} v_a}{(1 - c/100)} \tag{5-27}$$

$$E_y = \frac{v_w E_{y\text{-}w}}{(1 - c/100)} + \frac{v_a E_{y-a}}{(1 - c/100)} \tag{5-28}$$

$$G_{xy} = \frac{v_w G_{xy-w}}{(1-c/100)} + \frac{v_a G_{xy-a}}{(1-c/100)} \tag{5-29}$$

$$\mu_{i-xy} = v_w \mu_{w-xy} + v_a \mu_{a-xy} \tag{5-30}$$

Where $E_x$ (GPa), $E_y$ (GPa), $G_{xy}$ (GPa) and $\mu_{xy}$ were the elastic constants for RVE. $E_{x\text{-}w}$, $E_{y\text{-}w}$, $G_{xy\text{-}w}$ and $\mu_{xy\text{-}w}$ were the elastic constants for wood and $E_{x\text{-}a}$, $E_{y\text{-}a}$, $G_{xy\text{-}a}$ and $\mu_{xy\text{-}a}$ were the elastic constants for adhesive. $c$ was the compression ratio for wood.

The strength indices of RVE in principal directions were also calculated including tensile ($T$), compression ($C$) and shear strength ($S$) based on the adhesive fraction and wood fraction. The strength indices in principal directions for RVE were predicted as follows in the Eqs.:

$$T_x = v_w T_{x-w} + v_a T_{x-a} \tag{5-31}$$

$$T_y = v_w T_{y-w} + v_a T_{y-a} \tag{5-32}$$

$$C_x = v_w C_{x-w} + v_a C_{x-a} \tag{5-33}$$

$$C_y = v_w C_{y-w} + v_a C_{y-a} \tag{5-34}$$

$$S = v_a S_a + v_w S_w \tag{5-35}$$

Where $T_x$ (MPa), $T_y$ (MPa), $C_x$ (MPa), $C_y$ (MPa) and $S$ (MPa) were the strength indices for RVE. $T_{x\text{-}w}$, $T_{y\text{-}w}$, $C_{x\text{-}w}$, $C_{y\text{-}w}$ and $S_w$ were the strength indices for wood. $T_{x\text{-}a}$, $T_{y\text{-}a}$, $C_{x\text{-}a}$, $C_{y\text{-}a}$ and $S_a$ were the strength indices for adhesive. Some wood veneer mechanical properties were tested and obtained in Table 5-1. The values were with the limitations compared with previous investigations [241, 242].

Table 5-1. Average elastic constants and strengths for wood species and PF.

| Species | $E_x$ Gpa | $E_y$ GPa | $G_{xy}$ GPa | $\mu_{xy}$ | $C_x$ MPa | $C_y$ MPa | $T_x$ MPa | $T_y$ MPa | $S$ MPa |
|---|---|---|---|---|---|---|---|---|---|
| Masson pine veneer | 6.85 | 0.33 | 0.44 | 0.31 | 24.50 | 0.85 | 12.4 | 1.5 | 1.77 |
| Poplar veneer | 6.45 | 0.27 | 0.38 | 0.33 | 25.10 | 0.83 | 10.5 | 1.2 | 1.5 |
| PF | 8.8 | 8.8 | 3.18 | 0.40 | 35 | 35 | 70 | 70 | 15 |

### 5.3.3 Prediction of mechanical property parameters in RVE

Based on the calculated elastic constants and strength indices of RVE, macro-mechanical properties [modulus of elasticity (MOE), modulus of rupture (MOR), shear modulus (G), shear strength (SS)] of laminated woods were predicted according to classical lamination theory.

The stiffness coefficient matric of $\boldsymbol{D}_{ij}$ could be obtained, and MOE ($E$, GPa) and G (GPa) for laminated- wood could be calculated. MOR (MPa) of laminated-wood was predicted based on the strength indices including $T_x$, $T_y$, $C_x$, $C_y$ and $S$ according to last ply failure criterion and Tsai-Hill strength theory.

$$D_{ij} = \frac{1}{3}\sum_{k=1}^{N}\left(\overline{Q_{ij}}\right)_k (z_k^3 - z_{k-1}^3) \tag{5-36}$$

$$E = 12/(t^3 d_{11})\ E = 12/(t^3 d_{11}) \tag{5-37}$$

$$G = 12/(t^3 d_{33}) \tag{5-38}$$

$$F.I.=\left(\frac{\sigma_x}{X}\right)^2+\left(\frac{\sigma_y}{Y}\right)^2+\left(\frac{\tau_{xy}}{S}\right)^2-\frac{\sigma_x\sigma_y}{X^2}<1 \quad (5\text{-}39)$$

Where $\boldsymbol{D}_{ij}$ (kN·mm) was the matrix of bending stiffness for laminated-wood. $\boldsymbol{Q}_{ij}$ (GPa) was the matrix of reduced stiffness for laminated-wood. $z_k$ (mm) was the coordinate for different RVEs in the direction of z. $t$ (mm) was the height of laminated-wood. $d_{11}$ (kN·mm)$^{-1}$, $d_{33}$ (kN·mm)$^{-1}$ were the elements in the inverse matrix of $\boldsymbol{D}_{ij}$. $\sigma_x$ (MPa), $\sigma_y$ (MPa) and $\tau_{xy}$ (MPa) were the stress for RVE, $X$ represented $T_x$ or $C_x$ for RVE, and $Y$ represented $T_y$ or $C_y$ for RVE.

SS ($\tau$, MPa) for RVE was predicted based on its longitudinal and transverse tensile strength according to the Tsai-Hill strength theory. SS distribution of wood composites could be obtained from the theory of Koseki as follows [243]:

$$\left(\frac{\tau_{xy}}{T_x}\right)^2+\left(\frac{-\tau_{xy}}{T_y}\right)^2-\left(\frac{\tau_{xy}}{T_x}\right)\left(\frac{-\tau_{xy}}{T_x}\right)=1 \quad (5\text{-}40)$$

$$\tau=\min\{E\left(\frac{\tau_{xy}}{E_x}\right)\} \quad (5\text{-}41)$$

Where $E_x$ (GPa) was elastic constant for RVE and $E$ (GPa) was MOE for laminated-wood. $\tau$ (MPa) was shear strength for laminated-wood.

## 5.4 Materials and methods

### 5.4.1 Materials

Wood veneer of masson pine (*Pinus massoniana Lamp.*) and poplar (*Populus tomentosa*) were selected from Guangdong Province and Jiangsu Province of China. The veneers were oven-dried at 50°C for 24h and then saved in the container under

60%RH and 25°C in order to obtain an equilibrium moisture content. The moisture content of veneers was 8 ± 3% with the dimension of 400 mm (length) × 400 mm (width) × 1.2 mm (height). The density of masson pine and poplar was 0.53 and 0.44 g/cm$^3$. The solid content of PF adhesive was 47% and the mole ratio of formaldehyde to phenol was 2 to 1. The viscosity of PF adhesive was 359 mPa·s. The density of PF was 1.10 g/cm$^3$.

### 5.4.2 HVEF-treated laminated-wood

The adhesive of 150 g/m$^2$ were applied to single wood surface and different laminated-wood composites (5-ply, 7-ply and 9-ply) were assembled. The assembly was set in the plate electrostatic field within a hot pressing machine as described in previous study. The electrostatic field voltage was set to 60 kV and the temperature was settled at 145°C. The pressure on the laminated-wood was 1MPa and the press duration was 1min/mm. HVEF treatment was applied during the whole press time. Ten repetitions were conducted for each condition. The compression ratios for masson pine laminated-wood composites were 12.56±0.35% (5-ply), 10.35±0.30% (7-ply) and 7.40±0.42% (9-ply); the compression ratios for poplar laminated-wood composites were 13.74±0.31% (5-ply), 11.20±0.22% (7-ply) and 8.65±0.25% (9-ply).

### 5.4.3 Fluorescence microscopy analysis

Samples were taken from the fixed position at the interphase of the composite material adhesive layer, and the samples were fixed on the sliding slicer with the size of 5mm×5mm× 30μm (length × width × thickness). The slices were heated in a

baking machine for 24h (50°C). After cooling, the slices were soaked with 1% saffron staining (Safraninet) for 20 min. The stained slices were then dehydrated and the ethanol solution (concentrations ranged from 55%, 65%, 75%, 85% to 100%) was changed every 10 min. After dehydration, the slices are immersed in xylene/anhydrous ethanol (volume ratio 1/1) mixture (10 min), and then immersed in pure xylene solution for 10 min. After the slices are removed, the slices are sealed with gum and set aside. Fluorescence microscopy with ultraviolet light source (OLYMPUSBX51) was used in this experiment.

### 5.4.4 X-ray vertical density profile analysis

X-ray vertical density profile analysis is an effective nondestructive testing technology for investigating the density distribution of the interphase of composite materials, which is beneficial to analyzing the distribution of the interphase adhesives of composite materials, and evaluating the quality and properties of the bonding materials. The sample is selected from the fixed area of the composite material, the size is 5mm×5mm (length × width), and the thickness is determined by the thickness of the composite material. Grecondax-5000 instrument is used, the test accuracy is 0.02mm, the ambient temperature is 25℃, and the humidity is 60%.The density of wood is mainly calculated according to this formula:

$$\rho = \frac{1}{\mu t} \ln \frac{I_0}{I} \qquad (4\text{-}1)$$

Where, $I_0$ is the initial intensity (X-ray), $I$ is the test intensity, $t$ is the thickness of the sample, and $\mu$ is the wavelength and the correlation constant (μ= 7).

### 5.4.5 Nano indentation test method

The sample was selected from the fixed area of the laminated veneer with a dimension of 5mm×5mm×5mm (length × width × height). The surface with glue line was selected for observation, and was cut flat with a diamond knife. Before measurement, the sample was stored at 20°C and 60% humidity for 24 h. The speed of the indentation head approaching the sample was 5nm/s, the peak load was 200μN (American IMICRO), and the time of pressure holding and pressure relief was 5s respectively. 40 to 50 scanning points were selected on the wood cell wall with a step size of 0.05mm, and the longitudinal modulus of elasticity was obtained by nano-indentation.

### 5.4.6 Mechanical property test method

In this paper, the mechanical properties of composite materials such as modulus of elasticity, modulus of rapture, shear modulus and shear strength were tested by Sans mechanical testing machine. The loading speed was 2mm/min. The methods were as follows.

Modulus and strength of masson pine and poplar veneer in principal directions were measured according to the standard of ASTM D4761-19, GB/T 14017-2009 and GB/T 1938-2009. MOE, MOR, G and SS of laminated-wood composites were measured according to EN 789-2005 and GB/T 20241-2006. The speed of loading was 2 mm/min. Ten repetitions were conducted for each mechanical test.

## 5.5 Results and analysis

### 5.5.1 Interfacial properties of laminated-wood under HVEF induction

In this study, the bonding interphase properties of the five-layer laminated-wood were firstly discussed, and fluorescence microstructures of the bonding interphase between Masson's pine and poplar were obtained by ultraviolet light source (as shown in Fig. 5-2 (b) and (e), and Fig. 5-3 (b) and (e)). In the untreated samples, it could be observed from the transverse and longitudinal sections that the adhesive penetrated deeply and the distribution of the adhesive at the interphase was discontinuous and dispersed. A large amount of the adhesive penetrated into the internal structure of the wood through the lumen or tracheids. After HVEF treatment, more adhesives were continuously and uniformly distributed along the interphase, and a large number of wood lumen (poplar) and tracheids (masson pine) were filled with adhesive at the interphase. By calculating the penetration depth of the adhesive, it could be obtained that the average penetration depth of the untreated sample was: Masson pine (855μm) < poplar (1130μm); the average penetration depth of masson pine (245μm) was lower than that of poplar (430μm) after HVEF treatment.

In addition, the vertical density distribution of the sample was shown in Figures 5-2 (f) and 5-3 (f). As could be seen from the figure, after the HVEF treatment, the distribution range of adhesives at the interphase narrowed and the density at the interphase increased significantly. Moreover, the maximum density at the interphase of masson pine was higher than that of poplar. The difference of this result is mainly

attributed to the difference of lignin content and diameter of cell in different tree species. In previous related studies, it was also found that the density at the interphase of the composite material increased significantly after treated by a HVEF [169,174]. This was mainly because the increase of surface energy and free radicals provided more reaction sites for the crosslinking reaction between wood chemical groups and adhesives. According to Equation (5-26), the volume fraction of the adhesive along the thickness of the sample could be calculated according to the density distribution of the composite material. It could be seen from Figures 5-2 (g) and 5-3 (g) that the volume fraction of the adhesive at the bonding interphase increased significantly after treated by a HVEF.

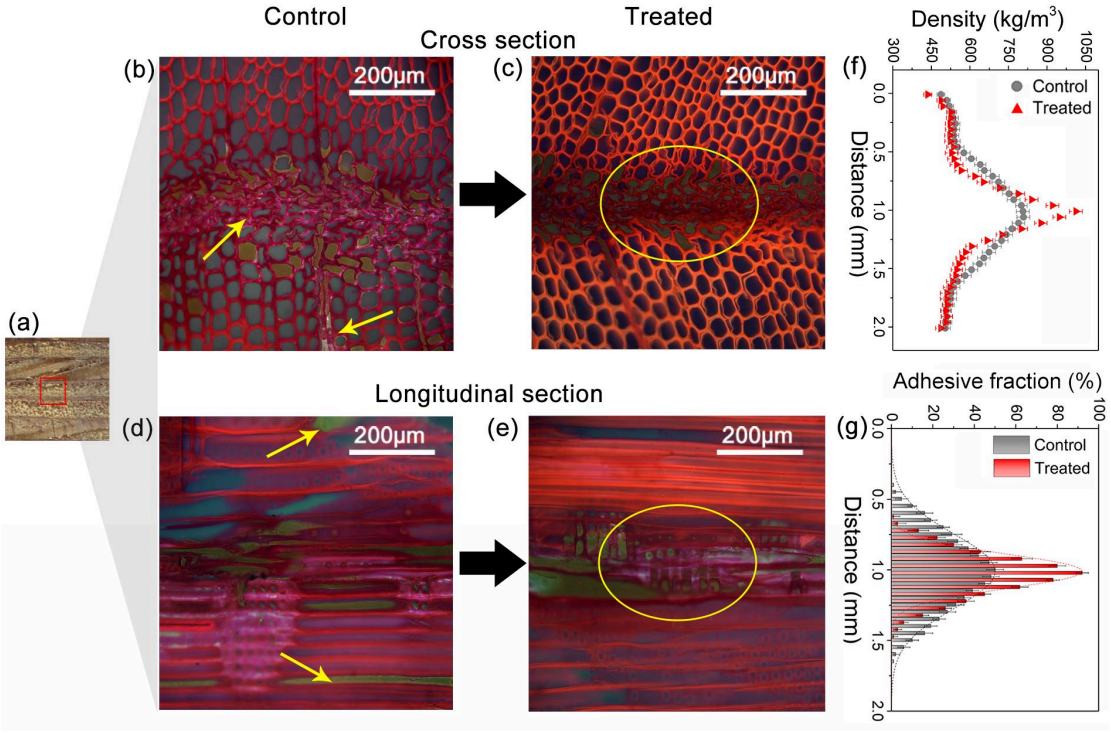


Fig.5-2 Micrographs obtained from single bonding interphase of (a) 5-ply masson pine laminated-wood. The comparison between (b) control (cross section), (d) control (longitudinal section), (c) HVEF-treated sample(cross section), (e) HVEF-treated samples (longitudinal section), (f) VDPand (g) adhesive fraction for bonding interphase of 5-ply masson pine laminated-wood.

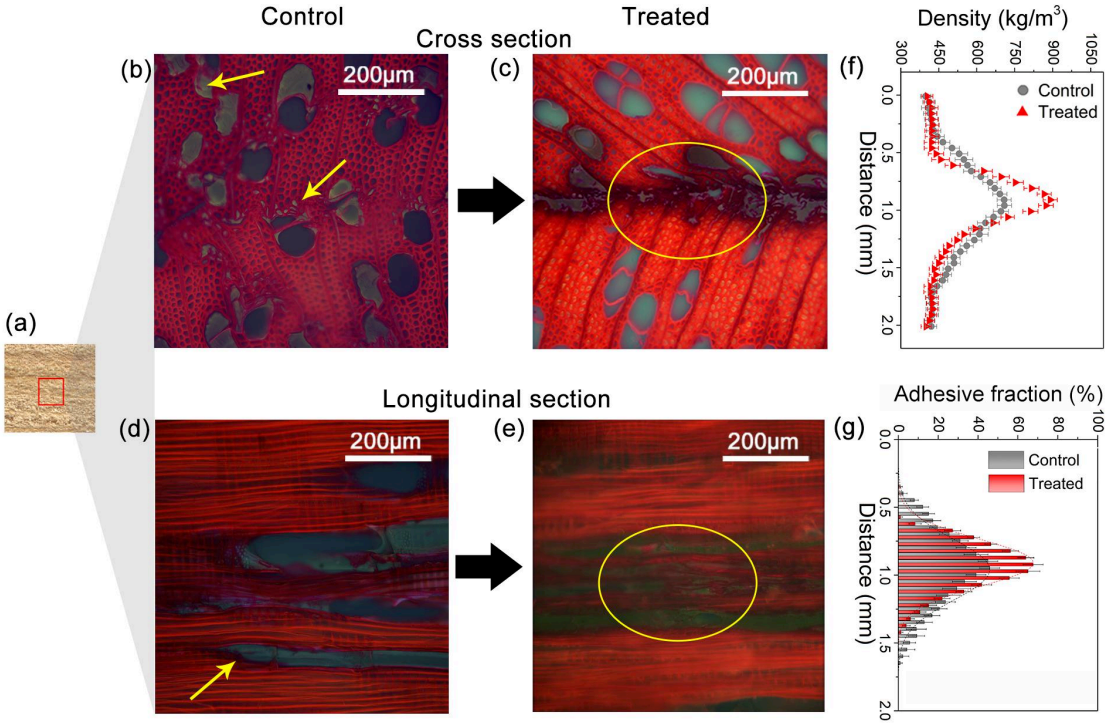


Fig.5-3 Micrographs obtained from single bonding interphase of (a) 5-ply poplar laminated-wood. The comparison between (b) control (cross section), (d) control (longitudinal section), (c) HVEF-treated sample(cross section), (e) HVEF-treated samples (longitudinal section), (f) VDPand (g) adhesive fraction for bonding interphase of 5-ply poplar laminated-wood.

### 5.5.2 Mechanical property of RVE element

In order to obtain the interfacial bonding properties of composites accurately, it is necessary to test the stiffness and strength of the composites as a whole and at the interphase. At the interphase of composite materials, different penetration forms and distributions of adhesives have a great influence on the stress transfer at the interphase, thus reflecting the degree of cross-linking reaction between wood and adhesive and the mechanical properties of the interphase [244-246].

The elastic constants of the RVE elements in the untreated and treated samples, including $E_x$, $E_y$, $G_{xy}$ and $\mu_{xy}$, and the distribution of the elastic constants at the interphase were predicted by formulas (5-27) to (5-30) according to the changes of the volume fraction of the adhesives before and after the treatment of the HVEF as shown in Table 5-1 and Figure 5-2 (g) and 5-3 (g). It could be seen from Fig. 5-4 that, after the HVEF treatment, the values of all elastic constants of masson pine and poplar materials at the bonding interphase were significantly higher than those of the untreated samples.The increment of $E_x$ value at the interphase of masson pine and poplar was 16.70% and 12.19%, respectively.

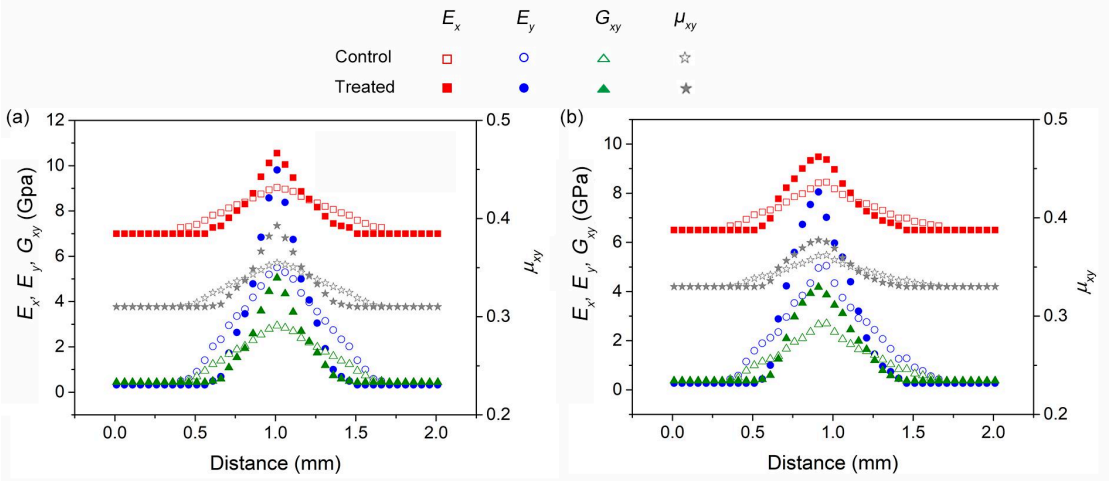


Fig.5-4 Elastic constants distribution for (a) masson pine and (b) poplar single bonding interphase in 5-ply laminated-wood before and after HVEF treatment.

In addition, in order to further verify the accuracy of $E_x$ values in the RVE unit, the experimental values ($E_{NI}$) obtained from the nano-indentation test (NI) were compared with $E_x$ (as shown in Fig. 5-5) using the nano-indentation test. As shown in Fig. 5-5 (b), test point per 50μm was selected in the red box range, and 40 to 50 points were selected on the wood cell wall (Fig. 5-6). After HVEF treatment, $E_{NI}$ at the

interphase of masson pine and poplar samples significantly increased (as shown in Fig. 5-5 (a)). At the same time, the hardness distribution at the interphase of the composite material was also obtained (as shown in Figure 5-5 (c)). It could be concluded that, after treated by a HVEF, the hardness at the interphase of the adhesive layer of the two samples increased significantly. These results were due to the higher density and volume fraction of the adhesive at the bonding interphase of the samples treated by HVEF. Previous studies have shown that the increase of density at the interphase has a positive effect on the modulus of elasticity and other properties of composites [247,248]. Since the test points in the nanoindentation test were all cell walls or the mixture of cell walls and adhesives, the elastic constant $E_x$ was predicted by using the compression modulus of solid wood (masson pine: $E_c$ =11.0 GPa, poplar: $E_c$ =9.2 GPa). It was evident that the relative errors of $E_x$ and $E_{NI}$ were less than ±15% (correlation $R^2$>90%, level 0.01) for both the masson pine and poplar composites in the untreated and treated samples. In the samples, the relative errors of $E_x$ and $E_{NI}$ could be attributed to the uneven distribution of adhesives and the change of mechanical properties of wood cell walls under hot pressing conditions [249,250]. Therefore, it could be explained that the distribution of adhesives could be obtained from the distribution of density at the interphase, so as to predict the elastic constant of RVE element, and further obtain the distribution characteristic method of elastic constant at the interphase of composite materials. On this basis, the influence of HVEF treatment on the interfacial and mechanical properties of composites was further quantified.

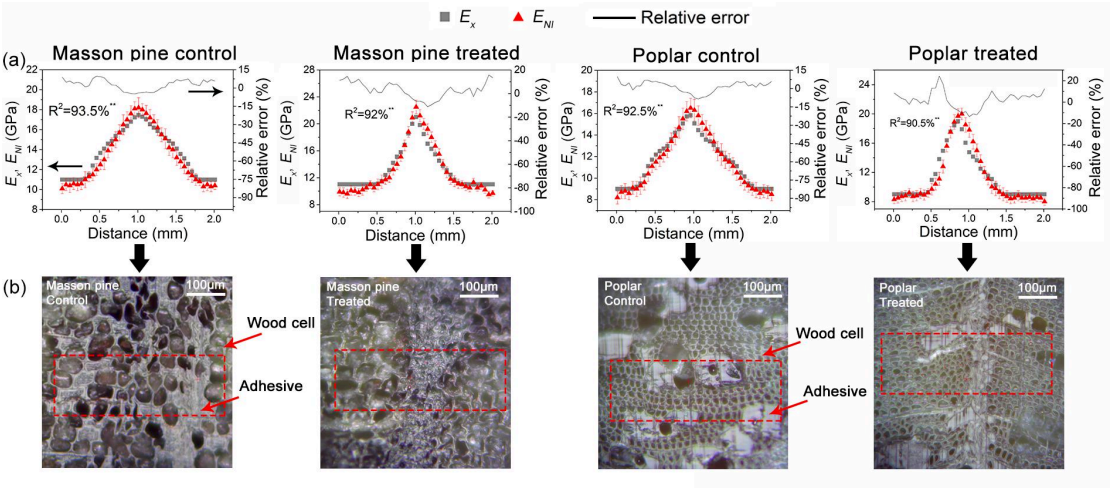


Fig.5-5 (a) ENI obtained from NI measurement for 5-ply masson pine and poplar laminated-wood compared with the predicted . Correlation coefficient (R2) and relative errors obtained between Ex and ENI. (b) Micrographs of indentation surface for masson pine and poplar samples. (c) Hardness of indentation surface for masson pine and poplar samples. Relative errors: $[(E_x\text{-}E_{NI})/E_{NI}]\times100\%$

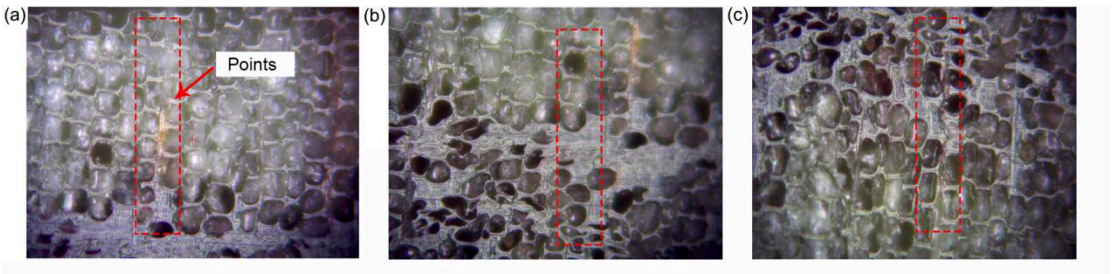


Fig.5-6 Diagram for indentation points selected along the thickness of laminated-wood bonding interphase from (a), (b) and (c).

### 5.5.3 Prediction and verification of mechanical properties of laminates

As shown in Fig. 5-7 (a) ~ (b), it represented the distribution of density and adhesives of the five-layer composite plate. At the same time, similar results were obtained for seven-layer and nine-layer laminates (as shown in Fig. 5-7 (c) ~ (f)). After HVEF treatment, the density and the volume fraction of the adhesive at the bonding interphase of each laminate increased significantly. The average density increment at the bonding interphase was as follows: masson pine, +21.4% (nine-ply)

< +25.7% (seven-ply) < +31.2% (five-ply); poplar, +14.7% (9-ply) < +20.5% (7-ply) < +24.8% (5-ply). More plies meant higher laminated thickness, leading to a larger distance between top and down electrodes. The amounts of free radicals and ions concentration among wood surface and reaction intensity between adhesive and wood were correlated with the distances between two electrodes [251]. The density and volume fraction of adhesives at the interphase of masson pine laminates were higher than those of poplar laminates regardless of the number of laminated-wood. This was similar to the results of previous studies, mainly due to the high lignin content in masson pine material, and the lignin content was proportional to the content of free radicals.

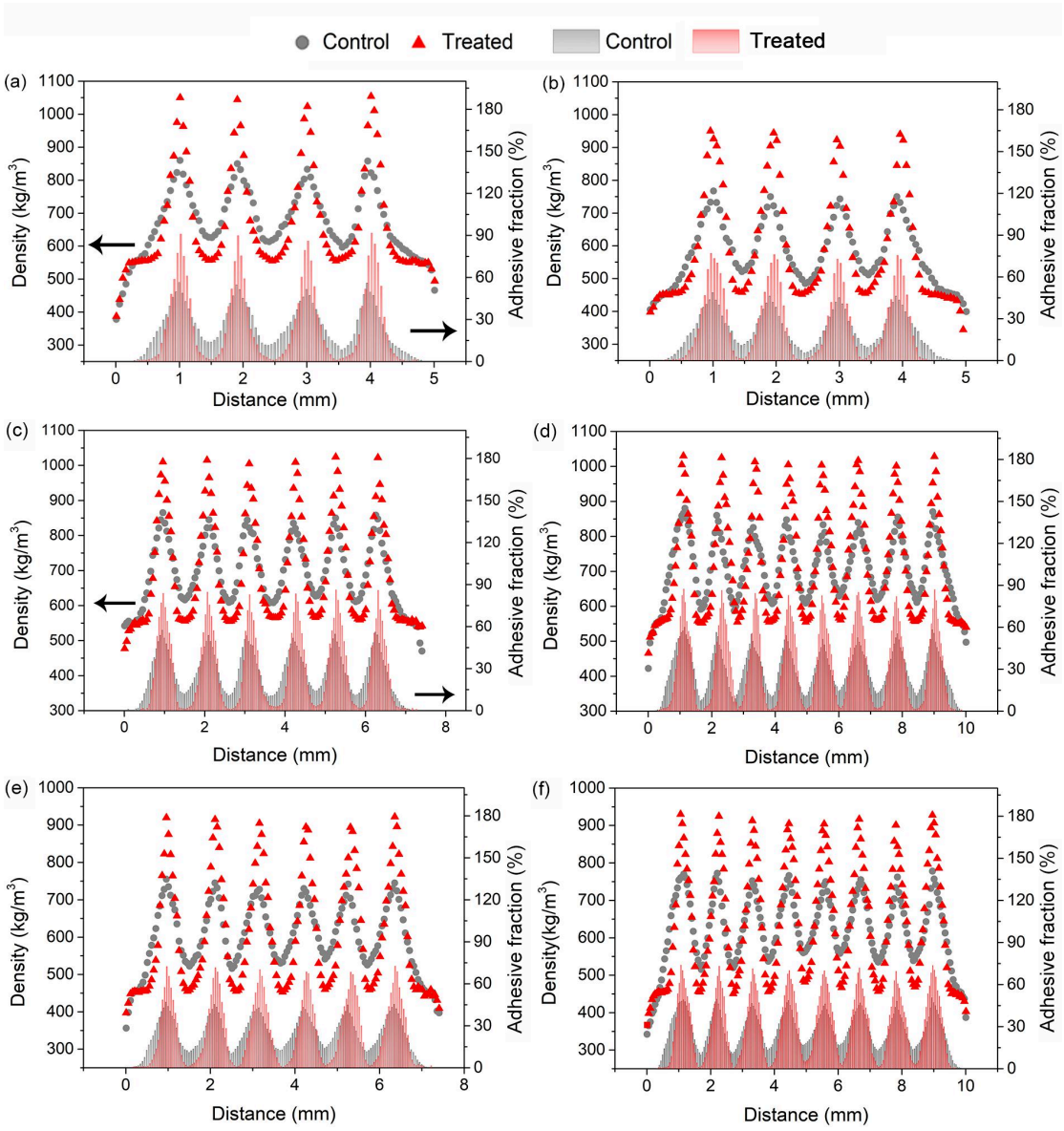


Fig.5-7 VDP and adhesive fraction for (a) 5-ply masson pine laminated-wood, (b) 5-ply poplar laminated-wood, (c) 7-ply masson pine laminated-wood, (d) 7-ply poplar laminated-wood, (e) 9-ply masson pine laminated-wood, (f) 9-ply poplar laminated-wood compared with the control.

The distribution of elastic constants ($E_x$, $E_y$, $G_{xy}$ and $\mu_{xy}$) and strength index parameters ($T_x$, $T_y$, $C_x$, $C_y$ and $S$) along the thickness direction of the composite were predicted based on the distribution of density (Fig. 5-8 (a), (b) and Fig. 5-9 (a) ~ (d)). As shown in Fig. 5-8 (c) ~ (f), Fig. 5-10 and Fig. 5-11, the elastic constant and

strength index of seven-layer and nine-layer laminates have similar distribution along the thickness direction. It could be seen from the figure that the elastic constant and strength index of the laminated plate were distributed in a quasi-sinusoidal curve along the thickness direction. In addition, compared with untreated specimens, the elastic constants and strength indexes of masson pine or poplar laminates treated by HVEF significantly increased.

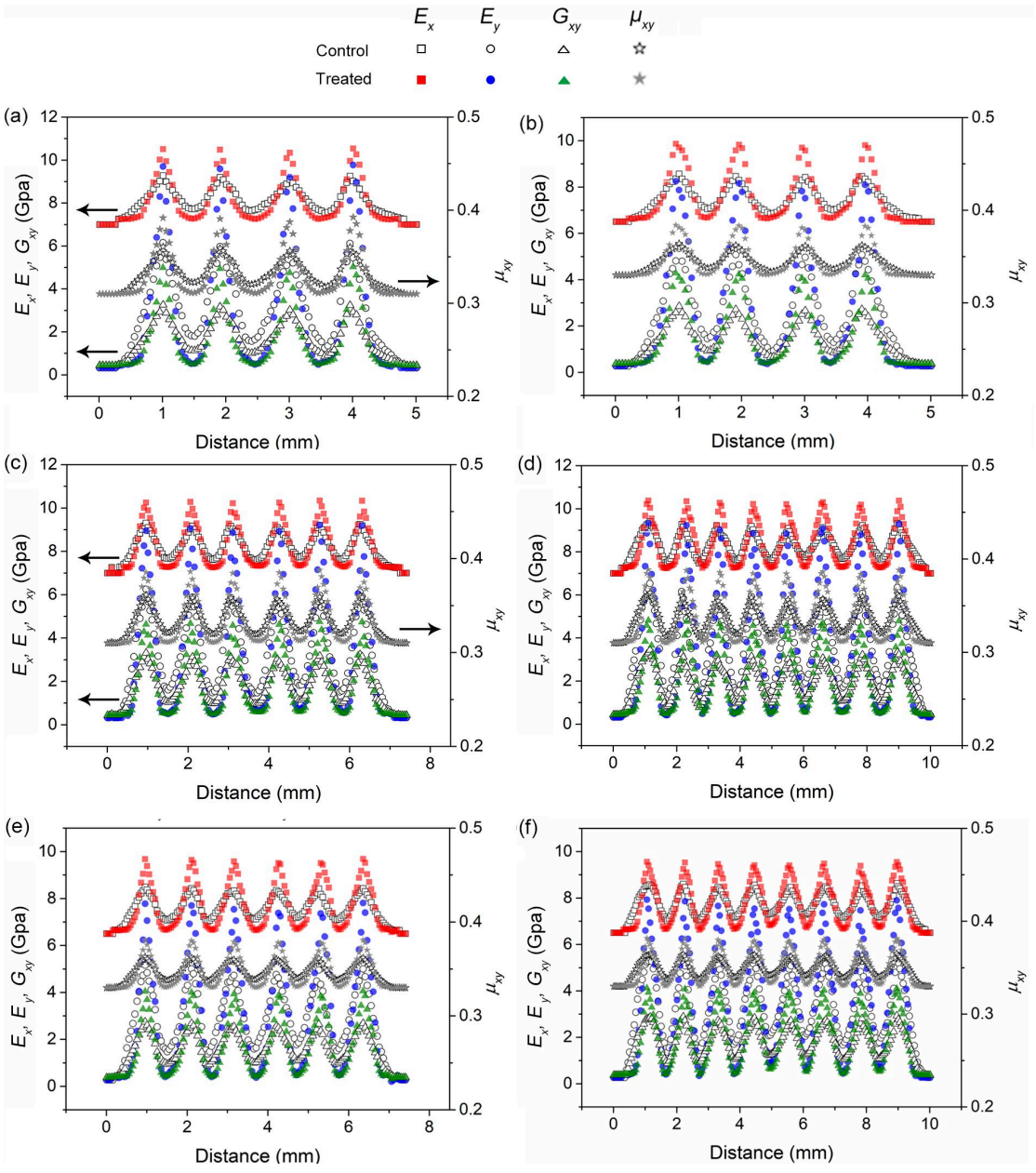


Fig.5-8 Elastic constants distribution for (a) 5-ply masson pine laminated-wood, (b) 5-ply poplar

laminated-wood, (c) 7-ply masson pine laminated-wood, (d) 7-ply poplar laminated-wood, (e) 9-ply masson pine laminated-wood, (f) 9-ply poplar laminated-wood compared with the control.

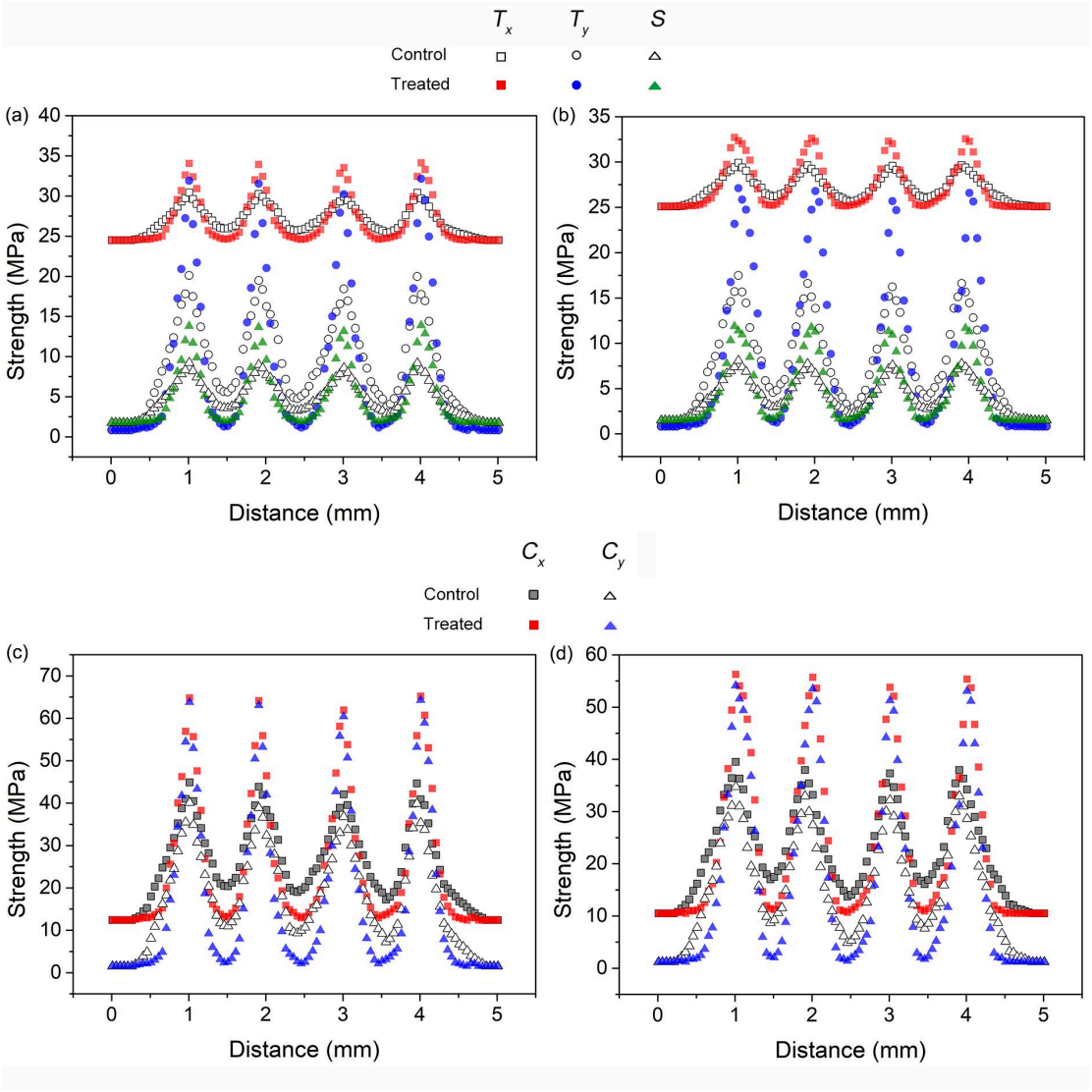


Fig.5-9 Strength indices distribution for 5-ply masson pine laminated-wood (a) Tx, Ty, S, (c) Cx, Cy; for 5-ply poplar laminated-wood (b) Tx, Ty, S, (d) Cx, Cy and compared with the control.

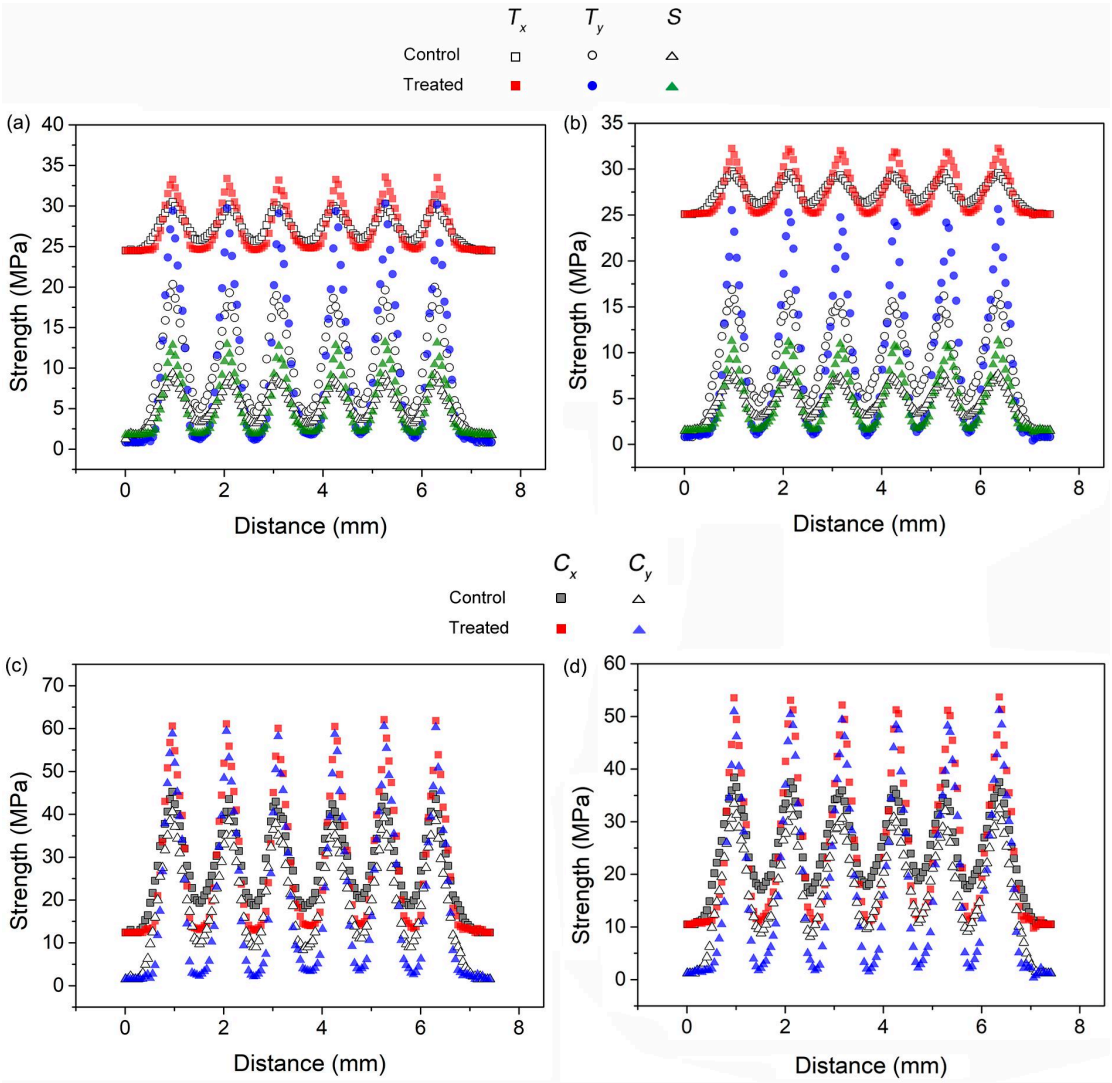


Fig.5-10 Strength indices distribution for 7-ply masson pine laminated-wood (a) Tx, Ty, S, (c) Cx, Cy; for 7-ply poplar laminated-wood (b) Tx, Ty, S, (d) Cx, Cy and compared with the control.

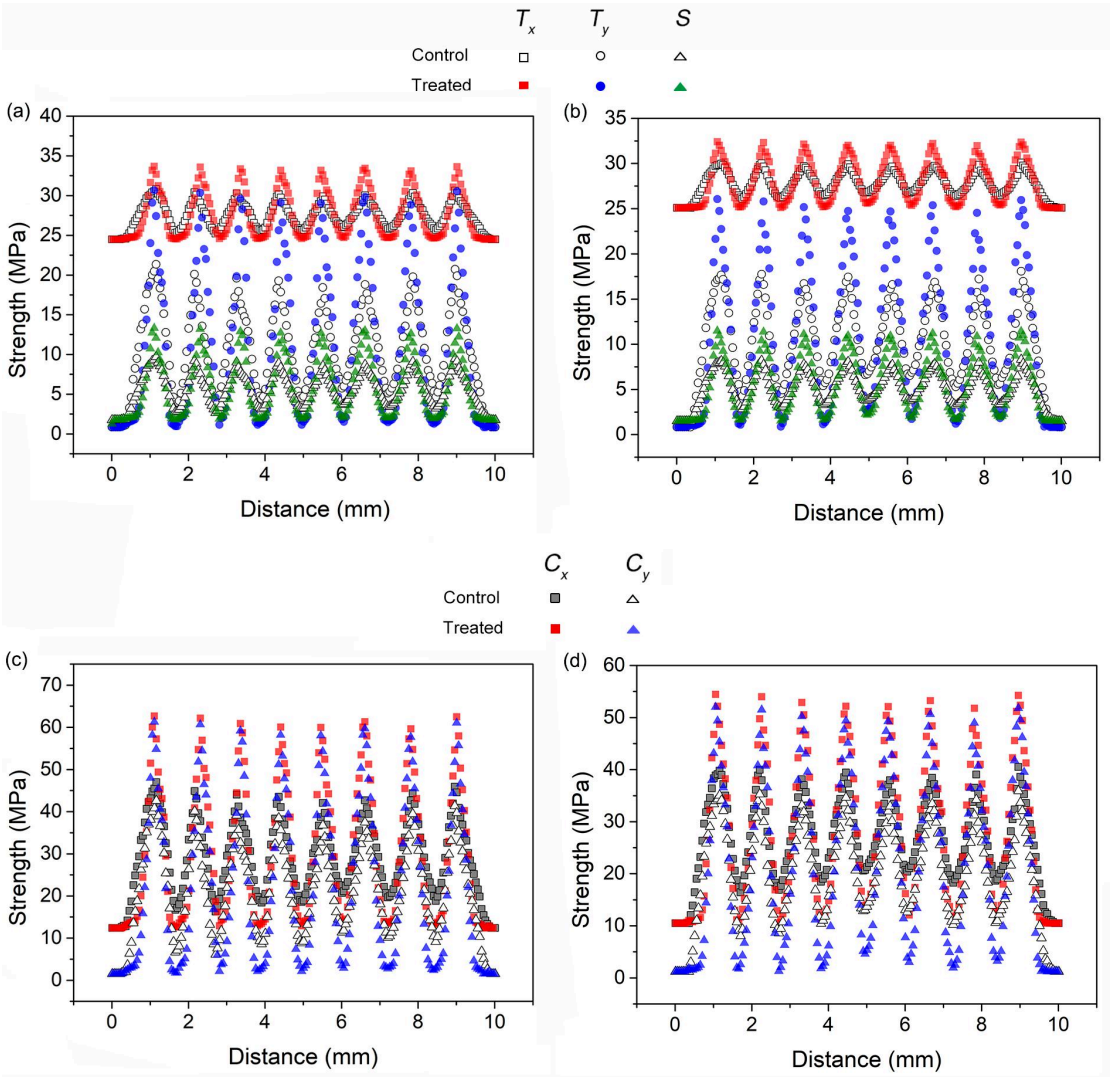


Fig.5-11 Strength indices distribution for 9-ply masson pine laminated-wood (a) Tx, Ty, S, (c) Cx, Cy; for 9-ply poplar laminated-wood (b) Tx, Ty, S, (d) Cx, Cy and compared with the control.

According to the predicted distribution of elastic constants and strength index parameters of laminates, the mechanical properties of laminates, including modulus of elasticity (MOE), modulus of rapture (MOR), shear modulus (G) and shear strength (SS), were predicted by using the formulas (5-36) ~ (5-41) and the theory of laminates. As shown in Fig. 5-12 and Fig. 5-13, the predicted values and tested values of MOE, MOR, G and SS of the laminates with different layers of masson pine and poplar were

presented respectively. It could be seen from the figure that the mechanical properties of laminated plates significantly increased after treated by a HVEF, and their mechanical properties increase with the increment of the number of laminated plates [252,253]. By comparing the predicted and measured values, the maximum relative error of the mechanical properties of the laminates was less than 30% (correlation coefficient $R^2$>80%, at the level of 0.01), regardless of whether the specimens have been treated by HVEF or not. In addition, the predicted values of MOE and MOR were lower than the measured values, while the predicted values of G and SS were higher than the measured values. This change was due to not considering thermal stress and humidity in the process of preparation. These factors could affect the interphase and mechanical performance of laminated plates [254]. Bonding interphase was not ideally uniform, and some local stresses occurred under shear loads [255]. In summary, according to the predicted results of the stiffness and strength distribution of laminated plates and the comparison between the predicted and measured values, it could be shown that the RVE element model can be used to quantify the induced effect of HVEF treatment on the stiffness and strength distribution along the thickness of laminated composite materials and interphase.

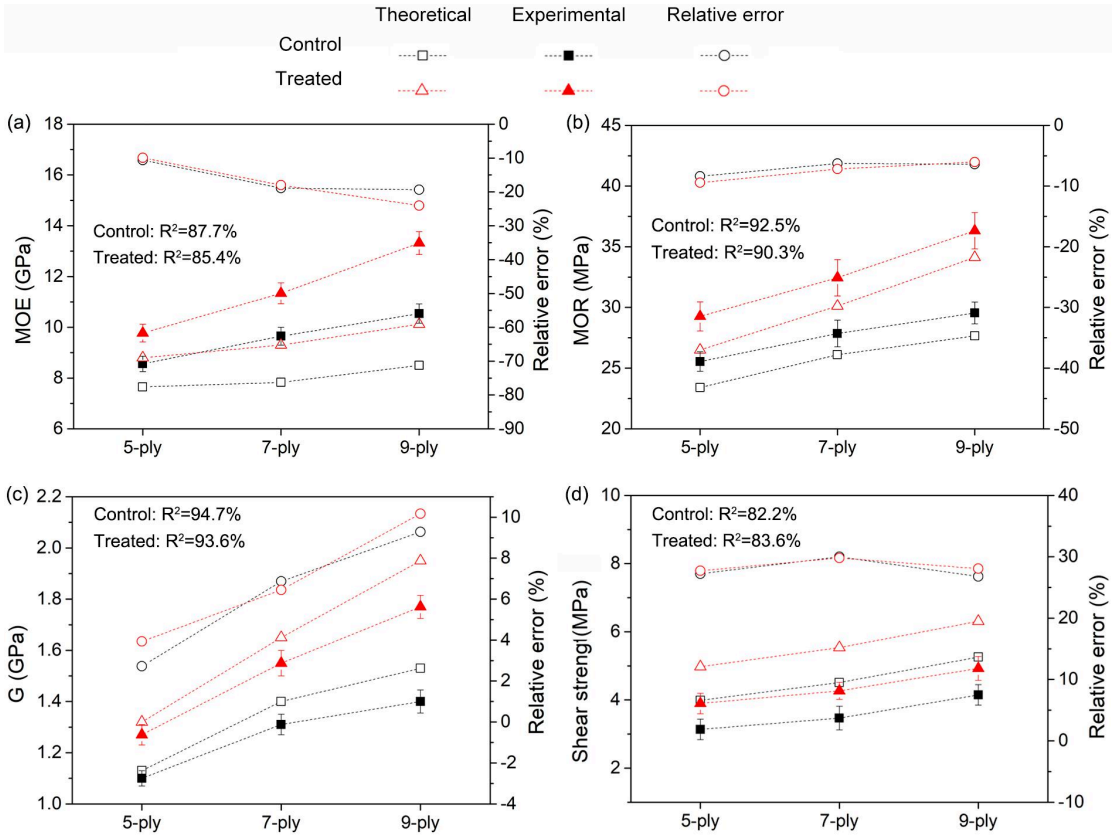


Fig.5-12 Correlation coefficients and relative errors obtained between theoretical and experimental values for (a) MOE, (b) MOR, (c) G and (d) SS of masson pine laminated-wood.

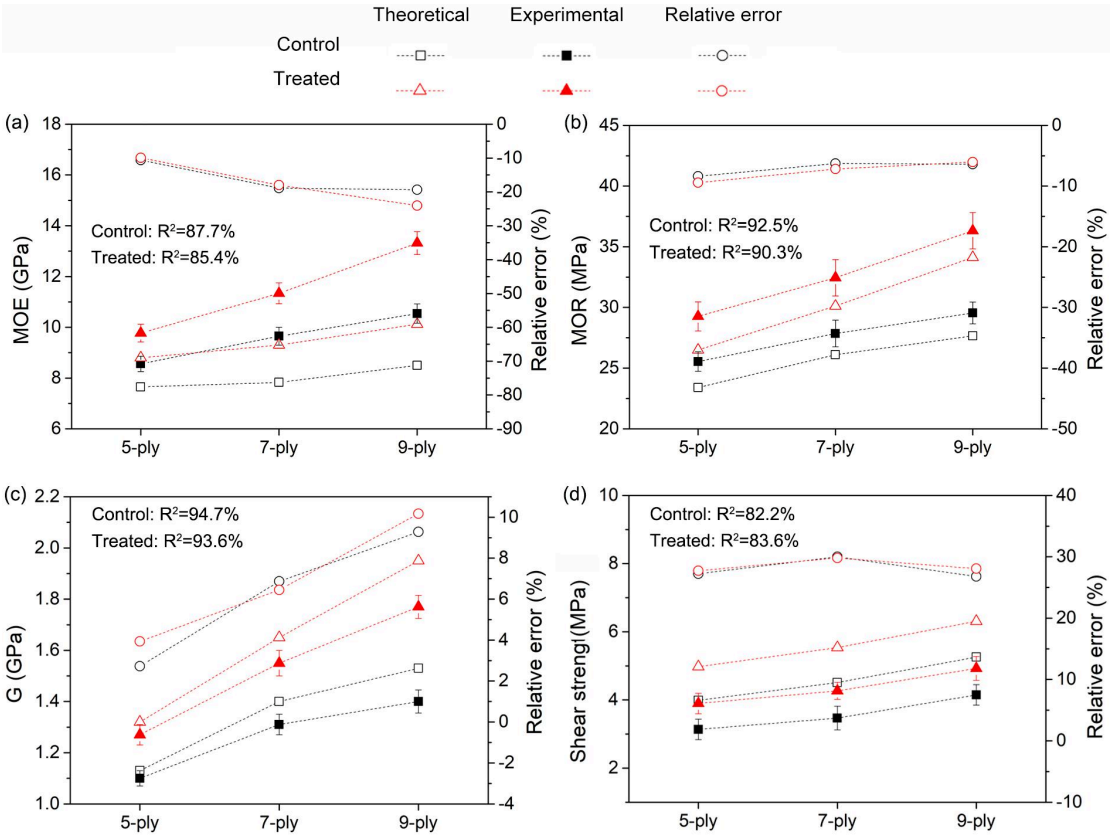


Fig.5-13 Correlation coefficients and relative errors obtained between theoretical and experimental values for (a) MOE, (b) MOR, (c) G and (d) SS of poplar laminated-wood.

## 5.6 summary

In this study, a prediction approach was proposed to predict the (distributions of) stiffness and strength of HVEF-treated laminated-wood composites base on the density profile along thickness direction. The characteristics of bonding interphase, and the distribution of adhesive fraction after HVEF treatment were investigated. RVE with a thickness of 50 μm was proposed to model stiffness and strength distributions in laminated-wood.

(1) After HVEF treatment, the penetration depth of the adhesive at the interphase of the laminates decreased significantly. The average penetration depth of the untreated samples was: masson pine (855μm) < poplar (1130μm). The average

penetration depth of masson pine (245μm) was lower than that of poplar (430μm) after HVEF treatment. In addition, after HVEF treatment, the distribution range of adhesives at the interphase was significantly narrowed, and the density at the interphase significantly increased. After HVEF treatment, the mechanical properties of the laminates increased significantly, and the mechanical properties increased with the increment of the number of laminates.

(2) The volume fraction of the adhesive along the thickness of the sample can be calculated according to the density distribution of the composite before and after HVEF treatment. According to the change of the volume fraction of the adhesive and the theoretical formula of the laminates, the elastic constants of the RVE element in the untreated and treated samples were predicted. The experimental values ($E_x$) obtained by the nanoindentation test ($E_{NI}$) were compared with those obtained by the nanoindentation test ($E_x$). The relative error between $E_x$ and $E_{NI}$ was less than ±15% (correlation $R^2$>90%, at the level of 0.01).

(3) According to the predicted distribution of elastic constants and strength index parameters of RVE element, the mechanical properties of laminated composite materials, including modulus of elasticity (MOE), modulus of rapture (MOR), shear modulus (G) and shear strength (SS), were predicted by using composite mechanics, laminated plate theory and MATLAB calculation program. By comparing the predicted values with the measured values, the maximum relative error of the mechanical properties of the laminates is less than 30% (the correlation coefficient R2>80%, at the level of 0.01) regardless of whether the specimens have been treated

by HVEF or not. It could be concluded that the RVE element model can be used to quantify the stiffness and strength distribution along the thickness direction of the laminated plate composites and the interphase treated by HVEF, and the mechanical model of the stiffness and stress distribution of the laminated interphase induced by HVEF could be built, so as to predict the mechanical properties of the composite materials.

# Chapter VI Conclusions and Research Prospects

## 6.1 General conclusion

In this study, the advanced equipments such as ESR (electron spin resonance), dynamic contact angle device, X-ray photoelectron spectrometer, rotational rheometer, fluorescence microscope and nano-indentation device were selected in order to investigate the effects of HVEF on the physicochemical properties of wood and bamboo, the effects of HVEF on the chemical structure and rheological properties of adhesives under a series of HVEF parameters. The aggregation effect of adhesive at bonding interface induced by HVEF has also been revealed and the micro-mechanical prediction model is established.

The main conclusions of this study are as follows:

1. After HVEF treatment, the surface activity of wood and bamboo increased significantly. Moreover, with the increase of voltage/time, the surface free radicals, O/C ratio and the number of oxygen groups increased significantly while the contact angle decreased. Under the condition of 60kV, the surface activity highly increased. The increment of free radicals was 26%, the decrease of initial contact angle was 22%, the decrease of equilibrium contact angle was 23%, the increment of free energy component was 43% ~ 75%, the increment of O/C ratio was 34%, the increment of oxygen-containing groups were 39% (C–OH), 149% (C–O or C=O) and 97% (O–C=O), respectively. Varied surface characteristics of different species and different sections were obtained under HVEF treatment. The change ratio was based on the surface characteristic parameters: cross section < tangential section < radial section; ayous < poplar < masson pine < Chinese fir. Under HVEF, the triggered silver particles reacted with

wood functional groups with different oxidation forms of Ag (0), Ag (I) and Ag (III). The highest concentration of silver particles in wood samples was 10.71%. Nano-scale silver particles were obtained with a certain crystal morphology and the average particle size was less than 50 nm. For bamboo, the surface activity of treated bamboo skin was significantly higher than that of bamboo pith. Under the condition of 60kV, the free radical, O/C ratio and oxygen-containing groups of bamboo skin increased by 35%, 32%, 33% (C–OH), 136% (C–O or C=O) and 71% (O–C=O) respectively. Therefore, under HVEF treatment, the physical and chemical properties of wood and bamboo can be significantly improved, which is conducive to improving the interphase properties of composite materials.

2. With the increase of voltage/time, significantly improved inter-molecular reactions of urea formaldehyde resin and phenol formaldehyde resin were obtained. After 60kV/8 min treatment, significant increment of the characteristic peaks of C–O groups were obtained. Under HVEF treatment, the temperature/frequency dependence of the rheological behaviors of the two resins changed significantly. In the temperature spectrum test, the viscosity, storage modulus and loss modulus of urea formaldehyde resin and phenol formaldehyde resin increased significantly after treatment. There was no significant difference in the increment of rheological property parameters between the two resins under various treatment conditions, but the reaction characteristics of the two adhesives were different with the water factor. In the frequency spectrum test, with the increase of temperature constant, the increment of viscosity, storage modulus and loss modulus of urea formaldehyde resin and phenol formaldehyde resin decreased. Therefore, the degree of inter-molecular polymerization of

phenol formaldehyde and urea formaldehyde resin can be significantly improved and the viscoelasticity of the resin can be improved under HVEF treatment.

3. After HVEF treatment, the distribution of adhesive at the bonding interphase was continuous and uniform. The penetration depth was significantly reduced. The density and bonding strength at the bonding interphase were significantly increased, and the delamination rate was reduced. After treatment, the maximal density at interphase is 1081 kg/m$^3$, which was 32% higher than the control. The bonding strength increased from 0.66MPa to 1.25MPa and the wood breaking rate increased to 85%, and the delamination rate decreased to 5.97%. Varied effects of HVEF treatment on different sections (C, cross section, T, tangential section and R, radial section) and different species were achieved. According to the change ratio of the interface characteristics, the sequence was: C-C < T-T < T-T$_\perp$ < R-T < R-R; ayous < poplar < masson pine < Chinese fir. The results showed that the improvement of the interphase properties of softwood induced by HVEF was higher than that of hardwood. According to the correlation analysis, the increase of lignin content significantly increased with the increment of free radicals, the decrease of penetration depth and the increment of bonding strength. However, there was a negative correlation between the content of extract, the diameter of cell cavity and the decrease of penetration depth and the increment of bonding strength. For bamboo material, the bonding strength was significantly improved after HVEF treatment. The bonding strength of bamboo skin and bamboo skin was 9.51MPa, and the bamboo failure ratio was 60%. In the combination of bamboo pith and bamboo pith, the maximum bamboo failure ratio was 85%, which was increased by 70%. Therefore, under HVEF treatment, the continuous and uniform distribution of bonding interphase adhesives

can be obtained, which can significantly improve the bonding performance of wood bamboo composite, and is conducive to the efficient utilization of wood bamboo composite.

4. According to the vertical density profile at the bonding interface, the laminated stiffness and stress distribution model of the bonding interface has been established. The results showed that the relative error was less than ±15%. Based on the distribution model, the macroscopic mechanical properties of composite are predicted with the combination of composite mechanics and laminated plate theory, including elastic modulus, bending strength, shear modulus and shear strength. The results showed that the prediction error of mechanical properties is less than 30%. With the stiffness and strength distribution model, the effect of HVEF treatment can be quantitatively characterized and the mechanical properties of HVEF treated composites can be predicted. As a result, strengthening mechanism of bonding interphase can be revealed with the the stiffness and strength distribution model.

## 6.2 Research Outlook

In view of the deficiencies in this research and the subsequent research work that needs to be carried out, the following research prospects and suggestions are put forward:

(1) This thesis clarified the mechanism of the influence of HVEF induction on the bonding characteristics of biomass materials and its interphase. Under different HVEF treatment conditions, the effects of HVEF induction on the surface properties of biomass materials, reaction mode of the adhesive and mechanical properties of the bonding interphase of biomass composites were explored. The strengthening

mechanism of the adhesive aggregation effect on the bonding interphase was revealed. In the future research work, we should also combine HVEF theory, wood physical and chemical theory under different temperature and humidity conditions to further explore the change law of the bonding interphase based on the macroscopic and microscopic mechanical properties after HVEF treatment, to reveal the effect of HVEF on the adhesive penetration form and mechanical properties depending on temperature and humidity, and to further multi scale explore the mechanical properties of composite materials.

(2) In addition, it is also necessary to perfect and improve the HVEF equipment (change the form of output voltage, plate material, etc.), to use the related theories of HVEF, and to combine analysis methods and analytical equipment such as spectroscopy, thermal and chemistry. In-depth analysis and research on the physical and chemical properties of materials from a microscopic perspective, and then analysis of the migration and movement of adhesive molecules based on the perspective of molecular dynamics. In addition, the HVEF-induced stress distribution mechanical model of the bonding interphase constructed in the study should be further applied to new composite materials, prepared from different types of biomass materials and environmentally friendly biomass-based adhesives to improve the universality of the mechanical model Therefore, it can improve the bonding enhancement mechanism and bonding theory of composite materials under the induction of HVEF.

## References


[1] Zhang H, Zhou X, Lu X, et al. Research on the non-gluing of Moso bamboo by linear vibration friction welding [J]. Journal of Nanjing Forestry University (Natural Science Edition), 2015, 39(5): 135-138.

[2] Yin T, Lu X, Han Z. Surface modification of carbon fiber and bonding performance of carbon fiber reinforced larch laminated timber [J]. Journal of Forestry Engineering, 2018, 3(2): 16-22.

[3] Yue K, Liu W, Lu X, et al. Research on basic mechanical properties of fast-growing poplar modified timber [J]. Forestry Practical Technology, 2011, 6(6): 57-59.

[4] Lu X, Wang Z, Du Y, et al. Prediction model of fast-growing poplar veneer in-plane shear modulus [J]. Journal of Nanjing Forestry University (Natural Science Edition), 2006, 30(1): 93-94.

[5] Lu X, He Q, Yao Y, et al. The natural frequencies and their influencing factors of the sole wood of two international general table tennis rackets [J]. Journal of Forestry Engineering, 2016, 1(1): 16-20.

[6] Zhan T, Yue L, Sun L, et al. Prediction model for longitudinal flexural elastic modulus of white parasol wood [J]. Journal of Nanjing Forestry University (Natural Science Edition), 2014, 38(3): 109-114.

[7] Wang Z, Fu H, Luo H, et al. Rolling shear properties of fast-growing poplar cross-layer orthogonal glulam [J]. Journal of Nanjing University of Technology (Natural Science Edition), 2016, 38(05): 116-120.

[8] Shen G, Hu G. Mechanics of Composite Materials [M]. Beijing: Tsinghua University Press, 2006.

[9] Zheng X, Zheng X, Jin L. Research progress of multi-scale methods in mechanical analysis of composite materials [J]. Progress in Mechanics, 2010, 40(1): 41-56.

[10] WANG H, ZHAO T, YAN Y, et al. Synthesis of resol–layered silicate nanocomposites by reaction exfoliation with acid-modified montmorillonite [J]. Journal of Applied Polymer Science, 2010, 92(2): 791-797.

[11] CUST DIO J, BROUGHTON J, CRUZ H. A review of factors influencing the durability of structural bonded timber joints [J]. International Journal of Adhesion & Adhesives, 2009, 29(2): 173-185.

[12] Li K. Study on the interface mechanics of wood composite materials (1) [J]. International Wood Industry, 2001, 1(1): 4-9.

[13] MANFREDI L B, PUGLIA D, TOMASUCCI A, et al. Influence of Clay Modification on the Properties of Resol Nanocomposites [J]. Macromolecular Materials & Engineering, 2008, 293(11): 878-886.

[14] Cheng R. The formation process of bonding strength during wood bonding [J]. Wood processing machinery, 2004, 15(6): 32-34.

[15] Gu J. Adhesives and Coatings [M]. Beijing: China Forestry Publishing Press, 2012.

[16] Li J. Biomass Composite Materials Science [M]. Beijing: Science Press, 2008.

[17] GINDL W, DESSIPRI E, WIMMER R. Using UV-Microscopy to Study Diffusion of Melamine-Urea-Formaldehyde Resin in Cell Walls of Spruce Wood [J]. Holzforschung, 2002, 56(1): 103-107.

[18] FURUNO T, IMAMURA Y, KAJITA H. The modification of wood by treatment with low molecular weight phenol-formaldehyde resin: a properties enhancement with neutralized phenolic-resin and resin penetration into wood cell walls [J]. Wood Science & Technology, 2004, 37(5): 349-361.

[19] JAKES J, FRIHART C, HUNT C, et al. X-ray methods to observe and quantify adhesive penetration into wood [J]. Journal of Materials Science, 2019, 54(8): 215-229.

[20] PENG G Y, WANG Y R, REN H Q, et al. Investigation of Characteristic Microstructures of Adhesive Interface in Wood/Bamboo Composite Material by Synchrotron Radiation X-Ray Phase Contrast Microscopy [J]. Spectroscopy & Spectral Analysis, 2013, 33(3): 829-833.

[21] MODZEL G, KAMKE F A, CARLO F D. Comparative analysis of a wood: adhesive bondline [J]. Wood Science & Technology, 2011, 45(1): 147-158.

[22] XU D, ZHOU H, MENG Y, et al. Characterization of adhesive penetration in wood bond by means of scanning thermal microscopy (SThM) [J]. Holzforschung, 2015, 70(4): 323-330.

[23] JEONG B, PARK B D. Effect of molecular weight of urea–formaldehyde resins on their cure kinetics, interphase, penetration into wood, and adhesion in bonding wood [J]. Wood Science and Technology, 2019, 53(4): 665-685.

[24] LE E A, NAIRN J A. Measuring interfacial stiffness of adhesively bonded wood [J]. Wood Science & Technology, 2014, 48(6): 1109-1121.

[25] HAMID N H A, AHMAD M, SURATMAN M N, et al. Adhesive Bonding Strength and Adhesive Penetration of Two Malaysian Medium Hardwoods [J]. Advanced Materials Research, 2013, 748(8): 170-174.

[26] SURATMAN M N. Adhesive Penetration in Laminated Oil Palm Trunk Veneer [J]. Journal of Tropical Forest Science, 2013, 25(4): 467-474.

[27] PAN Y F, XIAO H N, WANG W C, et al. Characterization of PVAc Adhesive Penetration and its Effect on Wood Properties [J]. Advanced Materials Research, 2014, 1033-1034(173): 1271-1274.

[28] GAVRILOVIĆ-GRMUŠA I, DUNKY M, DUNKY M, et al. Influence of Pressure on the Radial and Tangential Penetration of Adhesive Resin into Poplar Wood and on the Shear Strength of Adhesive Joints [J]. Bioresources 2016, 11(1): 2238-2255.

[29] KONNERTH J, J GER A, EBERHARDSTEINER J, et al. Wood Adhesive Bondlines by Nanoindentation [M]. Dordrecht: Springer, 2007.

[30] GINDL W, GUPTA H S. Cell-wall hardness and Young's modulus of melamine-modified spruce wood by nano-indentation [J]. 2002, 33(8): 1141-1145.

[31] KONNERTH J, GINDL W. Mechanical characterisation of wood-adhesive interphase cell walls by nanoindentation [J]. Holzforschung, 2006, 60(4): 429-433.

[32] JAKES J E, HUNT C G, YELLE D J, et al. Synchrotron-based X-ray Fluorescence Microscopy in Conjunction with Nanoindentation to Study Molecular-Scale Interactions of Phenol–Formaldehyde in Wood Cell Walls [J]. ACS applied materials and interfaces, 2015, 7(12): 6584-6589.

[33] OBERSRIEBNIG M, VEIGEL S, GINDL-ALTMUTTER W, et al. Determination of adhesive energy at the wood cell-wall/UF interface by nanoindentation (NI) [J]. Holzforschung, 2012, 66(6): 781-787.

[34] MENDOZA M, HASS P, WITTEL F K, et al. Adhesive penetration of hardwood: a generic penetration model [J]. Wood Science & Technology, 2012, 46(1-3): 529-549.

[35] MAKOTO K, NOBORU N, SHINICHIRO N. Estimation of the internal shear strength distribution of the element for laminated veneer lumber by nonlinear least-squares method [J]. Journal of Wood Science, 2018, 64(5): 635-641.

[36] LE E, NAIRN J. Measuring interfacial stiffness of adhesively bonded wood [J]. Wood Science and Technology, 2014, 48(6): 1109-1121.

[37] GUGLIELMINO E, EPASTO G, CORIGLIANO P, et al. Experimental and theoretical analyses of Iroko wood laminates [J]. Composites Part B: Engineering, 2017, 112(1): 251-264.

[38] KAMKE F A. Adhesive penetration in wood - A review [J]. Wood & Fiber Science Journal of the Society of Wood Science & Technology, 2007, 39(2): 205-220.

[39] Zhang S, Zhao L, Bao F, et al. Study on composite materials of triploid Chinese white poplar wood (shavings) reinforced by glass fiber and flax shavings [J]. Forest Products Industry, 2001, 28(4): 9-16.

[40] Zhang S, Zhou Y, Liu X. Research on the cement matrix for wood composite materials [J]. Building Panel, 1997, 3(3): 5-12.

[41] He F, Yang Y. Carbon fiber reinforced wood composite material [J]. New chemical materials, 2003, 31(10): 9-12.

[42] Wang W, Wang Z, Lu X, et al. Research on laminated poplar veneer lumber reinforced by metal mesh [J]. Journal of Nanjing Forestry University (Natural Science Edition), 2003, 27(6): 9-12.

[43] COLEMAN J D. Process for reconsolidated wood production [D]. US, 1987.

[44] Tang L. Study on the Mechanism of Cold Plasma Modification on Surface and Interface of Wood Veneer [D]. Nanjing: Nanjing Forestry University, 2015.

[45] NOVAK I, POPELKA A, SPITALSKY Z, et al. Investigation of beech wood modified by radio-frequency discharge plasma [J]. Vacuum, 119(9): 88-94.

[46] N.ACDA M, E.DEVERA E, J.CABANGON R, et al. Effects of plasma modification on adhesion properties of wood [J]. International Journal of Adhesion and Adhesives, 2012, 32(1): 70-75.

[47] HUNNEKENS B, PETERS F, AVRAMIDIS G, et al. Plasma treatment of wood-polymer composites: A comparison of three different discharge types and their effect on surface properties [J]. Journal of Applied Polymer Science, 2016, 133(18): 43376.

[48] ALTGEN D, AVRAMIDIS G, VI L W, et al. The effect of air plasma treatment at atmospheric pressure on thermally modified wood surfaces [J]. Wood Science & Technology, 2016, 50(6): 1-15.

[49] UEHARA T, NISHIMURA H, FURUNO T, et al. Effect of corona discharge treatment on beech [Fagus crenata] wood meal [J]. Journal of Applied Polymer Science, 1993, 41(1): 1695-1706.

[50] UEHARA T, SAKATA I. Effect of corona discharge treatment on cellulose prepared from beech wood [J]. Journal of Applied Polymer Science, 1990, 41(7-8): 1695-1706.

[51] SAKATA I, MORITA M, TSURUTA N, et al. Activation of wood surface by corona treatment to improve adhesive bonding [J]. Journal of Applied Polymer Science, 1993, 49(7): 1251-1258.

[52] RUPONEN J, LINDROOS T, ROHUMAA A, et al. Influence of surface activation on silver birch veneer properties [C]. Lahti: International Scientific Conference on Hardwood Processing, 2017.

[53] HALLER P, BEYER E, WIEDEMANN G, et al. Experimental study of the effect of a laser beam on the morphology of wood surfaces [C]. Vienna: International Symposium Wood Based Materials, 2002.

[54] MIKLEČIĆ J, JIROUŠ-RAJKOVIĆ V. Influence of Thermal Modification on Surface Properties and Chemical Composition of Beech Wood (Fagus sylvatica L.) [J]. Drvna Industrija, 2016, 67(1): 65-71.

[55] PETRIČ M, KRIČEJ B, PAVLIČ M, et al. Surface properties of wood thermally modified in vacuum at 212°C [C]. Slovenia: Proceedings of the Sixth European Conference on Wood Modification, 2012.

[56] SERNEK M, BOONSTRA M, PIZZI A, et al. Bonding performance of heat treated wood with structural adhesives [J]. Holz Als Roh Und Werkstoff, 66(3): 173-180.

[57] BEKHTA P, SEDLIACIK J, TYMYK D. The effect of chemical treatment of wood veneer surfaces on their bondability [J]. Acta Facultatis Xylologiae, 2015, 57(2): 71-79.

[58] OLAKANMI E O, OGUNESAN E A, VUNAIN E, et al. Mechanism of fiber/matrix bond and properties of wood polymer composites produced from alkaline treated Daniella oliveri wood flour [J]. Polymer Composites, 2015, 37(9): 2657-2672.

[59] Zhang Q, Gao Q, Li L, et al. Study on the relationship between surface free energy and bonding strength of poplar veneer treated with coupling agent [J]. Forest Products Industry, 2015, 42(10): 14-17.

[60] Wang D, Cao Y, Wang C, et al. Effect of silane coupling agent on properties of eucalyptus veneer-polyvinyl chloride membrane composites [J]. Journal of Beijing Forestry University, 2016, 38(2): 120-123.

[61] LU J, WU Q, JR H S. Chemical coupling in wood fiber and polymer composites: A review of coupling agents and treatments [J]. Wood and Fiber Science, 2000, 32(1): 88-104.

[62] Yin T, Lu X, Han Z. Adhesive properties of modified glass fiber cloth reinforced larch composites [J]. Journal of Forestry Engineering, 2016, 1(4): 45-50.

[63] DEVI A, SRIVASTAVA D. Studies on the blends of cardanol-based epoxidized novolac type phenolic resin and carboxyl-terminated polybutadiene (CTPB) [J]. Materials Science & Engineering A, 2007, 458(1): 336-347.

[64] Gong Y, Deng Z, Wu Q, et al. Research progress of high-performance modified phenolic resin [J]. Materials Review,2013, 27(11): 83-88.

[65] NAIR C P R. Advances in addition-cure phenolic resins [J]. Progress in Polymer Science, 2004, 29(5): 401-498.

[66] WANG M, WEI L, TONG Z. A novel condensation–addition-type phenolic resin (MPN): Synthesis, characterization and evaluation as matrix of composites [J]. Polymer, 2005, 46(21): 9202-9210.

[67] CUI J, LU X, ZHOU X, et al. Enhancement of mechanical strength of particleboard using environmentally friendly pine (Pinus pinaster L.) tannin adhesives with cellulose nanofibers [J]. Annals of Forest Science, 2015, 72(1): 27-32.

[68] Huang Z, Wang H, Kou Y, et al. Preparation and characterization of nano-cellulose modified phase change energy storage materials [J]. Thermosetting resin, 2014, 6(6): 30-33.

[69] Lin Q, Yang G, Liu J. Application and mechanism study of nano-silica modified urea-formaldehyde resin [J]. Journal of Fujian College of Forestry, 2005, 25(2): 97-102.

[70] HWANG H J, JUNG S L, CHO K H, et al. Tribological performance of brake friction materials containing carbon nanotubes [J]. Wear, 2010, 268(3-4): 519-525.

[71] LEI H, DU G, PIZZI A, et al. Influence of Nanoclay on Phenol-Formaldehyde and Phenol-Urea-Formaldehyde Resins for Wood Adhesives [J]. Journal of Adhesion Science & Technology, 2010, 24(8-10): 1567-1576.

[72] PIZZI, A. Recent developments in eco-efficient bio-based adhesives for wood bonding: opportunities and issues [J]. Journal of Adhesion Science & Technology, 20(8): 829-846.

[73] MANSOURI H R, NAVARRETE P, PIZZI A, et al. Synthetic-resin-free wood panel adhesives from mixed low molecular mass lignin and tannin [J]. European Journal of Wood and Wood Products, 2011, 69(2): 221-229.

[74] DABBABI I, GIMELLO O, ELALOUI E, et al. Organosolv Lignin-Based Wood Adhesive. Influence of the Lignin Extraction Conditions on the Adhesive Performance [J]. Polymers, 2016, 8(9): 340.

[75] HE Q, ZIEGLER-DEVIN I, CHRUSCIEL L, et al. Lignin-first integrated steam explosion process for green wood adhesive application [J]. ACS Sustainable Chemistry & Engineering, 2020, 8(13): 5380-5392.

[76] Li L, Zhu L, Zhu P. Analysis of China's Bamboo Resources and Bamboo Industry Development Status [J]. Southern Agriculture, 2017, 11(1): 6-9.

[77] Chen G. Preparation and mechanical properties of glued bamboo laminate [D]. Hunan: Central South University of Forestry and Technology, 2014.

[78] WAHAB M M A, CROCOMBE A D, BEEVERS A, et al. Coupled stress-diffusion analysis for durability study in adhesively bonded joints [J]. International Journal of Adhesion & Adhesives, 2002, 22(1): 61-73.

[79] YU W K, CHUNG K F, CHAN S L. Axial buckling of bamboo columns in bamboo scaffolds [J]. Engineering Structures, 2005, 27(1): 61-73.

[80] Zhang Q. Talking about my country's Bamboo-based Artificial Panels [J]. Forest Products Industry, 1989, 4(4): 5-8.

[81] DU C G, JIN C D, LI G Y. Study on Gluing Properties and Surface Wettability of Radial Bamboo Strips [J]. Advanced Materials Research, 2013, 671-674: 1774-1778.

[82] MENG F D, YU Y L, ZHANG Y M, et al. Surface chemical composition analysis of heat-treated bamboo [J]. Applied Surface Science, 2016, 371(15): 383-390.

[83] Tang Y, Yuan Y. Study on the Anticorrosive and Antifungal Treatment of Bamboo [J]. Wood Industry, 1990, 2(2): 1-6.

[84] Wang F, Wang W. Preliminary study on the current situation and problems of bamboo-based wood-based panels in my country [J]. China Wood-based Panels, 2007, 14(12): 1-4.

[85] Wang X, Zhao X, Gao Li, et al. Bamboo-wood composite is an important way to use bamboo efficiently [J]. Wood processing machinery, 2002, 13(4): 25-27.

[86] RAO J, BAO L, WANG B, et al. Plasma surface modification and bonding enhancement for bamboo composites [J]. Composites Part B: Engineering, 2017, 138(

[87] LI B, LI J, ZHOU X, et al. Study of Gliding Arc Plasma Treatment for Bamboo-Culm Surface Modification [J]. Forests, 2019, 10(1086.

[88] GUAN M, HUANG Z, ZENG D. Shear Strength and Microscopic Characterization of a Bamboo Bonding Interface with Phenol Formaldehyde Resins Modified with Larch Thanaka and Urea [J]. Bioresources, 2016, 11(492-502.

[89] MENG F-D, YU Y, ZHANG Y-M, et al. Surface chemical composition analysis of heat-treated bamboo [J]. Applied Surface Science, 2016, 371(

[90] LI T, CHENG D-L, W LINDER M, et al. Wettability of oil heat-treated bamboo and bonding strength of laminated bamboo board [J]. Industrial Crops and Products, 2015, 69(

[91] Chen G, Li J. Research on Improving the Bonding Performance of Bamboo [J]. Bamboo Research Transactions, 1991, 1(1): 37-43.

[92] ATANDA P, AKINLUWADE K, ADESINA O, et al. Effect of Alkali-treated Bamboo Fibers on Some Mechanical Properties of Virgin High Density Polyethylene [J]. Archives of Current Research International, 2017, 8(3): 1-7.

[93] LI X B, SHUPE T F, HSE C Y. Wettability of three Honduran bamboo species [J]. Journal of Bamboo & Rattan, 2004, 3(2): 159-167.

[94] LEE S H, WANG S. Biodegradable polymers/bamboo fiber biocomposite with bio-based coupling agent [J]. 37(1): 0-91.

[95] Ren P, Wang Z, Gao L, et al. Effect of coupling agent on bamboo surface wettability and bonding strength [J]. Adhesion, 2011, 7(1): 50-53.

[96] WANG C, WANG S, CHENG H, et al. Mechanical properties and prediction for nanocalcium carbonate-treated bamboo fiber/high-density polyethylene composites [J]. Journal of Materials Science, 2017, 52(19): 11482-11495.

[97] Yu W, Yu Y, Jiang Z. Surface bonding properties of bamboo [J]. Bamboo Research Transactions, 2006, 25(1): 30-36.

[98] Fu F, Hua Y. The influence of blank assembly method on the bonding strength of bamboo curtain board [J]. Journal of Nanjing Forestry University (Natural Science Edition), 1995, 19(1): 33-36.

[99] Chen G, Sun Z, Chen G, et al. Influence of billet assembly methods on the bonding properties of bamboo-wood composite laminated timber [J]. Journal of Central South University of Forestry and Technology, 2013, 33(12): 166-169.

[100] Deng B, Wu Z. Study on the effect of carbonization treatment on the performance of bamboo substrate bonding and paint [J]. Furniture, 2013, 1(1): 63-67.

[101] Chang Q, Hong H, Bai C, et al. Design of high-frequency hot press for bamboo recombined material [J]. Wood processing machinery, 2008, 6(6): 24-26.

[102] ZHANG H, PIZZI A P, ZHOU X, et al. The study of linear vibrational welding of moso bamboo [J]. Journal of Adhesion Science and Technology, 2018, 32(1): 1-10.

[103] KEMP B A, NIKOLAYEV I, SHEPPARD C J. Coupled electrostatic and material surface stresses yield anomalous particle interactions and deformation [J]. Journal of Applied Physics, 2016, 119(14): 1-7.

[104] SAVILLE D A. ELECTROHYDRODYNAMICS:The Taylor-Melcher Leaky Dielectric Model [J]. Annual Review of Fluid Mechanics, 2003, 29(1): 27-64.

[105] ZHANG J, LIU J. Effect of high voltage electric field on structure and property of PEDOT:PSS film [J]. Semiconductors, 2017, 51: 1611-1614.

[106] ARUN N, SHARMA A, SHENOY V B, et al. Electric-Field-Controlled Surface Instabilities in Soft Elastic Films [J]. Advanced Materials, 2006, 18(5): 660-663.

[107] JANKOWIAK A, COLLARDEY F, BLANCHART P. Electrical behaviour at high voltage on surface of SiC-β'-SiAlON ceramic composites [J]. Journal of The European Ceramic Society, 2005, 25(1): 13-18.

[108] SOUZA A L, LOPES I. Electric field distribution along the surface of high voltage polymer insulators and its changes under service conditions [C]. Toronto: 2006 IEEE International Symposium on Electrical Insulation, 2006.

[109] Wang D, Tang J, Tao J, et al. Charge accumulation characteristics of polymer surface after flashover and corona under DC voltage [J]. High Voltage Technology, 041(11): 3618-3627.

[110] Liu X, Lin H, Liang Y, et al. Study on the effect of microsecond pulse creeping discharge in the air on the surface characteristics of epoxy resin [J]. Transactions of the China Electrotechnical Society, 030(13): 158-165.

[111] KILIC A, SHIM E, POURDEYHIMI B. Measuring electrostatic properties of fibrous materials: A review and a modified surface potential decay technique [J]. Journal of Electrostatics, 2015, 74(4): 21-26.

[112] RICHMAN D E. Conformational responses to changes in the state of ionization of titrable groups in proteins [J]. Holzforschung, 2015, 54(6): 604-608.

[113] ASTORGA Q A M, SAKAMOTO W, CHIERICE G, et al. A new high voltage polymer insulator for electrical distributionsystems from oil of Mamona trees [C]. Virginia Beach: Electrical Insulation and Dielectric Phenomena, 1995.

[114] Xie Q, Zhang C, Yan J, et al. Surface charge accumulation and dissipation characteristics of insulating materials under non-uniform DC electric field [J]. Transactions of the China Electrotechnical Society, 034(004): 817-830.

[115] TREU A, LARN Y E. Impact of a low pulsed electric field on the fungal degradation of wood in laboratory trials [J]. International Biodeterioration & Biodegradation, 2016, 114(1): 244-251.

[116] TREU A, BARDAGE S, JOHANSSON M, et al. Fungal durability of polyaniline modified wood and the impact of a low pulsed electric field [J]. International Biodeterioration & Biodegradation, 2014, 87(2): 26–33.

[117] HATTORI T, TAMURA T. On the Effect of Electricity upon the Growth of Wood-destroying Fungi [J]. Japanese Journal of Phytopathology, 1939, 9(4): 211-222.

[118] TREU A, LARN Y E. Wood protection by means of electro osmotic pulsing technology (PLEOT) [C]. Lisbon: International Conference on Structural Health Assessment of Timber Structures, 2020.

[119] QIAN HE, TIANYI ZHAN, HAIYANG ZHANG, et al. Variation of surface and bonding properties among four wood species induced by high voltage electrostatic field (HVEF) [J]. Holzforschung, 2019, 73(10): 957-965.

[120] BJURMAN J. Growth inhibitory effects on blue-stain fungi of applied electricity fields [C]. Sweden: International Research Group on Wood Preservation conference, 1996.

[121] MESTECHKIN M. Condensation of fermion composite particles [J]. Journal of Computational Methods in Sciences & Engineering, 2011, 11(11): 127-142.

[122] Chen X, Cheng J, Yin X. Research progress and application of electrohydrodynamics [J]. Chinese Science Bulletin, 2003, 48(7): 637-646.

[123] CASTELLANOS A, P REZ A. Electrohydrodynamic Systems [M]. Berlin: Springer, 2007.

[124] Liu Y, Zhao G. Wood Resource Materials Science [M]. Beijing: China Forestry Press,2004.

[125] Qian J, Jin Y, Shen Z, et al. The influence of electric field intensity and action time on masson pine wood moisture content gradient [J]. Journal of Zhejiang A&F University, 2005, 22(2): 193-197.

[126] Qian J, Yu Y. The effect of electric field on poplar plywood [J]. Journal of Zhejiang A&F University, 1992, 16(3): 293-296.

[127] Qian J, Ye L, Zhang W. A Preliminary Study on the Gluing Effect of Poplar Wood by the Time of Electric Field [J]. Wood Industry, 2002, 3(3): 7-9.

[128] Qian J, Jin Y, Yu Y, et al. Gluing effect of potential difference between pads on Liu'an veneer [J]. Journal of Nanjing Forestry University (Natural Science Edition), 2002, 26(5): 41-43.

[129] MURR L E. Biophysics of Plant Growth in an Electrostatic Field [J]. Nature, 1965, 206(4983): 467-470.

[130] KRUEGER A P, REED E J. Biological Impact of Small Air Ions [J]. Science, 1976, 193(4259): 1209.

[131] Zhao J, Ma F, Yang W, et al. The effect of high voltage electrostatic field (HVEF) on swelling and chilling injury of soybean seeds [J]. Chinese Journal of Biophysics, 1995, 11(4): 595-598.

[132] Yan L, Bai X, Yu M, et al. Application of Electrostatic Technology in Agriculture [J]. Research on Agricultural Modernization, 1987, 8(5): 53-56.

[133] Xie J, Hua Z. Experimental study on freezing and thawing of food in high-voltage electrostatic field [J]. Food Science, 2000, 21(11): 14-18.

[134] YOSHIDA H, KITAJYO K, NAKAYAMA M. Electroosmotic dewatering under A.C. electric field with periodic reversals of electrode polarity [J]. Drying Technology, 1999, 17(3): 539-554.

[135] VIJH A K. Electroosmotic dewatering by a “new” method using a “gate” electrode: field effect transistor (FET) model or simply a multistage dewatering [J]. Drying Technology, 2002, 20(3): 705-710.

[136] VIJH A K. Some observations on electroosmotic dewatering (EOD) under A.C. electric field conditions [J]. Drying Technology, 2000, 18(1-2): 517-524.

[137] ISOBE S. Solid-liquid separation of agricultural products using twin screw press and electro-osmosis [J]. Japan Agricultural Research Quarterly, 1997, 31(2): 137-146.

[138] ORSAT V, RAGHAVAN G S V, SOTORINAL S, et al. Roller press for electro-osmotic dewatering of bio-materials [J]. Drying Technology, 1999, 17(3): 523-538.

[139] ASAKAWA Y. Promotion and retardation of heat transfer by electric fields [J]. Nature, 1976, 261(5557): 220-221.

[140] BAJGAI T R, HASHINAGA F. High electric field drying of Japanese radish [J]. Drying Technology, 2001, 19(9): 2291-2302.

[141] BAJGAI T R, HASHINAGA F. Drying of spinach with a high electric field [J]. Drying Technology, 2001, 19(9): 2331-2341.

[142] ISOBE S, BARTHAKUR N, YOSHINO T, et al. Electrohydrodynamic Drying Characteristics of Agar Gel [J]. Food Science & Technology International Tokyo, 1999, 5(2): 132-136.

[143] HASHINAGA F, KHAREL G P, SHINTANI R. Effect of Ordinary Frequency High Electric Fields on Evaporation and Drying [J]. Food Science & Technology International Tokyo, 1995, 1(2): 77-81.

[144] XU N, LIU W, HOU Q, et al. Effect of autohydrolysis on the wettability, absorbility and further alkali impregnation of poplar wood chips [J]. Bioresource Technology, 2016, 216(9): 317-322.

[145] ZHAN T, JIANXIONG L, JIALI J, et al. Viscoelastic Properties of the Chinese Fir (Cunninghamia lanceolata) during Moisture Sorption Processes Determined by Harmonic Tests [J]. Materials, 2016, 9(12): 1020.

[146] ZHAN T, JIANXIONG L, HAIYANG Z, et al. Changes of Time Dependent Viscoelasticity of Chinese Fir Wood and Its Frequency-Dependency during Moisture Desorption Processes [J]. Scientia Silvae Sinicae, 2017, 8(1): 1-7.

[147] CEN B, LIU Y, ZENG Z, et al. Mechanical behavior of novel GFRP foam sandwich adhesive joints [J]. Composites Part B: Engineering, 2017, 130(12): 1-10.

[148] ZHU M, SONG J, LI T, et al. Highly Anisotropic, Highly Transparent Wood Composites [J]. Advanced Materials, 28(26): 5181-5187.

[149] JONOOBI M, GHORBANI M, AZARHAZIN A, et al. Effect of surface modification of fibers on the medium density fiberboard properties [J]. European Journal of Wood & Wood Products, 2018, 76(6): 517-524.

[150] KROGELL J, KOROTKOVA E, ER?NEN K, et al. Intensification of hemicellulose hot-water extraction from spruce wood in a batch extractor – Effects of wood particle size [J]. Bioresource Technology, 2013, 143(9): 212-220.

[151] SERNEK M, RESNIK J, KAMKE F. Penetration of liquid urea-formaldehyde adhesive into beech wood [J]. Wood and Fiber Science, 1999, 31(1): 41-48.

[152] GERULLIS S, PFUCH A, SPANGE S, et al. Thin antimicrobial silver, copper or zinc containing SiOx films on wood polymer composites (WPC) applied by atmospheric pressure plasma chemical vapour deposition (APCVD) and sol–gel technology [J]. European Journal of Wood and Wood Products 2017, 76(8): 229-241.

[153] GASC N-GARRIDO P, MAINUSCH N, MILITZ H, et al. Copper and aluminium deposition by cold-plasma spray on wood surfaces: effects on natural weathering behaviour [J]. European Journal of Wood & Wood Products, 2016, 75(3): 1-10.

[154] ALTGEN D, AVRAMIDIS G, VIL W, et al. The effect of air plasma treatment at atmospheric pressure on thermally modified wood surfaces [J]. Wood Science & Technology, 50(6): 1227-1241.

[155] UEHARA T, SAKATA I. Effect of corona discharge treatment on cellulose prepared from beech wood [J]. Journal of Applied Polymer Science, 2003, 41(7-8): 1695-1706.

[156] KEMP B A, NIKOLAYEV I, SHEPPARD C J. Coupled electrostatic and material surface stresses yield anomalous particle interactions and deformation [J]. Journal of Applied Physics, 2016, 119(14): 111101-111635.

[157] CHIESA M, GIAMELLO E. Electron Spin Resonance Spectroscopy [M]. New York: John Wiley & Sons, Ltd, 2000.

[158] NADIR A, TURKER D, ZEKI C, et al. Wettability of fire retardant treated laminated veneer lumber (LVL) manufactured from veneers dried at different temperatures [J]. Bioresources, 2009, 4(4): 1536-1544.

[159] YOUNG T. An Essay on the Cohesion of Fluids [J]. Philosophical Transactions of the Royal Society of London, 1805, 95(1): 65-87.

[160] JIE-RONG C, WAKIDA T. Studies on the surface free energy and surface structure of PTFE film treated with low temperature plasma [J]. Journal Of Applied Polymer Science, 1997, 63(13): 1733-1739.

[161] SUN Y, ROYER M, DIOUF P N, et al. Chemical Changes Induced by High-Speed Rotation Welding of Wood — Application to Two Canadian Hardwood Species [J]. Journal of Adhesion Science & Technology, 2010, 24(8-10): 1383-1400.

[162] DORRIS G M, GRAY D G. The surface analysis of paper and wood fibers by Esca - electron spectroscopy for chemical analysis. Applications to cellulose and lignin [J]. 1978, 61(3): 545–552.

[163] HON D N S, FEIST W C. Free radical formation in wood: The role of water [J]. Wood Science, 1981, 14(1): 41-48.

[164] SOLODOVNIKOV S P, KOROTEEV M P, KAZIEV G Z, et al. Electron spin resonance study of the cavitated larch wood [J]. Russian Journal of General Chemistry, 2011, 81(1): 158-159.

[165] MONROLIN N, PRAUD O, PLOURABOU F. Electrohydrodynamic ionic wind, force field, and ionic mobility in a positive dc wire-to-cylinders corona discharge in air [J]. Physical Review Fluids, 2018, 3(6): 1-10.

[166] BA ULS-CISCAR J, PRATELLI D, ABEL M L, et al. Surface characterisation of pine wood by XPS [J]. Surface & Interface Analysis, 2016, 48(7): 589-592.

[167] TRUSS R W, WOOD B, RASCH R. Quantitative surface analysis of hemp fibers using XPS, conventional and low voltage in-lens SEM [J]. Journal of Applied Polymer Science, 2016, 133(8): 43023.

[168] PANDEY K K. A study of chemical structure of soft and hardwood and wood polymers by FTIR spectroscopy [J]. Journal of Applied Polymer Science, 1999, 71(12): 1969-1975.

[169] HE Q, ZHAN T, JU Z, et al. Influence of high voltage electrostatic field (HVEF) on bonding characteristics of Masson (Pinus massoniana Lamb.) veneer composites [J]. European Journal of Wood and Wood Products, 2018, 77(10): 105-114.

[170] MARIAN J E, STUMBO D A, MAXEY C W. Surface texture of wood as related to glue joint strength [J]. Forest Products Journal, 1958, 8(12): 345-351.

[171] LEE N H, LI C, CHOI J-H, et al. Comparison of moisture distribution along radial direction in a log cross section of heartwood and mixed sapwood and heartwood during radio-frequency/vacuum drying [J]. Journal of Wood Science, 2004, 50(6): 484-489.

[172] SCHIMLECK L R, JONES P D, PETER G F, et al. Nondestructive estimation of tracheid length from sections of radial wood strips by near infrared spectroscopy [J]. Holzforschung, 2005, 58(4): 375-381.

[173] KUROWSKA A, KOZAKIEWICZ P, BORYSIUK P. An attempt at the use of laboratory density analyzer for determination of solid wood cross section density distribution [J]. Forestry and Wood Technology 2010, 71(1): 435-439.

[174] HE Q, ZHAN T, ZHANG H, et al. The effect of high voltage electrostatic field (HVEF) treatment on bonding interphase characteristics among different wood

sections of Masson pine (Pinus massoniana Lamb.) [J]. Holzforschung, 2018, 72(7): 557-565.

[175] MENEZES A C, CARLOS G J, ARLETE C J. Colorimetric characteristics of different anatomical sections of muirapiranga (Brosimum sp.) wood [J]. Cerne, 2011, 17(2): 231-235.

[176] GEFFERT A, VYBOHOVA E, GEFFERTOVA J. Characterization of the changes of colour and some wood components on the surface of steamed beech wood [J]. Acta Facultatis Xylologiae, 2017, 59(1): 49-57.

[177] KANG H-Y, LEE W-H, JANG S-S, et al. Polyethylene Glycol Treatment of Han-Ok Round Wood Components to Prevent Surface Checking [J]. Bioresources, 2017, 12(2): 1-10.

[178] MAEKAWA T, FUJITA M, SAIKI H. Periodical analysis of wood structure. III. Evaluation of two-dimensional arrangements of softwood tracheids on transverse sections [J]. Bulletin of the Kyoto University Forests (Japan), 1990, 10(62): 275-281.

[179] FENGEL D. Structure and Function of the Membrane in Softwood Bordered Pits [J]. Holzforschung, 1972, 26(1): 1-9.

[180] HE G, YAN N. Effect of wood species and molecular weight of phenolic resins on curing behavior and bonding development [J]. Holzforschung, 2005, 22(6): 26-640.

[181] HIZIROGLU S, ZHONG Z W, ONG W K. Evaluating of bonding strength of pine, oak and nyatoh wood species related to their surface roughness [J]. Measurement, 2014, 49(1): 397-400.

[182] MIRZAEI B, SINHA A, NAIRN J A. Assessing the role of adhesives in durability of laminated veneer lumber (LVL) by fracture mechanics [J]. Holzforschung, 2016, 70(8): 763-771.

[183] POLETTO M, ZATTERA A J, FORTE M M C, et al. Thermal decomposition of wood: Influence of wood components and cellulose crystallite size [J]. Bioresource Technology, 2012, 109(1): 148-153.

[184] SANDERMANN W, AUGUSTIN H. Chemische Untersuchungen über die thermische Zersetzung von Holz-Zweite Mitteilung: Untersuchungen mit Hilfe der Differential-Thermo-Analyse [J]. Holz als Roh- und Werkstoff, 1963, 21(8): 305-315.

[185] AMMANN S, SCHLEGEL S, BEYER M, et al. Quality assessment of glued ash wood for construction engineering [J]. European Journal of Wood and Wood Products, 2016, 74(1): 67-74.

[186] HE Q, ZHAN T, ZHANG H, et al. Facile preparation of high anti-fungal performance wood by high voltage electrostatic field (HVEF) [J]. Journal of Cleaner Production, 2020, X(X): X.

[187] DORAU B, ARANGO R, GREEN F. An Investigation into the Potential of Ionic Silver as a Wood Preservative [C]. Nevada: Proceedings from the Woodframe Housing Durability and Disaster Issues Conference, 2004.

[188] SALAITA G N, HAZOS Z F, HOFLUND G B. Surface characterization study of the thermal decomposition of Ag2CO3 using X-ray photoelectron spectroscopy and electron energy loss spectroscopy [J]. Journal of Electron Spectroscopy and Related Phenomena, 107(1): 73-81.

[189] HUI, YANG, YAN-YU, et al. Preparation and antibacterial activities of Ag/Ag+/Ag3+ nanoparticle composites made by pomegranate (Punica granatum) rind extract [J]. Results in Physics, 2016, 6(6): 299-304.

[190] BIAN H, LUO J, WANG R, et al. Recyclable and Reusable Maleic Acid for Efficient Production of Cellulose Nanofibrils with Stable Performance [J]. ACS Sustainable Chemistry and Engineering, 2019, 7(24): 20022-20031.

[191] GU Y, BIAN H, WEI L, et al. Enhancement of Hydrotropic Fractionation of Poplar Wood Using Autohydrolysis and Disk Refining Pretreatment: Morphology and Overall Chemical Characterization [J]. Polymers, 2019, 11(4): 685.

[192] XIA H, YANG G. Facile synthesis of inorganic nanoparticles by a precipitation method in molten ε-caprolactam solvent [J]. Journal Of Materials Chemistry, 2012, 22(35): 18664-18670.

[193] YAO Q, WANG C, FAN B, et al. One-step solvothermal deposition of ZnO nanorod arrays on a wood surface for robust superamphiphobic performance and superior ultraviolet resistance [J]. Scientific Reports, 2016, 6(1): 35505.

[194] KIM S W, JUNG J H, LAMSAL K, et al. Antifungal Effects of Silver Nanoparticles (AgNPs) against Various Plant Pathogenic Fungi [J]. Mycobiology, 2012, 40(1): 53-58.

[195] TAO L, CHENG D L, W LINDER M E P, et al. Wettability of oil heat-treated bamboo and bonding strength of laminated bamboo board [J]. Industrial Crops and Products, 2015, 69(1): 15-20.

[196] JAVADIAN A, WIELOPOLSKI M, SMITH I F C, et al. Bond-behavior study of newly developed bamboo-composite reinforcement in concrete [J]. Construction and Building Materials, 2016, 122(9): 110-117.

[197] ZHONG Y, WU G, REN H, et al. Bending properties evaluation of newly designed reinforced bamboo scrimber composite beams [J]. Construction and Building Materials, 2017, 143(3): 61-70.

[198] SUPOMO H, DJATMIKO E B, ZUBAYDI A, et al. Analysis of the Adhesiveness and Glue Type Selection in Manufacturing of Bamboo Laminate Composite for Fishing Boat Building Material [J]. Marine Systems and Technologies, 2018, 874(1): 155-164.

[199] WEI Y, WANSI F, BIN Z, et al. Research status and suggestion on specification bamboo bonding interface [J]. Journal of Forestry Engineering, 2016, 5(5): 1-7.

[200] FENGEL D, SHAO X. A chemical and ultrastructural study of the Bamboo species Phyllostachys makinoi Hay [J]. Wood Science and Technology, 1984, 18(2): 103-112.

[201] HE Q, ZHAN T, ZHANG H, et al. Robust and durable bonding performance of bamboo induced by high voltage electrostatic field treatment [J]. Industrial Crops and Products, 2019, 137(5): 149-156.

[202] XU G, WANG L, LIU J, et al. FTIR and XPS analysis of the changes in bamboo chemical structure decayed by white-rot and brown-rot fungi [J]. Applied Surface Science, 2013, 280(8): 799-805.

[203] WANG J, SUN Q, SUN F, et al. Layer-by-layer self-assembly of reduced graphene oxide on bamboo timber surface with improved decay resistance [J]. European Journal of Wood and Wood Products, 2018, 76(4): 1223-1231.

[204] WEN H E, YOU J, JIANG S, et al. Isolation and characterization analysis of cellulose nanocrystal from Moso bamboo [J]. Journal of Nanjing Forestry University, 2013, 4(4): 23-29.

[205] LI X, SUN C, ZHOU B, et al. Determination of Hemicellulose, Cellulose and Lignin in Moso Bamboo by Near Infrared Spectroscopy [J]. Scientific Reports, 2015, 5(11): 17210.

[206] HUANG X, KOCAEFEA D, BOLUK Y, et al. Study of the degradation behavior of heat-treated jack pine (Pinus banksiana) under artificial sunlight irradiation [J]. Polymer Degradation and Stability, 2012, 97(7): 1197-1214.

[207] AND F P L, RIALS T G, SIMONSEN J. Relationship of Wood Surface Energy to Surface Composition [J]. Langmuir, 1998, 14(2): 536-541.

[208] WANG X Q, REN H Q, ZHAO R J, et al. [FTIR and XPS spectroscopic studies of photodegradation of Moso Bamboo (Phyllostachys pubescens Mazel)] [J]. Spectroscopy and Spectral Analysis, 2009, 29(7): 1864.

[209] XU C, ZHOU G, QIU H, et al. Analysis of the microscopic mechanism of coal wettability evolution in different metamorphic states based on NMR and XPS experiments [J]. Rsc Advances, 2017, 7(76): 47954-47965.

[210] PARK B D, KIM Y S, SINGH A P, et al. Reactivity, chemical structure, and molecular mobility of urea–formaldehyde adhesives synthesized under different conditions using FTIR and solid-state 13C CP/MAS NMR spectroscopy [J]. Journal Of Applied Polymer Science, 2003, 88(11): 2677-2687.

[211] STEELE R. Catalysis of the reaction of urea-formaldehyde precondensates on cellulose [J]. Journal of Applied Polymer Science, 1960, 4(10): 45-54.

[212] Du G, Lei H, PIZZI A. Thermomechanical performance analysis of urea-formaldehyde resin during curing [J]. Journal of Beijing Forestry University, 2009, 31(3): 110-114.

[213] Chen Y. Precuring characteristics and control mechanism of urea-formaldehyde resin [D]. Beijing: Chinese Academy of Forestry, 2015.

[214] Zhan T. Study on the viscoelastic response mechanism of wood in the process of moisture adsorption and desorption [D]. Beijing: Chinese Academy of Forestry, 2016.

[215] Yu H, Zhang J, Wang Y, et al. Research on rheology and viscoelasticity of phenolic resin jelly [J]. Journal of Southwest Petroleum University (Natural Science Edition), 2011, 33(3): 159-164.

[216] Zhang R, Tang L, Qian Y, et al. The effect of oxygen plasma treatment time on the surface wettability of poplar veneer [J]. Wood processing machinery, 2010, 4(4): 25-27.

[217] LU X, PIZZI A. Curing conditions effects on the characteristics of thermosetting adhesives-bonded wood joints — Part 1: Substrate influence on TTT and CHT curing diagrams of wood adhesives [J]. Holz als Roh- und Werkstoff, 1998, 56(5): 339.

[218] Wu Z. Basic Electrostatics [M]. Beijing: Peking University Press, 2010.

[219] Liang Y, Ding C. Electrohydrodynamic analysis of the principle of high-voltage electric field drying technology [C]. Qingdao: The 12th Annual Conference of the Electrostatic Professional Committee of the Chinese Physical Society, 2005.

[220] NEARN W T. Wood-Adhesive Interface Relations [J]. Off Dig Fed Soc Paint Technol, 1965, 37(1): 720-733.

[221] ROWELL R M. Handbook Of Wood Chemistry And Wood Composites [M]. Florida: CRC Press, 2005.

[222] FUCHENG B, YOUKE Z, JIANXIONG L. Relationship between permeability and fine structure of common Chinese fir and mason pine wood [J]. Journal of Beijing Forestry University, 2003, 25(1): 1-5.

[223] ZHAO Y, BAO F. Theoretical analysis on the relationship between softwood longitudinal permeability and its structure [J]. Scientia Silvae Sinicae, 1998, 34(4): 88-95.

[224] SANDERMANN W, AUGUSTIN H. Chemische Untersuchungen über die thermische Zersetzung von Holz—Dritte Mitteilung: Chemische Untersuchung des Zersetzungsablaufs [J]Holz als Roh- und Werkstoff, 1964, 22(10): 377-386.

[225] LO K S, LIEW K C. Effect of extraction solvent on mechanical properties of particleboard produced from cultivated Acacia hybrid [J]. Journal of the Indian Academy of Wood Science, 8(1): 46-49.

[226] HASHIM R, HOW L S, SULAIMAN O, et al. Effect of extractive removal on dimensional stability and bonding properties of particleboard made from hybrid of Acacia [J]. Journal of the Institute of Wood Science, 2001, 15(5): 261-266.

[227] ZHAOHUI W, ZEHUI W, XIGEN R. Studies on radial variation in density of moso bamboo using X-ray scanning [J]. Scientia Silvae Sinicae, 2004, 40(3): 111-116.

[228] DIXON P, GIBSON L. The structure and mechanics of Moso bamboo material [J]. Journal of the Royal Society, Interface / the Royal Society, 2014, 11(99): 1-7.

[229] TSUJINO T, TAKEUCHI N, KAWAI T. Bending strengths of wood beams of rectangular cross-sections by rigid body spring model II. The case where the cause of rupture is shear failure [J]. Mokuzai Gakkaishi, 1999, 45(1): 9-16.

[230] ANSHARI B, GUAN Z W, WANG Q Y. Modelling of Glulam beams pre-stressed by compressed wood [J]. Composite Structures, 2017, 165(3): 160-170.

[231] SUSAINATHAN J, EYMA F, DE LUYCKER E, et al. Experimental investigation of compression and compression after impact of wood-based sandwich structures [J]. Composite Structures, 2019, 220(5): 236-249.

[232] SMARDZEWSKI J, WOJCIECHOWSKI K W. Response of wood-based sandwich beams with three-dimensional lattice core [J]. Composite Structures, 2019, 216(6): 340-349.

[233] FOSCHI R O, BARRETT J D. Glued-laminated beam strength: a model [J]. J Struct Div, 1980, 106(8): 1735-1754.

[234] TETSUJI TSUJINO N T, TAKURO HIRAI. Predicting the Modulus of Rupture of Glued-Laminated Beams by the Rigid Bodies-Spring Model [J]. Mokuzai Gakkaishi, 2005, 51(5): 303-310.

[235] KEITA OGAWA H I, MASAKI HARADA, HIROFUMI NAGAO, HIDEO KATO, ATSUSHI MIYATAKE. Monte-Carlo Simulation Model for Predicting the Tensile Strength Distribution of Cross Laminated Timber [J]. Journal of the Society of Materials Science Japan, 2018, 67(12): 1087-1093.

[236] T. TSUJINO N T, T. KAWAI. Bending strengths of wood beams of rectangular cross-sections by rigid body spring model II. The case where the cause of rupture is shear failure [J]. Mokuzai Gakkaishi, 1999, 45(1): 9-16.

[237] He M, Yang J, Zhang S. Wood structure design [M]. Beijing: China Building Industry Press, 2008.

[238] Osamu Watanabe. Fundamentals of Wood Application [M]. Shanghai: Shanghai Science and Technology Press, 1986.

[239] Lu X, Chen Y. Fast-growing poplar veneer along the grain elastic modulus prediction model [J]. Journal of Nanjing Forestry University (Natural Science Edition), 2002, 26(3): 9-13.

[240] Lu X, Huang H, Du Y. Prediction model of transverse grain elastic modulus of fast-growing poplar veneer [J]. Journal of Nanjing Forestry University (Natural Science Edition), 2003, 27(2): 21-24.

[241] CAI Z. Wood-Based Composite Board [M]. New Jersey: John Wiley and Sons, 2012.

[242] UEDA K. Elastic Constants of Solid Wood and of Plywood [J]. Journal of the Society of Materials Science, Japan, 1971, 20(1): 1181-1187.

[243] MAKOTO K, NOBORU N, SHINICHIRO N. Estimation of the internal shear strength distribution of the element for laminated veneer lumber by nonlinear least-squares method [J]. Journal Of Wood Science, 2018, 65(4): 635-641.

[244] JEONG B, PARK B-D. Effect of molecular weight of urea–formaldehyde resins on their cure kinetics, interphase, penetration into wood, and adhesion in bonding wood [J]. Wood Science and Technology, 2019, 54(3): 665-685.

[245] GROOM L H, LEICHTI R J. Effect of Adhesive Stiffness and Thickness on Stress Distributions in Structural Finger Joints [J]. Journal Of Adhesion, 44(1-2): 69-83.

[246] WEI X, WEI Y. Influence of adhesive thickness on local interface fracture and overall strength of metallic adhesive bonding structures [J]. International Journal of Adhesion and Adhesives, 2013, 40(1): 158–167.

[247] BADER M, NEMETH R, KONNERTH J. Micromechanical properties of longitudinally compressed wood [J]. European Journal of Wood and Wood Products, 2019, 77(2): 341-351.

[248] RINDLER A, HANSMANN C, KONNERTH J. The effect of moisture on the mechanical response of wood, adhesive and their interphase by means of nanoindentation [J]. Wood Science and Technology, 2019, 53(5): 729-746.

[249] WU Y, WANG S, ZHOU D, et al. Use of Nanoindentation and Silviscan to Determine the Mechanical Properties of 10 Hardwood Species [J]. Wood and Fiber Science Journal of the Society of Wood Science and Technology, 2009, 41(1): 64-73.

[250] ANTIKAINEN T, ROHUMAA A, HUGHES M, et al. Comparison of the accuracy of two on-line industrial veneer moisture content and density measurement systems [J]. European Journal of Wood and Wood Products, 2014, 73(11): 61-68.

[251] KIERCZYŃSKI K, ŻUKOWSKI P. The influence of strong electric fields on the DC conductivity of the composite cellulose, insulating oil, and water nanoparticles [C]. Constanta: Advanced Topics in Optoelectronics, Microelectronics, and Nanotechnologies, 2016.

[252] MUHAMMAD-FITRI S, SUFFIAN M, WAR W M N, et al. Mechanical properties of plywood from batai (*paraserianthes falcataria*), eucalyptus (*eucalyptus pellita*) and kelempayan (*neolamarckia cadamba*) with different layer and species arrangement [J]. Journal of Tropical Forest Science, 2018, 30(1): 58-66.

[253] ASHORI A, GHOFRANI M, REZVANI M H, et al. Development and Material Properties of Reinforced Plywood Using Carbon Fiber and Waste Rubber Powder [J]. Polymer Composites, 2016, 39(3): 1-10.

[254] THOEMEN H, HUMPHREY P E. Modeling the physical processes relevant during hot pressing of wood-based composites. Part I. Heat and mass transfer [J]. Holz als Roh- und Werkstoff, 2006, 64(2): 125-133.

[255] CHENG G, ZHANG H, HUNT J F, et al. Determining shear modulus of thin wood composite materials using a cantilever beam vibration method [J]. Construction and Building Materials, 2016, 121(6): 285-289.

## Academic papers published during the degree study

(1) **Qian He**, Tianyi Zhan*, Haiyang Zhang, Zehui Ju, Lu Hong, Nicolas Brosse, Xiaoning Lu*, Facile preparation of high anti-fungal performance wood by high voltage electrostatic field (HVEF), *Journal of cleaner production*, 2020, 260: 120947. (IF=6.39).

DOI: 10.1016/j.jclepro.2020.120947

(2) **Qian He**, Isabelle Ziegler-Devin, Laurent Chrusciel, Sebastien Ngwa Obame, Lu Hong, Xiaoning Lu, Nicolas Brosse*, Lignin-first integrated steam explosion process for green wood adhesive application, *ACS sustainable chemistry and engineering*, 2020, 8(13):5380-5392. (IF=6.97) DOI: 10.1021/acssuschemeng.0c01065

(3) **Qian He**, Tianyi Zhan*, Haiyang Zhang, Zehui Ju, Lu Hong, Nicolas Brosse, Xiaoning Lu*, Robust and durable bonding performance of bamboo induced by high voltage electrostatic field treatment, *Industrial crops and products*, 2019, 137: 149-156. (IF=4.19)

DOI: 10.1016/j.indcrop.2019.05.010

(4) **Qian He**, Tianyi Zhan*, Haiyang Zhang, Zehui Ju, Lu Hong, Nicolas Brosse, Xiaoning Lu*, Variation of surface and bonding properties among four wood species induced by a high voltage electrostatic field (HVEF), *Holzforschung*, 2019, 73(10): 957-965. (IF=2.58)

DOI: 10.1515/hf-2018-0190

(5) **Qian He**, Tianyi Zhan, Zehui Ju, Haiyang Zhang, Lu Hong, Nicolas Brosse, Xiaoning Lu*, Influence of high voltage electrostatic field (HVEF) on bonding characteristics of Masson (Pinus massoniana Lamb.) veneer composites, *European journal of wood and Wood products*, 2019, 77(1): 105-114. (IF=1.90) DOI: 10.1007/s00107-018-1360-6

(6) **Qian He**, Tianyi Zhan*, Haiyang Zhang, Zehui Ju, Chunping Dai, Xiaoning Lu*, The effect of high voltage electrostatic field (HVEF) treatment on bonding interphase characteristics among different wood sections of Masson pine (Pinus massoniana Lamb.), *Holzforschung*, 2018, 72(7): 557-565. (IF=2.58) DOI 10.1515/hf-2017-0168

(7) **Qian He**, Tianyi Zhan*, Haiyang Zhang, Zehui Ju, Lu Hong, Nicolas Brosse, Xiaoning Lu*, Prediction of stiffness and strength distributions in laminated-wood treated by high voltage electrostatic field (HVEF), *Materials today communications*, accepted, 2020.

(8) Lu Hong, **Qian He**, Zehui Ju, Haiyang Zhang, Nicolas Brosse, Xiaoning Lu*, Effect of vacuum hot pressing on the bonding quality and heat transfer performance of plywood, *European Journal of Wood and Wood Products*, 2020, 4, published online.

DOI: 10.1007/s00107-020-01531-y

(9) Zehui Ju, **Qian He**, Haiyang Zhang, Tianyi Zhan, Liangsong Chen, Suxia Li, Lu Hong  Xiaoning Lu*, Steam explosion of windmill palm fiber as the filler to improve the acoustic property of rigid polyurethane foams, *Polymer Composites*, 2020, 4, published online.

DOI: 10.1002/pc.25585

(10) Zehui Ju, **Qian He**, Tianyi Zhan, Haiyang Zhang*, Lin Sun, Lu Hong, Xinyi Shi, Xiaoning Lu*, Steam Exploded Peanut Shell Fiber as the Filler in the Rigid Polyurethane Foams. *Journal of Renewable Materials*, 2019, 7(11), 1077-1091.

DOI: 10.32604/jrm.2019.07525

(11) Haiyang Zhang*, **Qian He**, Xiaoning Lu, A. Pizzi, Changtong Mei, Xianxu Zhan, Energy Release Rate Measurement of Welded Bamboo Joints, *Journal of Renewable Materials*, 2018, 6(5), 450-456. DOI:10.7569/JRM.2017.634180

(12) Junfeng Wang, Xuan Wang, **Qian He**, Yaoli Zhang, Tianyi Zhan*, Time-temperature-stress equivalence in compressive creep response of Chinese fir at high-temperature range, *Construction and Building Materials*, 2020, 235, 117809.

DOI: 10.1016/j.conbuildmat.2019.117809

(13) Tianyi Zhan*, Fengze Sun, Chao Lv, **Qian He**, Xuan Wang, Kang Xu, Yaoli Zhang, Liping Cai, Evaluation of moisture diffusion in lignocellulosic biomass in steady and unsteady states by a dynamic vapor sorption apparatus, *Holzforschung*, 2019, 73(12), 1113-1119.

DOI: https://doi.org/10.1515/hf-2019-0063.

(14) Junfeng Wang, Xuan Wang, Tianyi Zhan*, Yaoli Zhang*, Chao Lv, **Qian He**, Lu Fang, Xiaoning Lu, Preparation of hydro-thermal surface-densified plywood inspired by the stiffness difference in sandwich structure of wood, *Construction and Building Materials*, 2018, 177, 83-90. DOI: 10.1016/j.conbuildmat.2018.05.135

## Conference reports：

(1) **Qian He**, Tianyi Zhan, Haiyang Zhang, Zehui Ju, Lu Hong, Nicolas Brosse,

Xiaoning Lu*, Comparison of bonding performance between plywood and laminated veneer lumber induced by high voltage electrostatic field, 2019, MATEC Web of Conferences, 275:01013.

DOI: 10.1051/matecconf/201927501013

(2) **Qian He**, Tianyi Zhan, Haiyang Zhang, Zehui Ju, Lu Hong, Nicolas Brosse, Xiaoning Lu*, Highly mechanical performance of laminated veneer lumber Induced by high voltage electrostatic field, 2019, Modular and Offsite Construction multi-conference.

DOI: 10.29173/mocs78

**Abstract**: Improving the mechanical strength of wood and bamboo composite is an important way to promote product upgrading and industrial development. In this study, ESR (electron spin resonance), dynamic contact angle device, X-ray photoelectron spectrometer, rotational rheometer, fluorescence microscope and nano-indentation device were selected in order to investigate the effects of HVEF on the physicochemical properties of wood and bamboo, the effects of HVEF on the chemical structure and rheological properties of adhesives under a series of HVEF parameters. The aggregation effect of adhesive at bonding interface induced by HVEF has also been revealed and the micro-mechanical prediction model is established. The results are as follows: 1) After HVEF treatment, the surface activity of wood and bamboo increased significantly. Moreover, with the increase of voltage/time, the surface free radicals, O/C ratio and the number of oxygen groups increased significantly while the contact angle decreased. 2) With the increase of voltage/time, significantly improved inter-molecular reactions of urea formaldehyde resin and phenol formaldehyde resin were obtained. 3) After HVEF treatment, the distribution of adhesive at the bonding interphase was continuous and uniform. The penetration depth was significantly reduced. The density and bonding strength at the bonding interphase were significantly increased, and the delamination rate was reduced. 4) According to the vertical density profile at the bonding interface, the laminated stiffness and stress distribution model of the bonding interface has been established. The results showed that the prediction error of mechanical properties was less than 30%.

**Keywords**: wood/bamboo materials, high voltage electric field, surface activation, bonding interphase, bonding strength.